

A SYNERGETIC APPROACH TO PRODUCE DURABLE, HIGHLY
RECYCLED PAVEMENT MIXTURES

A Dissertation
Submitted to
the Temple University Graduate Board

In Partial Fulfillment
of the Requirements for the Degree
DOCTOR OF PHILOSOPHY
(Civil Engineering)

by
Ahmed Abdalla
May 2022

Examining Committee Members:

Ahmed F. Faheem (Ph.D.), Advisory Chair, Civil Engineering Department
Joseph Thomas Coe (Ph.D.), Civil Engineering Department
Bechara E. Abboud (Ph.D.), Civil Engineering Department
Eve Walters (Ph.D.), External Member, Environmental Engineering Department

ABSTRACT

Recently, Sustainable engineering has become a necessity due to the limited availability of virgin materials, environmental concerns, and the lack of economic resources. According to the United Nations, "Sustainable engineering is the process of using resources in a way that does not compromise the environment or deplete the materials for future generations." However, developing cost-efficient and long-term road infrastructure has always been a challenge. Therefore, novel solutions are required to extend the pavement life cycle and minimize raw materials utilization to overcome this challenge. This research focuses on integrating the waste material to produce rheological engineered asphalt mixtures as pavement material. This study utilized three wastes, which are Off-spec fly ash (OFA), Reclaimed Asphalt Pavement (RAP), and finally, a bio-oil extracted from Spent Coffee Ground (SCG).

OFA is a viable source for recycling due to the quantities produced yearly and deposited in landfills. For many years fly ash has been effectively used as a partial replacement for Portland cement in producing different types of concrete, embankments, and soil stabilization. Most of the underutilized fly ash is Off-Spec. That was the motive behind adopting the OFA in this study. This study aims to investigate the fly ash's interaction with the asphalt binder as an additive rather than a filler. Few studies evaluated this hypothesis regarding fly ash as an additive. Moreover, this research's novelty comes as there is a lack of research evaluating the fly ash-asphalt physio-chemical interaction.

RAP utilization in roads infrastructure became a current state of practice. Most state Departments of Transportation (DOTs) have been using RAP at a composition average of about 20% of the mix by mass. This study focuses on maximizing the utilization of the RAP content through using a bio-oil extracted from the SCG as a new promising rejuvenator.

Spent coffee ground is not well recycled, and almost six million tons are sent to landfills every year. This waste was found to release methane into the atmosphere; methane is the second-most abundant greenhouse gas and has a global warming potential up to 86 times greater than CO₂, which is highly harmful to the environment.

In this study, the overreaching goal is to develop a green, innovative, and sustainable approach by recycling three different types of wastes (OFA, RAP, and SCGO) to achieve high-performance asphalt pavements. In addition, this study documents the science-based approach to successfully integrating these wastes as substitutes to the asphalt binder.

Results show that some OFAs are associated with improved rheological performance, damage healing, and cracking resistance as an asphalt binder additive. The improvement is attributed to the level of interaction between the binder and the physical and chemical characteristics of the OFA. The use of rejuvenators further improved the aging resistance of the ash blends, suggesting high potential synergy, especially the proposed SCGO rejuvenator, which promotes utilizing it as a promising eco-friendly rejuvenator in the asphalt pavement industry. After engineering a product built by OFA and rejuvenators, these results have been validated by mixtures' scale testing.

62% optimum RAP content is suggested to be utilized with an 11% dosage of the proposed SCGO rejuvenator as binder replacement. For the new engineered OFA/rejuvenators products, a 30% optimum RAP content is suggested to be used. Finally, Life Cycle Assessment (LCA) is conducted to evaluate the environmental potential of utilizing multi recycled materials in the Hot Mix Asphalt (HMA) industry. The results show a reduction in environmental impacts with RAP utilization and the new eco-friendly products (OFA and SCGO rejuvenator). Shifting HMA plant fuel to natural gas instead of Heavy Fuel Oil (HFO) offers considerable potential environmental benefits. Adopting the Ultrasonic Assisted-oil Extraction (UAE) as SCGO rejuvenator extraction method showed less energy and solvent consumption than the Soxhlet extraction, resulting in less environmental impacts.

Keywords: Asphalt Binder; Sustainability; Recycling; Pavement Performance; Off-spec Fly Ash (OFA); Coal Combustion Waste (CCW); Reclaimed Asphalt Pavement (RAP); Asphalt Aging; Spent Coffee Ground (SCG); Rejuvenator; Life Cycle Assessment (LCA).

*“Sometimes, It is not about the journey or the destination, but about the
people, you meet along the way.”*

ACKNOWLEDGMENTS

I want to express my deepest gratitude to all those who have supported me, all of whom I would not be here without!

First, I would like to extend my heartfelt appreciation to Dr. Ahmed Faheem, who gave me this life-changing opportunity. You have not only supported and mentored me as a student but as a person. I will always be grateful for your patience and guidance throughout my Ph.D. It was an honor being your student. Thank you!

I want to extend my gratitude to the committee members, Dr. Bechara Abboud, Dr. Joseph Coe, and the external examiner Dr. Eve Walters, for honoring me with being my Ph.D. defense committee members and their input in this research work.

I want to thank my “**Asphalt Abad**” fellows and brothers, Mohammed Alsaihi and Arash Hosseini. Thank you for supporting, helping, and accepting me among you and being brothers to me. Also, I would like to thank Dr. Ahmed Shabana for all the support and guidance he provided. You are a brother to me!

I also would like to thank the Electric Power Research Institute (EPRI) for the financial support, without which I would not have been able to conduct this research. Thanks are also due to the staff of the College of Engineering, who was of significant help during my Ph.D. studies at Temple University.

I would like to extend my deepest appreciation and thanks to my family. Thank you, my mother and father, for your continuous support, patience, belief, unconditional LOVE, and your continuous prayers that made me reach that far. I love you!

I would like to thank my sister Radwa and my brother Mohamed for the help and support that you always gave.

I want to send my deepest gratitude to Karl and Laurie Siebert for being my family. It means a lot to me. I love you!

Finally, I want to thank my fiancée and my future wife, Lauren, for her continuous support, understanding, and acceptance. I love you, Lauren!

Thank you to the people I met through the journey!

TABLE OF CONTENTS

ABSTRACT.....	ii
ACKNOWLEDGMENTS	vi
LIST OF FIGURES	xiii
LIST OF TABLES.....	xvii
GLOSSARY OF TERMS.....	xix
CHAPTER 1	1
1. INTRODUCTION AND SCOPE OF WORK.....	1
1.1. Background	1
1.2. Research Motivation	4
1.3. Hypothesis.....	10
1.4. Research Approach	10
1.4.1 (Chapter 2) Phase I: Mechanistic Investigation of the Interaction of Coal Combustion Waste (CCW) and Asphalt Binder.....	11
1.4.2 (Chapter 3) Phase II: The Influence of Spent Coffee Ground Bio-Oil (SCGO) as a Rejuvenating Agent on Cracking Susceptibility of Aged Binder and RAP.	12
1.4.3 (Chapter 4) Phase III: Evaluating the Synergy Between Off-spec Fly Ash (OFA) Additives & Bio-Based Rejuvenators in Recycled Asphalt Blends.....	13
1.4.5 (Chapter 5) Phase IV: Evaluating the Influence of the Proposed Fly Ash Product on Asphalt Mixtures with Different Rap Ratios.....	14
1.4.6 (Chapter 6) Phase V: Life Cycle Assessment of Eco-Friendly Asphalt Pavement	15
CHAPTER 2	16

2. MECHANISTIC INVESTIGATION OF THE INTERACTION OF COAL COMBUSTION WASTE (CCW) AND ASPHALT BINDER	16
2.1. Background and Phase Objective.....	16
2.2. Materials and Methods	20
2.2.1. Materials	20
2.2.2. CCW Chemical and Physical Testing.....	20
2.2.3. Laboratory Testing Methods to Evaluate Binder Blends.....	21
2.2.3.1. Chemical Analysis using FTIR.....	21
2.2.3.2. Rheological Time and Temperature Dependency.....	23
2.2.3.3. Damage Behavior.....	24
2.2.3.4. Low-Temperature Cracking Susceptibility using Bending Beam Rheometer (BBR)	26
2.3. Experimental Design	26
2.3.1. Fabrication of Blends.....	27
2.4. Testing Results and Discussion.....	28
2.4.1. Chemical and Physical Characterization of Fly Ash	28
2.4.1.1. CCW Chemical Composition	28
2.4.1.2. Particle Shape and Size Distribution of Fly Ash	29
2.4.1.3. Fractional Voids (Rigden Voids).....	32
2.4.2. Asphalt Blends Performance.....	34
2.4.2.1. Superpave Performance Grading Results	34
2.4.2.2. Analysis of Infrared Spectroscopy (FTIR)	37
2.4.2.3. Damage Healing Evaluation.....	40
2.4.2.4. Crossover Modulus (G_c^*).....	43
2.4.2.5. Low-Temperature Performance Evaluation	46
2.4.3. Discussion of the Findings.....	50
CHAPTER 3	52

3. THE INFLUENCE OF SPENT COFFEE GROUND BIO-OIL (SCGO) AS A REJUVENATING AGENT ON CRACKING SUSCEPTIBILITY OF AGED BINDER AND RAP.....	52
3.1. Background and Phase Objective.....	52
3.2. Materials and Methods.....	55
3.2.1. Experimental Design Overview	55
3.2.2. Spent Coffee Ground (SCG) Bio-oil Extraction (Soxhlet Extraction Process)	58
3.2.3. Fabrication of Blends	60
3.2.4. Glover Rowe Parameter (G-R), Crossover Frequency, and Modulus (ω_c), (G_c^*)	60
3.3. Test Results and Discussion.....	62
3.3.1. Analysis of Infrared Spectroscopy (FTIR)	62
3.3.2. Thermal Cracking and Relaxation Performance Evaluation	67
3.3.3. Frequency Sweep Test Results	70
3.3.4. Grover-Rowe Parameter (G-R).....	73
3.3.5. Crossover Modulus and Frequency (G_c^* , ω_c).....	76
3.3.6. Rejuvenators' Efficiency (RE) Analysis.	77
CHAPTER 4	81
4. EVALUATING THE SYNERGY BETWEEN UPCYCLED OFF-SPEC FLY ASH & BIO-BASED REJUVENATORS IN RECYCLED ASPHALT BLENDS	81
4.1. Phase Objective	81
4.2. Materials and Methods.....	81
4.2.1. Experimental Design Overview	81
4.2.2. Fabrication of Binder Blends	83
4.3. Test Results and Discussion.....	84
4.3.1. Analysis of Infrared Spectroscopy (FTIR)	84
4.3.2. Low-Temperature Performance Evaluation.....	90

4.3.3.	Grover-Rowe Parameter (G-R).....	96
4.3.4.	Crossover Modulus and Frequency (G_c^* , ω_c).....	101
4.3.5.	OFA/Rejuvenator Synergetic Efficiency (SE).....	104
CHAPTER 5	108
5.	EVALUATING THE INFLUENCE OF THE PROPOSED FLY ASH PRODUCT ON ASPHALT MIXTURES WITH DIFFERENT RAP RATIOS	108
5.1.	Phase Objective.....	108
5.2.	Materials and Methods.....	108
5.2.1.	Experimental Design.....	108
5.2.2.	Materials	110
5.2.3.	Mix Design and Production	112
5.2.4.	Compaction Evaluation.....	113
5.2.4.1.	Volumetric Properties [87]:.....	113
5.2.4.2.	Construction Densification Index (CDI):	114
5.2.5.	Rutting Evaluation	115
5.2.6.	Cracking Evaluation.....	117
5.3.	Results and Discussion.....	121
5.3.1.	Compaction Evaluation.....	121
5.3.1.1.	Volumetric Properties.....	122
5.3.1.2.	Asphalt Mixtures' Workability.....	129
5.3.2.	Rutting Evaluation (High-Temperature Performance)	133
5.3.3.	Cracking Evaluation (Intermediate-Temperature Performance)	137
5.3.3.1.	Optimum RAP Content According to the Intermediate Temperature Performance	144
5.3.4.	Thermal Cracking (Low-Temperature Performance).....	145
5.3.5.	Analysis of Test Method Sensitivity.....	151
CHAPTER 6	155
6.	LIFE CYCLE ASSESSMENT OF ECO-FRIENDLY ASPHALT PAVEMENT .	155
6.1.	Background	155

6.2. Phase Objective and Scope	160
6.2.1. Goal of the Study	160
6.2.2. System Description and Boundaries	161
6.2.3. Functional Unit	163
6.2.4. Life Cycle Inventory Analysis	163
6.2.4.1. Data Acquisition of Materials Extraction and Production.....	165
6.2.5. Life Cycle Impact Assessment (LCIA).....	175
6.3. Results and Discussion.....	176
6.3.1. Process Contribution Analysis.....	180
6.3.2. Scenario Analysis.....	187
CHAPTER 7	189
7. CONCLUSION AND RECOMMENDED FUTURE WORK.....	189
7.1. Phase I Conclusion and Recommended Work.....	189
7.2. Phase II Conclusion and Recommended Work.....	191
7.3. Phase III Conclusion and Recommended Work	193
7.4. Phase IV Conclusion and Recommended Work	196
7.5. Phase V Conclusion and Recommended Work	200
REFERENCES	202

LIST OF FIGURES

Figure 1-1. The difference between rigid and flexible pavement structures.	2
Figure 1-2. Moving 12-Month Total Vehicle Miles Traveled (VMT) From 1971 to 2021 [9].....	6
Figure 1-3. Net electric generation by energy source [11]	8
Figure 2-1. Illustration of Determination of Peak Areas for the Unmodified Binder after PAV Aging.....	23
Figure 2-2. Fatigue Failure in LAS Tests for the Unmodified Asphalt Binder: (a) Stress-Strain Curve, (b) PSE-Based Failure (After Wang et al., 2015 [46]), (c) Schematic Illustration for %Healing Calculation (After Xie et al., 2017 [45]).....	25
Figure 2-3. Experimental Program	27
Figure 2-4. SEM of Samples at 1000x Magnification: (a) BH (b) CS (c) GA (d) HT (e) RH (f) RO (g) SBH (h) WE	30
Figure 2-5. A Schematic Showing the Concept of Fixed Asphalt and Free Asphalt [44]	33
Figure 2-6. The Carbonyl Index (ICO) of the Investigated Blends/Binders.....	38
Figure 2-7. The Sulfoxide Index (ISO) of the Investigated Blends/Binders	39
Figure 2-8. Healing Performance of the Investigated Blends/Binders	40
Figure 2-9. Comparison of measured damage healing performance against predicted values	42
Figure 2-10. Crossover modulus (G_c^*) of the investigated blends/binders	44
Figure 2-11 Comparison of measured crossover modulus against predicted values	46
Figure 2-12 Low temperature cracking potential of the investigated Blends/Binders	47
Figure 2-13. Comparison of measured ΔT_c against predicted values	49
Figure 3-1. Experimental Program	57
Figure 3-2. (a) Soxhlet Bio-Oil Extraction equipment, and (b) Rotary Evaporator Equipment.	59
Figure 3-3. Absorption of the Investigated PAV Aged Rejuvenated and Unrejuvenated (a) ARAP-NC, (b) ARAP-AA, (c) ARAP-PMA, and (d) RAP-RS19.	66
Figure 3-4. ΔT_c of the Investigated RAP binders before and after 2nd cycle of PAV Aging.....	67
Figure 3-5. ΔT_c of the Investigated PAV Aged Rejuvenated and Unrejuvenated RAP binders.....	69

Figure 3-6. Correlation between The Carbonyl Index (ICO) and ΔT_c of the Investigated Rejuvenated and unrejuvenated RAP binders.....	69
Figure 3-7. Asphalt Complex Modulus and Phase angle Master Curves for (a) ARAP-NC, (b) ARAP-AA, (c) ARAP-PMA, and (d) RAP-RS19.....	73
Figure 3-8. G-R Parameter of the Investigated RAP binders before and after Subjection to PAV Aging.....	75
Figure 3-9. G-R Parameter of the Investigated PAV Aged Rejuvenated and Unrejuvenated RAP binders.	75
Figure 4-1. Phase II Experimental Program	83
Figure 4-2: The Carbonyl Index (ICO) and The Sulphoxide Index (ISO) of the Investigated Unmodified ARAP Binder/OFA blends at Different Aging Levels.	85
Figure 4-3: The Carbonyl Index (ICO) and The Sulphoxide Index (ISO) of the Investigated PMA ARAP Binder/ OFA blends at Different Aging Levels.	86
Figure 4-4: The Carbonyl Index (ICO) + The Sulphoxide Index (ISO) of the Investigated Rejuvenated Unmodified ARAP Binder/ OFA blends at Different Aging Levels.	88
Figure 4-5: The Carbonyl Index (ICO) + The Sulphoxide Index (ISO) of the Investigated Rejuvenated PMA ARAP Binder/ OFA blends at Different Aging Levels.....	89
Figure 4-6. ΔT_c of the Investigated Unmodified ARAP Binder/ OFA blends at Different Aging Levels.....	91
Figure 4-7: ΔT_c of the Investigated PMA ARAP Binder/ OFA blends at Different Aging Levels.....	92
Figure 4-8: ΔT_c of the Investigated Rejuvenated Unmodified ARAP Binder/ OFA blends at Different Aging Levels.	93
Figure 4-9: ΔT_c of the Investigated Rejuvenated PMA ARAP Binder/OFA blends at Different Aging Levels.	95
Figure 4-10. Correlation between The Carbonyl Index (ICO), The Sulphoxide Index (ISO), ICO+ISO, and ΔT_c of the Investigated Rejuvenated Unmodified and PMA Binder/OFA blends.	96
Figure 4-11: G-R Parameter of the Investigated Unmodified ARAP Binder/OFA blends at Different Aging Levels.	97
Figure 4-12: G-R Parameter of the Investigated PMA ARAP Binder/ OFA blends at Different Aging Levels.	98
Figure 4-13: G-R Parameter of the Investigated Rejuvenated Unmodified ARAP Binder/ OFA blends at Different Aging Levels.....	99
Figure 4-14: G-R Parameter of the Investigated Rejuvenated PMA ARAP Binder/ OFA blends at Different Aging Levels.....	101

Figure 5-1: Phase III Experimental Program	110
Figure 5-2: Graphical representation of the two aggregate structures used in the study	111
Figure 5-3: Description of the Definition of CDI and TDI [88]	115
Figure 5-4: Schematic of the indirect tension test. (a) Test apparatus with the specimen and environmental chamber, (b) Load-Displacement curve obtained from the test.	117
Figure 5-5: Semi-Circular Bend (SCB) test. (a) SCB Specimen and test apparatus, (b) Force-Displacement curve.	118
Figure 5-6: A typical force Load Point Displacement (LPD) curve from the SCB test After [96]	121
Figure 5-7: The influence of the introduction of the different fly ash products on %AV for the 15% RAP mixtures	124
Figure 5-8: The influence of the introduction of the different fly ash products on % VMA for the 15% RAP mixtures	124
Figure 5-9: The influence of the introduction of the different fly ash products on % VFA for the 15% RAP mixtures	126
Figure 5-10. The influence of the introduction of the different fly ash products on %AV for the 50% RAP mixtures	127
Figure 5-11. The influence of the introduction of the different fly ash products on %VMA for the 50% RAP mixtures	128
Figure 5-12. The influence of the introduction of the different fly ash products on %VFA for the 50% RAP mixtures	129
Figure 5-13: Effect of Fly Ash/ Rejuvenator Products on CDI values for Both Unmodified and PMA 15% RAP Mixtures.	131
Figure 5-14. Effect of Fly Ash/ Rejuvenator Products on CDI values for Both Unmodified and PMA 50% RAP Mixtures.	132
Figure 5-15: Effect of Fly Ash/ Rejuvenator Products on the Number of Gyration Corresponding to 115 mm Height for 100% RAP Mixtures.	133
Figure 5-16: Tensile Strength Obtained from IDT-HT Test for both unmodified and PMA 15% RAP Mixtures	135
Figure 5-17. Tensile Strength Obtained from IDT-HT Test for both unmodified and PMA 50% RAP Mixtures	136
Figure 5-18: Tensile Strength Obtained from IDT-HT Test for 100% RAP Mixtures ..	137
Figure 5-19. Two Specimens with the Same Fracture Energy and Different Flexibility Index	138
Figure 5-20: The Fracture Energy and the Flexibility Index of the Unmodified Binder 15% RAP Mixtures	139

Figure 5-21: The Fracture Energy and the Flexibility Index of the PMA Binder 15% RAP Mixtures	140
Figure 5-22. The Fracture Energy and the Flexibility Index of the Unmodified Binder 50% RAP Mixtures	141
Figure 5-23. The Fracture Energy and the Flexibility Index of the PMA Binder 50% RAP Mixtures	142
Figure 5-24: The Fracture Energy and the Flexibility Index of the 100% RAP Mixtures	143
Figure 5-25. Optimum RAP Content According to the Intermediate Temperature Performance	144
Figure 5-26. The Relation the Pre-peak Slope and the Fracture Energy for the tested Mixtures	145
Figure 5-27. The Fracture Toughness, Fracture Energy, and the Pre-Peak Slope of the Unmodified binder 15% RAP Mixtures	146
Figure 5-28: The Fracture Toughness, Fracture Energy, and the Pre-Peak Slope of the PMA 15% RAP Mixtures	147
Figure 5-29. The Fracture Toughness, Fracture Energy, and the Pre-Peak Slope of the Unmodified binder 50% RAP Mixtures	148
Figure 5-30. The Fracture Toughness, Fracture Energy, and the Pre-Peak Slope of the Unmodified binder 50% RAP Mixtures	149
Figure 5-31: The Fracture Toughness, Fracture Energy, and the Pre-Peak Slope of the 100% RAP Mixtures	150
Figure 6-1. Life Cycle Assessment Framework (After the ISO 14044) [107]	158
Figure 6-2. LCA System Boundary of The Study Based on FHWA’s Pavement LCA Framework [113].	162
Figure 6-3. LCIA Results Relative to the Control Scenario (LC0-0).....	179
Figure 6-4. Sub-process contribution on the Different Environmental Impacts.....	180
Figure 6-5. Relative Contribution of the Main Processes to the Total Impact Scores: (a) Acidification, (b) Carcinogenic, (c) Ecotoxicity, (d) Eutrophication, (e) Global Warming, (f) Non-carcinogenic, (g) Ozone depletion, (h) Respiratory effects, and (i) Smog.....	186
Figure 6-6. The Variation of the LCIA Results of Adopting the Ultrasonic Assisted-oil Extraction (UAE) Method as an Alternative Scenario Relative to the Baseline Scenario (Soxhlet Extraction).	188

LIST OF TABLES

Table 2-1. Chemical Requirements (ASTM C618-19).....	28
Table 2-2. Chemical Elemental Composition and LOI of the Investigated Fly Ashes.....	29
Table 2-3. Physical Properties of Fly Ash	31
Table 2-4. Continuous Performance Grade for Unmodified and PMA Blends.....	35
Table 2-5. Results of the Healing performance regression multivariate analysis.....	42
Table 2-6. Results of the crossover modulus regression multivariate analysis	45
Table 2-7. Results of the ΔT_c regression multivariate analysis	48
Table 2-8: Fly Ash Physio-chemical optimal range for blends performance	51
Table 3-1. Continuous Performance Grade (PG) for the Investigated Asphalt Binders and RAP.....	56
Table 3-2. Carbonyl Index (ICO) for Rejuvenated and Unrejuvenated RAP binders.....	63
Table 3-3. Crossover modulus and frequency values of the Investigated Unrejuvenated /Rejuvenated RAP binders.....	77
Table 3-4. Different Investigated Rejuvenators' Efficiency Summary	79
Table 4-1. Crossover modulus and frequency values of the Investigated Unrejuvenated /Rejuvenated ARAP binders/ OFA blends.	104
Table 4-2: OFA/Rejuvenator Synergetic Efficiency (SE)	106
Table 5-1: Properties of the RAP binder and aggregates.....	111
Table 5-2: Mix design details	113
Table 5-3: Proposed Guideline for High-Temperature IDT (HT IDT) to Minimize Pavement Rutting [99]	116
Table 5-4: Significance of Changes in Binder Type, RAP Content, and Fly Ash/ Rejuvenator Products on the Test Method Results Using ANOVA.....	151
Table 6-1. Scenarios of the Asphalt Mixtures Analyzed in LCA Study.....	166
Table 6-2. Life Cycle Inventory Data for Virgin Material Extraction Processes	166
Table 6-3. Life Cycle Inventory Data for RAP Production Processes (Per 1 Ton of RAP)	167
Table 6-4. Life Cycle Inventory Data for SCGO Extraction Processes (Per 1 Kg of SCGO).....	169
Table 6-5. Life Cycle Inventory Data for OFA/SCGO Aging Additive Production (Per 1 Kg of OFA/SCGO Aging Additive)	171

Table 6-6. Parameters Considered Calculating TE According to Equation (1).....	173
Table 6-7. Calculated Thermal Energy (TE) for 1 Tonne of Mixtures' production	174
Table 6-8. Transportation Distances Considered in the Case Study.....	175
Table 6-9. Characterization Factors are available for the media listed for each impact category After H. Gu and R. Bergman (2016) [125]	176
Table 6-10. Total LCIA Results for the Investigated Scenarios	177

GLOSSARY OF TERMS

AASHTO	American Association of State Highway and Transportation Officials
Ac	Acidification
%Va	Air Void
ACAA	American Coal Ash Association
ASTM	American Society for Testing and Materials
ARAP	Artificial RAP
AC%	Asphalt content
BBR	Bending Beam Rheometer
ICO	Carbonyl Index
CAM	Christensen-Andersen-Marasteanu
CCP	Coal Combustion Products
CCW	Coal combustion Waste
CoV	Coefficient of Variation
G*	Complex Modulus
CDW	Construction and Demolition Wastes
CDI	Construction Densification Index
ω_c	Crossover Frequency
G_c*	Crossover Modulus
DOT	Departments of Transportation
DSR	Dynamic Shear Rheometer
Ec	Ecotoxicity

ESAL	Equivalent Single Axle Load
Eu	Eutrophication
FAA's	Federal Aviation Administration
FI	Flexibility Index
FGD	Flue Gas Desulfurization
FTIR	Fourier-Transform Infrared Spectroscopy
FE	Fracture Energy
K_{IC}	Fracture Toughness
GER	Global Energy Requirement
GW	Global Warming
G-R	Glover-Rowe
GHG	Greenhouse gases
HDV	Heavy Duty Vehicle
HFO	Heavy Fuel Oil
PGH	High-Temperature Grade
HMA	Hot Mix Asphalt
HHC	Human Health Cancerous
HHN	Human Health Noncancerous
HHP	Human Health Particulate
IDT-HT	Indirect Tension test at High Temperatures
PGI	Intermediate-Temperature Grade
IRI	International Roughness Index

JMF	Job Mix Formula
LCA	Life Cycle Assessment
LCI	Life Cycle Inventory Analysis
LAS	Linear Amplitude Sweep
LPD	Load Point Displacement
LTOA	Long-Term Oven Aging
LTPPBind	Long-Term Pavement Performance Bind
PGL	Low-Temperature Grade
%G_{mm}	Maximum Theoretical Density
NAPA	National Asphalt Pavement Association
NCHRP	National Cooperative Highway Research Program
NMAS	Nominal Maximum Aggregate Size
OFA	Off-spec Fly Ash
OBC	Optimum Binder Content
OD	Ozone Depletion
PSD	Particle Size Distribution
PG	Performance Grade
PBO	Petroleum-Based oil
δ	Phase Angle
PSF	Photochemical Smog Formation
PMA	Polymer Modified Asphalt
PAV	Pressure Aging Vessel

PSE	Pseudo-Strain Energy
RAP	Reclaimed Asphalt Pavement
RAS	Recycled Asphalt Shingles
RE	Rejuvenators' Efficiency
RTFO	Rolling Thin Film Oven
SEM	Scanning Electron Microscopy-Energy Dispersive Spectroscopy
SCB	Semi-Circular Bend
STOA	Short-Term Oven Aging
Si	Silicon
S-VECD	Simplified Visco-Elastic Continuum Damage
SG	Specific Gravity
SCG	Spent Coffee Ground
SDA	Spray Dryer Absorber
SHRP	Strategic Highway Research Program
SBS	Styrene-Butadiene-Styrene
ISO	Sulfoxide Index
S	Sulfur
SA	Surface Area
SE	Synergetic Efficiency
TSR	Tensile Strength Ratio
USEA	The United States Energy Administration
TE	Thermal Energy

TRACI	Tool for the Reduction and Assessment of Chemical and Other Environmental Impacts
USLCI	U.S. Life Cycle Inventory
UAE	Ultrasonic Assisted-oil Extraction
VBO	Vegetable-Based Oil
VMT	Vehicle Miles Travelled
%VFA	Voids Filled with Asphalt
%VMA%	Voids in Mineral Aggregates
WMA	Warm Mix Asphalt
XRF	X-Ray Fluorescence

CHAPTER 1

INTRODUCTION AND SCOPE OF WORK

1.1. Background

The road industry started about (600 B.C.) by the Carthaginians [1]. The Romans eventually found that Carthaginians, their neighbors across the Mediterranean, threatened their empire. Accordingly, the Romans invaded Carthage in 146 B.C. That is why it is believed that the Romans adopted the practice of a military road system from the Carthaginians. It is estimated that the Romans built about 87,000 km of roads within their empire. However, the first paved road is believed to be in Egypt. This road is located near the Dahshur pyramids, 43 miles southwest of Cairo. This world's oldest known paved road is about a 7½-mile-long, 6-foot-wide road. It was made of limestone and sandstone slabs, built between 2600 and 2200 B.C. This Road is believed to be used to transport basalt on human-drawn sleds from a quarry on the Nile to building sites [2].

In 1870, the first asphalt rock roadway to be laid in the U.S. was accredited to chemist E.J. DeSmedt. He constructed a small experimental road made of European asphalt; the road was laid in front of the city hall in Newark, New Jersey. A year later, in 1871, in Washington, D.C, several asphalt-like pavements were laid. These pavements were composed of crushed rock and sand with coal tar pitch and creosote oil. These pavements were able to provide over 15 years of good service.

Then, in 1876, in Washington, D.C., the first sheet asphalt pavement composed of Trinidad Lake asphalt laid in the U.S. was on Pennsylvania Avenue [3].

Road paving went through many evolutions throughout history until it reached the current way it is right now. Today, there are two major categories of pavements. As shown in Figure 1-1, the first is the flexible pavement, and the second is the rigid pavement. Rigid pavements are constructed, basically, from cement concrete or reinforced concrete slabs. Cement concrete slabs are sufficiently strong to resist the applied loads from traffic. The rigid pavement has a high modulus of elasticity to distribute the load over a relatively wide soil area. On the other hand, flexible pavement structure flexes under the applied load, as shown in Figure 1-1, and that is why it is so named. Flexible pavement is designed as a layered system structure in which high-strength materials are placed on the top where the intensity of the stress is high, and less-strength materials are placed at the bottom where the stress intensity is low [3]–[5].

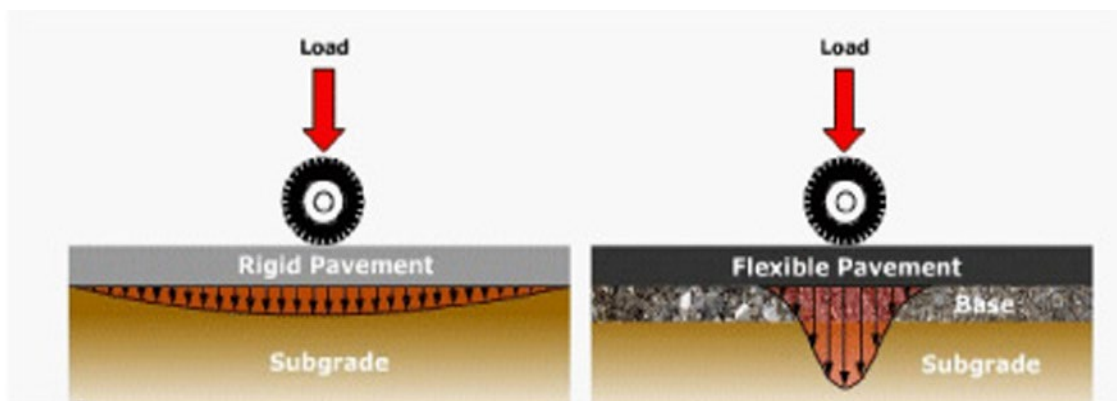


Figure 1-1. The difference between rigid and flexible pavement structures.

Generally, any flexible pavement consists of two main types of materials, asphalt binder, and aggregates. Typically, the asphalt cement is usually about 5%, and the aggregates correspond to the remaining 95% by mass. According to the American Society for Testing and Materials (ASTM), ASPHALT is identified as “A dark brown to black cementitious material in which the predominating constituents are bitumen’s which occur in nature or are obtained in petroleum processing.” The primary purpose of the asphalt binder in the Hot Mix Asphalt (HMA) appears from the name that it works as a waterproof, thermoplastic, viscoelastic binding, and adhesive material that either binding aggregate particles together or works as a bond between particles and an existing surface [6]. Asphalt cement or binder is a complex mixture of petroleum hydrocarbons with various chemical structures composed of hydrogen, carbon, and heteroatoms, such as oxygen, sulfur, nitrogen, vanadium, and nickel. Asphalt binder is a viscoelastic material, as at low temperatures, asphalt cement can be very elastic and brittle, and at high temperatures, it behaves to be very fluid (viscous). The asphalt binder behaves as a viscoelastic material at intermediate temperatures, combining elastic and viscous properties. The HMA mixing philosophy is to add asphalt binder content as possible for achieving durability, fatigue resistance, rutting resistance, and flexibility.

The other major component of any kind of pavement is the aggregates. According to the American Association of State Highway and Transportation Officials (AASHTO), aggregates can be classified as coarse and fine aggregates. According to (AASHTO Designation: M 145-91, 2012), sieve #10 size (2mm) can separate coarse and fine aggregates.

Therefore, whatever is retained on sieve #10 is considered coarse aggregates (gravel, boulders, and cobbles), and whatever passing sieve #10 is considered fine aggregates (sand and mineral fillers). Mineral fillers are defined as the fraction of the fine aggregates that pass sieve #200 size (0.075mm).

1.2. Research Motivation

According to the Federal Highway Administration FHWA, there are more than 4.1 million miles of public roads in the U.S. About 3 million miles of these enormous network are paved roads. 85% of the paved roads are surfaced with asphalt concrete (flexible pavement). On the other hand, almost 5% of the paved network are rigid pavement, and the remaining 10% are found to be composite pavements. Asphalt mixtures are used to pave roads, streets, highways, parking lots, airports, biking and walking trails, and other paved surfaces in the nation's transportation networks. Roughly 3,500 asphalt mix plants operate across the United States, producing about 350 million tons of asphalt pavement material per year. 65% of the asphalt pavement market is publicly funded highway projects. According to the National Asphalt Pavement Association (NAPA), the capital spending on highways, roads, and bridges by all levels of government (federal/state/local) totals about \$80 billion annually. Approximately 28,000 jobs are supported for each \$1 billion of federal spending invested in highway construction nationwide. From the previously mentioned statistics, the highways construction industry is considered one of the biggest nationwide.

As demonstrated in Figure 1-2, the total Vehicle Miles Travelled (VMT) in the United States increased by 175% from 1971 to 2021. Moreover, VMT is expected to increase by 50% in the next 20 years, and more importantly, freight movement is expected to double by 2025. The number of vehicles on the road was found to be increased by 266% from 1960 to 2019. On the other hand, the number of road miles only increased by 17 % over the same period [8]. Moreover, with rapid industrialization in developing nations, an increase in paved surfaces is anticipated.

The previously mentioned statistics could explain the great need to build high-quality roads and maintain their high performance over a long period. Accompanying the continuous yearly increased traffic, an escalating increase in crude oil prices. Accordingly, it is expected that the costs of asphalt mixture production to increase continuously every year. That motivated materials researchers to investigate novel materials, recycle different waste materials, and yield them to meet the specifications for high-performance transportation infrastructure.

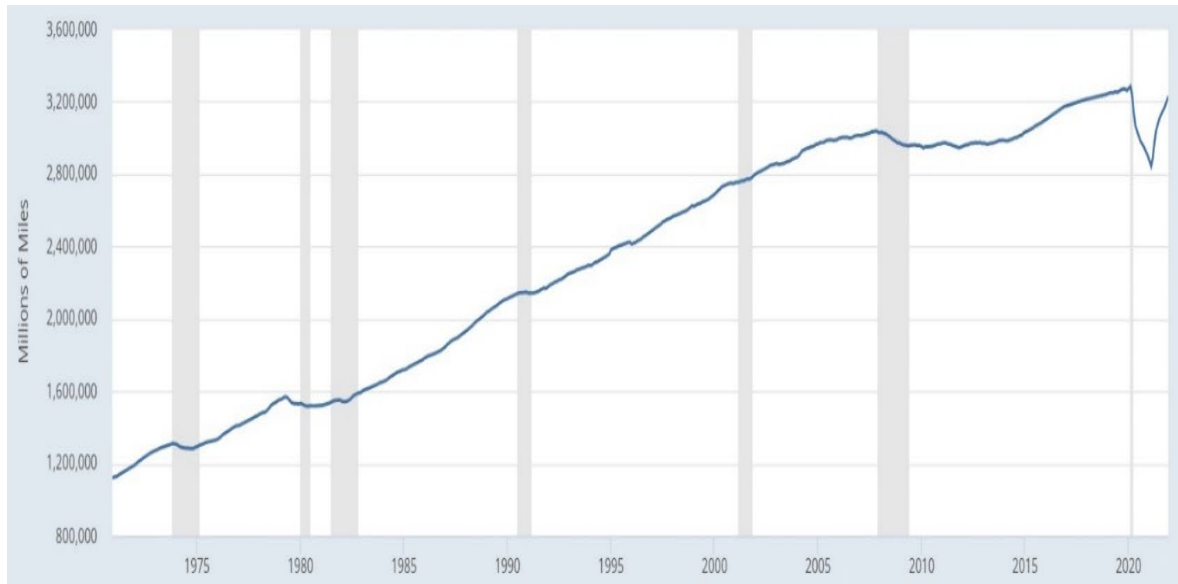


Figure 1-2. Moving 12-Month Total Vehicle Miles Traveled (VMT) From 1971 to 2021 [9]. Based on FHWA, about 36 million tons of the Recycled Asphalt Pavement (RAP) produced is reported to be used as a portion of recycled hot mix asphalt, in cold mixes, or as aggregate in granular or stabilized base materials. Less than 20% of the annual amount of RAP generated is disposed of in landfills or by the right of way and eventually reused. When asphalt mixtures are aged, they are prone to be more brittle, which leads to fracture under the environmental and mechanical effects. The fracture mainly happens when the asphalt binder loses its ability to bind the aggregate together. The previously illustrated phenomena become more common when RAP materials are used in the asphalt mixture since the utilized RAP is already aged and prone to aging-related distresses. Therefore, RAP being used, at a composition average of about 15% of the mix by mass and sometimes up to 50% in some cases, became a current state of practice.

Coal combustion Waste (CCW) is a viable source for recycling due to the large quantities produced yearly in the United States. According to the American Coal Ash Association (ACAA), 41% of produced CCW is disposed of in landfills in 2020, constituting more than 28.4 million tons [10]. There are widespread concerns that coal plants are closing and will be closed in the near future, as clean energy is taking over. However, coal-fueled electric power plants are expected to remain relatively steady through 2033. In fact, coal-fueled electric power is forecasted to have the lion's share of electricity production around the US, with more than 36% of the total electricity produced through 2033 [11], as shown in Figure 1-3. In 2019, more than 34% of the Coal Combustion Products (CCP) was fly ash. More than 63% of the produced fly ash was utilized in different fields. For many years fly ash has been effectively used as a partial replacement for Portland cement in producing different types of concrete, embankments, and soil stabilization. Fly ash is rarely used in flexible pavement construction. However, lately, there has been renewed interest in employing it as a mixed design component [12]–[15]. Less than 2.00% of the utilized fly ash in 2019 was used in the asphalt industry, and it was used as an asphalt filler [16]. This is considered a very minimal amount to be used in such a massive industry as the pavement industry. Asphalt mixtures are used to pave roads, streets, highways, parking lots, airports, biking and walking trails, and other paved surfaces in the nation's transportation networks.

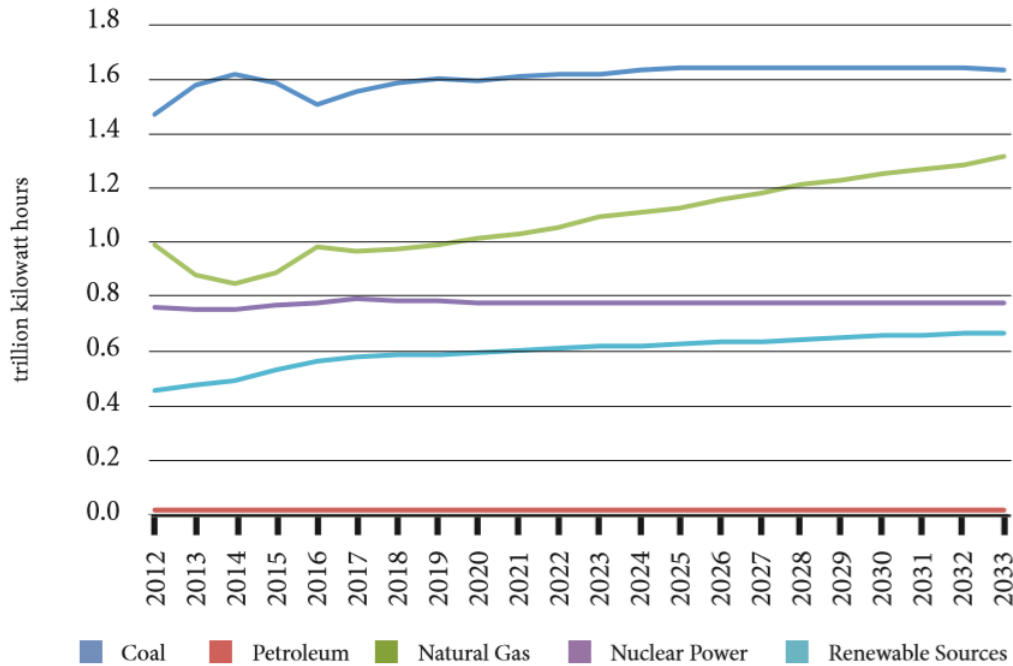


Figure 1-3. Net electric generation by energy source [11]

Another waste material is Spent Coffee Grounds (SCG). According to the U.S. Department of Agriculture, the world’s coffee production is 16.34 billion pounds per year.

According to World Economic Forum, more than 2 billion cups of coffee are consumed every day across the globe. Most of the coffee used to make those cups are thrown away, with six million tonnes sent to landfill every year. Decomposed coffee grounds were found to release methane into the atmosphere; methane is the second-most abundant greenhouse gas and has a global warming potential up to 86 times greater than CO₂, which is extremely bad for the environment [17].

In 2021, 1.5 billion tons of crushed stone valued at more than \$19 billion was produced by an estimated 1,410 companies operating 3,440 quarries and 180 sales region and (or)

distribution yards in 50 States. It is estimated that about 72% of crushed stone was used as a construction aggregate, mainly for road construction and maintenance; 16% for cement manufacturing; 8% for lime manufacturing; 2% for agricultural uses; and the remaining 2% for other chemicals, and miscellaneous uses and products. The price of crushed stones increased by 15% from 2017 to 2021, reaching \$13.0 per metric ton. Iron and steel slag substitute the crushed stone for roadbuilding. In addition, other sources such as RAP are increasingly substituted virgin aggregates. However, the percentage of total aggregate supplied by recycled materials remained very small in 2021 [18].

Asphalt concrete cost is increasing because of the increased traffic demands in crude oil and many other factors such as the rising energy costs. The dilemma was always and will be having a sustainable and efficient highway infrastructure that can endure a high service life with little maintenance and rehabilitation costs. That can explain the urgent need for developing cost-efficient and long-term road infrastructure.

This development shall be achieved by adopting innovative approaches that are green and environmentally sustainable. Having high-performance asphalt pavements with high durability in the presence of different types of recycled materials additives is an efficient technique that can significantly reduce the rising costs of rehabilitating and maintaining asphalt concrete pavements while offering a green and sustainable solution.

1.3. Hypothesis

Combining the beneficial effects of CCP and SCG can enhance the high, intermediate, and low-temperature performance of highly recycled asphalt mixtures, including Reclaimed Asphalt Pavement (RAP). Accordingly, developing an innovative, green, and sustainable framework that can reduce the maintenance and rehabilitation costs of asphalt concrete pavements.

One of the unique aspects of this study is the synergetic approach in utilizing waste material to produce asphalt mixtures. Each of the waste sources is incorporated in the study to complement/address a side effect of utilization of the other wastes while as well, improving asphalt mixtures' performance.

1.4. Research Approach

The overarching goal of this study is to develop a green, innovative, and sustainable approach through recycling three different types of waste (RAP, CCW, and SCG) in achieving high-performance asphalt pavements. To achieve this goal, the research is divided into five main phases. Each phase has a set of goals and tasks that need to be achieved to reach the main goal of the research.

Each phase will be discussed in detail in a separate chapter in this dissertation. In the following subsections, each phase is briefly demonstrated.

1.4.1 (Chapter 2) Phase I: Mechanistic Investigation of the Interaction of Coal Combustion Waste (CCW) and Asphalt Binder.

Previous studies show promising effects of some standard fly ash classes on asphalt. However, there is limited research into Off-spec Fly Ash (OFA). Multiple studies published presented fly ash as a unique additive compared to traditional mineral fillers. In this research, several coal combustion wastes (CCW) are examined in terms of their physio-chemical interaction with asphalt binders. Eight types of CCW are blended with two types of asphalt binders: unmodified and Polymer Modified Asphalt (PMA). The physical properties and chemical composition of the CCW are characterized. Testing is focused on identifying changes in binder performance after blending with the CCW to understand the role of the CCW. The experimental program is focused on damage healing, rheological performance, and Low-temperature cracking potential. All the blends are conditioned using the pressure aging vessel.

Oxidative aging is quantified through measurement of both carbonyl (ICO) and sulfoxide (ISO) indices by Fourier-Transform Infrared Spectroscopy (FTIR). Results show that some of the CCWs are associated with improved rheological performance, damage healing, and cracking resistance. The improvement is attributed to the level of interaction between the binder and the CCW and the physical and chemical characteristics of the CCW. Testing results demonstrate that synergy between the CCW particles and polymer modifiers needs further investigation. Statistical regression analysis is used to quantify the significance of influencing factors on the blend performance. The analysis revealed that the level of interaction between the CCW and the binder is measurable by the phase angle of the blend.

The CCW's silicon (Si), Sulfur (S) content, along with particle size distribution and specific gravity, are the significant chemical and physical properties influencing the blend performance. These findings propose a fruitful upcycling opportunity for some CCW as an enhancer of asphalt performance.

1.4.2 (Chapter 3) Phase II: The Influence of Spent Coffee Ground Bio-Oil (SCGO) as a Rejuvenating Agent on Cracking Susceptibility of Aged Binder and RAP.

This phase aims to deliver a new promising asphalt binder rejuvenator developed from Spent Coffee Ground to mitigate the effects of aging on the asphalt. The research relied on three different binders: two unmodified PG 64-22 binders and a Polymer Modified (PMA) PG 76-22 binder. Moreover, a field extracted RAP binder is utilized in evaluating the rejuvenator's efficiency. For this study, the proposed SCGO is compared against two market-available rejuvenators.

The experimental program relied on aging control binder samples for each asphalt type with no rejuvenation using the Rolling Thin Film Oven (RTFO) test, followed by the Pressure Aging Vessel (PAV) test for 20 hours to create Artificial RAP (ARAP) binder. Then, ARAP and RAP binders were blended with 5% by their weight with one of the two on-market rejuvenators (#1, #2) or the proposed SCGO rejuvenator. Testing results reveal that low-temperature relaxation was significantly improved for all the investigated samples after an additional PAV aging cycle, as ΔT_c values increased compared to the control binders. Further, samples' master curves were used to calculate the Glover-Rowe (G-R) parameter, Crossover frequency, and modulus (ω_c , G_c^*).

The results clearly showed the ability of the SCGO to reduce the aging rate and improve the rheological properties of RAP binders. Further, the FTIR test shows that the new SCGO rejuvenator reduces the oxidation levels of the aged RAP binders, as suggested by the carbonyl index. The new SCG bio-oil acquires the merit of being a promising eco-friendly rejuvenator in the asphalt pavement industry, with effectiveness comparable to the two market-available rejuvenators tested.

1.4.3 (Chapter 4) Phase III: Evaluating the Synergy Between Off-spec Fly Ash (OFA) Additives & Bio-Based Rejuvenators in Recycled Asphalt Blends

In this phase, four off-spec fly ashes were screened from phase I and blended with two types of asphalt binders; unmodified and PMA. The OFA inclusion in the binder is proposed as an additive to the binder rather than part of the aggregate fines.

The binders and blends were exposed to two cycles of PAV aging, rejuvenating after the first aging cycle using two market-available rejuvenators and the proposed SCG rejuvenator. Given the reported benefits of using some classes of fly ash with asphalt and promoting high-quality utilization of post-service reclaimed asphalt binders, the main goals of this phase are to evaluate the synergetic influence of the OFA and rejuvenator combination on asphalt binder aging. In addition, FTIR analysis was used to evaluate the chemical changes resulting from aging.

Loss of ductility in the binders was measured using ΔT_c as a measurement of the effect of aging on binder durability. Glover-Rowe (G-R) Parameter and Cross-over Modulus (G_c^*) were also used to determine the aging state of the rejuvenated binders. Results showed that

all fly ash additives either reduce or maintain the oxidation level as that of the neat binder. This indicates a slower aging rate for the ash blends than the binder alone for both cycles of PAV aging. The use of rejuvenators further improved the aging resistance of the ash blends, suggesting high potential synergy.

1.4.5 (Chapter 5) Phase IV: Evaluating the Influence of the Proposed Fly Ash Product on Asphalt Mixtures with Different Rap Ratios

In this phase, three off-spec fly ashes were screened from phase III and were blended with two different rejuvenators; the petroleum-based rejuvenator (Rej.#2) and the proposed vegetable-based SCGO rejuvenator. The new blends are hereafter referred to as OFA/rejuvenator products. In addition, three ratios of RAP were studied for this phase 15%, 50%, and 100% RAP contents.

Two binders were used in this study; a neat PG 64-22 binder and a Styrene-Butadiene-Styrene (SBS) Polymer Modified (PMA) binder PG 76-22 for the 15% RAP and 50% RAP mixtures. The new OFA/rejuvenator products are introduced to the different mixtures, then evaluated through Indirect Tension test for high-temperature performance and Semi-Circular Bend (SCB) for both intermediate and low-temperature performance. Moreover, the influence of the OFA/rejuvenator products on mixtures' workability is evaluated. The main objective of this phase is to validate the findings of the previous phases on the mixtures' scale. Also, identify the optimum RAP content to be utilized with SCGO rejuvenator and OFA/rejuvenator products.

1.4.6 (Chapter 6) Phase V: Life Cycle Assessment of Eco-Friendly Asphalt Pavement

In this Phase, a comparative Life Cycle Assessment (LCA) is conducted to evaluate the environmental potential of utilizing multi recycled materials in the Hot Mix Asphalt (HMA) industry. These Materials are Reclaimed Asphalt Pavement (RAP), Off-spec Fly Ash (OFA), and the proposed Spent Coffee Ground bio-oil (SCGO). A comparative analysis is performed on producing one ton of HMA considering multiple scenarios, which stem from virgin materials extraction, recycled materials production, transportation, and HMA production. The study analyzed six percentages of RAP replacement to aggregate and asphalt binder, 0%, 15%, 30%, 50%, 80%, and 100% RAP. Moreover, 11% of virgin asphalt binder is replaced by two proposed products. The first product is the SCGO, which is utilized alone as an asphalt binder rejuvenator with the highest two RAP rate scenarios, 80 and 100%. The second product is a blend of the OFA with the SCGO with a 2:1 ratio, which is evaluated with all the investigated scenarios.

After assessing the baseline scenario, an alternative scenario is investigated. The alternative scenario is changing the SCGO extraction technique from Soxhlet to Ultrasonic Assisted-oil Extraction (UAE). Open-LCA software is used for modeling all the investigated scenarios in the light of TRACI v.2.1 impact assessment methodology in this case study. The results show a reduction in environmental impacts with RAP utilization and the new eco-friendly products. In addition, adopting the UAE as SCGO rejuvenator extraction method showed less energy and solvent consumption than the Soxhlet extraction, resulting in less environmental impacts.

CHAPTER 2

MECHANISTIC INVESTIGATION OF THE INTERACTION OF COAL COMBUSTION WASTE (CCW) AND ASPHALT BINDER

2.1. Background and Phase Objective

Coal combustion Waste (CCW) is a viable source for recycling due to the large quantities produced yearly in the United States. According to the American Coal Ash Association (ACAA), 41% of produced CCW is disposed of in landfills in 2020, constituting more than 28.4 million tons [10]. For many years fly ash has been effectively used as a partial replacement for Portland cement in producing different types of concrete, embankments, and soil stabilization. Fly ash is rarely used in flexible pavement construction. However, lately, there has been renewed interest in employing it as a mix design component [12]–[15]. However, the focus of this recent interest is directed mainly to standard fly ash classes. These classes of fly ash are already utilized at a steadily increasing rate, according to the ACAA [19]. On the other hand, other CCWs are underutilized at an alarmingly high rate. Material like Flue Gas Desulfurization (FGD) scrubber has less than 5% utilization [10]. Most of the underutilized materials are formed when coal-burning power plants burn coal at low temperatures to minimize their CO₂ and SO₂ emissions. Therefore, these types of CCW are referred to as Off Spec Fly Ash (OFA). They may have high carbon and sulfur contents, hindering off-spec ash use with cementitious materials.

In the literature related to the interaction of particulates with the asphalt binder, papers have been published since the early 1900s. Many of these studies labeled these particulates as

fillers. Typically, fly ash is treated as a filler in most studies. However, in a study sponsored by the National Cooperative Highway Research Program (NCHRP), the researchers suggested that fly ash's influence on the binder does not match that of the mineral fillers [20]. The study researchers followed up with additional experimentations to evaluate the interaction between fillers and asphalt binders, including fly ash. This study incorporated particulates (mineral fillers and fly ash) with the binders at different volume concentrations. Testing evaluated the stiffness change and tack strength of the blends. The results confirmed the observation of the NCHRP study, where the fly ash interaction with binders was unique. Later, two studies evaluated mixture compaction and performance by replacing 10% of the binder with fly ash while keeping the aggregate structure (gradation) constant. The first study by Faheem et al. in 2017 used three types of fly ash, including one off-spec ash. The results showed that using 10% fly by weight of the asphalt binder did not change the compaction effort required to achieve density targets. The laboratory performance testing of the mixtures focused on testing moisture damage resistance, fatigue life, and thermal cracking. The reported results show a significant increase in fatigue life measured as the number of cycles to 50% drop of the complex dynamic modulus. The moisture damage tensile strength ratio (TSR) following the AASHTP T283 procedure indicated no change in the TSR even with the lower asphalt binder content. Mixture thermal cracking tested using the semi-circular bending geometry resulted in a significant fracture energy increase at -18°C [21]. In addition, the ash containing mixes exhibited lower stiffness at this temperature compared to the control mixes (containing 10% more binder). The research team repeated similar work for off-spec ash with warm mix asphalt [22]. The

published results follow the exact same trend. These results suggest that fly ash may interact with the binder as an additive rather than a filler. Few studies evaluated this hypothesis regarding fly ash as an additive. *Bautista et al. (2015)* investigated the rheological performance of asphalt binders with different types of CCWs in terms of correlation with fly ash's chemical and physical properties [23]. *Faheem et al. (2017)* validated that some CCWs can work as enhancers and extenders to the binder. The authors also demonstrated that some CCW products could enhance the mixture of aging resistance, moisture damage resistance, fatigue life, and thermal cracking resistance [21]. In 2017, *Saha et al.* investigated the structure of asphalt blends with fly additives using atomic force microscopy. They reported that the addition of fly ash could increase the area of the micelle structures and correlated the area to the complex modulus of blends [24].

Nevertheless, this research's novelty comes as there is a lack of research evaluating the fly ash-asphalt physio-chemical interaction. This could be influenced by the difficulty of quantifying such interaction or due to the complex nature of the asphalt binders [25]. However, there were decent efforts made by many researchers studying asphalt-filler interactions, but not fly ash-asphalt physio-chemical interaction [26]–[29].

Recently, two studies have been published focusing on the physicochemical interaction of fly ash and asphalt. In a paper published in 2021, Li and Yang evaluated morphological and chemical characteristics of asphalt blended with limestone and fly ash particulates at 50% dosage by mass. The authors clearly indicate that fly ash is not an inert filler.

The authors concluded that the physicochemical interaction of the fly ash and asphalt blends resulted in better aging resistance performance than limestone and asphalt blends [15]. Muhammad et al. conducted a comprehensive study on asphalt mixtures containing fly ash and bone glue. The authors claimed that the fly ash and bone glue modified the asphalt binder. The testing results showed that the fatigue life measured by the four-point-bending beam fatigue test is 89.5% higher when the binder is replaced with 10% bone glue and 6% fly ash. These two recent studies are among the very few research treating fly ash as an additive rather than a filler [14].

Given the above discussion, this phase aims to investigate the interaction between asphalt binders and different CCWs. The main hypothesis is that some of the CCWs act as additives. The following objectives are selected to test this hypothesis:

- Obj 1. Investigate various OFA sources' chemical and physical properties and evaluate their physio-chemical influence on the aging and healing capability of binder and ash blends.
- Obj 2. Quantify change in the chemical composition of the blend of OFA and binder under simulated aging.
- Obj 3. Quantify damage performance of the blend under the viscoelastic regime and elastic regime.
- Obj 4. Highlight the rheological profile of the blends.

This study's objective could establish a new market for some OFAs as upcycled additives.

2.2. Materials and Methods

2.2.1. Materials

Two binders are selected in this study; a neat PG 64-22 binder and a Styrene-Butadiene-Styrene (SBS) Polymer Modified (PMA) binder PG 76-22. Eight types of CCW are mixed with the two types of binders at 10% by weight. This dosage is selected to be following previously published studies [13], [21], [22]. The eight types of fly ash were obtained from eight different electric power plants in six different states. GA, BH, SBH, RH, WE, RO, HT, and CS CCWs are procured from different power plants in Alabama, Georgia, Georgia, Mississippi, Wisconsin, South Carolina, Missouri, and South Carolina. This is intended to reflect the variability in the coal sources used nationwide.

2.2.2. CCW Chemical and Physical Testing

The physical and chemical properties of the CCW are obtained through several tests. The Specific Gravity (SG) was measured with Le Chatelier Flask for Density per ASTM C188-17. The Rigden Voids test was conducted according to the European Standard EN1097-4. Particle Size Distribution (PSD) was determined according to ASTM D4464 using laser light scattering with alcohol solution instead of distilled water to avoid cementation and acquire more precise results. The laser light scattering results were used to calculate the specific Surface Area (SA), D_{10} , D_{50} , and D_{90} Parameters. The D_{10} , D_{50} , and D_{90} can be defined as follows: D_{90} means the percentage of particles finer than this size is 90%. D_{10} means the percentage of particles finer than this size is 10%. D_{50} means the portion of particles with diameters smaller and larger than this value is 50%, also known as the median

diameter. The chemical elemental analysis was obtained using X-Ray Fluorescence (XRF) following ASTM D6247- 18. In addition, the shape of the particle of fly ash was investigated using Scanning Electron Microscope (SEM).

2.2.3. Laboratory Testing Methods to Evaluate Binder Blends

To evaluate an additive to the asphalt binder, it is necessary to quantify the change in the binder's fundamental behavior. To evaluate the claim that the CCW is acting as an additive, it is necessary to investigate the changes in the rheology of the asphalt binder to distinguish between the influence of inert particulate inclusion (filler) or an additive that contribute to the overall performance of the binder matrix. Laboratory methods reported for evaluating binder additives are numerous. For this paper, this section will focus only on the following methods:

- 1- Chemical analysis using Fourier Transform Infrared Spectroscopy (FTIR)
- 2- Full performance grading PG testing is conducted per AASHTO M320
- 3- Rheological analysis of time and temperature dependency using master curves using the dynamic shear rheometer (DSR)
- 4- Damage analysis and healing using the DSR.

2.2.3.1. Chemical Analysis using FTIR

This method relies on passing a beam of infrared radiation through a sample, and a spectrometer analyzes the transmitted radiation. The spectrum of transmitted radiation, either in terms of transmittance or absorbance, shows absorbed radiations at specific

wavelengths. This absorbed radiation at a particular wavelength corresponds to the absorbance due to vibration or rotation of a particular chemical bond when the frequency of vibration (or rotation) of the bond matches that of infrared radiation. Traditionally, the functional groups of carbonyl (C=O) and sulfoxides (S=O) are used to evaluate the asphalt binder and monitor its changes through different levels of oxidative aging. Many studies discussed using this method to evaluate chemical changes in the binder in the presence of additives [30]–[35]. A detailed method for quantifying the carbonyl index (ICO) and the sulfoxide index (ISO) is reported by *Grenfell et al. (2009)* [36]. The authors proposed the following equations to calculate both indices:

$$\textit{The Carbonyl Index (ICO)} = \frac{\textit{Area around } 1700 \textit{ cm}^{-1}}{\textit{Area around } 1460 \textit{ cm}^{-1} + \textit{Area around } 1375 \textit{ cm}^{-1}} \quad \textit{Equation 2-1}$$

$$\textit{The Sulfoxide Index (ISO)} = \frac{\textit{Area around } 1030 \textit{ cm}^{-1}}{\textit{Area around } 1460 \textit{ cm}^{-1} + \textit{Area around } 1375 \textit{ cm}^{-1}} \quad \textit{Equation 2-2}$$

The numerator in previous equations corresponds to the peak area due to the stretching of ketonic bonds. The denominator in the Equation corresponds to the bending of C–H bonds in the spectrum of the binder sample. The relative area in a particular spectrum is considered instead of the height or magnitude of the peaks. The areas around the peaks of interest are calculated by constructing a baseline from valley to valley, as shown in Figure 2-1.

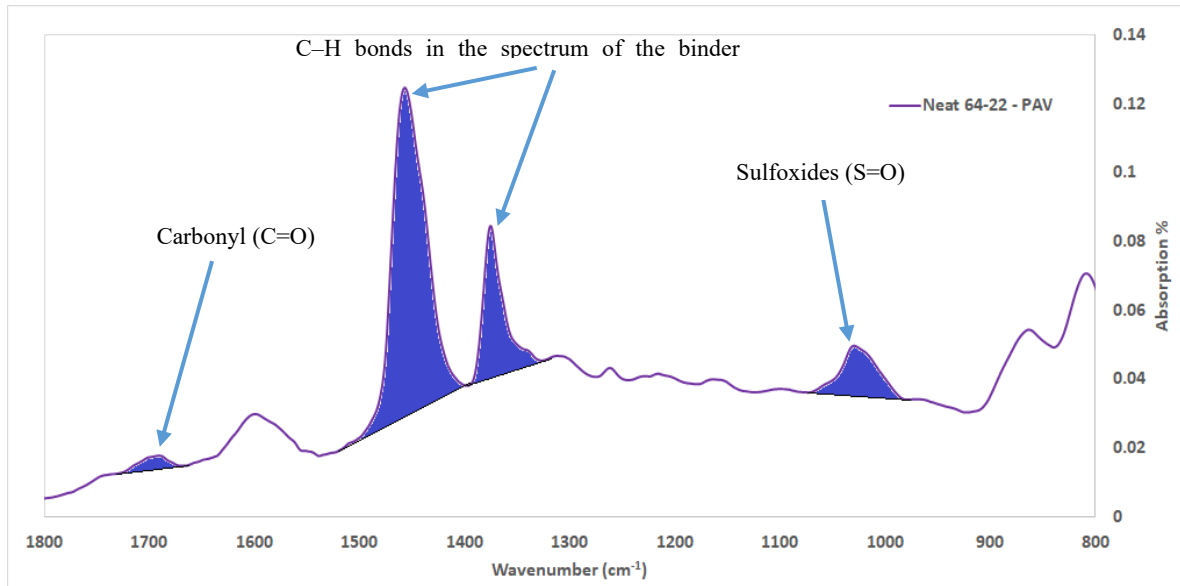


Figure 2-1. Illustration of Determination of Peak Areas for the Unmodified Binder after PAV Aging

2.2.3.2. Rheological Time and Temperature Dependency

The master curves for the complex modulus (G^*) and phase angle (δ) are constructed using DSR frequency sweep testing. For PG 64-22 binder/blends, testing is conducted at different temperature levels; 10°C, 22°C, 34°C, 46°C, 58°C, 64°C, and 70°C covering a frequency range from 100 to 0.1 rad/s at each temperature. For PMA 76-22 binder/blends, the test was held at 10°C, 22°C, 34°C, 46°C, 58°C, 70°C, and 76°C covering the same range of frequencies. The amplitude strain was set to 0.1% for both intermediate and high temperatures (10-34°C, 46-76°C) respectively to achieve linear viscoelastic range behaviors for the blends/binder tested. Two samples of each blend/binder are tested, achieving a Coefficient of Variation (COV) not exceeding 10%. The constructed master curves are then used to compare the different blends and calculate the crossover modulus G_c^* .

2.2.3.3. *Damage Behavior*

Studying the damage behavior of asphalt binders has received the attention of many researchers. Given the viscoelastic nature of the asphalt, it is necessary to study damage under different schemes. This study will focus on damage and healing of the binder at a temperature range where the binder is behaving as a viscoelastic polymer (viscous and elastic components are equal).

2.2.3.3.a. *Damage Healing Characterization*

Xie et al. (2017) developed a new procedure based on a Linear (strain) Amplitude Sweep (LAS) test to quantify healing performance, as explained in Figure 2-2 [37]. This protocol is a four steps procedure. First, a continuous LAS test is conducted at the intermediate temperature - determined as the intermediate temperature of the performance grade (PG). The first step is conducted to define the strain level where damage starts to occur. Second, a new binder sample is subjected to the LAS loading until it arrives at the specific strain amplitude corresponding to the previously determined damage level. Third, a rest period is applied while maintaining the temperature. Eventually, the LAS loading is resumed from the strain amplitude applied prior to the rest period. As demonstrated in Figure 2-2-c, the percent healing (%Hs) can be quantified from the change in the accumulated damage growths through Equation (2-3), where S1 and S2 are damage intensities before and after applying the rest period, respectively.

Wang et al. (2015) developed a new approach to analyzing the data through simplified viscoelastic continuum damage (S-VECD). As described in Figure 2-2-a and b, the new

failure criterion analysis is based on Pseudo-Strain Energy (PSE). Wang et al. (2015) proved that trends in stored PSE effectively define the failure for the LAS tests of asphalt binders. Moreover, the new proposed failure definition is material-dependent, which makes it effective in capturing the change in binder behavior after the introduction of an additive [38].

$$\%H_s = \frac{S_1 - S_2}{S_1}$$

Equation 2-3

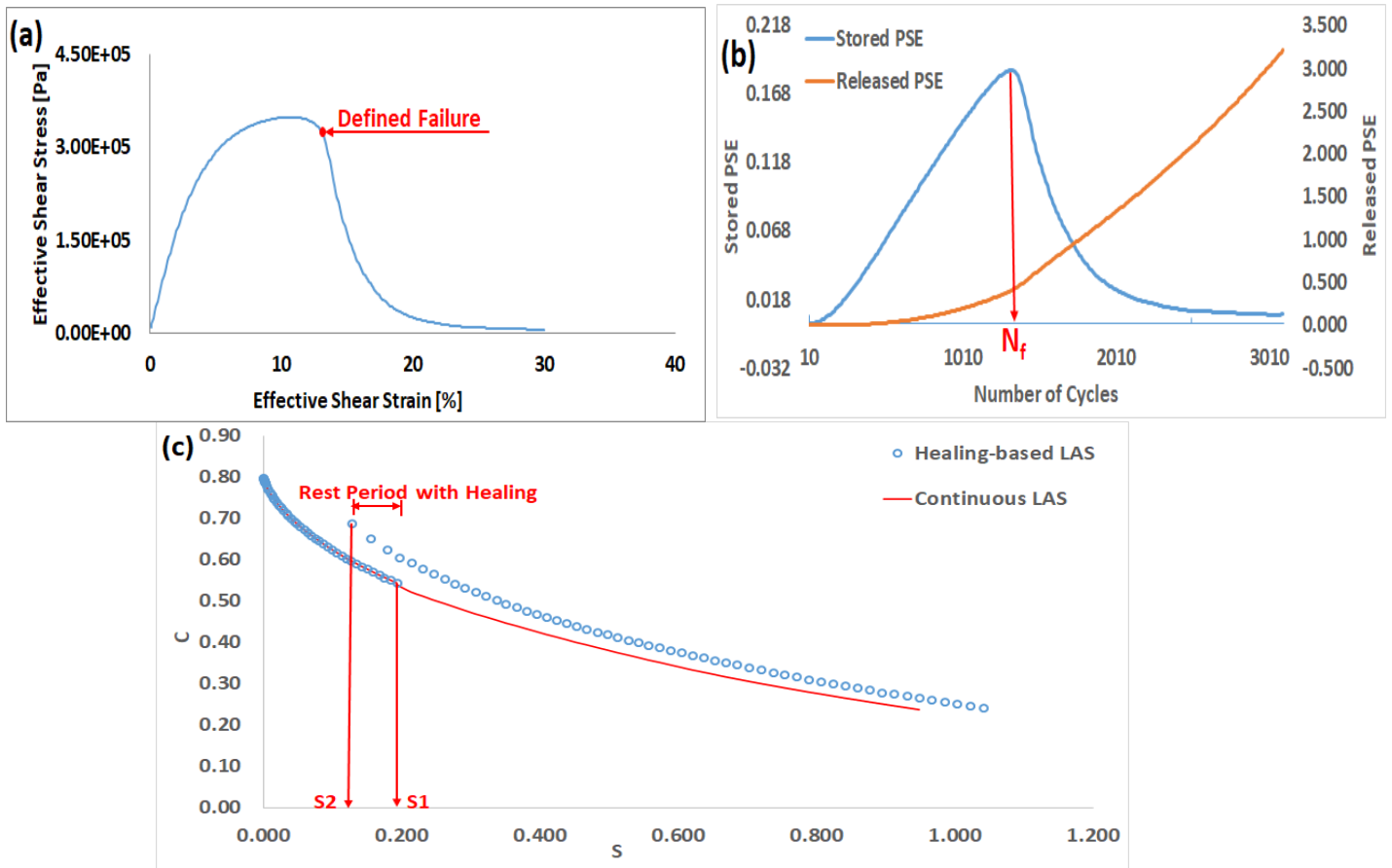


Figure 2-2. Fatigue Failure in LAS Tests for the Unmodified Asphalt Binder: (a) Stress-Strain Curve, (b) PSE-Based Failure (After Wang et al., 2015 [46]), (c) Schematic Illustration for %Healing Calculation (After Xie et al., 2017 [45])

2.2.3.4. Low-Temperature Cracking Susceptibility using Bending Beam Rheometer (BBR)

This test follows the creep loading of an asphalt beam at a low temperature. This test is used to quantify the stiffness (S) of the binder under sustained loading as well as the rate of increase in stiffness (m). For practical reasons, the load is sustained for 60 seconds to record S(60s) and m(60s) as the parameters used to evaluate and compare binders' performances. The standard practice sets an acceptable level of S is less than 300MPa and for m-value is greater than 0.3. Anderson et al. (2011) introduced the ΔT_c parameter, the numerical difference between the critical low temperature corresponds to stiffness, S at 300 MPa, and critical temperature corresponds to the m-value of 0.300 [39]. In other words, ΔT_c is a numerical index value for gauging the binder's ability to compensate the increase in stiffness with relaxation. Some studies have suggested acceptable values for this parameter, a crack warning value of -2.5°C was suggested by Anderson et al., and a cracking limit value of -5°C was suggested by Rowe when an identifiable risk of cracking for the binder occurs [39], [40].

2.3. Experimental Design

To achieve the objectives, an experimental design is illustrated in Figure 2-3. Experimental tasks addressing the four objectives of the study are labeled accordingly. All asphalt blends are conditioned with rolling thin film oven (RTFO), then pressure aging vessel (PAV) for 20 hours to induce oxidative aging.

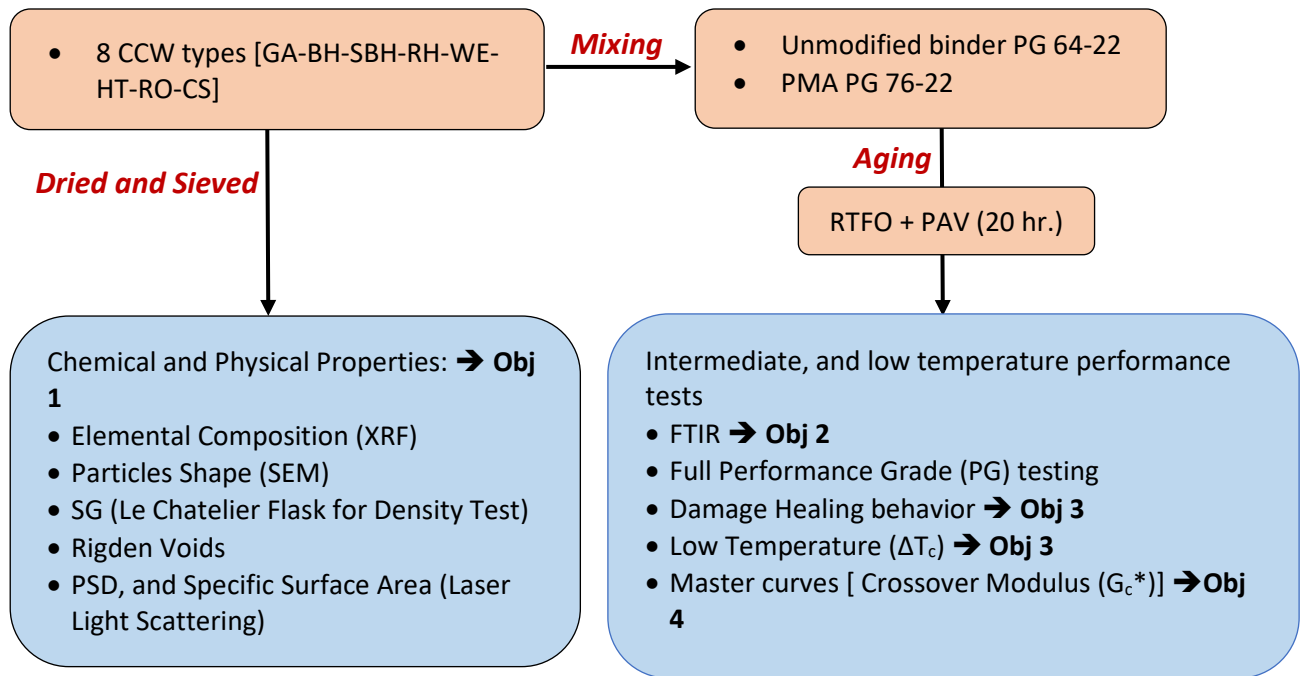


Figure 2-3. Experimental Program

2.3.1. Fabrication of Blends

The process of blending starts with heating the PG-64-22 binder to $135\pm 5^{\circ}\text{C}$, and the polymer-modified PG 76-22 binder to $155\pm 5^{\circ}\text{C}$. CCWs are heated to the same temperatures as binders before blending. The CCW sample is loaded incrementally to the binder and dispersed using a high shear mixer. The blending process is completed in 30 minutes. This process yielded 16 blends; 8 CCW blended with two binders. It is important to mention that the un-blended control samples are exposed to the same protocol to avoid fabrication/conditioning bias.

2.4. Testing Results and Discussion

In this section, the results are presented in three parts. The first part discusses the chemical and physical characterization of CCW. Further, the second section discusses the blend's performance. Finally, the second part is coupled with regression analysis to identify the statistically significant parameters influencing the reported results.

2.4.1. Chemical and Physical Characterization of Fly Ash

2.4.1.1. CCW Chemical Composition

As shown in Table 2-1, the ASTM C618-19 determines the limits for classifying the different types of fly ash.

Table 2-1. Chemical Requirements (ASTM C618-19)

	Class		
	N	F	C
Silicon dioxide (SiO ₂) + aluminum oxide (Al ₂ O ₃) + iron oxide (Fe ₂ O ₃) [SAF], min, %	70.0	50.0	50.0
Calcium oxide (CaO), %	Report Only	18.0 max	>18.0
Sulfur trioxide (SO ₃), max, %	4.0	5.0	5.0
Loss on ignition, max, %	10.0	6.0	6.0

The results from the XRF test are reported in Table 2-2. Comparing the composition of the CCW samples tested to Table-1 for classification results in identifying GA and RO as Class F fly ash. The remaining is classified as OFA.

Table 2-2. Chemical Elemental Composition and LOI of the Investigated Fly Ashes

CCW	SiO₂, %	Al₂O₃, %	Fe₂O₃ %	SAF	CaO, %	SO₃, %	LOI, %	Class Interpretation
GA	52.02	22.42	15.54	89.97	3.00	0.82	0.93	F
BH	6.61	3.22	2.39	12.22	52.74	16.82	8.92	OFA
SBH	23.15	16.01	4.93	44.09	26.16	7.01	13.24	OFA
RH	41.77	17.40	3.69	62.86	22.41	6.48	1.77	OFA
WE	31.77	15.55	4.88	52.20	27.59	10.24	1.55	OFA
RO	57.57	25.63	10.49	93.68	0.90	0.08	3.87	F
HT	25.71	13.99	4.50	44.20	34.32	11.13	5.68	OFA
CS	39.04	21.84	3.04	63.92	16.94	13.24	3.52	OFA
Average	34.70	17.01	6.18	57.89	23.01	8.23	4.94	

OFA= Off-spec Fly Ash

2.4.1.2. Particle Shape and Size Distribution of Fly Ash

Scanning electron microscope (SEM) images are presented in Figure 2-4. Standard classes of fly ash (Class C and Class F) are typically characterized by their spherical shapes, as shown in Figures 2-4-c and 2-4-f. All the OFA contain a mix of spherical and irregular shapes. The differences in the coal-burning processes can be the main reason for the variation in the fly ash shape [41]. In addition, per the supplying utilities, some of the OFAs are residual material created from the combination of fly ash and the reagent lime from the scrubber unit used to absorb acidic exhaust gases. Samples belonging to this class are demonstrated in Figures 2-4-d and 2-4-g. These materials are referred to as spray dryer absorber (SDA).

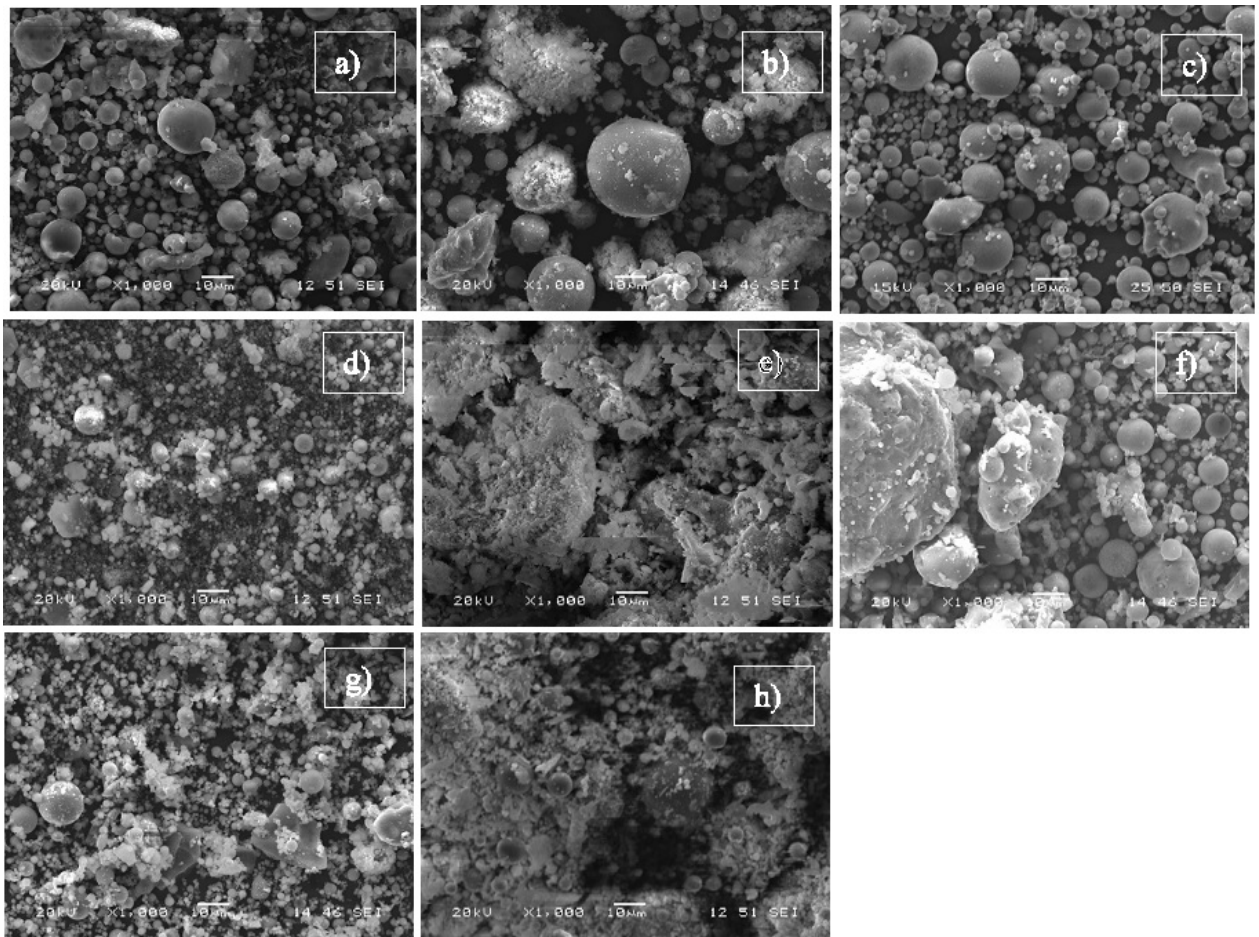


Figure 2-4. SEM of Samples at 1000x Magnification: (a) BH (b) CS (c) GA (d) HT (e) RH (f) RO (g) SBH (h) WE

Table 2-3 demonstrates the D_{10} , D_{50} , and D_{90} as estimated from the particle size distribution data. This information is obtained based on conducting laser diffraction (ASTM D4464-10) on the samples. A group of CCWs (SBH, GA, WE, and HT) is characterized by the presence of very fine particles. This is demonstrated by the size of D_{10} falling within the 0.94-1.02 μm size range.

The specific surface area (SA) obtained from the same test is considered surrogate to the particulates' binder adsorbing capacity. Generally, the SA of powder particles varies

inversely with the particle size; the larger the surface area, the finer the particle distribution, and the greater the particle adsorbing capacity. Table 2-3 shows the specific surface area. It is noticed that the SA of BH, RH, RO, and CS fly ash are below the average, indicating that they are on the coarser side. As expected, finer CCW (GA, SBH, and HT) exhibit higher SA values.

Table 2-3. Physical Properties of Fly Ash

Coding Name	Fly ash class	Specific gravity (g/cm³)	Rigden Voids %	D₁₀ (μm)	D₅₀ (μm)	D₉₀ (μm)	Specific Surface area (cm²/g)	D₉₀-D₁₀ D₅₀
GA	F	2.47	28.89%	1.00	11.70	64.40	28,179	5.42
BH	Off-spec	2.40	56.85%	1.30	6.75	220.95	18,339	32.54
SBH	Off-spec	2.39	42.37%	0.90	12.00	106.90	29,405	8.83
RH	Off-spec	2.58	56.76%	2.50	26.10	95.65	13,568	3.57
WE	Off-spec	2.64	34.25%	1.00	23.30	113.00	24,293	4.81
RO	F	2.30	38.15%	2.53	28.65	103.85	15,042	3.54
HT	Off-spec	2.59	42.20%	1.00	6.95	133.80	26,959	19.11
CS	Off-spec	2.25	48.20%	3.40	31.20	63.50	13,677	1.93
Average	————	2.45	43.46%	1.71	18.32	112.75	21,183	9.97

2.4.1.3. Fractional Voids (Rigden Voids)

The capacity of the particulates to hold asphalt binder can be estimated using the voids entrapped in a compacted sample of filler. The void content is estimated by compacting dry fillers in a mold using a specified compaction effort. The concept is similar to the Fine Aggregate Angularity test utilized in the Superpave system to measure the angularity of fine aggregates (AASHTO 304) but includes a standard compaction device to pack the filler. Rigden introduced the measurement of fractional voids in 1947. Hence, most researchers refer to the fractional voids test as the “Rigden Voids” test [42], [43].

Rigden considered the asphalt required to fill the voids in the dry compacted sample as fixed asphalt, while excess asphalt is considered free asphalt. Rigden postulated that the percent free asphalt is the main factor defining the consistency of filled systems and reported that changes in viscosity are independent of asphalt characteristics or any particulate characteristics other than the fractional voids. Based on these findings, it was concluded that the chemical differences between various particulates are of less significance. Figure 5 illustrates the concept proposed by Rigden.

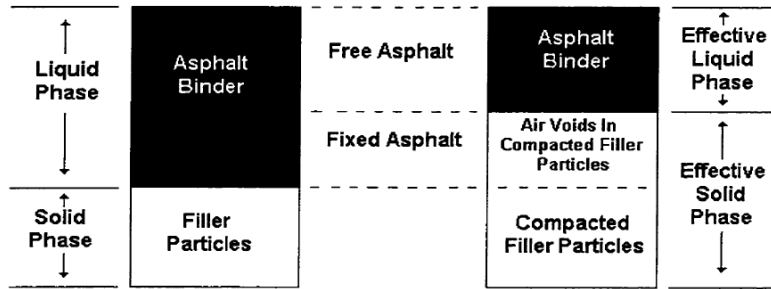


Figure 2-5. A Schematic Showing the Concept of Fixed Asphalt and Free Asphalt [44]

The results of the Rigden Voids test reported in Table 2-3 show a wide range of values. The maximum value is associated with BH at 56.85%, which also possesses the coarsest particles. The minimum value is associated with GA at 28.89%. It is also among the finest of the CCWs studied. Based on Rigden's stipulation, these two CCWs should be the most and least influential, respectively, when blended with the binders.

The following sections discuss whether the CCW included in this study follows Rigden's postulation. The CCW will act as fillers if their effect on the binder is directly correlated to their physical properties and inclusion load. The literature studies discussed in the introduction of this suggest that some classes of CCWs deviate from acting as fillers. This study will add to this knowledge body and demonstrate the rheological changes in the blended system due to the presence of the CCWs. To achieve this goal, the selected CCW selected for testing are showing a wide range of compositional and physical properties to such that the changes in the properties of the system can be studied and correlated to the CCW characteristics.

2.4.2. Asphalt Blends Performance

2.4.2.1. Superpave Performance Grading Results

In Table 2-4, the continuous Performance Grade (PG) is presented. The high PG (PGH) is determined using the Superpave parameter of $G^*/\sin\delta$. The low PG (PGL) is determined using the BBR Superpave stiffness (S) and relaxation (m) parameters. The PGH represents the maximum summer temperature the blend can be employed. Similarly, the PGL is related to the lowest winter temperature before failure occurs in the binder. Finally, intermediate PG (PGI) is measured using the DSR where it corresponds to the temperature at which $G^* \cdot \sin\delta$ is equal to 5000kPa. The lower PGI is commonly interpreted as higher fatigue resistance since it is indicative of the ability of the system to maintain flexibility under repeated loading.

Table 2-4. Continuous Performance Grade for Unmodified and PMA Blends.

Continuous PG	Unmodified binder PG 64-22			PM binder PG 76-22		
	PGH	PGL	PGI	PGH	PGL	PGI
Control Binder	67.40	$\frac{S -26.70}{m -25.66}$	22.95	79.40	$\frac{S -25.63}{m -24.90}$	23.70
GA	68.80	$\frac{S -24.89}{m -25.44}$	23.70	80.95	$\frac{S -24.96}{m -25.45}$	22.45
BH	70.00	$\frac{S -24.40}{m -24.36}$	24.00	83.00	$\frac{S -22.90}{m -23.08}$	25.70
SBH	69.00	$\frac{S -23.56}{m -25.72}$	23.65	81.85	$\frac{S -24.28}{m -25.10}$	24.25
RH	68.90	$\frac{S -23.89}{m -26.34}$	23.15	81.75	$\frac{S -24.20}{m -22.85}$	25.40
WE	68.20	$\frac{S -24.51}{m -26.49}$	23.00	81.10	$\frac{S -24.53}{m -24.88}$	24.85
RO	69.00	$\frac{S -24.61}{m -25.43}$	23.20	81.80	$\frac{S -25.43}{m -25.01}$	24.80
HT	69.30	$\frac{S -24.26}{m -24.95}$	24.10	81.70	$\frac{S -24.05}{m -24.96}$	25.25
CS	69.40	$\frac{S -23.86}{m -24.50}$	25.05	82.65	$\frac{S -24.45}{m -24.57}$	23.80

Following the influence of the CCW on each binder, for the PG64-22 binder, the true high grade deviated from the control binder by at most +2.6°C with BH blend. This deviation changed the high standard grade to PG70. The rest of the blends show a minimal increase in the high grade not exceeding +2°C. For the PGI, all the blends increased in value. The blend with CS shows the most increase of 2.10°C. The remainder of the blends shows a less stiffening effect, with a maximum increase of 1.15°C for the blend with HT. The least increase is the blend with WE, which shows a minimal increase of 0.05°C. For PGL, the

critical temperature associated with the stiffness increased for all blends. The maximum increase is associated with SBH, where the critical temperature increased from -26.70°C for the control blend to -23.56°C for the blend with SBH. Interestingly, the associated for the critical temperature relaxation index (m-value) showed a decrease from -25.66°C to -25.72°C . This is a minor difference; however, it indicates that while the blend increased in low-temperature stiffness, it did not lose its ability to relax thermal stresses. Therefore, given that both the control and the SBH blend are graded as PG64-22, the SBH blend is expected to show superior resistance to cracking given its higher m-value.

The same trend is observed for the PMA PG76-22 for the true high grade. The maximum increase in the PGH is associated with the BH blend at $+3.6^{\circ}\text{C}$. This increase changes the standard grade to PG82. The other blend that changed grade is the blend with CS, where the PGH changed by 3.25°C . The remainder of the blends maintained the same grade. For PHI, the maximum increase is observed with the BH, RH, and HT blends. Interestingly, most of the remaining blends are hovering around the control value within a range of 1.00°C . In fact, the blend with GA shows a PGI of -1.25°C less than the control. For the PGL, all the blends show a minimal increase in the critical temperature associated with the stiffness. On the other hand, a group of blends (GA, SBH, WE, and HT) shows improvement in the thermal relaxation index (m-value).

It is important to note that the maximum increase in the PGH for both binders is associated with the BH blend. The BH CCW possesses the highest value of the Rigden voids at 56.9%. Therefore, this is aligned with the postulation of Rigden and other researchers. However,

the stiffness measures at the intermediate and low temperatures show different trends. A CCW with a similar Rigden voids value is RH at 56.8%. The blend with this CCW is associated with a much lower increase in stiffness as measured by the PGH and PGI, comparable to values similar to other CCWs with lower Rigden voids values. For example, the PGH for RH with the PG64 binder is 68.9°C, and the PGH for GA is 68.8°C. Noting that the GA has the lowest Rigden voids value at 28.9% contradicts Rigden's postulation. Furthermore, the blend with the RH improved is associated with an improved low-temperature relaxation at low temperature for the same binder. In contrast, GA is associated with a small reduction in relaxation. This could mean that BH acts as a filler while the RH interacts with the binder and enhances its performance.

2.4.2.2. Analysis of Infrared Spectroscopy (FTIR)

Carbonyl and Sulfoxide Indices are shown in Figures 2-6 and 7, respectively. The data shown are the average of four specimens. The spectral peaks of interest for the sulfoxide peak were 1030 cm^{-1} and the carbonyl peak at 1700 cm^{-1} . To analyze the carbonyl and sulfoxide groups with the presence of fly ash, these spectra are normalized using a reference of bending of C–H bonds in the spectrum of the binder sample. The higher the carbonyl and sulfoxide indices, the higher the level of oxidative aging. As shown in Figure-6, the presence of fly ash with the unmodified binder is associated with reduced levels of ICO by a range of -54%, with RH fly ash, to -17% with CS fly ash. For the PMA blends, the presence of the CCWs, except with RO and RH, is associated with reduced ICO by a range varying from -36% with HT fly ash to -23% with SBH. The two CCWs not associated

with a reduction in the ICO for the PMA are associated with a small increase. RO is associated with a +9.16% increase in the ICO, while RH is associated with an increase of +4.58% only.

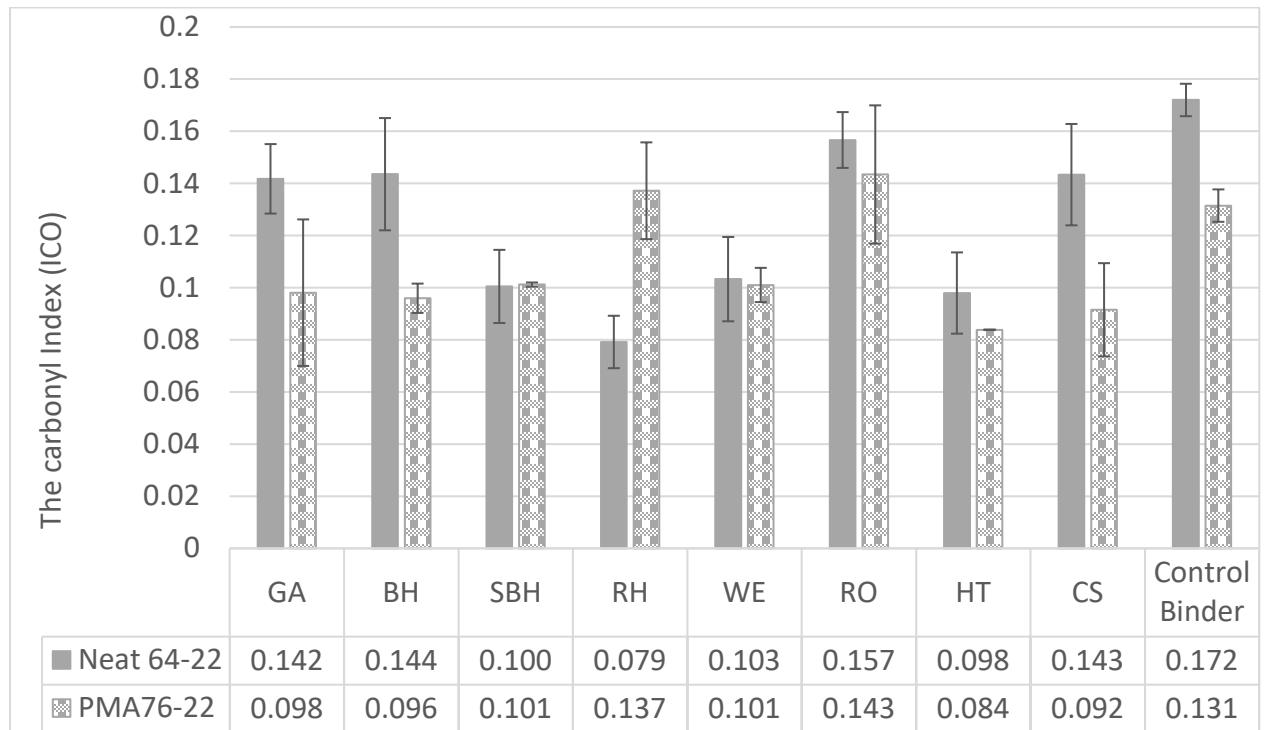


Figure 2-6. The Carbonyl Index (ICO) of the Investigated Blends/Binders

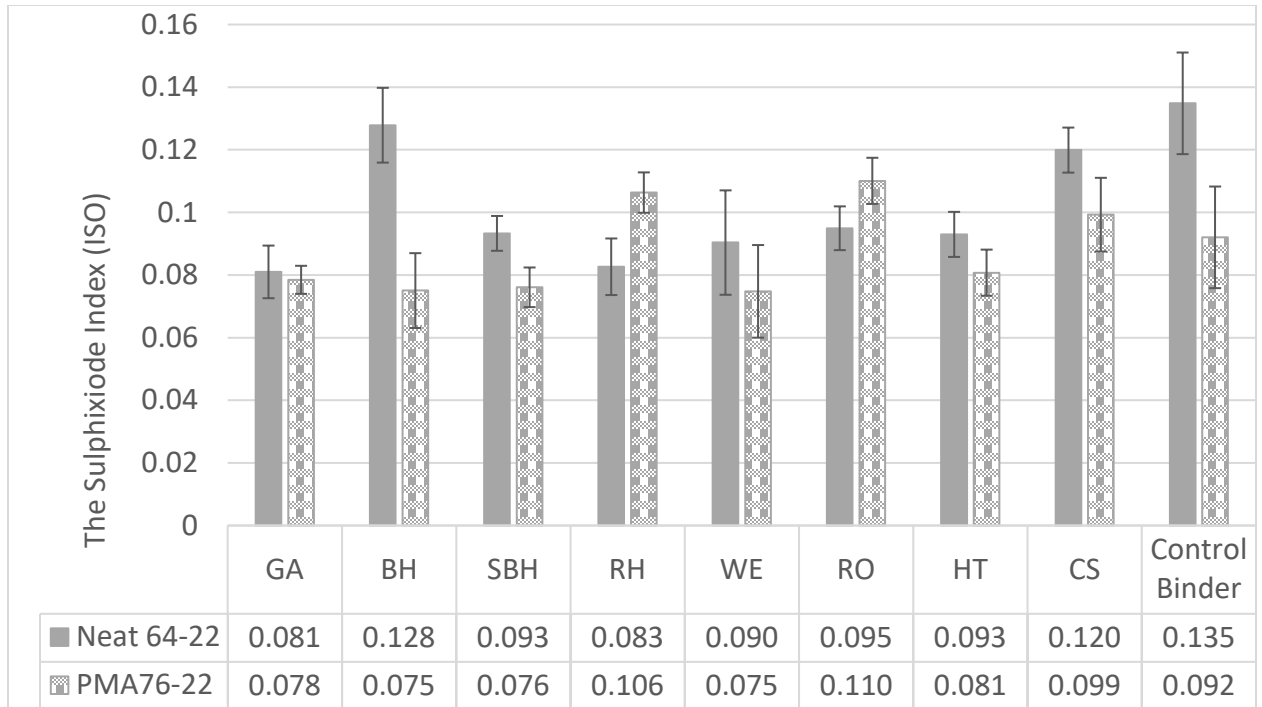


Figure 2-7. The Sulfoxide Index (ISO) of the Investigated Blends/Binders

The sulfoxide index (ISO) data demonstrated in Figure 2-7 shows the same trend. For the unmodified binder, all CCWs are associated with a reduction in the ISO by a range of -40%, with GA, to -5% with BH. For the PMA blends, the presence of fly ash, except with RO, RH, and CS, also reduced the oxidative aging index by a range that varies from -19% with WE fly ash to -12% with HT fly ash. The increase in the ISO associated with RO, RH, and CS is 19.57%, 15.22%, and 7.61%, respectively. As can be noted, both RO and RH negatively affect the aging indices of the polymer-modified binder. This may suggest that the inclusion of these particulates in a system already loaded with polymer causes some negative interaction. These results are not conclusive at this stage, but the only common property for these CCW is that they possess the smallest specific surface area and the

tightest size range as measured by particle size distribution. Further testing will focus on these CCWs to evaluate if particle size distribution plays a role in the blend performance.

2.4.2.3. *Damage Healing Evaluation*

Figure 2-8 demonstrates the results of the healing test for both binders. For the unmodified binder blends, the addition of all the CCWs is associated with an increase in the healing capability, except for GA. BH, RO, and CS are associated with the highest level of healing of about 20% more than the control binder. All the other blends are associated with more than a 10% increase in healing.

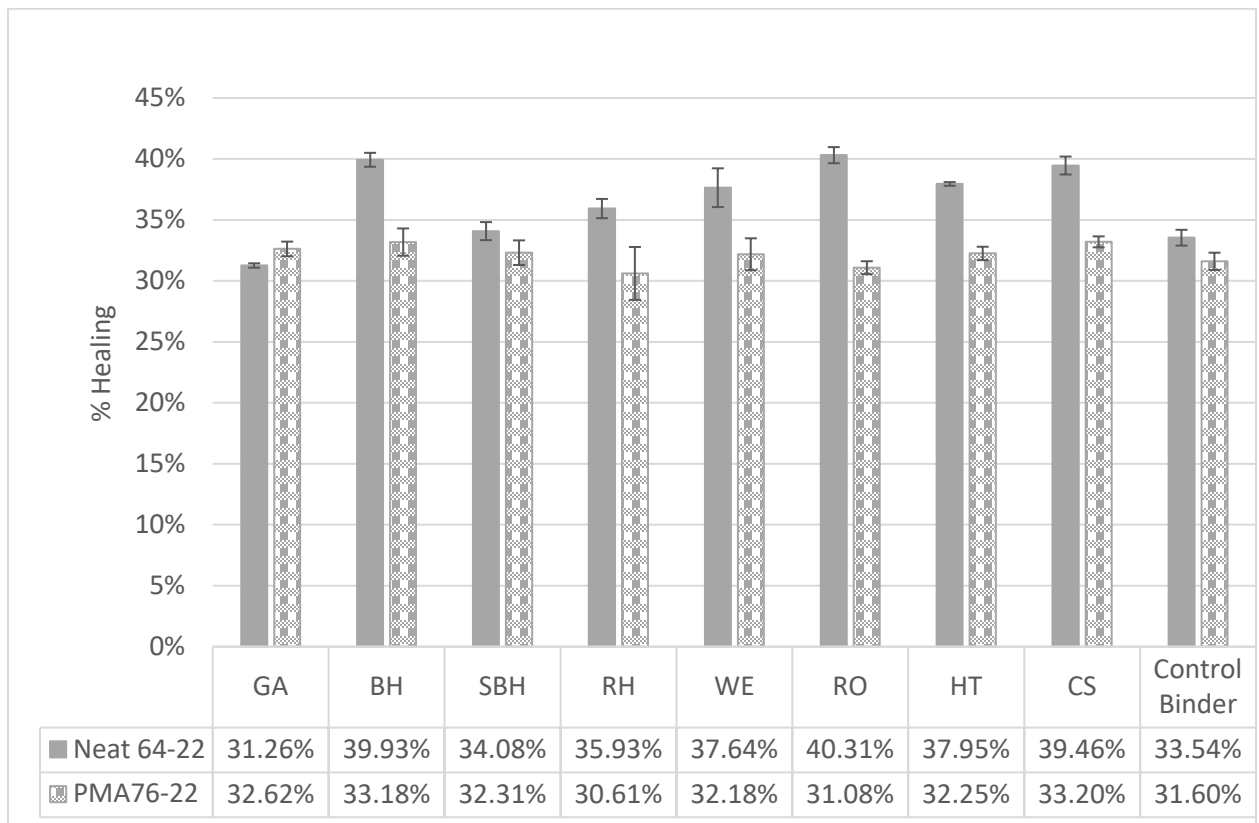


Figure 2-8. Healing Performance of the Investigated Blends/Binders

For the PMA blends, the damage healing results show minimal change compared to the control binder. That is expected as some polymer-modified binders tend to show a higher degree of stiffening due to aging. SBS modified binder is found to be prone to molecular breakdown due to oxidation, which leads to significant loss of the elastic recovery response [45], [46]. Therefore, the healing capacity may be affected by the polymer.

The difference in response between the two binders indicates that the binder and the added CCW dominate the damage healing mechanism. It also illustrates that the interaction of the CCW and the polymer may be a critical factor. To quantify the interaction, regression analysis is used to identify statistically influential parameters.

2.4.2.3.a. Fly Ash Physio-chemical Influence on Asphalt Binder's Healing Performance

Given the results presented in Figure 2-8, it is expected that the regression analysis will reveal both binder and CCW properties as the significant factors influencing healing. The details of the regression model are shown in Table 2-5. As expected, the formulation of the model relies on the phase angle of the binder/blend after aging as the most significant independent variable, as demonstrated by the p-value. The model also reveals that $SO_3\%$, specific gravity of the CCW are significant parameters influencing the damage healing.

Table 2-5. Results of the Healing performance regression multivariate analysis

Term	Estimate	Std Error	t Ratio	Prob> t
Intercept	-0.6051	0.2327	-2.6000	0.0232
SO ₃ , %	0.0029	0.0009	3.0738	0.0096
Specific Gravity (g/cm ³)	-0.0968	0.0394	-2.456	0.0303
Phase angle (δ) at intermediate temperature (°)	0.0240	0.0048	4.9401	0.0003

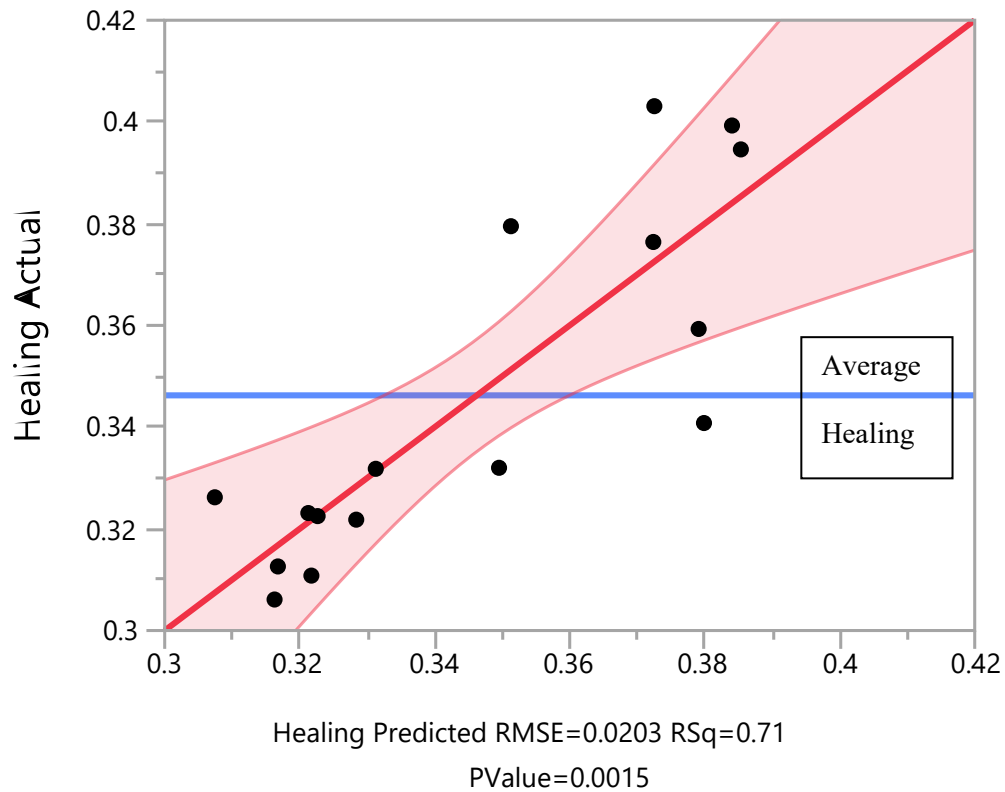


Figure 2-9. Comparison of measured damage healing performance against predicted values
As seen in Figure 2-9, the regression model values are in solid agreement with the measured values. Examining the regression parameters, the coefficients of the independent variables

follow expected trends and follow fundamental materials principles. It is essential to comment on having the phase angle of the blend as part of the model. In typical particulate viscoelastic composites, the particulates' presence is associated with an increase in stiffness and reduction in phase angle. This is due to the differential flow of the matrix and the particulates in the blends. However, the phase angle is a good measure of synergy when the particulates contribute to the flow. Therefore, the inclusion of such parameters in the model serves as a strong indication of the ability of the particulate additive to contribute to the overall blend performance. As for sulfur, it has been reported in many studies that it has softening effect on asphalt and increases durability [47]–[52]. Accordingly, showing up in the regression model as a significant parameter conforms with the reports from other researchers. The statistical results confirm the stipulation that the CCW influences the blend as an additive, not as a filler.

2.4.2.4. *Crossover Modulus (G_c^*)*

The crossover modulus is a valid rheological parameter to quantify the change in the material. Crossover modulus is defined as the complex shear modulus when the phase angle equals 45° , where the storage modulus equals the loss modulus. It has been used as means to evaluate the influence of additives on binders' aging behavior. The crossover modulus is inversely related to aging [53]. In this study, the crossover modulus (G_c^*) was determined from the master curves of complex shear modulus and phase angle through frequency sweep tests. The reference temperature was chosen as 15°C in this study. Two

samples of each blend/binder were tested in the DSR frequency sweep test achieving a Coefficient of Variation (CoV) not exceeding 10%.

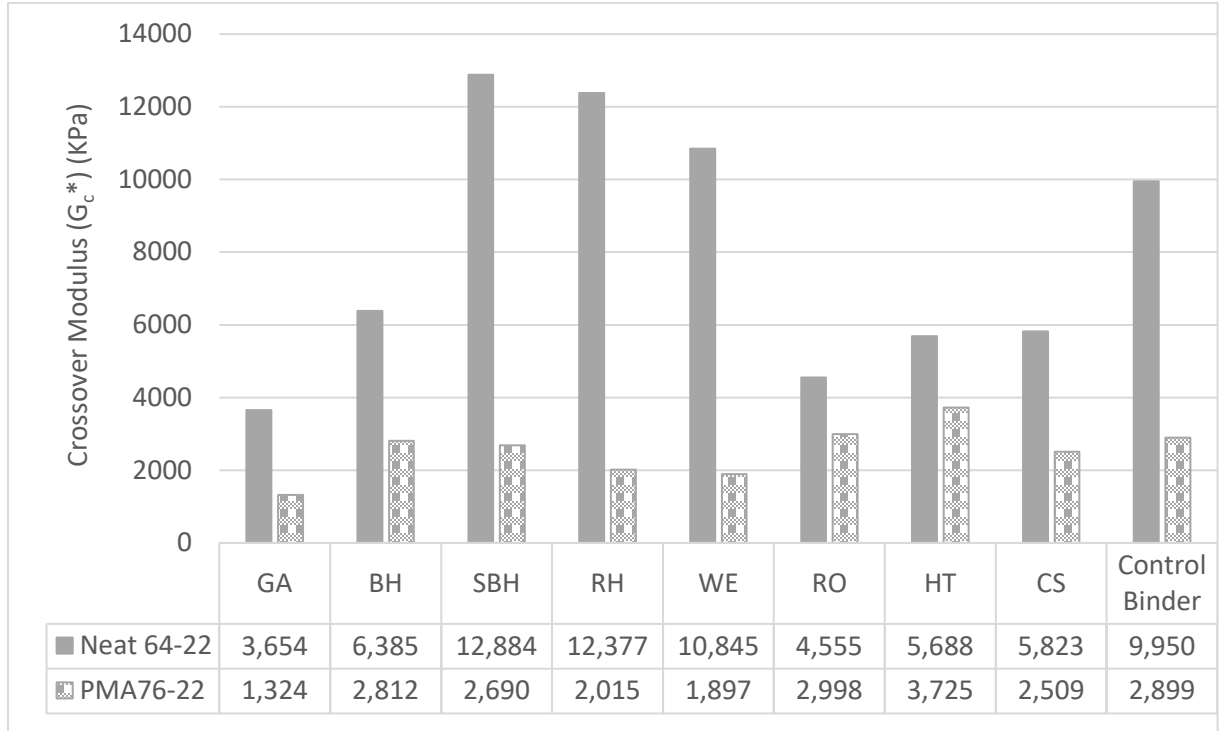


Figure 2-10. Crossover modulus (G_c^*) of the investigated blends/binders

Figure 2-10 shows the crossover modulus of the investigated blends/binders. For blends based on the unmodified binder, the addition of SBH, RH, WE are associated with an increase in G_c^* of 29%, 24%, and 9%, respectively. On the other hand, the remaining CCWs are associated with a reduction in the G_c^* . For the PMA's blends, only HT and RO show improvement. The G_c^* increased by 28% and 3%, respectively. Examining both healing and G_c^* , HT is associated with improved performance, and it is among the finest ash used as determined by its specific surface area. Regression analysis is used to highlight the statistically significant parameters influencing the observed results.

2.4.2.4.a Fly Ash Physio-chemical Influence on Asphalt Binder's Aging Indicator (G_c^*)

The regression analysis reveals a high correlation between $SiO_2\%$ and the blend measured Phase angle after one cycle of PAV at intermediate temperature. The regression results are shown in the following Table 2-6.

Table 2-6. Results of the crossover modulus regression multivariate analysis

Term	Estimate	Std Error	t Ratio	Prob> t
Intercept	-133283.1473	20129.9929	-6.6211	<.0001
$SiO_2, \%$	-83.0078	29.94235	-2.7723	0.0158
Phase angle (δ) at intermediate temperature ($^\circ$)	2907.4419	417.6719	6.9611	<.0001

Table 2-6 shows the significance of the two independent variables, silicon (Si) and the phase angle (δ). While the model shows a strong correlation power, as demonstrated by the high R^2 value of 80%, it also conforms with the healing model in showing the phase angle as the most critical parameter for capturing the physio-chemical influence of the CCW. On the other hand, the significant contribution of the Si conforms with reports from the literature. It has been reported by Zhang et al. (2019) and Guo and Tan (2021) to be a significant factor in the interaction between the particulates and asphalt binder [28], [29].

Figure 2-11 compares the asphalt blends' crossover modulus's predicted value for both unmodified and PMA binders against the measured values shown in the following plot. This comparison tests the strength of the fit. It is important to note that the presentation of such a figure illustrates the distribution of the data along with the range of G_c^* . While the correlation coefficient is an essential parameter in measuring the statistical fit, examining

the distribution of the data reveals additional information. The data points are well distributed around the line of equality and around the average value. More importantly, the correlation does not seem to be influenced by a subset of the data points. This confirms that the crossover modulus significantly depends on the parameters in the model. This continues to confirm that some of the CCWs are not acting as fillers, but their interaction with the binder can improve performance as additives.

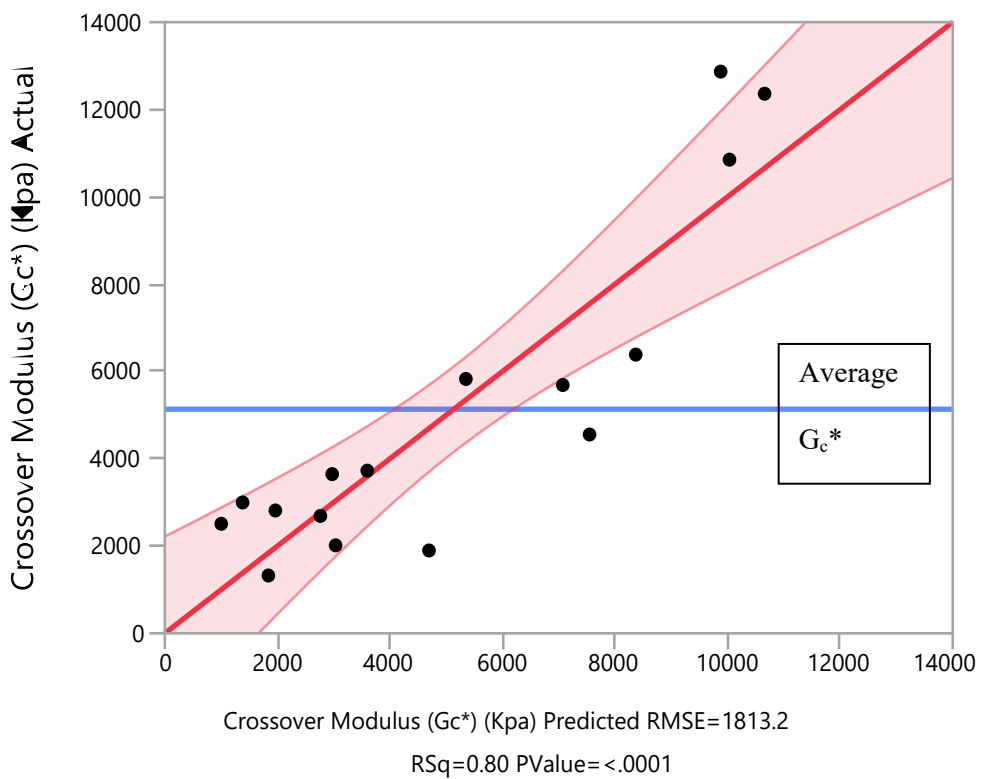


Figure 2-11 Comparison of measured crossover modulus against predicted values

2.4.2.5. Low-Temperature Performance Evaluation

The ΔT_c is used for evaluating cracking potential at low temperatures for aged binders. The lower the value ΔT_c , the lesser the ability of the binder to relax the thermal stresses. In

addition, the higher the level of aging, the lower the value of the ΔT_c . Therefore, this parameter has been used as a measure to evaluate the ability of additives to retain the binder's flexibility under different levels of aging [54]. Figure 2-12 demonstrates the results of this test for both binders. It is worth mentioning that although the CoV is high for the measured ΔT_c , both the critical low temperature corresponds to stiffness, S at 300 MPa, and critical temperature corresponds to the m-value of 0.300 did not exceed CoV 6.0%, which indicates high testing repeatability.

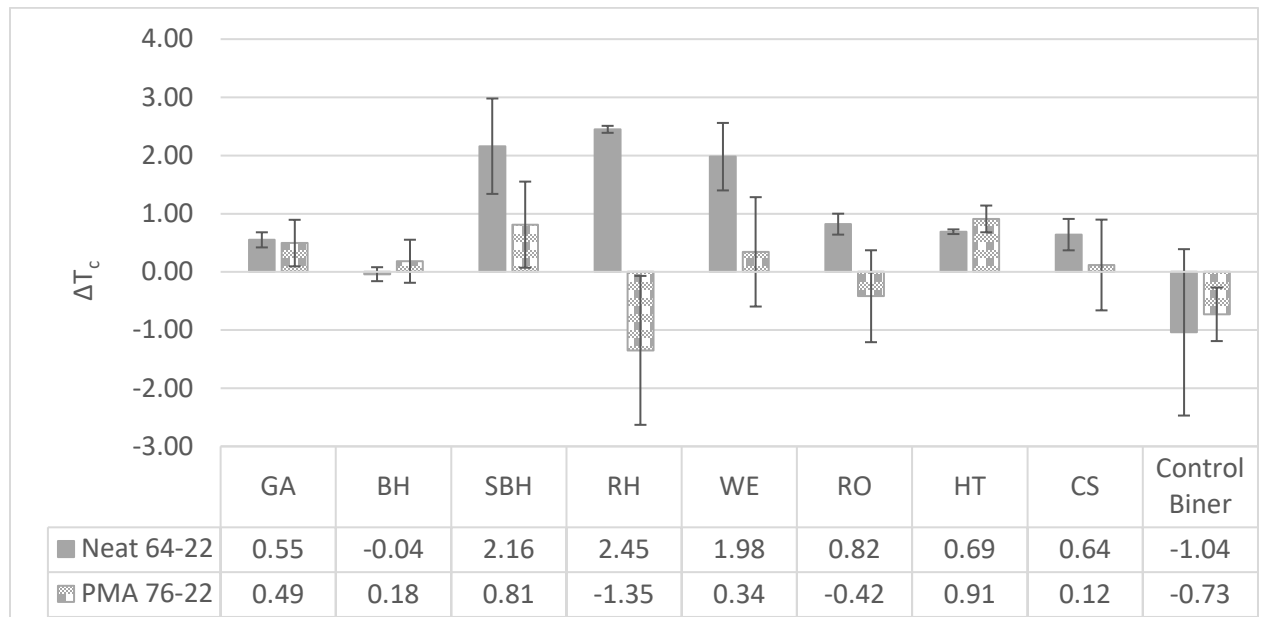


Figure 2-12 Low temperature cracking potential of the investigated Blends/Binders

The results of the ΔT_c parameter continue the trend of mixed results based on the binder type. The most significant increase in the ΔT_c for the unmodified binder is found for RH, followed by the WE. In general, all blends maintained a ΔT_c value close to zero or above, indicating that they maintained their low-temperature thermal stress relaxation even after long-term aging. More importantly, they all show improved results compared to the control

binder. Evaluating the PMA blends, some of the blends show improved ΔT_c after aging by more than 200%. In general, most blends show either preserve the binder ΔT_c or improve it. The only blend that is not associated with improved performance is the one with RH.

The results confirm the trend of previous observations that the interaction between some of the CCWs products and the asphalt binder reduces the detrimental effects of aging, which is believed to preserve the binder's ability to resist potential thermal cracking. Combining the observations from healing and resistance to cracking after aging reveals a very promising trend.

2.4.2.5.a. Fly Ash Physio-chemical Influence on Asphalt Binder's Low-Temperature Performance (ΔT_c)

For ΔT_c , the regression analysis reveals that it is highly correlated to D_{10} , specific gravity, the carbonyl Index (ICO), and the measured blend phase angle after one cycle of PAV at intermediate temperature. The regression results are shown in the following Table 2-7.

Table 2-7. Results of the ΔT_c regression multivariate analysis

Term	Estimate	Std Error	t Ratio	Prob> t
Intercept	-22.8164	4.3151	-5.2875	0.0003
Specific Gravity (g/cm ³)	-3.3321	0.9805	-3.3981	0.0059
D_{10} (μm)	-0.3497	0.1327	-2.6349	0.0232
The carbonyl Index (ICO)	-24.5841	4.4057	-5.5801	0.0002
Phase angle (δ) at intermediate temperature ($^\circ$)	0.7207	0.0925	7.7913	<.0001

Figure 2-13 compares the predicted value of the ΔT_c for both unmodified and PMA binders against the measured values in the following plot. The Figure shows a high level of coefficient of correlation at 88%. However, R^2 should not be the only gauge for significance for a regression model. Examining the significant parameters used in the model, they include ash physical properties (Specific Gravity and D_{10}), a measure of blend aging sensitivity (ICO), and a measure of the viscoelastic interaction of the ash and the binder represented by the phase angle (δ). More importantly, the contribution of each of these parameters follows the expected scientific fundamentals of materials science.

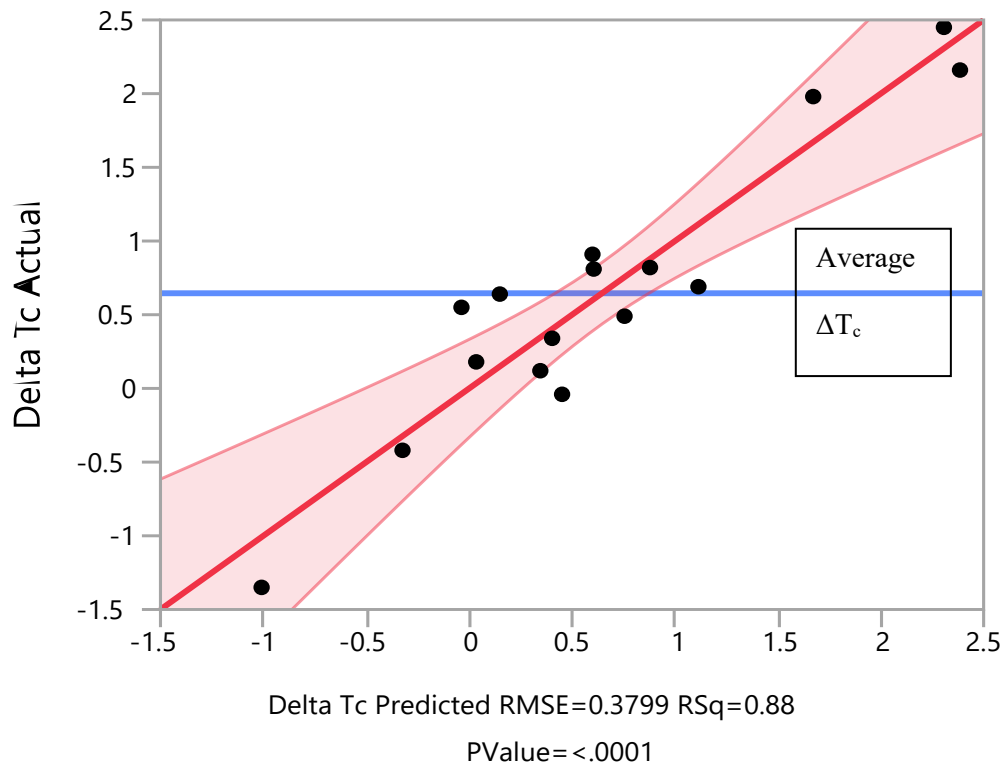


Figure 2-13. Comparison of measured ΔT_c against predicted values

2.4.3. Discussion of the Findings

The results and analysis presented in this phase show that significant improvements in asphalt performance can be attained in the presence of some types of fly ash. However, since most fly ashes used in this testing program are off-spec, they do not follow standardized formulation. This is one of the reasons, most of this class of ash gets deposited in landfills. This phase study provides strong evidence for the prospect of upcycling off-spec fly ash to be utilized as a high-value additive in the asphalt industry.

Based on the blends level testing and the regression analysis, optimal ranges for ash physical and chemical properties can be suggested. The range of these properties is selected based on the observed mastic performance as demonstrated by the various tests conducted in the study. Therefore, using the regression models and defining satisfactory performance of mastics based on healing performance higher than 34%, Crossover Modulus higher than 6000 KPa, and ΔT_c higher than -2.5, the proposed optimal ranges can be calculated. This study proposes these ranges since no such recommendations are available in the literature. Furthermore, since they are based on regression model equations, these ranges are presented here to guide future research into OFA utilization.

This performance limit of 34% was chosen as it is higher than the healing values for both unmodified binder and PMA. For the crossover modulus (G_c^*), the range between the unmodified binder and the PMA is vast. Accordingly, a value near the average was specified, 6000 KPa. For the ΔT_c parameter, two limits could be referred to. These two limits are -2.5°C , which was suggested by Anderson et al., and a cracking limit value of

-5°C, which was suggested by Rowe when an identifiable risk of cracking for the binder occurs. Accordingly, the lower value was chosen. The intermediate temperature phase angle after one cycle of aging for all binders/mastics was found to vary between 46.7 to 50.7. Accordingly, the average value of the unmodified binder (49.5) is adopted as a limit, since it is higher than the PMA blends average. The Phase angle can be controlled based on the binder type and the percentage of fly ash to be mixed with the binder. The carbonyl Index (ICO) was set to be less than 0.172, as it is the lowest value of the two investigated binders. Table 2-8 shows the suggested optimal range of OFA properties for utilization with asphalt binder. According to this table's limits, and in light of the performance results, **BH, SBH, RH, and WE** are screened out of the eight investigated OFA and chose to move further in phase three of this study.

Table 2-8: Fly Ash Physio-chemical optimal range for blends performance

Cross Over Modulus (Gc*)	Target Gc*	SiO₂, %	
	6,000.00 KPa	< 42.00%	
Healing Performance	Target Healing %	SO ₃ , %	Specific Gravity (g/cm ³)
	> 34.00%	> 6.40 %	< 2.64
ΔT_c	Target ΔT _c	Specific Gravity (g/cm ³)	D ₁₀ (μm)
	-2.50	< 2.64	< 2.50

CHAPTER 3

THE INFLUENCE OF SPENT COFFEE GROUND BIO-OIL (SCGO) AS A REJUVENATING AGENT ON CRACKING SUSCEPTIBILITY OF AGED BINDER AND RAP.

3.1. Background and Phase Objective

Applying reclaimed asphalt pavement (RAP) and recycled asphalt shingles (RAS) in new pavement construction can have significant environmental and economic advantages. Studies show that the reuse of RAP saves approximately \$2.5 billion annually, avoiding the need for vast landfill space and preserving natural resources [55]–[58]. State departments of transportation (DOTs) limit the amount of RAP to be utilized in a ton of asphalt mixture due to the potential adverse effects of RAP on the performance of the resulting pavement. However, most DOTs allow up to 20% RAP with the asphalt mixtures used [59].

There are three different environmental benefits of reusing RAP. First, it reduces road construction materials waste by incorporating them into new construction projects [60]. Second, reducing energy consumption and emissions caused by asphalt binder production. Asphalt binder production causes the highest energy consumption and emissions, such as aggregates, among pavement materials. Using RAP, the required binder decreases, which eventually results in less energy consumption and fewer emissions [68], [62]. Third, the landfill space required for the disposal of RAP is reduced [63].

Zaumanis *et al.* [61] compared the costs of conventional asphalt mixtures to those of asphalt mixtures containing RAP. Different RAP (0–100%) material percentages were considered in their study. The authors found that using 50% RAP materials decreased the construction cost by almost 29% of its original cost.

The aged bitumen in RAP loses some of the light components of maltenes during aging, which changes the balance between the asphaltene and the maltene portions. Mogawer *et al.* [64] showed that aged bitumen has higher stiffness and lower workability than unaged bitumen. Low workability prevents achieving proper compaction in the field, leading to premature failure. Thus, replacing some of the bitumen in new pavement construction with RAP bitumen disturbs the colloidal balance of the overall blend. Many studies researched the chemical performance of aged asphalt binder and RAP. It has been proved that aging increases the carbonyl and sulfoxide contents in bitumen and makes it more susceptible to forming aromatic conjugates [30], [31], [35], [65].

Many researchers use recycling agents (also referred to as rejuvenators). Using rejuvenators can enhance aged bitumen's chemical and rheological performance in RAP. Bio-oil additives are utilized in the asphalt binder industry as asphalt modifiers (<10% asphalt replacement), asphalt extenders (25–75% asphalt replacement), and direct alternative binders (100% asphalt replacement) [66]. Bio-oils sources can be categorized into three categories. The first category is agricultural or forest production wastes that include but are not limited to crop residues (like maize straw), wood wastes (like sawdust and bark), and urban organic wastes (like microalgae). The second category is animal wastes that include but are not limited to swine manure bovine feces. Finally, the third category is post-consume oil wastes that include but are not limited to cooking oil/residues,

waste auto engine oil/residues, cottonseed, and soybean oil residues [67], [68]. Many studies indicated that most of these materials could restore the balance lost after aging between Asphaltene maltenes and Aromatics by using different contents [68]–[73].

Zhang *et al.* [74] evaluated a bio-based rejuvenator derived from waste wood as an asphalt recycling agent. The study showed that using the wood waste rejuvenator can increase the viscous components and reduce the stiffness of the aged asphalt binder. The high content of light compounds in the bio-oil balanced the chemical compounds of the aged asphalt. As a result, the rutting resistance, fatigue resistance, and low-temperature crack resistance of the aged asphalt binder were restored by the bio-oil significantly. Xinxin *et al.* [75] proposed a waste Vegetable Based Oil (VBO) as an asphalt binder rejuvenator. The researchers concluded that the optimum dosage to be used is 13.4 wt %. Compared with virgin asphalt, the rutting property of rejuvenated asphalt and the workability were found to be slightly poorer. On the other hand, the fatigue and low-temperature properties have been significantly enhanced.

Pahlavan *et al.* [69] examined the merits of coliquefying high protein algae with high-lipid swine manure to form a bio-oil containing a high concentration of nitrogen-containing fused aromatics to intercalate into oxidized asphaltene nanoaggregates. It was found that high-lipid swine manure bio-oil can rejuvenate the aged asphalt found in the reclaimed asphalt pavement by restoring the aged asphalt binder's original chemical balance and molecular conformation. Elkashef *et al.* [76] introduced soybean oil-derived material to be utilized as a potential asphalt binder rejuvenator. The results suggested that this material is a viable candidate as a rejuvenator. Using the soybean oil-derived rejuvenator at a low dosage improved the fatigue and low-temperature properties of aged asphalt binder. In

addition, it led to a notable decrease in the complex shear modulus accompanied by an increase in the phase angle, which is an indication of reversing the effect of aging.

This phase evaluates spent coffee ground extracted oil as a new asphalt binder rejuvenator. The proposed rejuvenator is investigated to study its effect on aged asphalt binder, Artificial RAP (ARAP), and RAP's rheological and cracking performance. In addition, the proposed SCGO is compared to two different market rejuvenators. Rejuvenator #1 is a Vegetable based Oil (VBO), and the other, rejuvenator #2, is a Petroleum-based oil (PBO).

3.2. Materials and Methods

3.2.1. Experimental Design Overview

The experimental program is presented in Figure 3-1. The program relies on three different binders: Two unmodified PG 64-22 binders and a Polymer Modified (PMA) PG 76-22 binder. These binders are used to create artificial RAP (ARAP) for a full testing program with two available rejuvenators and the proposed SCGO rejuvenator. In addition, an extracted RAP binder is used to confirm the results of the ARAP with rejuvenators. The RAP binder was extracted and recovered from the RAP mixes per AASHTO T-164. Table 3-1 lists the high, intermediate, and low-temperature Performance Grade (PG) for the investigated binders and RAP.

Table 3-1. Continuous Performance Grade (PG) for the Investigated Asphalt Binders and RAP

Tested Binder	High Temperature			Low Temperature (PAV 20 hr.)		Continuous PG
	Original ¹	RTFO ²	Inter. Temp. ³	S/MPa ⁴	m-slope ⁵	
NC PG 64-22	67.4	68.5	22.9	-26.7	-25.7	67-25
AA PG 64-22	69.5	70.0	24.0	-24.1	-23.3	69-23
PMA PG 76-22	79.4	81.4	23.7	-25.6	-24.90	79-24
RAP-RS19	87.3	————	23.3	-29.4	-27.5	87-27

¹ Temperature corresponds to $|G^*|/\sin(\delta)=1.0$ KPa

² Temperature corresponds to $|G^*|/\sin(\delta)=2.2$ KPa

³ Temperature corresponds to $|G^*|\sin(\delta)=5000$ KPa

⁴ Temperature Corresponds to Stiffness= 300 MPa

⁵ Temperature corresponds to m-value =0.3

Three different rejuvenators were used in this study. Two market rejuvenators, VBO and PBO, are referred to as rejuvenators #1 and #2, respectively. In addition, a new Vegetable-based SCGO rejuvenator is introduced in this research.

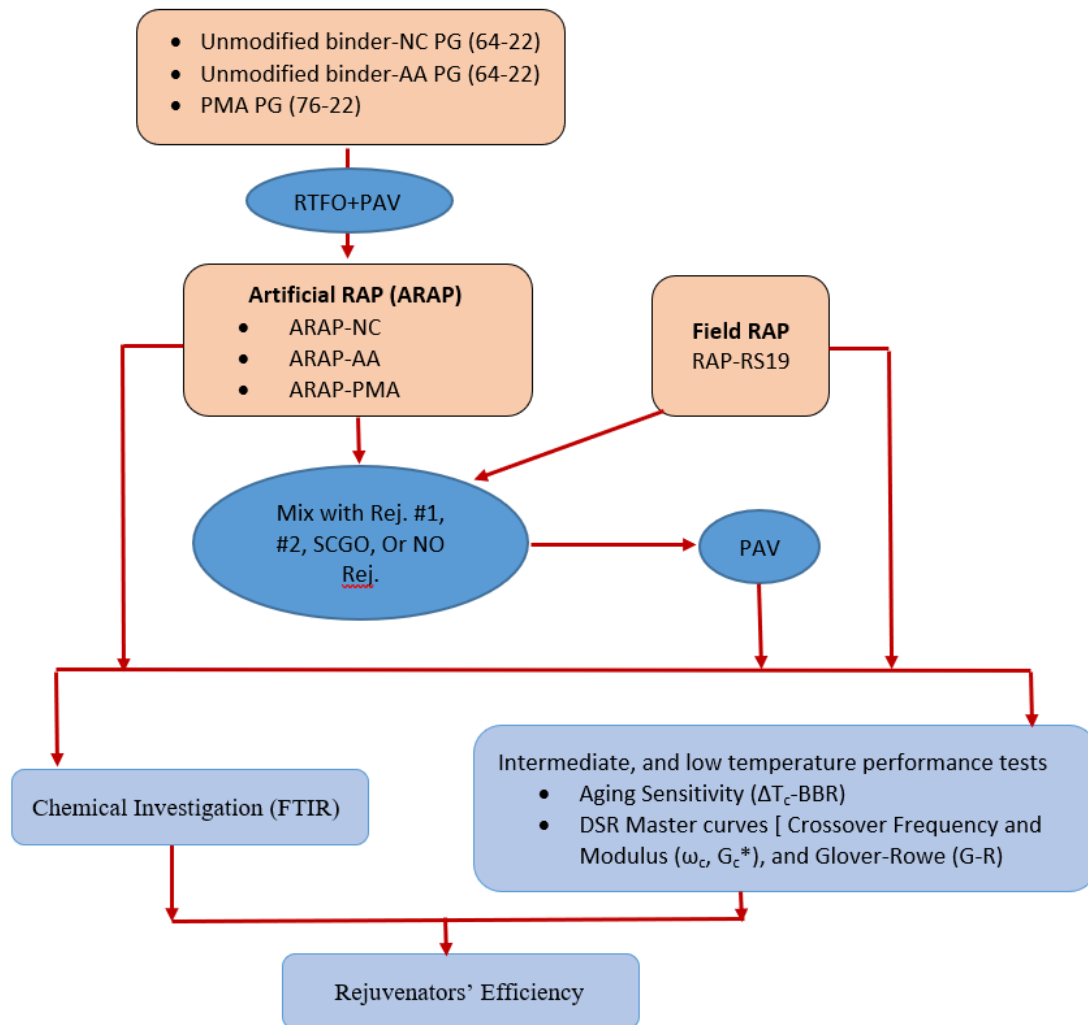


Figure 3-1. Experimental Program

The aging characterization of the blends and binders is quantified using Fourier-transform infrared spectroscopy (FTIR). The test is used to calculate the Carbonyl functional group (C=O) increase in asphalt samples with oxidative aging. In addition, aging-dependent rheological behavior is also investigated and utilized to quantify the aging behavior of the samples. Therefore, the testing program includes Low-temperature performance using the bending beam rheometer (BBR) test according to AASHTO PP-42 to measure the low-temperature ductility.

The Glover-Rowe (G-R) parameter, crossover frequency, and crossover modulus (ω_c and G_c^*) are also evaluated for the investigated RAP binders. Finally, all samples are tested using two replicates to achieve a coefficient of variation not exceeding 10%.

In general, rejuvenator dosage is determined based on achieving one of the following three conditions: first, restoring the low-temperature grade (PGL) of the binder blend to that of the base binder, or second, restoring the high-temperature grade (PGH) of the binder blend to that of the base binder, or third, achieving ΔT_c equal to -5 [77]. For this study, achieving ΔT_c equal to or less than -5°C was set for choosing the rejuvenator dosage. This criterion led to using a 5% dosage for the rejuvenators.

3.2.2. Spent Coffee Ground (SCG) Bio-oil Extraction (Soxhlet Extraction Process)

The soxhlet extraction procedure was adopted for SCG bio-oil extraction, as the Soxhlet apparatus is available in Temple University facilities. The Soxhlet procedure was performed to separate the lipids from the SCG. As demonstrated in Figure 3-2-a, a round-bottom flask was filled with 150 milliliters of n-hexane and placed on the heating source. a Soxhlet thimble, a borosilicate glass filter that will hold the coffee grounds while filtering out the lipids, is weighed before and after filling it with the dried SCG and is placed into the extraction chamber of the Soxhlet, which was placed on top of the round bottom flask. The water-cooled reflux condenser is placed on top of the Soxhlet extractor.

The self-sustaining process is continued as follows:

- 1- The hexane boiled, and its vapor traveled up the bypass arm.
- 2- The vapor condensed in the reflux condenser and dripped down.

- 3- The coffee lipids dissolved in the hexane, and the hexane-lipid mixture accumulated until its surface was leveled with the siphon arm.
- 4- The hexane-lipid mixture is drained back into the round-bottom flask, and the cycle is kept repeating.

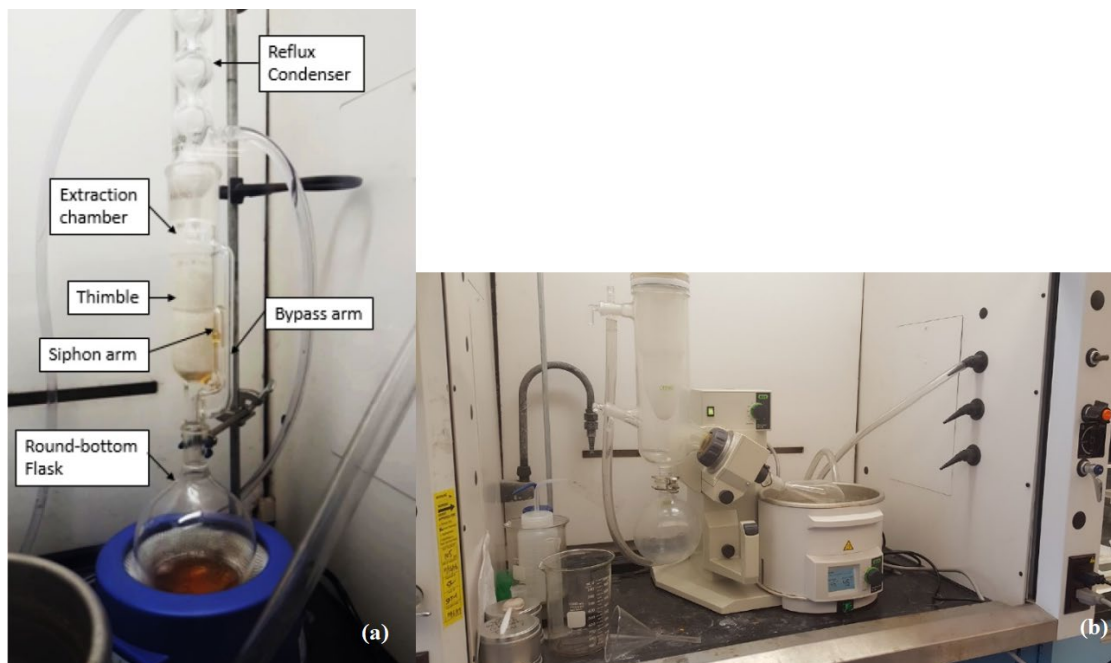


Figure 3-2. (a) Soxhlet Bio-Oil Extraction equipment, and (b) Rotary Evaporator Equipment.

Following the Soxhlet extraction, a rotary evaporator (shown in Figure 3-2-b) was used to remove the hexane from the lipid-hexane mixture. The mixture was poured into the round bottom flask, which rotates in a warm water bath. The hexane vapor was pulled through the apparatus via vacuum, cooled by a dry-ice condenser, and deposited into another flask for reuse. This process ran until the hexane no longer dripped from the condenser. Only coffee lipids were left in the rotating flask. Then, the coffee lipids (bio-oil) were let to sit overnight in an open container inside the fume hood to ensure complete evaporation of the volatile hexane.

3.2.3. Fabrication of Blends

For producing Artificial RAP (ARAP), a sample of the binders for each asphalt type with no rejuvenation was exposed to short-term aging using the Rolling Thin Film Oven (RTFO) test per AASHTO T 240. The RTFO aging was followed by the Pressure Aging Vessel (PAV) test for 20 hours following AASHTO R 28. The testing matrix included a control "non-rejuvenated" ARAP and field RAP to serve as a baseline for comparisons. Then, ARAP and RAP were blended with 5% by their weight with one of the two on-market rejuvenators (#1, #2) or the new proposed SCGO rejuvenator using a high shear mixer. The blending process was completed over 30 minutes. Following the application of the rejuvenators, the samples were put through an additional PAV cycle. It is important to note that the un-rejuvenated ARAP and RAP binders' samples were exposed to the same mixing protocol as a control sample to avoid fabrication/conditioning bias influencing the ARAP and RAP properties. This process yielded four RAP binders (three ARAP binders and one field RAP binder) and sixteen unrejuvenated/rejuvenated samples (Three ARAP binders, one RAP, with three rejuvenators, and no rejuvenator).

3.2.4. Glover Rowe Parameter (G-R), Crossover Frequency, and Modulus (ω_c), (G_c^*)

The Glover-Rowe (G-R) parameter is utilized to evaluate the effect of aging on the blends' ductility. Before the Strategic Highway Research Program (SHRP) was established, the ductility test (at 15°C) was used to assess binders for susceptibility to cracking at intermediate temperature. In 2005, Glover conducted a comprehensive study on the aging of asphalt binder, and in that study, Glover presented the DSR function ($G''/(\eta'G')$) measured at 0.005 rad/sec and 15°C [78]. The DSR function strongly correlated with the ductility test [78]. Anderson et al. [79] conducted a field study in which the DSR function

was validated as a good candidate for identifying loss of ductility that may lead to non-load associated cracking in pavements. The G-R parameter shown in Equation (3-1) was a reformulation of the DSR function [80]:

$$G - R = \frac{G^*(\cos\delta)^2}{\sin\delta} \quad \text{(Equation 3-1)}$$

Where,

G^* - complex shear modulus (kPa); and

δ - phase angle (degree).

The crossover frequency and modulus (ω_c , G_c^*) are rheological parameters that quantify aging susceptibility. Crossover modulus is defined as the complex shear modulus when the phase angle equals 45° , where the storage modulus equals the loss modulus. The crossover modulus is a unique point on the material's viscoelastic spectrum, not depending on the test frequency and temperature. Increased crossover values indicate an increased viscous and elastic component of the materials. The crossover modulus is inversely related to aging. The frequency sweep tests determined the crossover modulus G_c^* from the master curves of complex shear modulus and phase angle.

Similar to the crossover modulus, the crossover frequency (ω_c) corresponds to the frequency at which the phase angle (δ) is 45° or $G' = G''$, which indicates the equal contribution of the elastic and viscous components of G^* . Some rejuvenators mainly act as a softener by influencing the viscous component of asphalt. Other rejuvenators restore both the viscous and elastic performance of aged asphalt. It has been shown that nearly all so-called rejuvenators soften the aged bitumen and increase its crossover frequency, which

measures bitumen's vicious behavior. However, not all rejuvenators increase the crossover modulus, which measures the extent of polydispersity. Asphalt binder's polydispersity increases with aging and is inversely related to crossover modulus [58], [81]. Therefore, crossover modulus and frequency are reliable tools for evaluating rejuvenator efficiency. A concurrent increase in crossover modulus and crossover frequency is needed to show successful rejuvenation and not only softening agent [58], [81].

The crossover frequency and modulus (ω_c , G_c^*) and Glover-Rowe Parameter (G-R) were obtained through the DSR frequency sweep test. The DSR frequency sweep test was conducted on all blends and binders. For PG 64-22 blends/binders and field RAP, the test was conducted at 10, 22, 34, 46, 58, 64, and 70°C, over a frequency range from 100 to 0.1 rad/s at each temperature. For PMA PG 76-22 blends and binder, the test was held at 10, 22, 34, 46, 58, 70, and 76°C over a frequency range from 100 to 0.1 rad/s. The amplitude strain was set to 0.1% to attain linear viscoelastic range behaviors for the blends and binder tested.

3.3. Test Results and Discussion

3.3.1. Analysis of Infrared Spectroscopy (FTIR)

Table 3-2 shows the change in the FTIR results for the different investigated ARAP and RAP at different aging levels. Thus, FTIR monitored the main changes in the chemical functional groups between the two aging levels for the different investigated ARAP and RAP. The data shown are the average of four replicates. The spectral peak of interest was for the carbonyl peak at 1700 cm^{-1} . To analyze the carbonyl group with the presence of rejuvenators, these spectra were normalized using a reference of bending of C–H bonds in

the spectrum of the binder sample. The higher the carbonyl index, the greater the oxidation level and aging accordingly.

As mentioned above, the different rejuvenators are introduced to the ARAP and RAP, then subjected to PAV aging cycle. Figure 3-3 shows the influence of the different rejuvenators when blended with the investigated RAP binders. Rejuvenator#1 is a vegetable-based bio-oil (VBO), and rejuvenator#2 is Petroleum-Based bio-oil (PBO). The new proposed SCGO also has a VB nature. The ester group ($1,735\text{cm}^{-1}, 750\text{cm}^{-1}$) referred to in Figure 3-3 can clearly distinguish between the PBO and VBO, as the VBO contains the ester groups.

Table 3-2. Carbonyl Index (ICO) for Rejuvenated and Unrejuvenated RAP binders.

Asphalt Binder /RAP	ARAP@1 st PAV or Field RAP	@ 2 nd PAV		RAP + Rej. #1 @ 2 nd PAV		RAP + Rej. #2 @ 2 nd PAV		RAP + SCGO @ 2 nd PAV	
		ICO	Relative to RAP*	ICO	Relative to RAP	ICO	Relative to RAP	ICO	Relative to RAP
NC PG 64-22	0.172	0.168	-2.59%	0.157	-8.87%	0.133	-22.76%	0.169	-1.87%
AA PG 64-22	0.125	0.160	28.17%	0.145	16.12%	0.178	42.81%	0.110	-12.28%
PMA PG 76-22	0.131	0.138	4.61%	0.121	-8.28%	0.116	-11.45%	0.120	-8.51%
RAP-RS19	0.139	0.141	1.61%	0.144	3.76%	0.145	4.29%	0.139	0.00%

*RAP term includes both Artificial RAP and field extracted RAP

Table 3-2 lists the calculated values of ICO for the different investigated RAP binders. The results show that further aging applied on both the ARAP and RAP binders is causing minimal changes in measured ICO. Only ARAP-AA binder is showing a noticeable increase in ICO by 28%.

Both rejuvenators #1 and #2 are found not to positively influence the aging index ICO when introduced to ARAP-AA and RAP-RS19. Rejuvenator#1 drops the ICO by 8.9% and 8.3% when introduced to the ARAP-NC and ARAP-PMA binders. Introducing rejuvenator

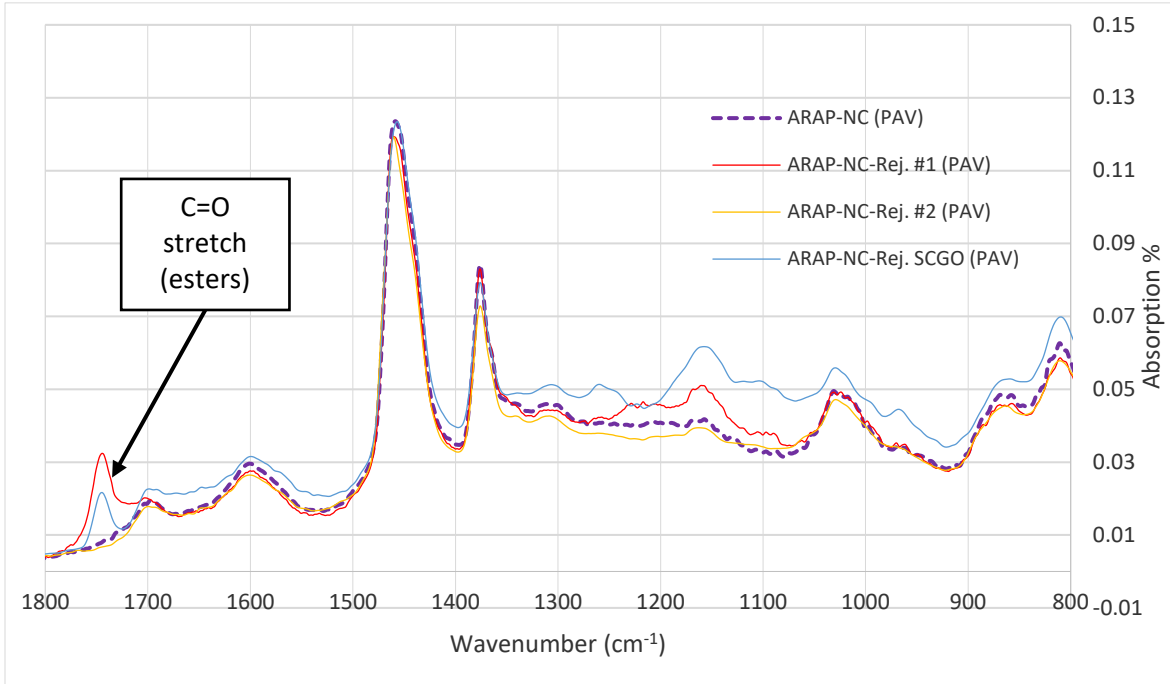
#2 to ARAP-NC and ARAP-PMA drops the aging index ICO values by 22.8% and 11.5%, respectively.

The SCGO rejuvenator is the only rejuvenator showing a consistent reduction in the ICO aging index when introduced to the different investigated ARAP/RAP. It drops the ICO values by 1.9%, 12.3%, and 8.5% when blended with the ARAP-NC, ARAP-AA, and ARAP-PMA, respectively. Furthermore, the new SCGO is the only rejuvenator that maintained the ICO level of the field RAP at a constant level after the second cycle of PAV.

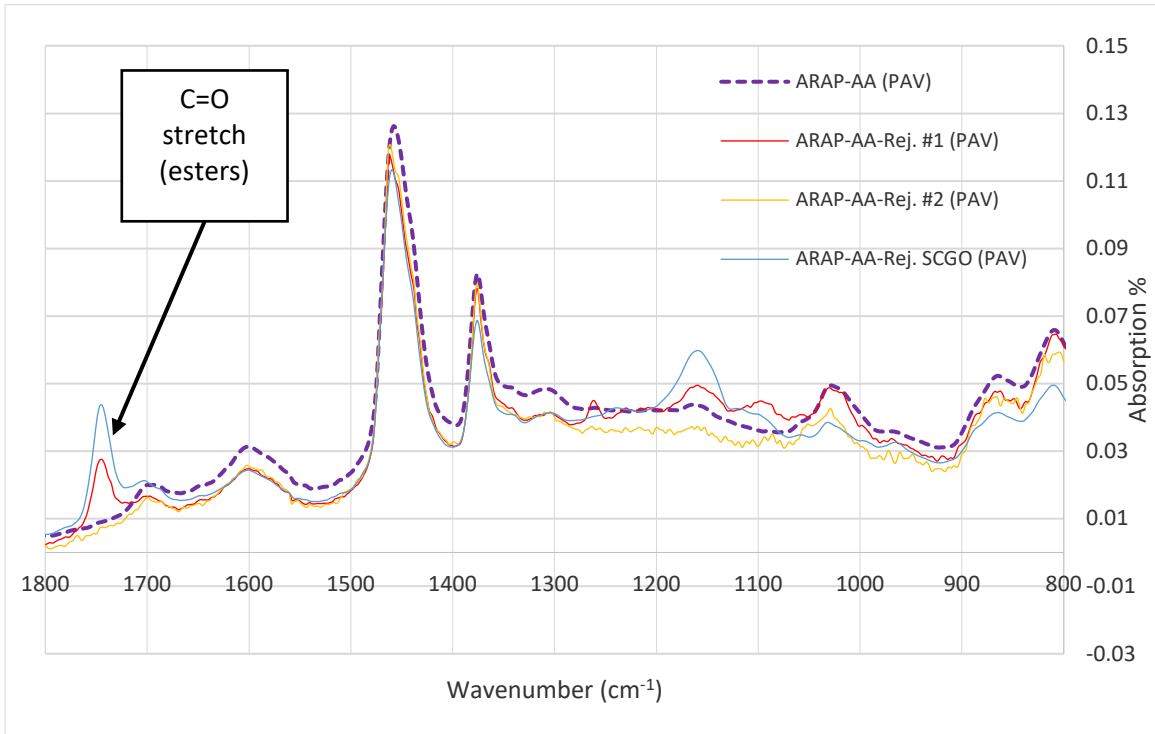
Understandably, the results of spectroscopy indices provide a more qualitative evaluation. This is because (1) it depends on small samples that may have issues representing the bulk material, and (2) the approximate method in calculating the areas under the appropriate peaks of the output. Therefore, from the previous results, it can be concluded that the introduction of the VBO rejuvenators, especially the new proposed SCGO, is associated with the higher recovery of PAV-aged RAP binders. That could be due to the predominance constitution of esters with saturated and unsaturated fatty acids for the VBO rejuvenators. On the other hand, the PBO rejuvenators are products with a predominance of polar aromatic molecules. These interpretations have been referred to by several authors [27], [60], [74]–[76], [82], [83].

The asphalt binder aging process is very complex, with changes in its chemical composition and rheological properties. The chemical composition change is irreversible, including oxidation, loss of volatiles, and formation of highly polar functional groups. On the other hand, the rheological properties change a reversible process related to physical

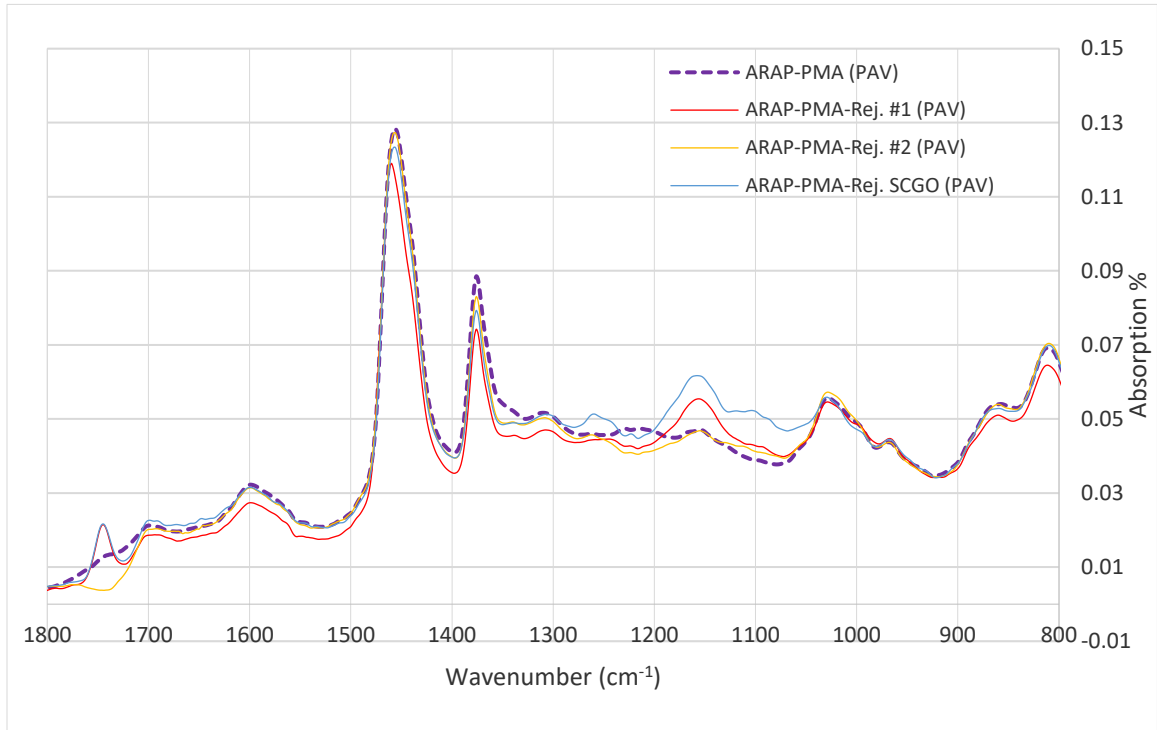
hardening attributed to the reorganization of the binder molecules [83]. Accordingly, cracking and ductility-related evaluation is conducted.



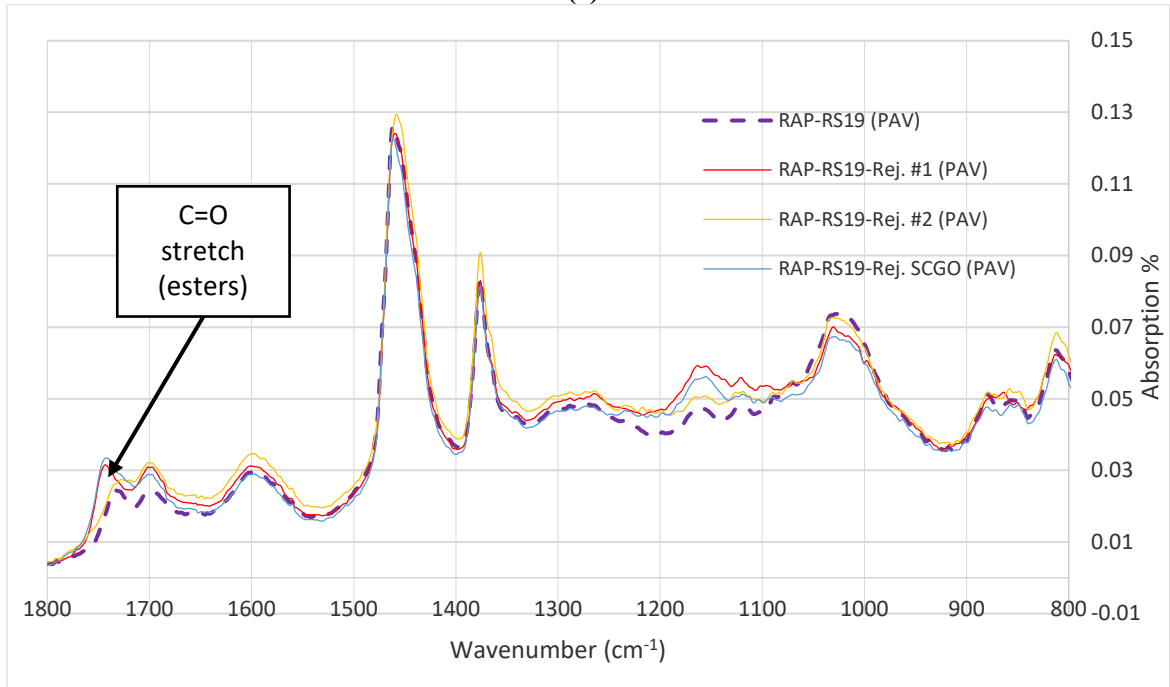
(a)



(b)



(c)

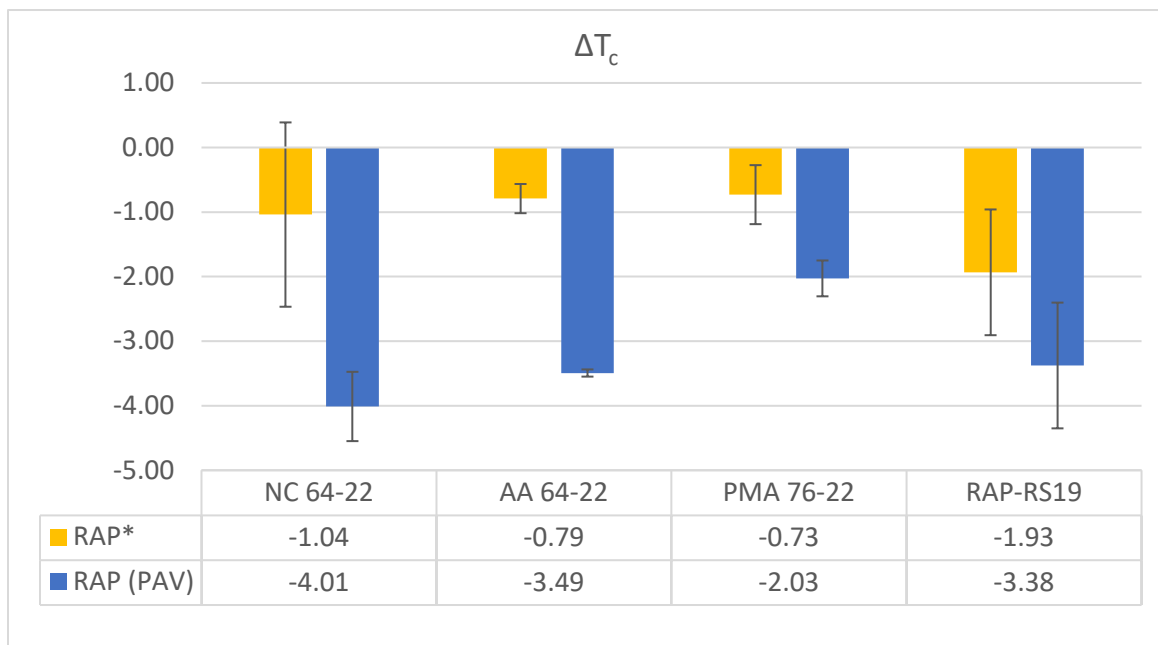


(d)

Figure 3-3. Absorption of the Investigated PAV Aged Rejuvenated and Unrejuvenated (a) ARAP-NC, (b) ARAP-AA, (c) ARAP-PMA, and (d) RAP-RS19.

3.3.2. Thermal Cracking and Relaxation Performance Evaluation

ΔT_c is used for evaluating the age-related cracking potential at low temperatures. The lower the value of ΔT_c , the lesser the ability of the binder to relax under thermal stresses as the pavement ages. Figures 3-4 and 3-5 demonstrate the results related to low-temperature performance. Figure 3-4 depicts that all the investigated RAP binders are more susceptible to aging. The ARAP-AA is more prone to thermal cracking than the other investigated RAP binders, as its ΔT_c value drops the most by 343%. On the other hand, ARAP-NC, ARAP-PMA, and RAP-RS19 binders' ΔT_c values are found to drop by 286%, 178%, and 75%, respectively.



***RAP term includes both Artificial RAP and field extracted RAP**

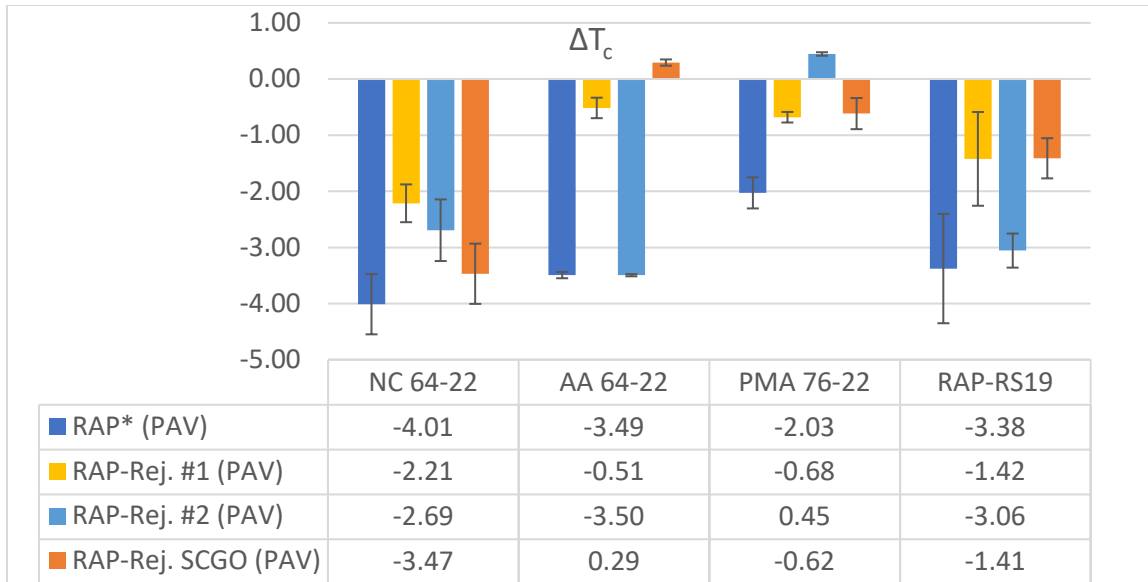
Figure 3-4. ΔT_c of the Investigated RAP binders before and after 2nd cycle of PAV Aging

Figure 3-5 demonstrates the effect of the different rejuvenators when introduced to the different RAP binders. In general, introducing rejuvenators to the aged RAP binders increases the resistance to thermal cracking. Rejuvenator#1 is found to improve the

performance of ARAP-NC and RAP-RS19 by 45% and 26%, respectively, as measured by ΔT_c . Rejuvenator#2, the PBO rejuvenator, has no significant improvement in thermal cracking resistance when introduced to ARAP-AA and RAP-RS19 but significantly increases ΔT_c for ARAP-PMA by 122%.

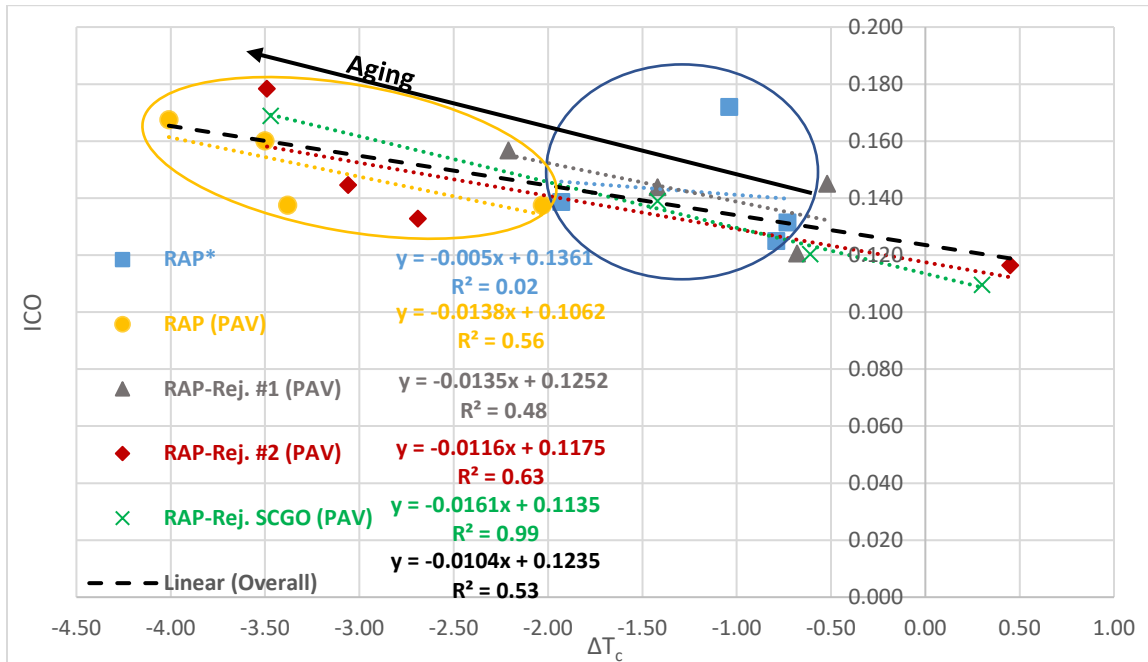
The new proposed SCGO significantly enhances the resistance to thermal cracking when introduced to all the investigated RAP binders. The ΔT_c values ARAP-NC, ARAP-AA, ARAP-PMA, and RAP-RS19 are found to increase by 13%, 110%, 70%, and 26%, respectively, compared to their corresponding PAV aged unrejuvenated RAP. These results show the effectiveness of SCGO in retarding the aging of the different binders compared to the two on-market rejuvenators. Especially when introduced to the ARAP-AA and RAP-RS19. It is important to note that all results of blends and binder are within acceptable performance as recommended by Anderson *et al.* [39].

Figure 3-6 shows the ICO index correlation with the ΔT_c . It is clear that the PBO has the lowest rejuvenating effect compared to the VBO rejuvenators. On the contrary, as illustrated, the VBO rejuvenators can retard the aging indices to a level exceeding RAP binders' original condition before being subjected to PAV aging.



*RAP term includes both Artificial RAP and field extracted RAP

Figure 3-5. ΔT_c of the Investigated PAV Aged Rejuvenated and Unrejuvenated RAP binders.



*RAP term includes both Artificial RAP and field extracted RAP

Figure 3-6. Correlation between The Carbonyl Index (ICO) and ΔT_c of the Investigated Rejuvenated and unrejuvenated RAP binders.

3.3.3. Frequency Sweep Test Results

The tested binders' stiffness and phase angle were obtained from the asphalt binder frequency weep test. The Christensen-Andersen-Marasteanu (CAM) model, as shown in Equation (3-2), was used to construct the asphalt and RAP master curves. The shift factor was estimated based on the Williams–Landel–Ferry WLF equation. Figure 3-7 depicts the complex modulus and the phase angle master curves for the tested asphalt binder and RAP.

$$|G^*| = \frac{G_g^*}{\left[1 + \left(\frac{\omega_c}{\omega_r}\right)^k\right]^{\frac{m_e}{k}}} \quad (\text{Equation 3-2})$$

where

$|G^*|$ = complex shear modulus (Pa);

G_g^* = glassy modulus (Pa);

ω_c = crossover frequency (rad/s);

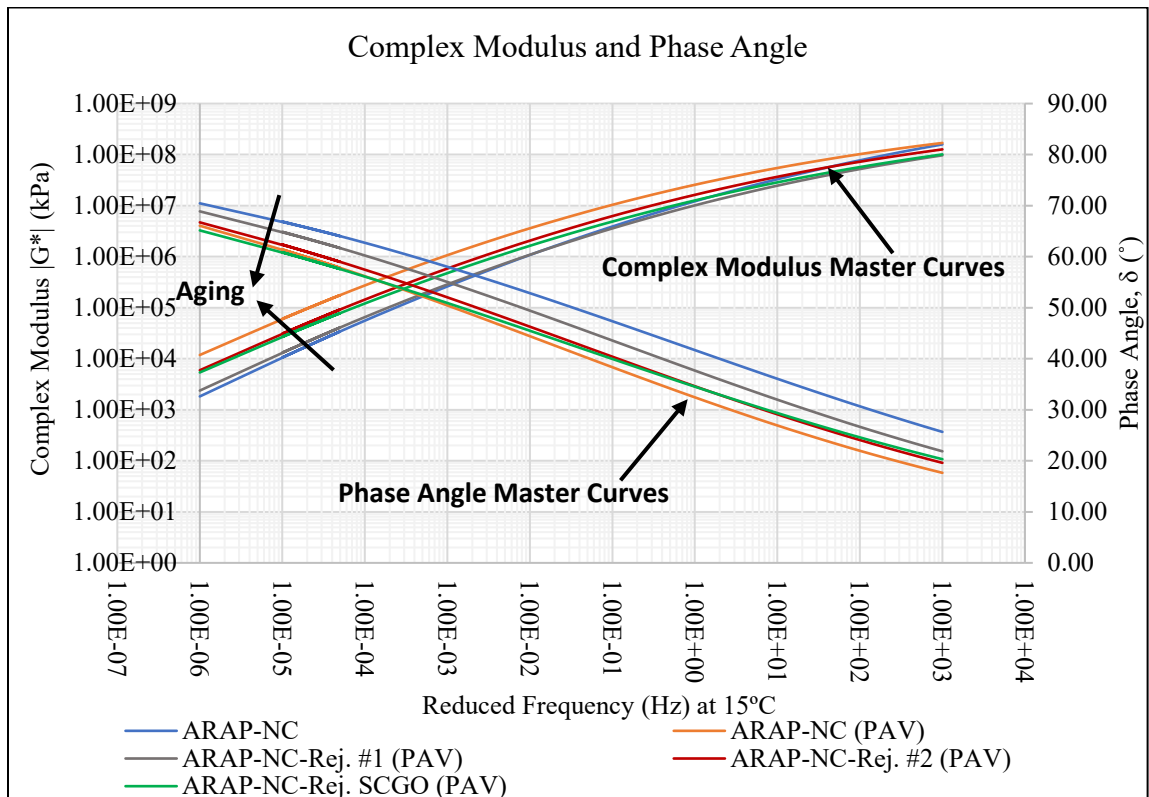
ω_r = reduced frequency (rad/s); and

m_e, k = fitting coefficients.

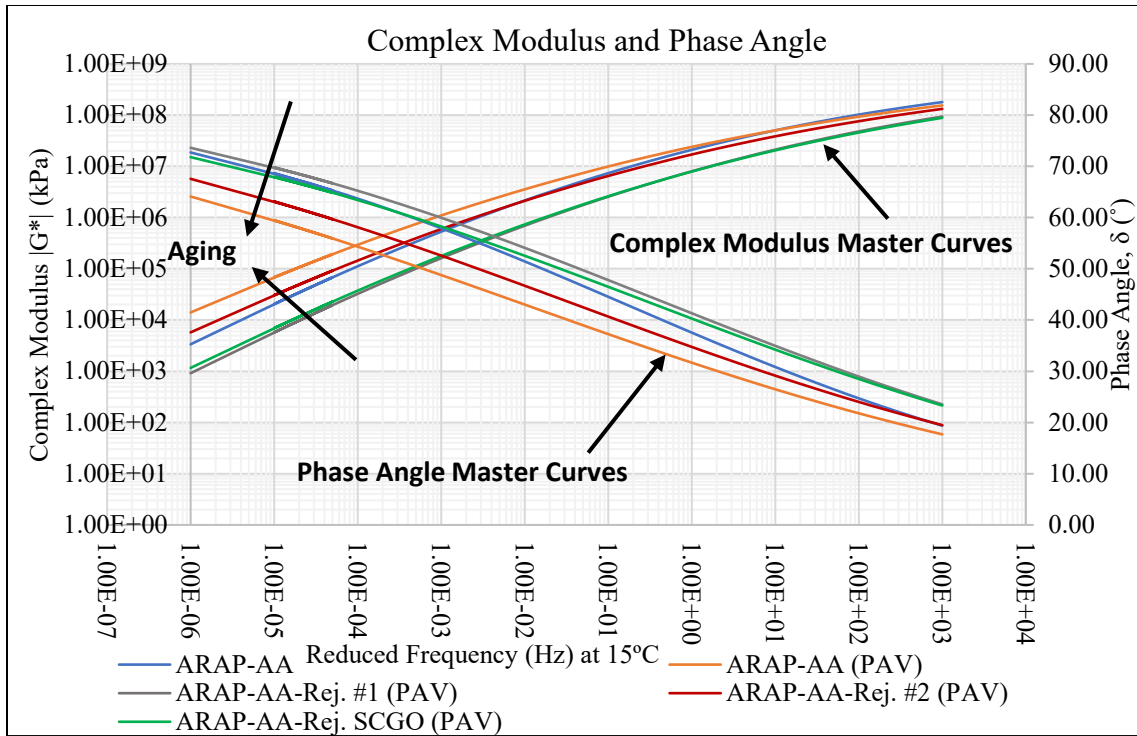
The complex modulus increases and the phase angle decreases when the investigated asphalt binders are subjected to the second round of PAV aging and when RAP is subjected to PAV aging. As expected, introducing the different rejuvenators to the aged asphalt binder reduces the stiffness. The VBO rejuvenators have a more dominant effect following the FTIR results trends than the PBO. Introducing rejuvenator#1 to the unmodified binder NC reduces its stiffness and increases its phase angle, accordingly enhancing its elastic component. As shown in Figure 3-7-a, rejuvenator#1 enhances the elastic component to a

limit higher than the binder after its first round of PAV aging. The PBO rejuvenator#2 performs the least with both investigated unmodified binders. It has an intermediate performance with the PMA binder and the real extracted RAP.

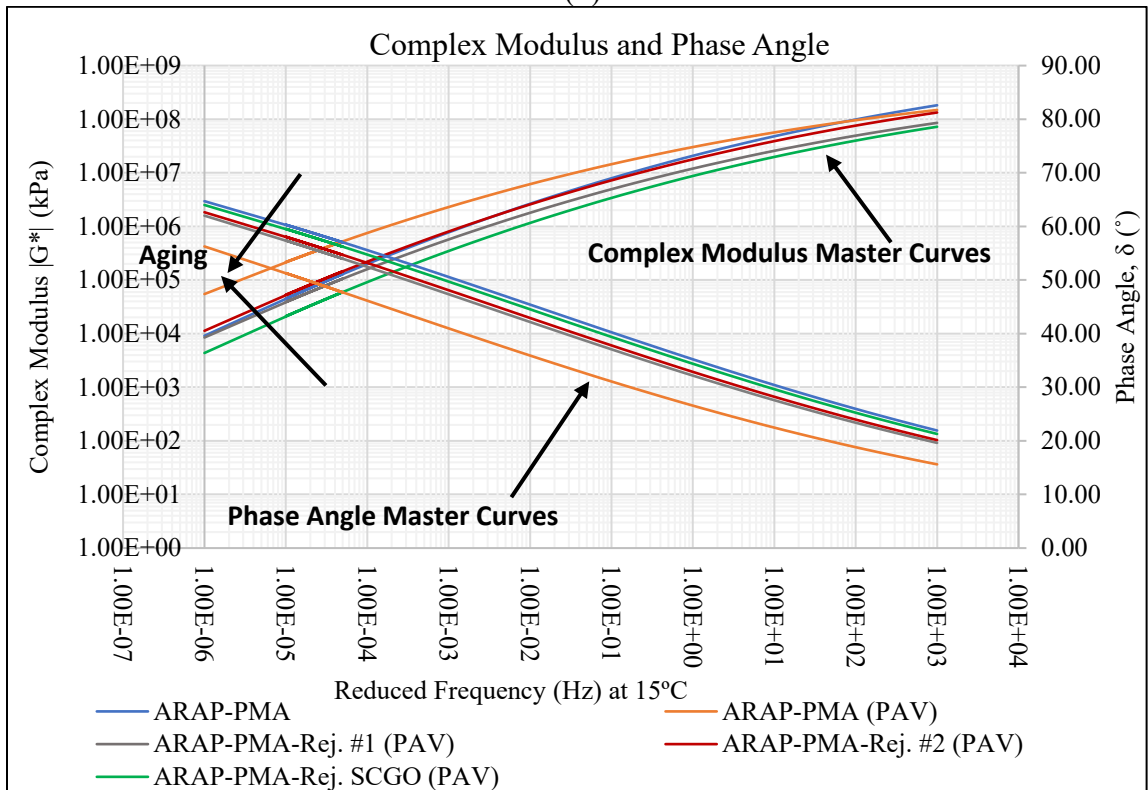
The proposed SCGO performs efficiently with unmodified binder AA, PMA binders, and the extracted RAP compared to the two market rejuvenators. Furthermore, it is found that introducing the SCGO enhances the elastic component of the PAV-aged binder and more effectively with the RAP, as shown in Figures 3-7-b to -d.



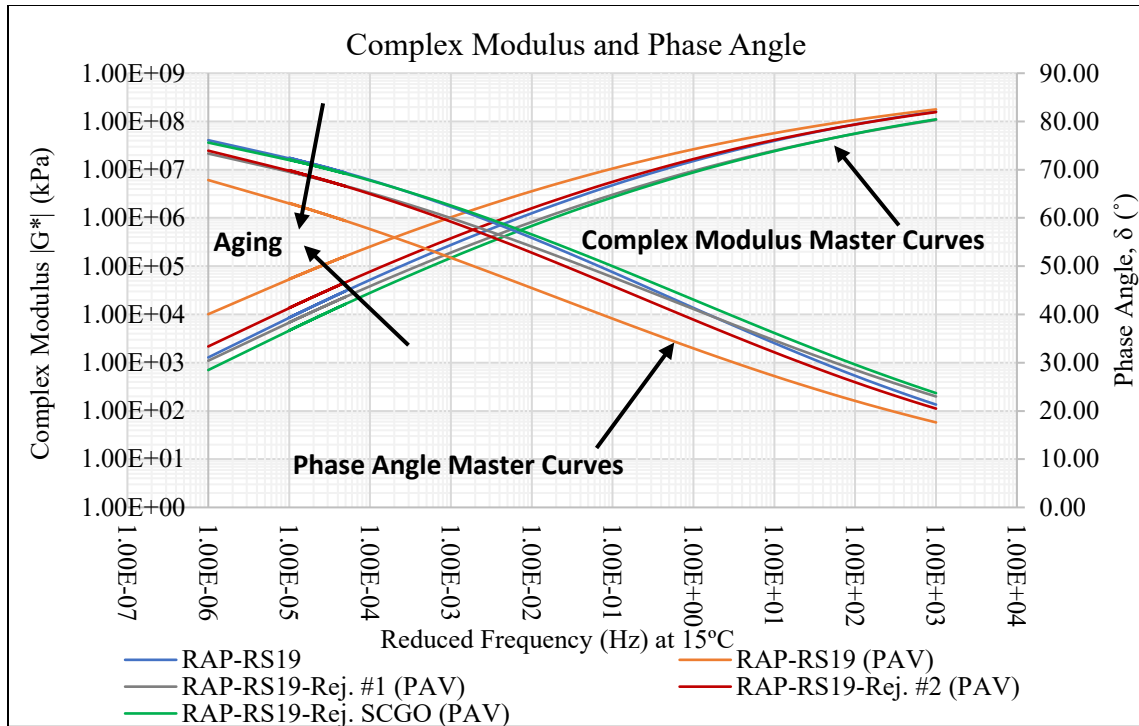
(a)



(b)



(c)



(d)

Figure 3-7. Asphalt Complex Modulus and Phase angle Master Curves for (a) ARAP-NC, (b) ARAP-AA, (c) ARAP-PMA, and (d) RAP-RS19.

3.3.4. Grover-Rowe Parameter (G-R)

The G-R parameter is an aging indicator calculated from the DSR frequency sweep test results, used to evaluate the cracking resistance of an asphalt binder. Durability thresholds were translated into $G-R = 180$ kPa (corresponding to a 5 cm ductility and 0.0009 MPa/s for the initial DSR function) to indicate the onset of cracking (warning). $G-R = 600$ kPa (corresponding to 3 cm ductility, 0.003 MPa/s DSR function) was used to indicate extensive block cracking (limit) [39], [78].

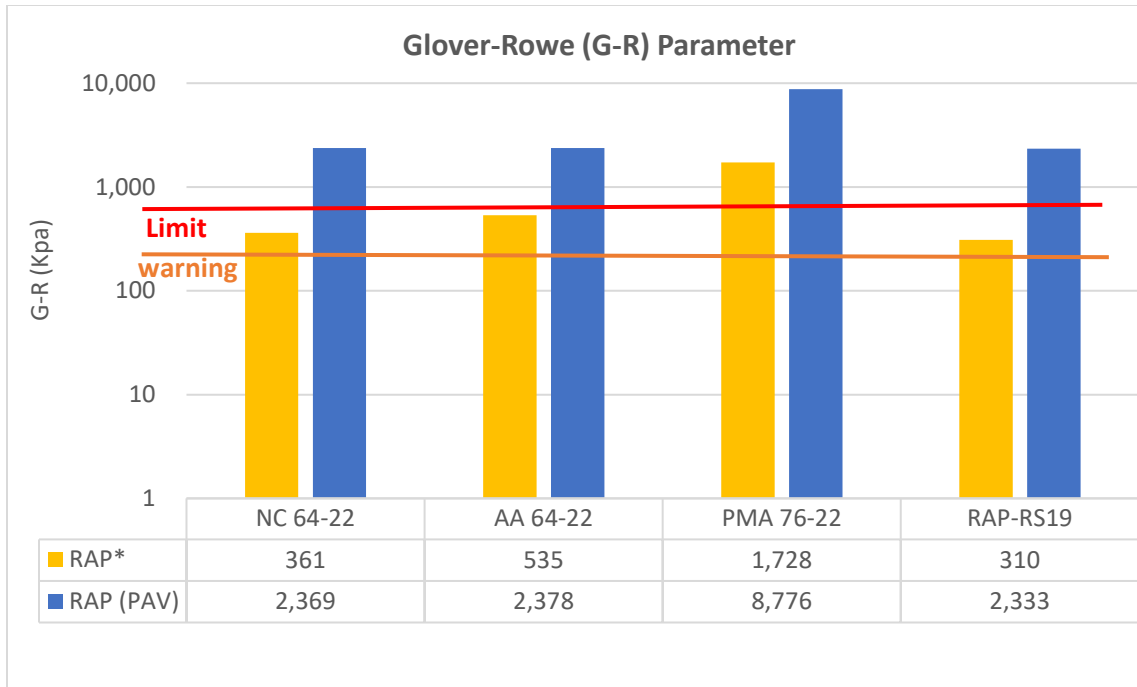
Figure 3-8 shows the results of the G-R parameter for the different investigated RAP at different aging levels. To begin with, all the RAP binders exceed the warning cracking limit (180 KPa). However, only the ARAP-PMA exceeds the cracking limit line (600 KPa). The reason behind that could be the polymerization of the asphalt binder, as the PMA

binder is stiffer than the unmodified binder when aged. As expected, the different investigated RAP binders are more prone to fatigue cracking when exposed to a cycle of PAV aging, as suggested by the G-R parameter.

Figure 3-9 depicts the results of the investigated PAV aged rejuvenated and unrejuvenated RAP binders. The VBO rejuvenator#1 has the highest performance when introduced to ARAP-NC and ARAP-AA. It reduces the susceptibility to the intermediate temperature cracking by 80% and 90% for ARAP-NC and ARAP-AA binders, respectively, compared to their corresponding unrejuvenated PAV aged RAP binders. On the contrary, when introduced to the different RAP binders, the PBO rejuvenator#2 has the lowest performance. Compared to the unrejuvenated PAV aged RAP binders, it enhances the intermediate temperature performance by 50%, 48%, 76%, and 84% for the ARAP-NC, ARAP-AA, ARAP-PMA, and RAP-RS19, respectively.

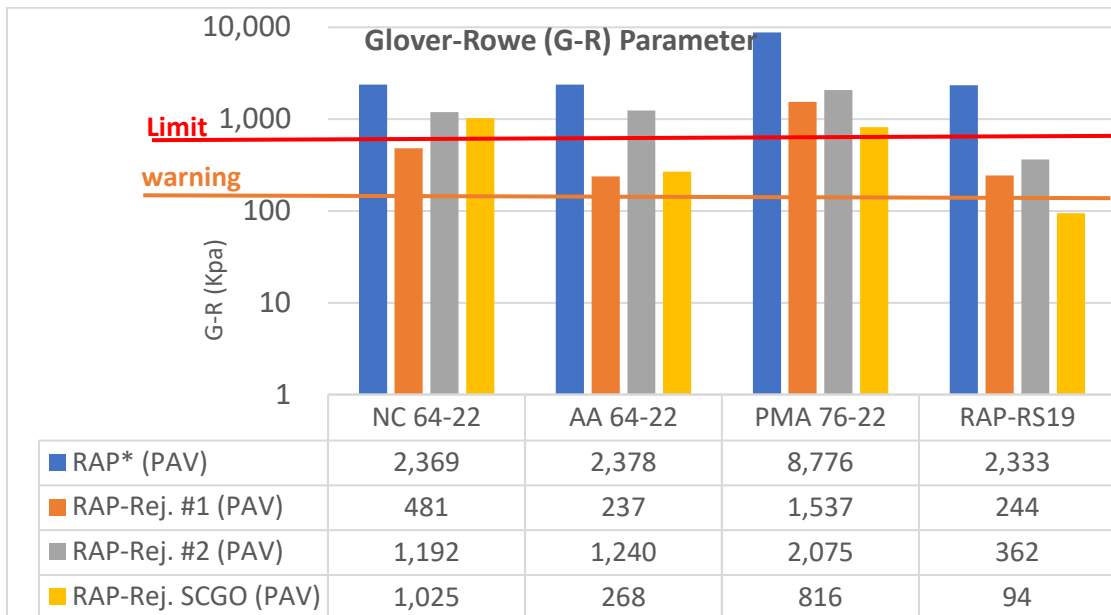
The proposed VBO rejuvenator reduces the susceptibility to the intermediate temperature cracking the most with the ARAP-PMA binder and RAP-RS19. Relative to unrejuvenated PAV aged RAP, it reduces the G-R values by 91% and 96% for the ARAP-PMA and RAP-RS19, respectively.

Both VBO rejuvenators enhance the intermediate temperature performance to a limit lower than the extensive cracking limit (600 KPa) with the ARAP-AA binder. Also, the new SCGO, VBO rejuvenator, reduces the RAP-RS19's susceptibility to the intermediate temperature cracking to a limit lower than the warning cracking limit (160 KPa). In general, the VBO rejuvenators show the ability to improve intermediate temperature performance higher than the PBO rejuvenator.



*RAP term includes both Artificial RAP and field extracted RAP

Figure 3-8. G-R Parameter of the Investigated RAP binders before and after Subjection to PAV Aging



*RAP term includes both Artificial RAP and field extracted RAP

Figure 3-9. G-R Parameter of the Investigated PAV Aged Rejuvenated and Unrejuvenated RAP binders.

3.3.5. *Crossover Modulus and Frequency (G_c^* , ω_c)*

Table 3-3 shows the crossover modulus and frequency results for the different investigated unrejuvenated/rejuvenated RAP binders. Following the previously illustrated results, the crossover modulus and frequency of the different investigated asphalt RAP binders decrease when subjected to PAV aging.

In general, introducing the rejuvenators restores the crossover modulus and frequency to values higher than the unrejuvenated PAV aged RAP binders. However, all the investigated rejuvenators did not restore the crossover modulus for the ARAP-NC. In contrast, the investigated rejuvenators could change the crossover frequency to a higher value than the unrejuvenated PAV-aged RAP binders. That suggests that the rejuvenator's synergetic behavior depends on the binder mixed with.

Following the previously discussed results, the VBO rejuvenators increase the aging resistance when introduced to the ARAP-AA. The VBO rejuvenator#1 has a higher viscoelasticity restoration when introduced to the ARAP-AA binder. On the other hand, the PBO rejuvenator #2 restores the viscoelastic components the most when introduced to the ARAP-PMA binder. As suggested by increasing the crossover modulus and frequency, the new SCGO rejuvenator is very promising in rejuvenating the RAP-RS19 binder. When introduced to the ARAP-PMA and ARAP-AA binders, it also shows an acceptable rejuvenation performance.

Table 3-3. Crossover modulus and frequency values of the Investigated Unrejuvenated /Rejuvenated RAP binders.

Asphalt Binder /RAP	Index	RAP*	RAP (PAV)	RAP-Rej. #1 (PAV)	RAP-Rej. #2 (PAV)	RAP-Rej. SCGO (PAV)
NC PG 64-22	G _c * (KPa)	9,950	4,777	4,172	4,073	2,879
	ω _c (Hz)	0.651	0.018	0.138	0.040	0.031
AA PG 64-22	G _c * (KPa)	9,485	3,742	5,283	4,165	4,708
	ω _c (Hz)	0.169	0.011	0.419	0.039	0.328
PMA PG 76-22	G _c * (KPa)	2,899	977	977	1,637	1,049
	ω _c (Hz)	0.012	0.000	0.003	0.004	0.008
RAP-RS19	G _c * (KPa)	11,211	4,972	6,881	8,131	8,339
	ω _c (Hz)	0.530	0.019	0.513	0.211	0.900

*RAP term includes both Artificial RAP and field extracted RAP

3.3.6. Rejuvenators' Efficiency (RE) Analysis.

The previous chemical and rheological illustrated aging indices will be utilized in this section for evaluating the investigated rejuvenators' efficiency. Equations (3-3) is used in evaluating the rejuvenator's chemical efficiency in reducing both carbonyl aging index.

$$RE_{ICO} = \frac{ICO_{Unrejuvenated\ RAP}}{ICO_{Rejuvenated\ Aged\ RAP}} \quad \text{Equation (3-3)}$$

Intermediate and low-temperature rheological performance enhancement by rejuvenators is evaluated through Equations (3-4), (3-5), (3-6), and 3-(7). According to these equations, the rejuvenator is considered efficient when it achieves a RE value higher than a value of 1.0.

$$RE_{\Delta T_c} = 1 + \frac{\Delta T_{cUnrejuvenated\ Aged\ RAP} - \Delta T_{cRejuvenated\ Aged\ RAP}}{\Delta T_{cUnrejuvenated\ Aged\ RAP}} \quad \text{Equation (3-5)}$$

$$RE_{G-R} = \frac{\text{Log } G-R_{Unrejuvenated\ Aged\ RAP}}{\text{Log } G-R_{Rejuvenated\ Aged\ RAP}} \quad \text{Equation (3-6)}$$

$$RE_{G_c^*} = \frac{\text{Log}G_c^* \text{ Rejuevntated Aged RAP}}{\text{Log}G_c^* \text{ Uejuevntated Aged RAP}} \quad \text{Equation (3-7)}$$

$$RE_{\omega_c} = \frac{\omega_c \text{ Rejuevntated Aged RAP}}{\omega_c \text{ Unejuevntated Aged RAP}} \quad \text{Equation (3-8)}$$

Table 3-4 demonstrates the different investigated rejuvenators' efficiency. Both rejuvenators #1 and #2 are chemically efficient for the ARAP-NC binder, reducing the Carbonyl index. They also have higher efficiency with improving the low-temperature thermal cracking resistance. Moreover, they improve the intermediate-temperature performance as they reduce the G-R parameter. However, both rejuvenators are found to perform as softeners since they increase the crossover frequency and do not increase the crossover modulus. The new proposed SCGO rejuvenator is following the same trend. However, it fails to reduce the carbonyl index when introduced to the ARAP-NC binder.

Table 3-4. Different Investigated Rejuvenators' Efficiency Summary

Rejuvenator Efficiency	Asphalt Binder Type	Rejuvenators' Chemical and Rheological Efficiency				
		ICO	ΔT_c	G-R	ω_c	G_c^*
RE#1	ARAP-NC	1.069	1.449	1.258	7.672	0.984
RE#2		1.261	1.329	1.097	2.224	0.981
RE#SCGO		0.993	1.135	1.121	1.746	0.940
RE#1	ARAP-AA	1.104	1.851	1.421	37.688	1.042
RE#2		0.897	1.003	1.091	3.475	1.013
RE#SCGO		1.461	2.086	1.390	29.512	1.028
RE#1	ARAP-PMA	1.141	1.665	1.237	17.070	1.000
RE#2		1.181	2.222	1.189	23.817	1.075
RE#SCGO		1.143	1.700	1.354	48.956	1.010
RE#1	RAP-RS19	0.979	1.580	1.411	26.310	1.038
RE#2		0.974	1.095	1.316	10.821	1.058
RE#SCGO		1.014	1.580	1.705	46.214	1.061

For the ARAP-AA binder, both VBO rejuvenators improve the chemical and rheological performance when introduced to the ARAP binder. The PBO rejuvenator#2 performs moderately with the ARAP-AA binder. However, it did not reduce the carbonyl index when introduced to the ARAP-AA binder. It has lower rejuvenation efficiency when compared to the VBO rejuvenators.

For the ARAP-PMA binder, the PBO rejuvenator#2 has superior rejuvenation efficiency compared to the VBO rejuvenators. In addition, it reduces the oxidation levels of ICO the most compared to the VBO rejuvenators. Moreover, it enhances the low-temperature thermal cracking resistance the most. However, the proposed VBO has the dominant improvement with the intermediate temperature performance when introduced to the ARAP-PMA binder.

For the field extracted RAP-RS19 binder, the proposed SCGO rejuvenator has the most significant rejuvenation efficiency. Moreover, it manages to improve both the chemical and rheological performance of the RAP. On the other hand, both obtained market rejuvenators #1 and #2 cannot reduce the carbonyl index. Compared to the VBO rejuvenators, the PBO rejuvenator has a lower rejuvenation efficiency when introduced to the RAP-RS19.

CHAPTER 4

EVALUATING THE SYNERGY BETWEEN UPCYCLED OFF-SPEC FLY ASH & BIO-BASED REJUVENATORS IN RECYCLED ASPHALT BLENDS

4.1. Phase Objective

The objectives of this phase are:

- Validate the desirable influence of fly ash additives on asphalt binder aging rate.
- Evaluate the synergy of engineered fly ash RAP and two market-available rejuvenators using two different binders (unmodified PG 62-22 and PMA PG 76-22).
- Evaluate the synergy of engineered fly ash RAP and SCGO rejuvenator.

4.2. Materials and Methods

4.2.1. *Experimental Design Overview*

The phase two experimental program is presented in Figure 4-1. The program relies on two different binders as a base in this study: unmodified PG 64-22 binder and Polymer Modified (PMA) PG 76-22 binder. Four OFA, screened from phase I, were mixed with the two types of binders at 10% by mass.

For this phase, a control sample of the binder for each asphalt type with no additives was prepared to serve as a reference. For producing Artificial RAP (ARAP), The binders and blends were exposed to short-term aging using the Rolling Thin Film Oven (RTFO) test

by AASHTO T 240. The RTFO aging was followed by the Pressure Aging Vessel (PAV) test for 20 hours, following AASHTO R 28. Testing samples of each binder and binder blends were conducted on the different investigated ARAP binders. Then, the ARAP binders/ blends were blended with 5% by mass with one of the two on-market rejuvenators or the new SCGO rejuvenator. The two market rejuvenators, Vegetable Based oil (VBO) and Petroleum Based Oil (PBO), are referred to as rejuvenators #1 and #2, respectively. Following the application of the rejuvenators, the samples were put through a second PAV cycle. The testing matrix also included control "non-rejuvenated" PAV-aged ARAP binder/fly ash blends to serve as a baseline for comparison.

Aging characterization of the Binder blends and binders were tested using Fourier-transform infrared spectroscopy (FTIR) to evaluate aging based on the fact that functional groups such as ketone (C=O) and sulfoxides (S=O) increase in asphalt samples with oxidative aging. In addition, aging-dependent rheological behavior was also investigated and utilized to quantify the aging behavior of the samples. Therefore, the testing program includes Low-temperature performance using the bending beam rheometer (BBR) test, per AASHTO PP-42, to measure the low-temperature ductility. Furthermore, the Glover-Rowe (G-R) parameter and crossover modulus (G_c^*) were also evaluated for the Binder blends and binders at all the aging levels and blending combinations. Finally, all samples were tested using two replicates to achieve a coefficient of variation not exceeding 10%.

As mentioned in the previous phase, rejuvenator dosage is determined based on achieving one of the three following conditions: first, restoring the low-temperature grade (PGL) of the binder blend to that of the base binder, or second, restoring the high-temperature grade (PGH) of the binder blend to that of the base binder, or third, achieving ΔT_c equal to -5

[77]. For this study, achieving ΔT_c equal to or less than -5°C was set for choosing the rejuvenator dosage. This criterion led to using a 5% dosage for the rejuvenators.

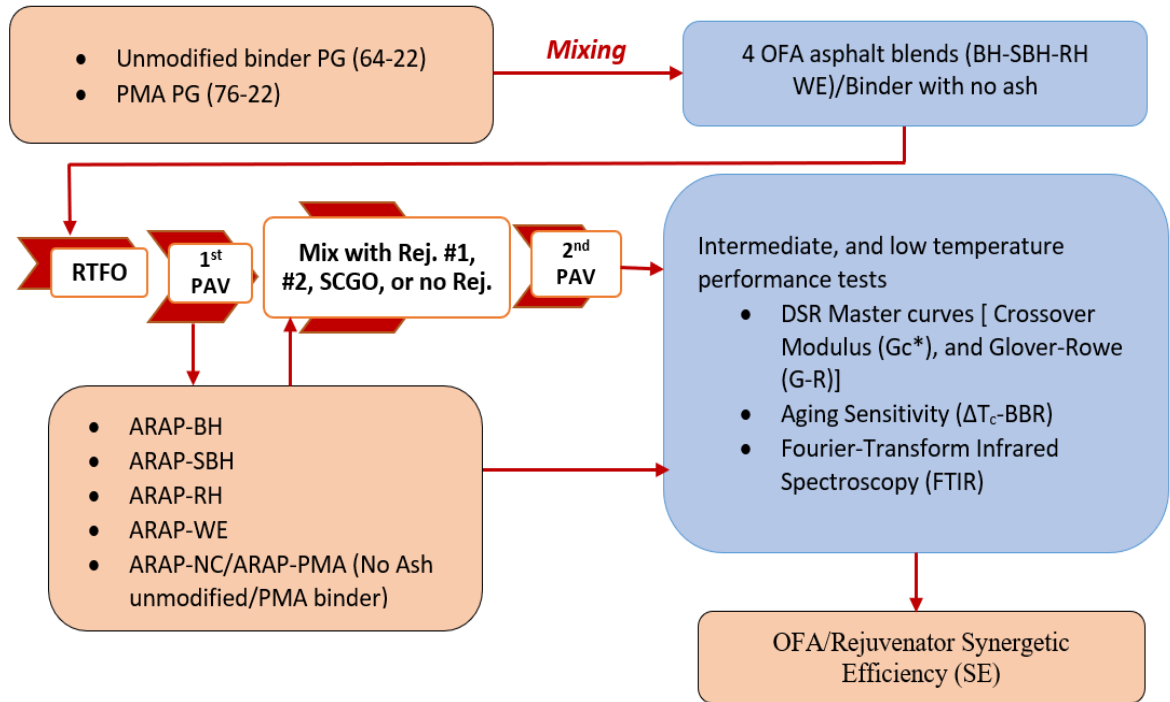


Figure 4-1. Phase II Experimental Program

4.2.2. Fabrication of Binder Blends

The neat binder was preheated in an oven at $135 \pm 5^\circ\text{C}$ for PG 64-22 asphalt and at $155 \pm 5^\circ\text{C}$ for PMA 76-22. Four OFA additives (BH, SBH, RH, and WE) were heated at the same temperature as the binders before blending. Next, the OFA powders were measured and added incrementally into the asphalt binder. A high shear mixer was used to disperse the agglomerates, producing what will be referred to as OFA blends. The blending process was completed over 30 minutes. First, the samples were put through the RTFO and first PAV cycles. Then, the two rejuvenators (#1, #2) and SCGO were blended with OFA blends, following the exact measuring and blending procedure. These were then put through a second PAV cycle. It is important to note that the un-blended (neat) binder samples without

additives were exposed to the same mixing protocol, as a control sample, with and without rejuvenators, to avoid fabrication/conditioning bias influencing the binders/ OFA blends properties.

This process yielded ten ARAP samples (two ARAP binders and eight ARAP OFA blends) and forty PAV aged ARAP samples (two ARAP binders, eight ARAP OFA blends, three rejuvenators, and no rejuvenator).

4.3. Test Results and Discussion

4.3.1. Analysis of Infrared Spectroscopy (FTIR)

The FTIR results, Carbonyl plus Sulfoxide Indices, are shown in Figures 4-2,3 and 4,5 for unrejuvenated and rejuvenated binder/ OFA blends, respectively. The data shown are the average of four replicates. The spectral peaks of interest were for the sulfoxide peak at 1030 cm^{-1} and the carbonyl peak at 1700 cm^{-1} . To analyze the carbonyl and sulfoxide groups with the presence of OFA and rejuvenators, these spectra were normalized using a reference of bending of C–H bonds in the spectrum of the binder sample. The higher the carbonyl and sulfoxide indices, the greater the oxidation level and aging accordingly. Figure 4-2 shows the change in the FTIR results for the unrejuvenated investigated ARAP binder/OFA blends at different aging levels.

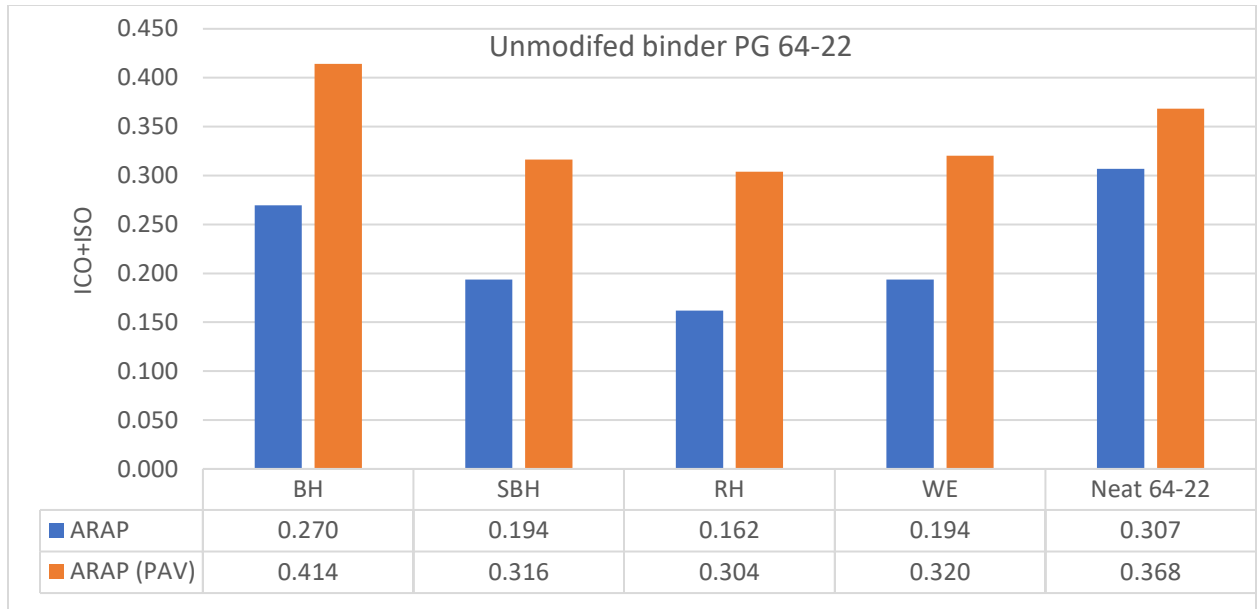


Figure 4-2: The Carbonyl Index (ICO) and The Sulphoxide Index (ISO) of the Investigated Unmodified ARAP Binder/OFA blends at Different Aging Levels.

Figure 4-2 shows that the OFA's presence is generally associated with oxidation-reduction for the investigated ARAP, as suggested by reduced ICO and ISO indices. For the unmodified ARAP binder/OFA blends, the RH-ARAP shows a drop of ICO+ISO indices by 47%, compared to the unmodified ARAP binder. After applying the PAV cycle on the ARAP binder/OFA blends, three out of the four OFA are associated with an oxidation-reduction compared to the unmodified ARAP PAV-aged binder. This suggests that the OFA blends are aging slower than the binder.

Figure 4-3 shows PMA ARAP binder/ OFA blends results for ICO+ISO indices. The results suggest that the presence of OFA, except for RH, is associated with lower aging levels than the ARAP-PMA binder. ARAP-BH blend shows a drop of oxidation indices by 24% compared to the ARAP-PMA binder.

The same trend continues after applying PAV aging cycle on the investigated ARAP binder/ OFA blends. ARAP-BH shows the maximum drop of oxidation indices by 37% compared to that of the ARAP-PMA PAV-aged binder. Studies have shown that some polymer-modified binders tend to show a higher degree of stiffening due to aging. For example, Styrene-Butadiene-Styrene (SBS) modified binders are especially prone to molecular breakdown due to oxidation, which leads to significant loss of the elastic response [45], [46]. The observed results for the FTIR agree with the literature showing a higher rate of formation of oxidative compounds.

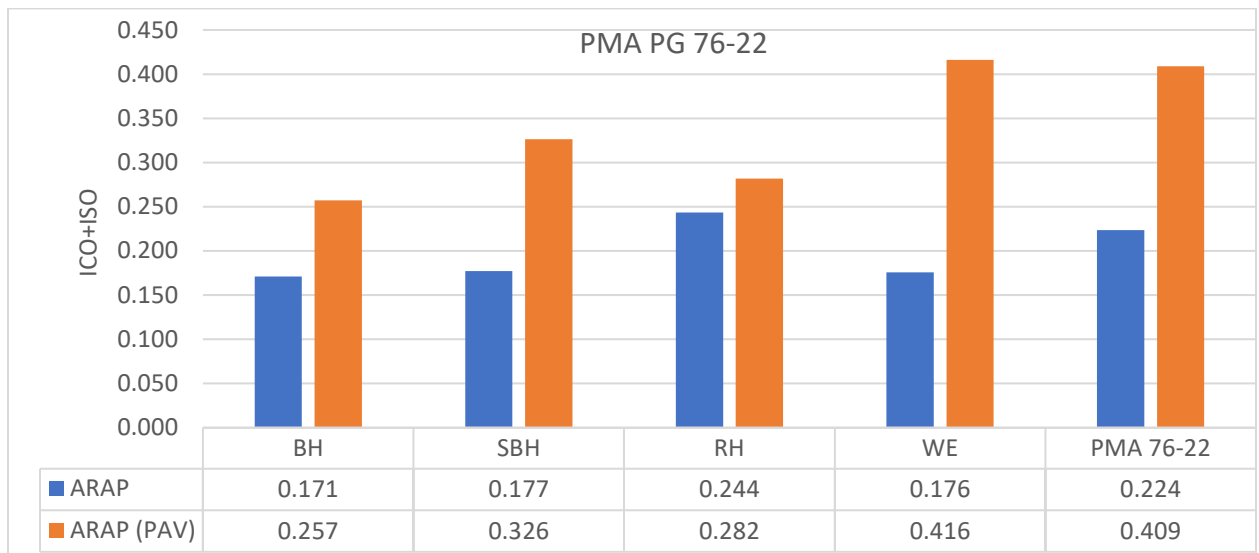


Figure 4-3: The Carbonyl Index (ICO) and The Sulphoxide Index (ISO) of the Investigated PMA ARAP Binder/ OFA blends at Different Aging Levels.

As mentioned above, after fabricating the different ARAP binder/ OFA blends, the samples are blended with the rejuvenators and subjected to the second round of PAV aging. Figures 3-4 and 5 show the results of the ICO+ISO for all the samples with and without rejuvenators after the second round of PAV for Unmodified and PMA ARAP binder/ OFA blends, respectively.

In order to discuss the results in Figure 4-4, first, we will discuss the unmodified PG64-22 binder. The results show that the unmodified ARAP PAV-aged binder responded to the introduction of all three rejuvenators with a reduction in the oxidation indices. In addition, the PBO, rejuvenator #2, shows higher oxidation resistance than the other two rejuvenators when introduced to the unmodified ARAP PAV-aged binder.

Note that the rejuvenators are introduced after the ARAP binder/ OFA blends are produced. As for the ARAP OFA blends, two trends can be observed. The first trend is observed with ARAP-WE, ARAP-RH, and ARAP-SBH. The aging indices are already lower than the unmodified ARAP-NC PAV-aged binder. Therefore, the introduction of the rejuvenators did not seem to change the aging sensitivity of these ARAP OFA blends, except with ARAP-RH/ Rej.#1. The second trend is observed for the ARAP-BH blend, where applying a cycle of PAV on it led to a significant increase in the oxidation indices. Introducing the rejuvenator reduced the indices values for the ARAP-BH blend, yet it stayed higher than the rejuvenated unmodified ARAP binder.

The SCGO rejuvenator consistently improved all ARAP OFA blends regarding oxidation indices, except with the SBH blend, indicating high synergetic interaction with OFA. The most reduced value of the ICO+ISO was observed with SCGO with ARAP-RH blend, with about a 21% reduction in ICO+ISO compared to the unrejuvenated Unmodified PAV-aged ARAP binder. In general, the overall influence of the SCGO is comparable to the market rejuvenators.

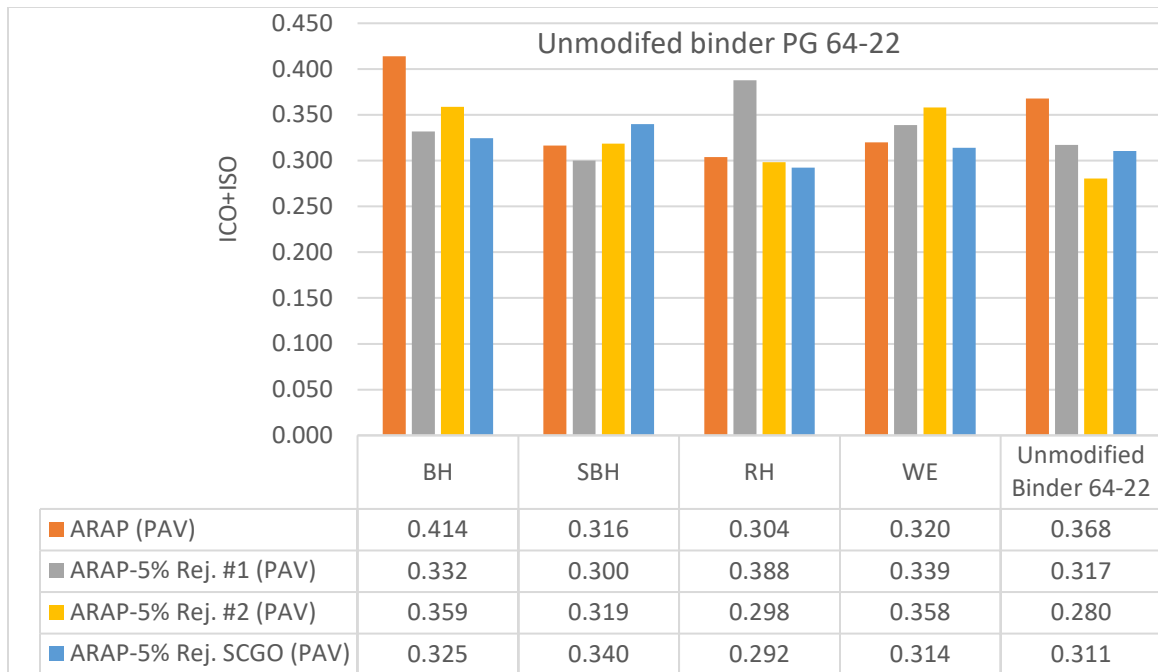


Figure 4-4: The Carbonyl Index (ICO) + The Sulphoxide Index (ISO) of the Investigated Rejuvenated Unmodified ARAP Binder/ OFA blends at Different Aging Levels.

Figure 4-5 shows the PMA ARAP binder/ OFA blends results. The discussion of the presented results also focuses on the ARAP-PMA binder, ARAP OFA blends, and the introduction of the new SCGO. The indices for the ARAP-PMA binder show a significant reduction with the introduction of all three rejuvenators, especially with the PBO rejuvenator #2. Regarding the ARAP OFA blends, all ARAP OFA blends, except for ARAP-WE, continue to show a lower unrejuvenated oxidation index value after exposure to the PAV cycle than the PMA ARAP PAV-aged binder. The introduction of the rejuvenators further reduced the oxidation index value. The VBO rejuvenator #1 lowers the oxidation indices when introduced to ARAP-SBH and ARAP-WE blends. Introducing rejuvenator #2 to all the investigated ARAP OFA blends is associated with oxidation indices reduction.

When introduced to the ARAP OFA blends, the new SCGO rejuvenator follows the rejuvenator #1 trend. It is found to be associated with reducing the aging level when introduced to ARAP-SBH and ARAP-WE. Rejuvenator #2 shows a dominating association with a reduced oxidation level compared to Rejuvenator #1 and the SCGO. These findings align with the results demonstrated in the previous phase.

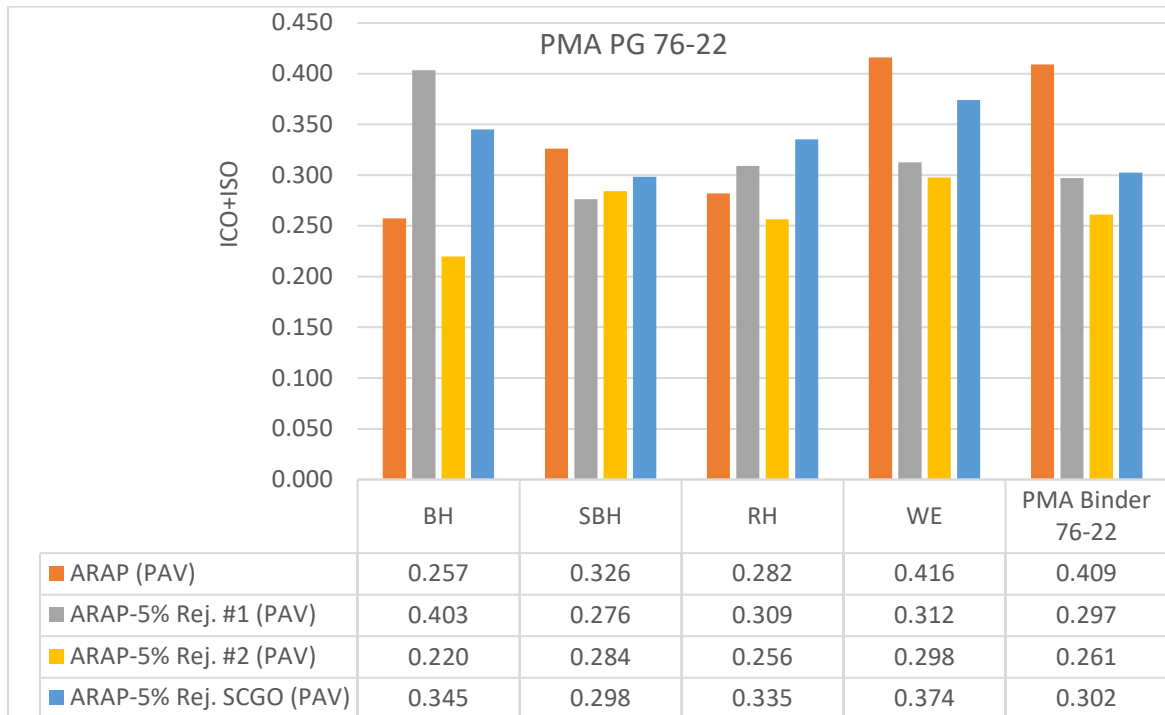


Figure 4-5: The Carbonyl Index (ICO) + The Sulphoxide Index (ISO) of the Investigated Rejuvenated PMA ARAP Binder/ OFA blends at Different Aging Levels.

As mentioned, the asphalt binder aging process is very complex. Two main mechanisms are associated with such a process: changes in its chemical composition and rheological properties. The chemical composition change is irreversible, including oxidation, loss of volatiles, and formation of highly polar functional groups. On the other hand, the rheological properties change a reversible process related to physical hardening attributed to the reorganization of the binder molecules [83].

Therefore, this study also relies on characterizing aging-dependent rheological properties. The tests used in the program can evaluate the change in the binder/Asphalt blends fundamental rheological performance under the different aging levels and concerning the presence of rejuvenation.

4.3.2. Low-Temperature Performance Evaluation

Figures 4-6 and 7 demonstrate the low-temperature rheological performance change for the unmodified and PMA ARAP binder/ OFA blends without rejuvenation, respectively.

As demonstrated in Figure 4-6, the presence of OFA generally improves the low-temperature performance of the unmodified ARAP OFA blends compared to the unmodified ARAP binder. ARAP-RH and ARAP-SBH have higher low-temperature relaxation and thermal cracking resistance by 336% and 308%, respectively, compared to the unmodified ARAP binder. It is expected that after applying another cycle of PAV aging on the binder/OFA blends, their relaxation ability will deteriorate. However, the OFA blends, except with ARAP-BH blend, are showing a slower rate of aging compared to the unmodified ARAP PAV-aged binder.

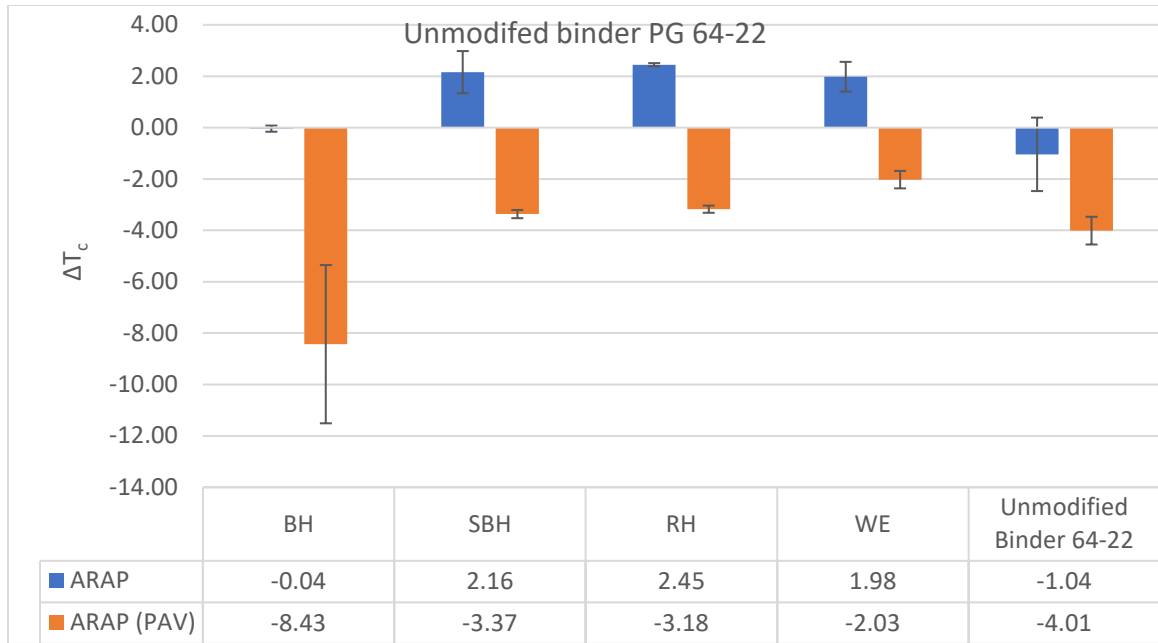


Figure 4-6. ΔT_c of the Investigated Unmodified ARAP Binder/ OFA blends at Different Aging Levels.

Figure 4-7 demonstrates that the presence of OFA, except with RH, is associated with improving the low-temperature performance of the PMA ARAP compared to the ARAP-PMA binder. ARAP-SBH shows higher resistance to thermal cracking by 211% compared to the ARAP-PMA binder. After applying a PAV cycle on the ARAP binder/OFA blends, it is expected to have lower ΔT_c , as the binder/OFA blends loses its ability to relax at lower temperature. However, the OFAs shows the ability to slow the aging rate compared to the PMA ARAP PAV-aged binder.

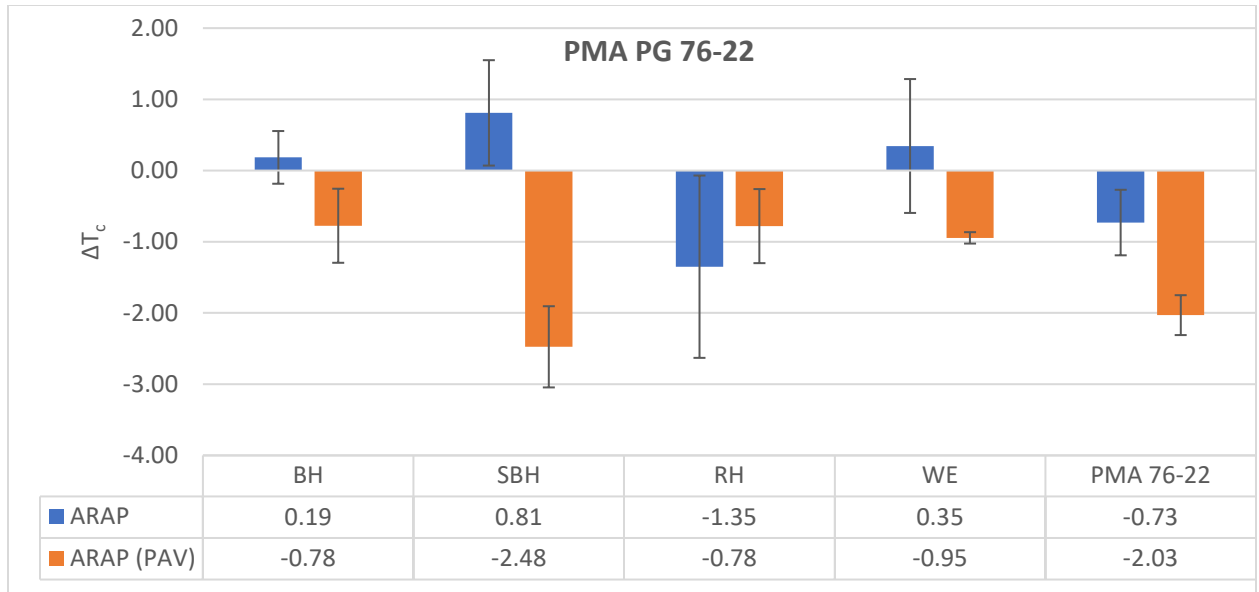


Figure 4-7: ΔT_c of the Investigated PMA ARAP Binder/ OFA blends at Different Aging Levels.

Figures 4-8 and 9 show the results of the ΔT_c for all the ARAP samples with and without rejuvenators after the second round of PAV for unmodified and PMA binder, respectively.

For the ARAP-NC binder, Figure 4-8 shows that introducing the three rejuvenators is associated with an improvement in thermal cracking resistance as measured by ΔT_c . For the ARAP OFA blends, the two on-market rejuvenators perform positively when introduced to both ARAP-BH and ARAP-SBH blends. Compared to the unrejuvenated Unmodified ARAP binder, introducing the VBO rejuvenator#1 to the different investigated ARAP OFA blends is associated with improving low-temperature relaxation, except with ARAP-RH blend. The PBO rejuvenator #2 is associated with improving the thermal cracking resistance when introduced to ARAP-SBH, and ARAP-RH, compared to the unrejuvenated unmodified ARAP binder.

The SCGO rejuvenator performs positively with all ARAP OFA blends compared to the unmodified ARAP binder. Furthermore, SCGO rejuvenator has a significant synergetic influence with ARAP-BH, ARAP-RH, and ARAP-WE blends compared to their corresponding unrejuvenated ARAP OFA blends. Overall, SCGO's interaction with ARAP-RH and ARAP-WE blends improves the thermal cracking resistance compared to all ARAP OFA blends/rejuvenation combinations.

These results show that the effectiveness of the blends to maintain ductility depends on their corresponding sources/types. Moreover, selecting the right combination of aging retarding additives can significantly improve the binder's durability and slow the loss of ductility.

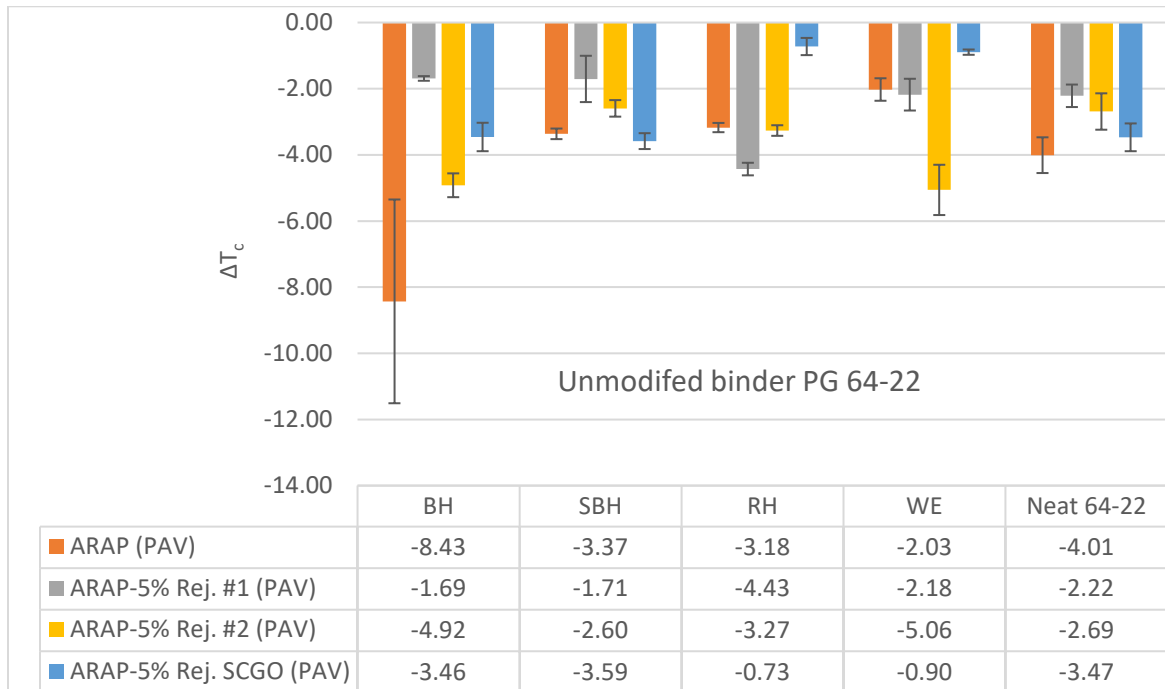


Figure 4-8: ΔT_c of the Investigated Rejuvenated Unmodified ARAP Binder/ OFA blends at Different Aging Levels.

Figure 4-9 shows the results of the ΔT_c for all the ARAP samples with and without rejuvenators after the second round of PAV for the PMA binder/OFA blends. Thermal cracking performance is enhanced for the ARAP-PMA binder when the three rejuvenators are introduced, as measured by ΔT_c .

As for the ARAP OFA blends, PBO rejuvenator #2 with ARAP OFA blends shows a reversal of ΔT_c values. That strongly conforms with phase II results. The VBO rejuvenator #1 positively influenced ARAP-WE and ARAP-SBH blends compared to their corresponding unrejuvenated ARAP OFA blends.

Regarding the SCGO rejuvenator, it is found that it cannot match the gains of the market-ready rejuvenators. However, SCGO rejuvenator, when introduced to ARAP-BH, ARAP-SBH, and ARAP-WE blends, showed an improvement in low-temperature ductility compared to the unrejuvenated PMA ARAP PAV-aged binder. It is important to note that all binder/OFA blends results are within acceptable performance as recommended by Anderson et al. (2011) [79]. In general, the PMA binder/OFA blends results are consistent with the hypothesis that such a binder class loses its ductility capacity with aging. This suggests that the improvements in the ΔT_c measured values are a combination of aging retarding due to the fly ash and softening due to the rejuvenators.

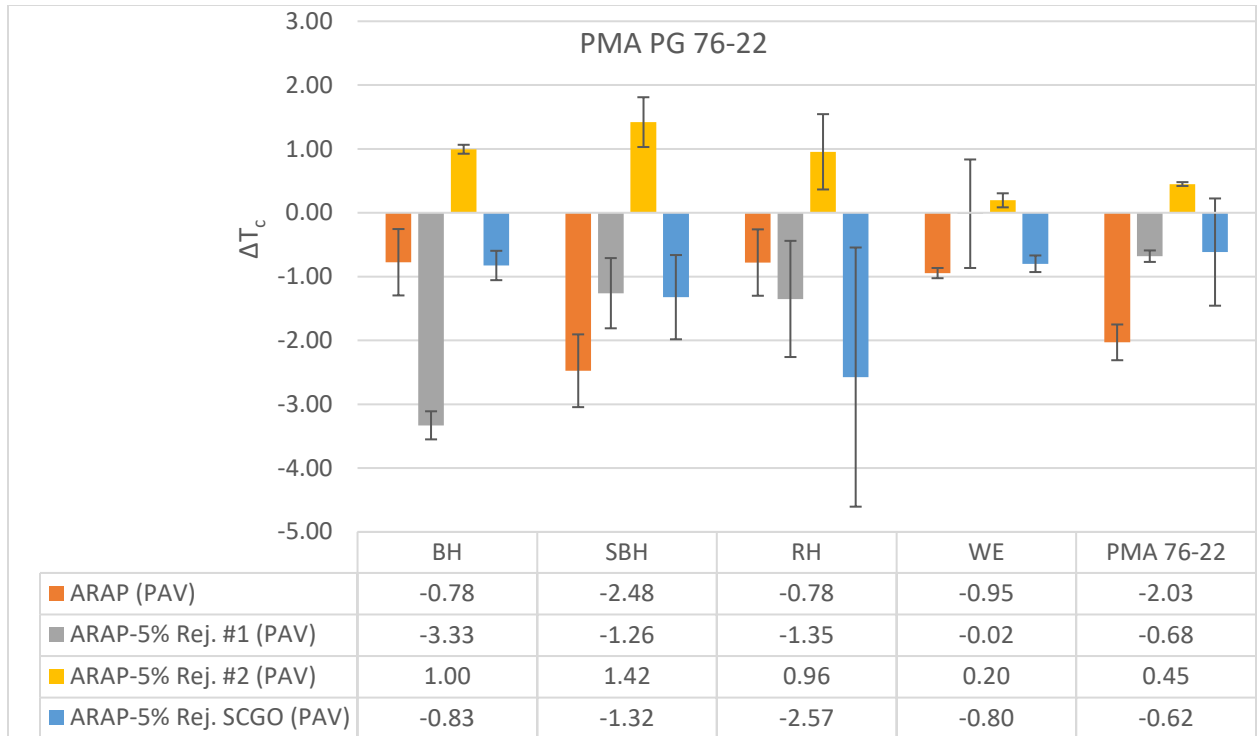


Figure 4-9: ΔT_c of the Investigated Rejuvenated PMA ARAP Binder/OFA blends at Different Aging Levels.

Figure 4-10 validates the relationship between the FTIR aging indices and the measured ΔT_c values for the blends. The ICO and ISO indices fairly correlate with the ΔT_c values with $R^2 = 0.53$. However, to understand what Index better correlates with the ΔT_c .

The relaxation at a lower temperature is associated with the Carbonyl Index ICO, translated in $R^2 = 0.66$. On the other hand, the sulfoxide index ISO did not show a good correlation to aging with $R^2 = 0.32$, which agrees with similar findings from previous research [82], [84]–[86].

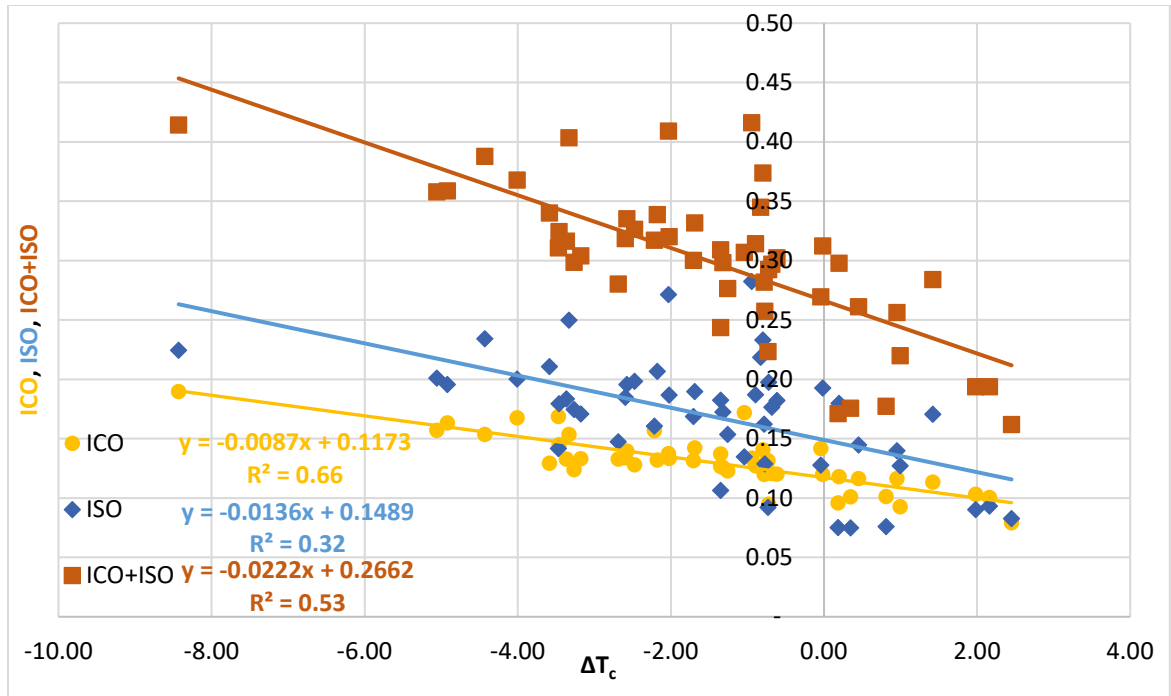


Figure 4-10. Correlation between The Carbonyl Index (ICO), The Sulphoxide Index (ISO), ICO+ISO, and ΔT_c of the Investigated Rejuvenated Unmodified and PMA Binder/OFA blends.

4.3.3. Grover-Rowe Parameter (G-R)

The G-R parameter is an aging indicator calculated from the DSR frequency sweep test results, used to evaluate the cracking resistance of an asphalt binder. Durability thresholds were translated into G-R = 180 kPa (corresponding to a 5 cm ductility and 0.0009 MPa/s for the initial DSR function) to indicate the onset of cracking (warning). G-R = 600 kPa (corresponding to 3 cm ductility, 0.003 MPa/s DSR function) was used to indicate extensive block cracking (limit) [39], [78].

Figures 4-11 and 12 demonstrate the G-R results for unmodified and PMA ARAP binder/OFA blends without rejuvenation. Figure 4-11 shows that OFA reduces the cracking resistance compared to the unmodified ARAP binder, except with the ARAP-SBH blend.

Only the ARAP-BH blend is found to exceed the extensive block cracking limit. The ARAP-BH blend has lower cracking resistance by 375% than the ARAP-NC binder.

After applying the additional PAV cycle on the investigated ARAP binder/ OFA blends, all ARAP binder/OFA blends samples significantly increased G-R values, indicating a lesser intermediate-temperature cracking resistance.

For the PMA ARAP binder/OFA blends, Figure 4-12 shows that OFA presence influences the intermediate temperature cracking resistance negatively compared to the ARAP-PMA binder. PMA ARAP binder/ OFA blends are found to exceed the extensive cracking block indication. However, after applying an additional PAV cycle on the investigated PMA ARAP binder/ OFA blends, ARAP-SBH and ARAP-RH blends have higher cracking resistance than ARAP-PMA binder. The ARAP-BH blend continues to perform poorly at all levels of aging.

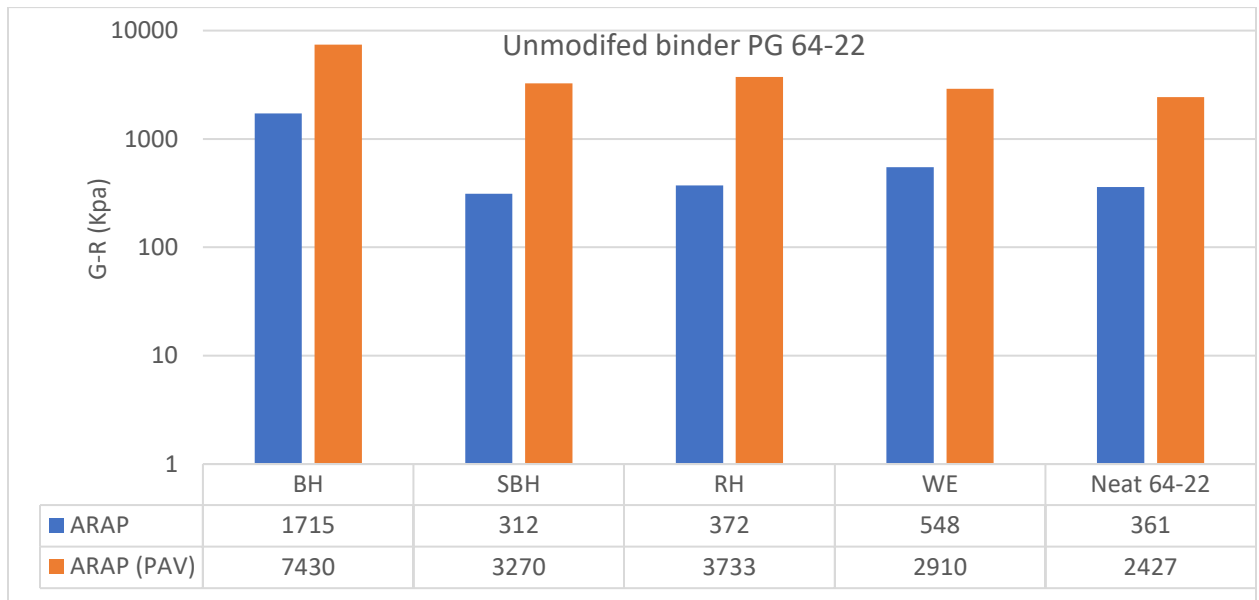


Figure 4-11: G-R Parameter of the Investigated Unmodified ARAP Binder/OFA blends at Different Aging Levels.

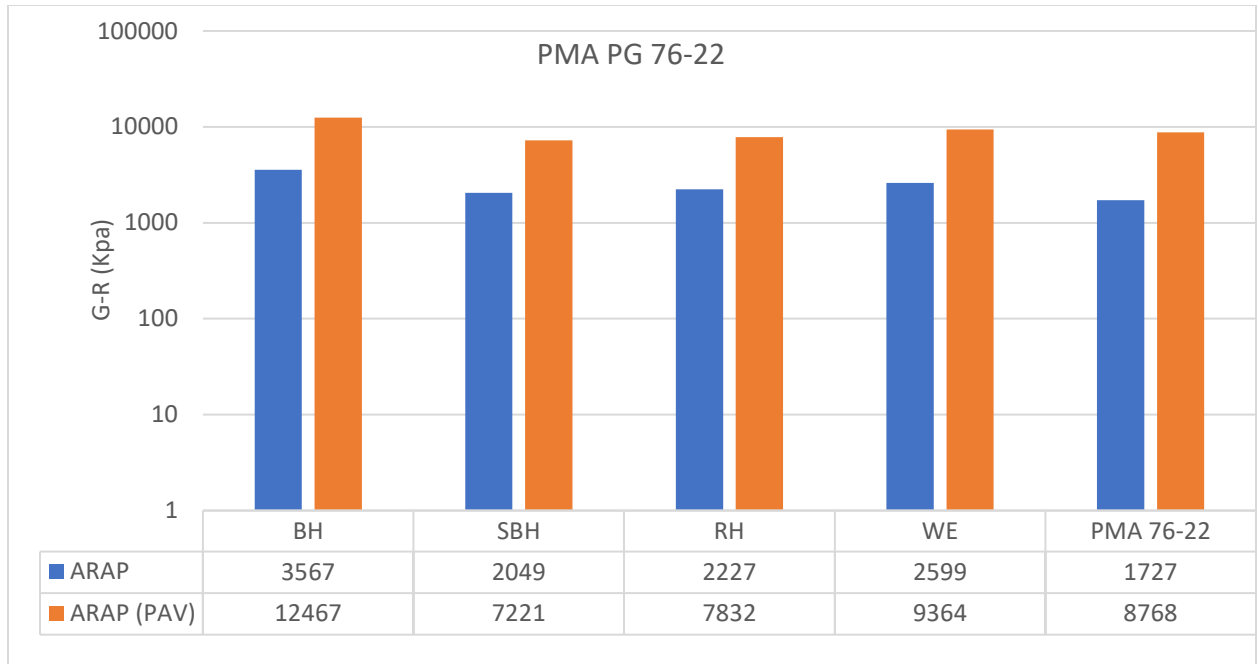


Figure 4-12: G-R Parameter of the Investigated PMA ARAP Binder/ OFA blends at Different Aging Levels.

Figures 4-13 and 14 illustrate the G-R results for unrejuvenated and rejuvenated unmodified and PMA ARAP binder/OFA blends, respectively.

Concerning the ARAP-NC binder, the rejuvenator's introduction is associated with reducing the G-R parameters, which translates to enhanced cracking resistance. Furthermore, both VBO rejuvenators #1 and SCGO have a superior influence on the ARAP-NC binder than the PBO rejuvenator #2.

Figure 4-13 shows that introducing the rejuvenators to the unmodified ARAP OFA blends enhances the intermediate temperature cracking resistance, as measured by the G-R parameter. The VBO rejuvenator #1 is found to positively enhance the cracking resistance when blended with all ARAP OFA blends, compared to their corresponding unrejuvenated ARAP OFA blends. Furthermore, rejuvenator #1 is found to have higher performance

when introduced to the ARAP-WE blend. On the other hand, the PBO rejuvenator #2 performs the worst compared to the other two rejuvenators. However, introducing rejuvenator #2 to the different investigated ARAP OFA blends improves the intermediate temperature cracking resistance. Furthermore, rejuvenator #2 is found to have higher performance when blended with the ARAP-SBH blend.

The new SCGO shows the highest reduction in the G-R (signifying improvement in cracking resistance) compared to the unrejuvenated ARAP OFA blends. Furthermore, SCGO rejuvenator with all types of OFA shows a significant synergetic influence on cracking resistance compared to its corresponding rejuvenated unmodified ARAP binder.

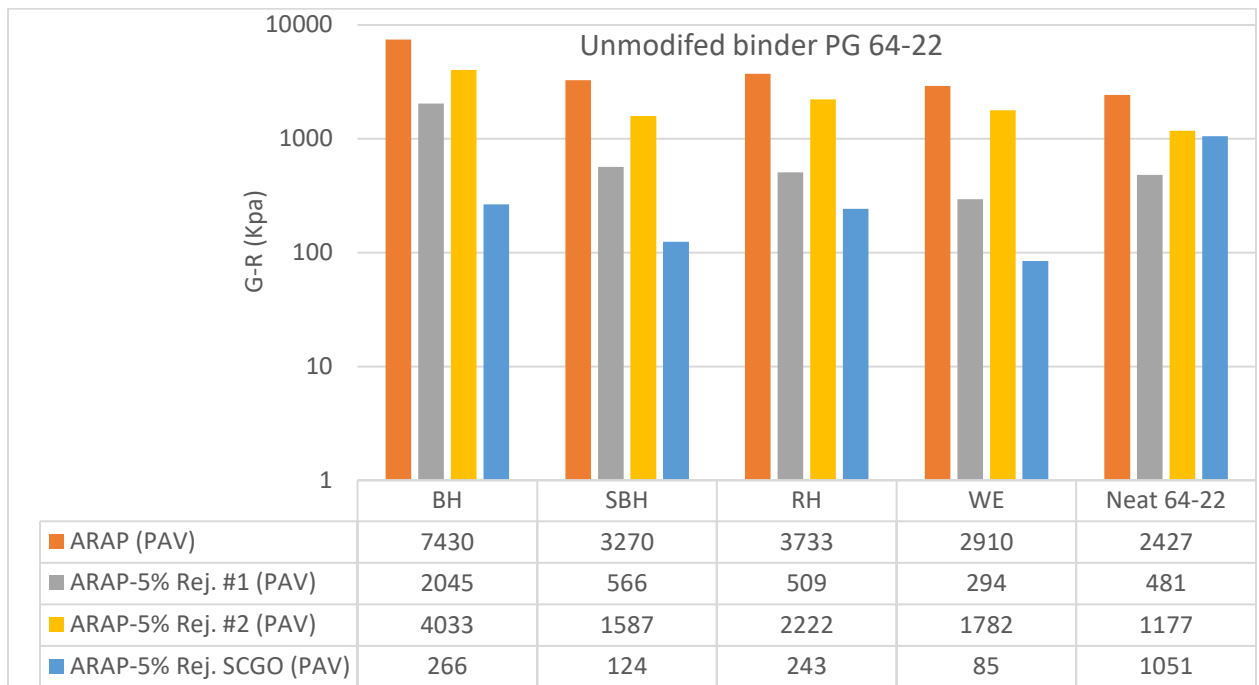


Figure 4-13: G-R Parameter of the Investigated Rejuvenated Unmodified ARAP Binder/ OFA blends at Different Aging Levels.

Following the unmodified binder trends, Figure 4-14 shows that the G-R parameter drops significantly when the ARAP-PMA binder is blended with the rejuvenators. Again, both

VBO rejuvenators #1 and SCGO have a superior influence on the ARAP-PMA binder than the PBO rejuvenator #2.

Introducing the rejuvenators to the PMA ARAP OFA blends enhances their intermediate temperature cracking resistance, as measured by the G-R parameter. The VBO rejuvenator #1 is found to positively enhance the cracking resistance when blended with all ARAP OFA blends, compared to their corresponding unrejuvenated ARAP OFA blends. Furthermore, rejuvenator #1 is found to have higher performance when introduced to the ARAP-WE. On the other hand, the PBO rejuvenator #2 performs the worst compared to the other two rejuvenators.

Nevertheless, introducing rejuvenator #2 to the different investigated ARAP OFA blends improves their intermediate temperature cracking resistance. Furthermore, rejuvenator #2 is found to have higher performance when blended with ARAP-SBH.

SCGO rejuvenator follows the same trend with PMA ARAP binder/ OFA blends. Introducing the new SCGO rejuvenator to the investigated ARAP OFA blends drops the G-R (improving cracking resistance) compared to their unrejuvenated ARAP OFA blends. Overall, SCGO with all ARAP OFA blends shows a significant positive synergetic influence on cracking resistance, compared to the other two rejuvenators. However, only the ARAP-BH blend experienced an improvement with the cracking resistance when mixed with SCGO rejuvenator compared to its corresponding rejuvenated ARAP-PMA binder.

Nevertheless, it is worth mentioning that all 24 ARAP OFA blends/rejuvenator combinations utilized with both binders enhance the intermediate temperature cracking resistance compared to the unrejuvenated PAV aged ARAP binders.

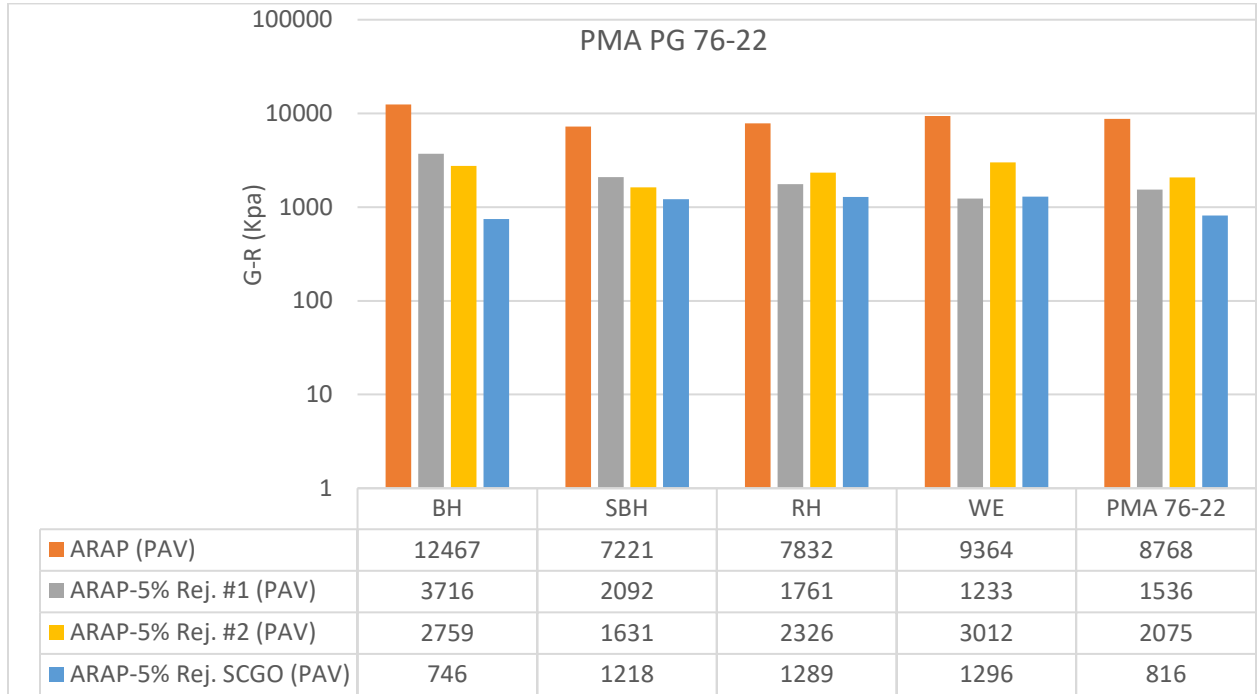


Figure 4-14: G-R Parameter of the Investigated Rejuvenated PMA ARAP Binder/ OFA blends at Different Aging Levels.

4.3.4. Crossover Modulus and Frequency (G_c^* , ω_c)

Table 4-1 shows the crossover modulus, and frequency results for the different investigated unrejuvenated/rejuvenated ARAP binders/OFA blends. For the unmodified ARAP-NC binder/OFA blends, the presence of OFA, except with ARAP-BH, is associated with an increase to both viscous and elastic components as suggested by the increase in the crossover modulus. Conversely, the crossover frequency drops by the presence of the OFA compared to the ARAP-NC binder.

The crossover modulus and frequency for all the investigated unmodified ARAP binder/OFA blends consistently drop after applying an additional cycle of PAV aging. However, the presence of OFA, except with ARAP-BH, is associated with an increase in the crossover modulus compared to the ARAP-NC PAV-aged binder. Following the previous trend, the crossover frequency drops by the presence of the OFA compared to the ARAP-NC binder.

For the PMA ARAP binder/OFA blends, Table 4-1 illustrates that the presence of OFA decreases the viscous and elastic components in ARAP Asphalt blends compared to the ARAP-PMA binder, as measured by the drop in the crossover modulus and frequency.

After applying an additional cycle of PAV on the investigated ARAP binder/ OFA blends, the crossover modulus and frequency consistently drop. However, as suggested by increasing crossover modulus, the PMA ARAP OFA blends show less aging susceptibility than the ARAP-PMA PAV-aged binder.

For rejuvenators, introducing the rejuvenators to the ARAP-NC binder did not increase the asphalt binder's crossover modulus, as it is supposed to perform. However, the rejuvenator's introduction is associated with increasing the ARAP-NC binder's crossover frequency.

For ARAP-NC OFA blends, rejuvenator #1 and #2's introduction to the OFA blends did not enhance aging resistance compared to their corresponding ARAP OFA blends after an additional cycle of PAV aging, except with ARAP-WE/rejuvenator#1. However, when introduced to ARAP-SBH and ARAP-WE blends, both market rejuvenators enhance their viscoelastic components compared to the rejuvenated ARAP-NC PAV-aged binder.

The new SCGO is found to perform significantly better compared to the other two rejuvenators. In addition, the synergy of ARAP OFA blends, when mixed with SCGO rejuvenator, is found to significantly improve the aging resistance compared to their corresponding unrejuvenated ARAP OFA blends and rejuvenated ARAP-NC PAV-aged binder. These significant findings promote the physio-chemical interaction between the ash and rejuvenators.

For the ARAP-PMA binder, Table 4-1 shows that introducing the rejuvenators to the ARAP PMA improves the aging resistance as evaluated through the crossover modulus and frequency. As for the ARAP OFA blends, introducing rejuvenator #1 to the ARAP OFA blends is less beneficial for aging resistance than the unrejuvenated ARAP OFA blends. On the other hand, rejuvenator #2's introduction to the ARAP OFA blends is associated with enhancing the aging resistance as measured by crossover modulus and frequency. Both rejuvenators #1 and #2, when introduced to the different ARAP OFA blends, improve the aging resistance compared to the rejuvenated ARAP-PMA PAV-aged binder.

SCGO rejuvenator moderately enhances the aging resistance as suggested by crossover modulus and frequency when introduced to the PMA ARAP OFA blends compared to the rejuvenated ARAP-PMA PAV-aged binder and unrejuvenated ARAP OFA blends. This promotes the positive role of the OFA/rejuvenators' synergetic effect on the binder.

Table 4-1. Crossover modulus and frequency values of the Investigated Unrejuvenated /Rejuvenated ARAP binders/ OFA blends.

<i>Asphalt Binder /RAP</i>	<i>Index</i>	<i>ARAP</i>	<i>RAP (PAV)</i>	<i>RAP-Rej. #1 (PAV)</i>	<i>RAP-Rej. #2 (PAV)</i>	<i>RAP-Rej. SCGO (PAV)</i>
<i>NC PG 64-22</i>	G_c^* (KPa)	9,948	4,778	4,171	4,131	2,876
	ω_c (Hz)	5.04	0.15	0.94	0.33	0.24
<i>BH</i>	G_c^* (KPa)	6,384	3,644	2,890	2,921	7,273
	ω_c (Hz)	0.33	0.02	0.10	0.04	3.79
<i>SBH</i>	G_c^* (KPa)	12,867	5,801	4,983	5,096	9,118
	ω_c (Hz)	2.53	0.12	0.98	0.28	9.0
<i>RH</i>	G_c^* (KPa)	12,361	5,290	4,636	3,909	5,883
	ω_c (Hz)	2.60	0.09	0.69	0.12	3.88
<i>WE</i>	G_c^* (KPa)	10,851	5,281	5,626	4,844	9,060
	ω_c (Hz)	1.92	0.13	1.49	0.23	10.58
<i>PMA 76-22</i>	G_c^* (KPa)	2,900	977	977	1,638	1,049
	ω_c (Hz)	3.35	0.06	0.59	1.10	1.56
<i>BH</i>	G_c^* (KPa)	2,814	1,471	1,007	2,462	1,931
	ω_c (Hz)	1.18	0.08	0.10	1.32	4.05
<i>SBH</i>	G_c^* (KPa)	2,689	1,636	1,417	3,240	2,027
	ω_c (Hz)	2.11	0.22	0.77	4.02	2.40
<i>RH</i>	G_c^* (KPa)	2,015	1,298	1,083	2,437	1,377
	ω_c (Hz)	1.46	0.12	0.60	1.57	1.26
<i>WE</i>	G_c^* (KPa)	1,898	1,198	977	1,872	1,279
	ω_c (Hz)	1.02	0.07	0.89	0.79	1.18

4.3.5. OFA/Rejuvenator Synergetic Efficiency (SE)

The previous chemical and rheological illustrated aging indices will be utilized in this section for evaluating the OFA/rejuvenator synergetic efficiency. Equation (4-1) evaluates the OFA/rejuvenator's chemical synergetic efficiency in reducing carbonyl and sulfoxide aging indices.

$$SE_{ICO+ISO}\% = \frac{-(ICO+ISO_{rejuvenated\ ARAP\ Blend} - ICO+ISO_{rejuvenated\ ARAP\ Binder})}{ICO+ISO_{Unrejuvenated\ Aged\ ARAP\ Binder}}\% \quad \text{Equation (4-1)}$$

Intermediate and low-temperature rheological performance enhancement by OFA/rejuvenator synergy is evaluated through Equations (4-2, 3, 4, and 5). According to these equations, the OFA/rejuvenator synergy is considered efficient when it achieves a positive SE value.

$$SE_{\Delta T_c}\% = \frac{\Delta T_c_{Rejuvenated\ ARAP\ Blend} - \Delta T_c_{Rejuvenated\ ARAP\ Binder}}{|\Delta T_c_{Unrejuvenated\ Aged\ ARAP\ Binder}|}\% \quad \text{Equation (4-2)}$$

$$SE_{G-R}\% = \frac{-(G-R_{rejuvenated\ ARAP\ Blend} - G-R_{rejuvenated\ ARAP\ Binder})}{G-R_{Unrejuvenated\ Aged\ ARAP\ Binder}}\% \quad \text{Equation (4-3)}$$

$$SE_{G_c^*}\% = \frac{G_c^*_{Rejuvenated\ ARAP\ Blend} - G_c^*_{Rejuvenated\ ARAP\ Binder}}{G_c^*_{Unrejuvenated\ Aged\ ARAP\ Binder}}\% \quad \text{Equation (4-4)}$$

$$SE_{\omega_c}\% = \frac{\omega_c_{Rejuvenated\ ARAP\ Blend} - \omega_c_{Rejuvenated\ ARAP\ Binder}}{\omega_c_{Unrejuvenated\ Aged\ ARAP\ Binder}}\% \quad \text{Equation (4-5)}$$

Table 4-2: OFA/Rejuvenator Synergetic Efficiency (SE)

Binder Type	Rejuvenator Type	ARAP OFA blends	OFA/Rejuvenator Synergetic Efficiency (SE) %				
			ICO+ISO	ΔT_c	G-R	G_c^*	ω_c
NC 64-22	Rej. #1	ARAP-BH	-4%	13%	-64%	-27%	-565%
		ARAP-SBH	5%	13%	-3%	17%	29%
		ARAP-RH	-19%	-55%	-1%	10%	-169%
		ARAP-WE	-6%	1%	8%	30%	369%
	Rej. #2	ARAP-BH	-21%	-56%	-118%	-25%	-194%
		ARAP-SBH	-10%	2%	-17%	20%	-30%
		ARAP-RH	-5%	-14%	-43%	-5%	-138%
		ARAP-WE	-21%	-59%	-25%	15%	-66%
	SCGO Rej.	ARAP-BH	-4%	0%	32%	92%	2389%
		ARAP-SBH	-8%	-3%	38%	131%	5928%
		ARAP-RH	5%	68%	33%	63%	2450%
		ARAP-WE	-1%	64%	40%	129%	6964%
PMA 76-22	Rej. #1	ARAP-BH	-26%	-131%	-25%	3%	-781%
		ARAP-SBH	5%	-29%	-6%	45%	298%
		ARAP-RH	-3%	-33%	-3%	11%	23%
		ARAP-WE	-4%	33%	3%	0%	474%
	Rej. #2	ARAP-BH	10%	27%	-8%	84%	351%
		ARAP-SBH	-6%	48%	5%	164%	4660%
		ARAP-RH	1%	25%	-3%	82%	760%
		ARAP-WE	-9%	-13%	-11%	24%	-485%
	SCGO Rej.	ARAP-BH	-10%	-10%	1%	90%	3968%
		ARAP-SBH	1%	-35%	-5%	100%	1336%
		ARAP-RH	-8%	-96%	-5%	34%	-467%
		ARAP-WE	-18%	-9%	-5%	23%	-601%

Table 4-2 demonstrates the different investigated OFA/rejuvenators' synergetic efficiency.

For the unmodified NC binder, rejuvenator #1 has a solid synergetic influence when introduced to ARAP-SBH, which enhances the chemical aging indices and intermediate and low-temperature rheological performance. The VBO rejuvenator#1 is found to have a consistent positive rheological influence when introduced to ARAP-WE. When introduced to the different investigated ARAP OFA blends, the PBO rejuvenator#2 shows low synergetic efficiency. On the other hand, the new proposed SCGO rejuvenator shows dominant positive synergetic influence with all the investigated ARAP OFA blends.

Its more significant synergetic influence appears when blended with ARAP-RH blend, enhancing measured chemical and rheological indices. The VBO rejuvenators generally perform better than the PBO rejuvenator when introduced to the different investigated ARAP OFA blends, especially with ARAP-WE.

For the PMA binder, the PBO rejuvenator#2 is found to have superior synergetic efficiency with the ARAP OFA blends, except with ARAP-WE, when compared to the VBO rejuvenators. The VBO rejuvenator #1 had a strong influence when introduced to ARAP-WE. The new proposed SCGO rejuvenator is found to perform fairly with both ARAP-BH and ARAP-SBH.

According to the above-illustrated results, only rejuvenator#2 and SCGO rejuvenator will be utilized with RH, SBH, and WE OFA in the mixture level testing to validate these significant findings in the next phase.

CHAPTER 5

EVALUATING THE INFLUENCE OF THE PROPOSED FLY ASH PRODUCT ON ASPHALT MIXTURES WITH DIFFERENT RAP RATIOS

5.1. Phase Objective

Three main milestones were defined for Phase III of the study:

- Produce the new fly ash products by utilizing asphalt binder rejuvenators as a delivery system for OFA.
- Validate the desirable influence of fly ash products on asphalt mixture high, intermediate, and low-temperature performance.
- Identify the optimum RAP content to be utilized with SCGO rejuvenator and OFA/rejuvenator products.

5.2. Materials and Methods

5.2.1. *Experimental Design*

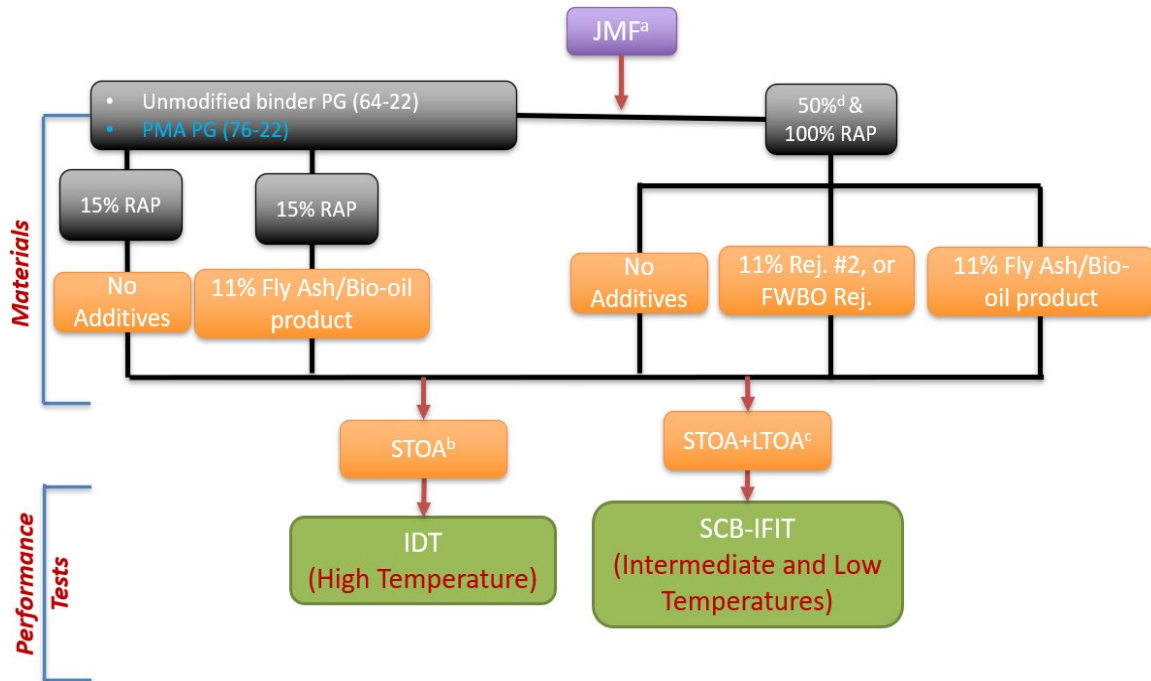
As shown in the flowchart for the experimental program in Figure 5-1, three ratios of RAP were studied for this phase. Two binders were used in this study; a neat PG 64-22 binder and a Styrene-Butadiene-Styrene (SBS) Polymer Modified (PMA) binder PG 76-22 for the 15% RAP and 50% RAP mixtures. Three OFAs were screened from the previous phase RH, SBH, and WE. The three fly ashes were blended with two types of rejuvenators: the PBO rejuvenator #2 and the new SCGO. The new OFA product is produced by blending the rejuvenator with RH, SBH, and WE in 1:1.2, 1:1.5, and 1:2 ratios.

This percentage achieves a dynamic viscosity close to the binder's viscosity at 155°C (mixing temperature). The OFA and the investigated rejuvenator were heated at 135°C for two hours. Then, the OFA powder was measured and added incrementally into the rejuvenator while using a high-shear mixer to disperse the agglomerates. The blending process was completed over 30 minutes.

The mixtures were subjected to two levels of aging: Short-Term Oven aging level (STOA) and Long-Term oven aging level (LTOA). The STOA mixtures were aged as prior to compaction for four hours at 135°C, while the LTOA mixtures were aged for an additional 120 hours at 85°C after short-term aging.

The experimental program included Three types of tests to evaluate the performance of the mixture at high, intermediate, and low temperatures.

1. Rutting resistance of the mixtures was determined using the Indirect Tension test at High Temperatures (IDT-HT) for STOA mixtures.
2. Cracking resistance at intermediate temperatures was determined using the Semi-Circular Bend (SCB) test for LTOA mixtures.
3. Cracking resistance at low temperatures was determined using the Semi-Circular Bend (SCB) test for LTOA mixtures.



^a JMF stands for Job Mix Formula

^b STOA stands for Short Term Oven Aging

^c LTOA stands for Long Term Oven Aging

^d the 50% RAP mixtures are investigated with the SCGO rejuvenator only

Figure 5-1: Phase III Experimental Program

5.2.2. Materials

This phase included one mix design. The mix design was developed with two binders and two RAP contents. The mix design developed adopting Nominal Maximum Aggregate Size (NMAS) of 12.5 mm. This was made to limit the number of variables included in the study. Table 5-1 shows the gradation of the RAP used and the rheological properties of RAP, including the high, intermediate, and low temperatures Performance Grades (PG). The binder content of the utilized RAP was determined through the ignition oven test as per AASHTO T 308, and it was found to be 5.7%.

Table 5-1: Properties of the RAP binder and aggregates

RAP Binder Properties	True High-Grade °C		High PG °C	True Interm. Grade °C	Interm. PG °C	True Low-Grade °C		Low PG °C	MSCR Results	
						Tc(S) °C	Tc(m) °C		J _{nr} 3.2 kPa ⁻¹	J _{nr} Diff %
		87.3		82	23.3	25	-29.4	-27.5	-22	4.7
RAP Aggregate Gradation	Sieve	1/2"	3/8"	#4	#8	#16	#30	#50	#100	#200
		97.6	83.4	41.2	24.6	15.2	7.7	2.8	0.8	0.2

The aggregates used are quartzite (coarse aggregate) and dolomite (fine aggregate). All aggregates, including the RAP, were fractionated into different particle sizes. The aggregates were then batched based on the aggregate blend for the given mix design. Worth mentioning that the aggregate structure was kept the same for any mix design, regardless of the RAP content. Figure 5-2 shows the aggregate structure for the mix designs.

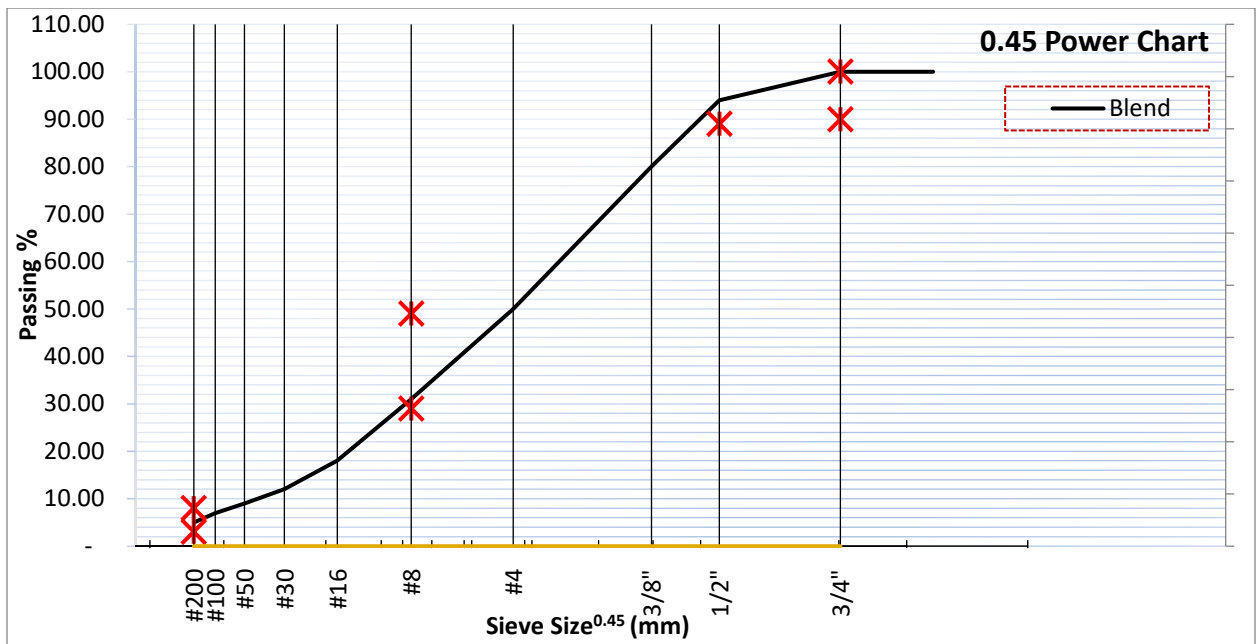


Figure 5-2: Graphical representation of the two aggregate structures used in the study

The mixing/Compaction temperatures were considered based on Hot Mix Asphalt (HMA) in this study. These were produced at the conventional asphalt mixing temperatures determined based on viscosity tests. The mixing/compaction temperatures for the unmodified and PMA binders were 155/145 and 165/155°C.

Two types of specimen sizes were produced. Volumetric specimens (4" in height); for which the target air content is 4.0% (based on AASHTO M-323 standard specification). The volumetric specimens (two replicas for each mix combination) were used to evaluate the compaction and volumetric properties of the mixtures. The same specimens were also used to evaluate rutting resistance using the IDT-HT test. Performance specimens (~6.5 inches in height), on the other hand, were compacted to an air content of $7\% \pm 0.5\%$. These specimens were used to evaluate the cracking performance of the mixtures using the Semi-Circular Bend (SCB) test (based on AASHTO TP-124 standard specification).

5.2.3. Mix Design and Production

Table 5-2 details the aggregate blends for each mix design. Table 5-2 provides the Optimum Binder Content (OBC) to achieve 4% air voids in the investigated mixtures and the RAP binder replacement in each mix.

Table 5-2: Mix design details

		15% RAP Mix- Control	15% RAP Mix- Fly Ash Additive	50% RAP Mix- Control	50% RAP Mix- Rej.	50% RAP Mix- Fly Ash Additive	100% RAP Mix- Control	100% RAP Mix- Rej.	100% RAP Mix- Fly Ash Additive
Aggregate Structure	Coarse-1	28.3%	28.3%	16.1%	16.1%	16.1%	0.0%	0.0%	0.0%
	Coarse-2	27.0%	27.0%	15.4%	15.4%	15.4%	0.0%	0.0%	0.0%
	Fine-1	29.0%	29.0%	16.5%	16.5%	16.5%	0.0%	0.0%	0.0%
	RAP	15.7%	15.7%	52.0%	52.0%	52.0%	100.0%	100.0%	100.0%
Mix Design Info.	OBC	5.2%	5.2%	4.7%	4.7%	4.7%	5.7%	6.3%	6.3%
	Virgin Binder	4.4%	3.8%	1.9%	1.4%	1.4%	0.0%	0.0%	0.0%
	RAP Binder	0.8%	0.8%	2.8%	2.8%	2.8%	5.7%	5.7%	5.7%
	Fly Ash/ Rejuvenator Additive	0.0%	0.6%	0%	0.0%	0.5%	0.0%	0.0%	0.6%
	Rejuvenator	0.0%	0.0%	0%	0.5%	0.0%	0.0%	0.6%	0.0%

5.2.4. Compaction Evaluation

The compaction characteristics of the mixtures were evaluated using the following:

5.2.4.1. Volumetric Properties [87]:

The three volumetric properties calculated were the Air Void (%Va) content, Voids in Mineral Aggregates (%VMA%), and Voids Filled with Asphalt (%VFA) as in Equations 5-1, 2, and 3, respectively.

$$\%Va = \left(1 - \frac{G_{mb}}{G_{mm}}\right) \times 100 \quad \text{Equation (5-1)}$$

$$\%VMA = \left(1 - \frac{G_{mb}(1-P_b)}{G_{sb}}\right) \times 100 \quad \text{Equation (5-2)}$$

$$\%VFA = \frac{\%VMA - \%Va}{\%VMA} \quad \text{Equation (5-3)}$$

Where:

G_{mb} is the bulk specific gravity of the compacted mixture,

G_{mm} is the Maximum theoretical specific gravity of the mixture,

G_{sb} bulk specific gravity of the aggregates in the mixture.

P_b is the asphalt binder percentage.

5.2.4.2. Construction Densification Index (CDI):

The CDI equals the area under the densification curve (produced by the SuperPave gyratory compactor) between the 8th gyration to the number of gyrations at 92% of the Maximum Theoretical Density ($\%G_{mm}$). This is a surrogate to the energy required to compact the pavement by roller compactors. The higher the CDI, the lower the workability of the mix. Figure 5-3 shows an illustration of the calculation of CDI. Figure 5-3 illustrates the benefit of using CDI to differentiate between compaction of two mixtures that both meet the volumetric requirements (4% air content at the design number of gyrations (N_{des})) but show significant differences in the energy required to achieve that target air content.

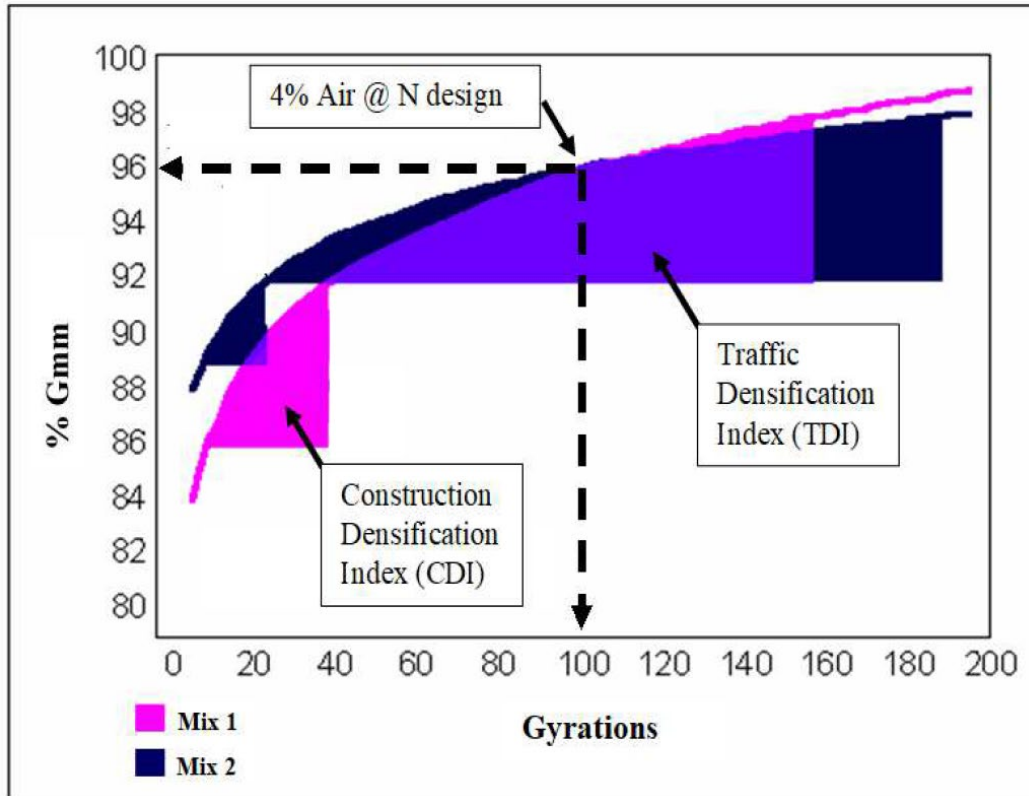


Figure 5-3: Description of the Definition of CDI and TDI [88]

5.2.5. Rutting Evaluation

Rutting is the permanent plastic deformation that occurs in the pavement with the repetition of loading cycles from traffic. In this study, the rutting resistance of the mixtures was evaluated using the IDT test at high temperatures. Based on the studies conducted by [89] (Geetha Srinivasan 2004) and (Christensen Jr and Bonaquist 2007) [89], [90], the IDT test in this study was conducted at a rate of 50 mm/min at a temperature 10°C below the yearly 7-day average maximum pavement temperature at a depth 20 mm below the pavement surface. Based on the Long-Term Pavement Performance Bind (LTPPBind), this temperature is 58°C for Pennsylvania. Thus, the IDT test was conducted at 48°C.

All specimens were conditioned at this temperature for two hours prior to testing. The test was conducted using MTS Landmark universal testing machine, and the specimens were placed inside an environmental chamber during the test. The test procedure and analysis used were based on the AASHTO T-283 standards. The tensile strength was determined using Equation (5-4):

$$S_t = \frac{2000 P}{\pi t D} \quad \text{Equation (5-4)}$$

Where S_t is the tensile strength in (kPa), P is the maximum load in N, t is the specimen thickness in mm, and D is the diameter of the specimen in mm. Figure 5-4 provides a schematic of the IDT-HT test and a sample of the Load-Displacement curve obtained from the test. Table 5-3 proposing Guideline for High-Temperature IDT (IDT-HT) [90].

Table 5-3: Proposed Guideline for High-Temperature IDT (HT IDT) to Minimize Pavement Rutting [99]

Design traffic level* (ESALs)	Rut resistance category	IDT strength range (kPa)
–	Very poor	< 50
< 0.3	Poor	50 to < 110
0.3 to < 3.0	Minimal	110 to < 170
3 to < 10	Fair	170 to < 270
10 to < 30	Good	270 to < 430
30 to < 100	Very Good	430 to < 660
100 to < 300	Excellent	660

*At 70 km/h (44 mph). To adjust the estimated traffic level to 70 km/h, multiply by $(70/v)$, where v is the average traffic speed in km/h.

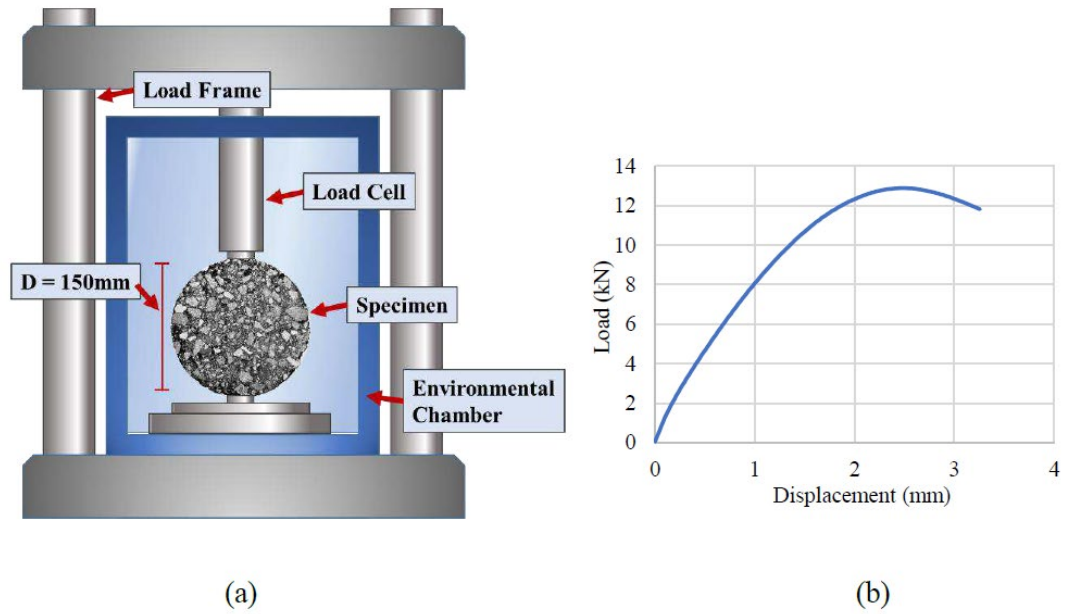
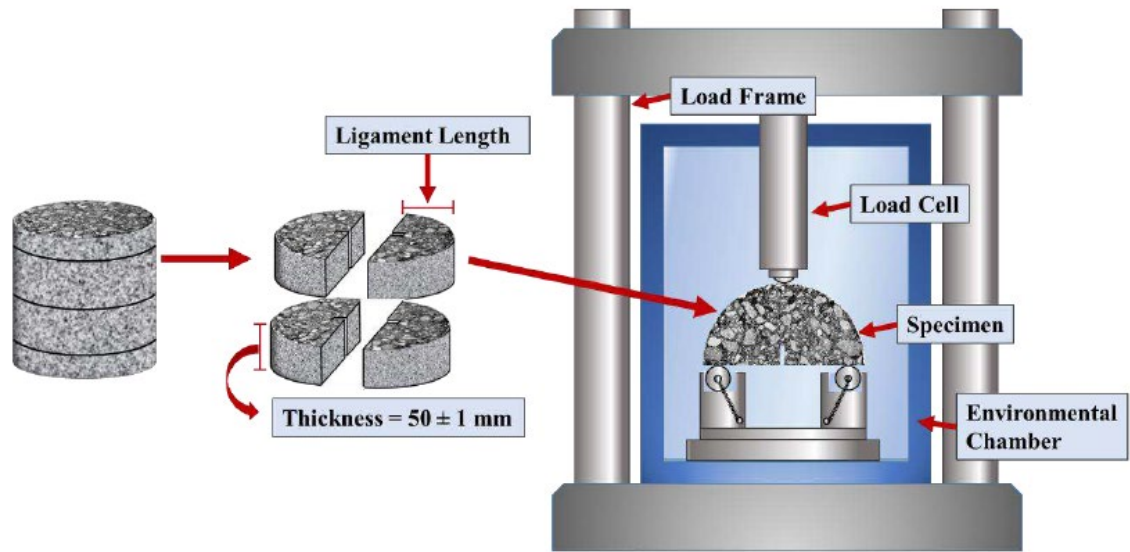


Figure 5-4: Schematic of the indirect tension test. (a) Test apparatus with the specimen and environmental chamber, (b) Load-Displacement curve obtained from the test.

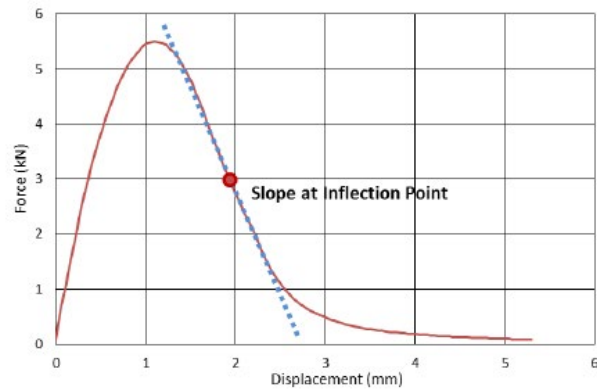
5.2.6. Cracking Evaluation

Cracking performance evaluation was made using the Semi-Circular Bend (SCB) test at intermediate and low temperatures (based on AASHTO TP-124 standard specification). The SCB is a three-point bending test run on half-disk asphalt mixture specimens. The mixtures were compacted to an air content of $7\% \pm 0.5\%$. Four half-disk specimens were obtained from each mixture sample. The half-disks have a thickness of 50 mm and an engineered notch (15 mm deep x 1.5 mm wide). Figure 5-5-(a) shows an SCB specimen with the notch. The test was run using the MTS universal testing machine at a 50 mm/min loading rate and 5mm/min [91] for intermediate and low temperatures, respectively.

The testing temperature was at 25°C for intermediate temperature, and at the low PG temperature -10°C [92]. The load-displacement curve was obtained from the test. Figure 5-5-b was used to determine the mixtures' fracture energy and flexibility index (FI).



(a)



(b)

Figure 5-5: Semi-Circular Bend (SCB) test. (a) SCB Specimen and test apparatus, (b) Force-Displacement curve.

The area under the curve is the work of fracture in (Joules). The work of fracture is then used to calculate the fracture energy in (Joules/m²) as follows in Equation (5-5) [93]:

$$\mathbf{Fracture\ Energy} = \frac{\mathbf{Work\ of\ Fracture}}{\mathbf{Thickness \times Ligament\ length}} \qquad \mathbf{Equation\ (5-5)}$$

The flexibility index (FI) is calculated by dividing the fracture energy by the slope of the post-peak curve at the inflection point, as shown in Equation (5-6). Higher FI values indicate more ductile failure behavior. Worth mentioning that the FI at low temperature was deemed because it was not discriminatory enough between mixtures, and the intermediate temperature testing at 25°C was adopted [94].

$$\mathbf{Flexibility\ Index} = \frac{\mathbf{Fracture\ Energy}}{\mathbf{|Slope|}} \qquad \mathbf{Equation\ (5-6)}$$

For the low-temperature performance evaluation, the fracture toughness and the pre-peak slope beside the fracture energy are calculated according to AASHTO TP 105-20. Fracture Toughness (K_{IC})—The fracture toughness, K_{IC}, is obtained as the stress intensity factor, K_I, at the critical load, P_c. The critical load is assumed to be the maximum load recorded during testing.

$$\frac{K}{\sigma_0 \sqrt{\pi a}} = Y_{I(0.8)} \quad \text{Equation (5-7)}$$

where:

$$\sigma_0 = \frac{P}{2rt} \quad \text{Equation (5-8)}$$

P = applied load (MN);

r = specimen radius (m); and

t = specimen thickness (m);

a = notch length (m); and

Y_I = the normalized stress intensity factor (dimensionless).

The mode I normalized stress intensity factor $Y_{I(0.8)}$ is independent of size and load but depends on the specimen's geometry and the loading configuration. The span length used in this study (i.e., 120mm) and the 150mm diameter of the specimen result in a span ratio of 0.8 or,

$$Y_{I\left(\frac{120}{150}\right)} = Y_{I(0.8)} \quad \text{Equation (5-9)}$$

$Y_{I(0.8)}$ is expressed as calculated in I.L.Lim; *et al.* (1993) [95] by:

$$Y_{I(0.8)} = 4.782 + 1.219 \left(\frac{a}{r}\right) + 0.063 \times e^{(7.045 \times \frac{a}{r})} \quad \text{Equation (5-10)}$$

The pre-peak slope is defined as the Stiffness (S). The stiffness (S) is calculated as the slope of the linear part of the ascending load average load line displacement curve. An example is shown in Figure 5-6.

The pre-peak slope of tangent in the loading phase was determined between $0.4 P_{\max}$ and $0.6 P_{\max}$ points following Nsengiyumva *et al.* (2015) [96].

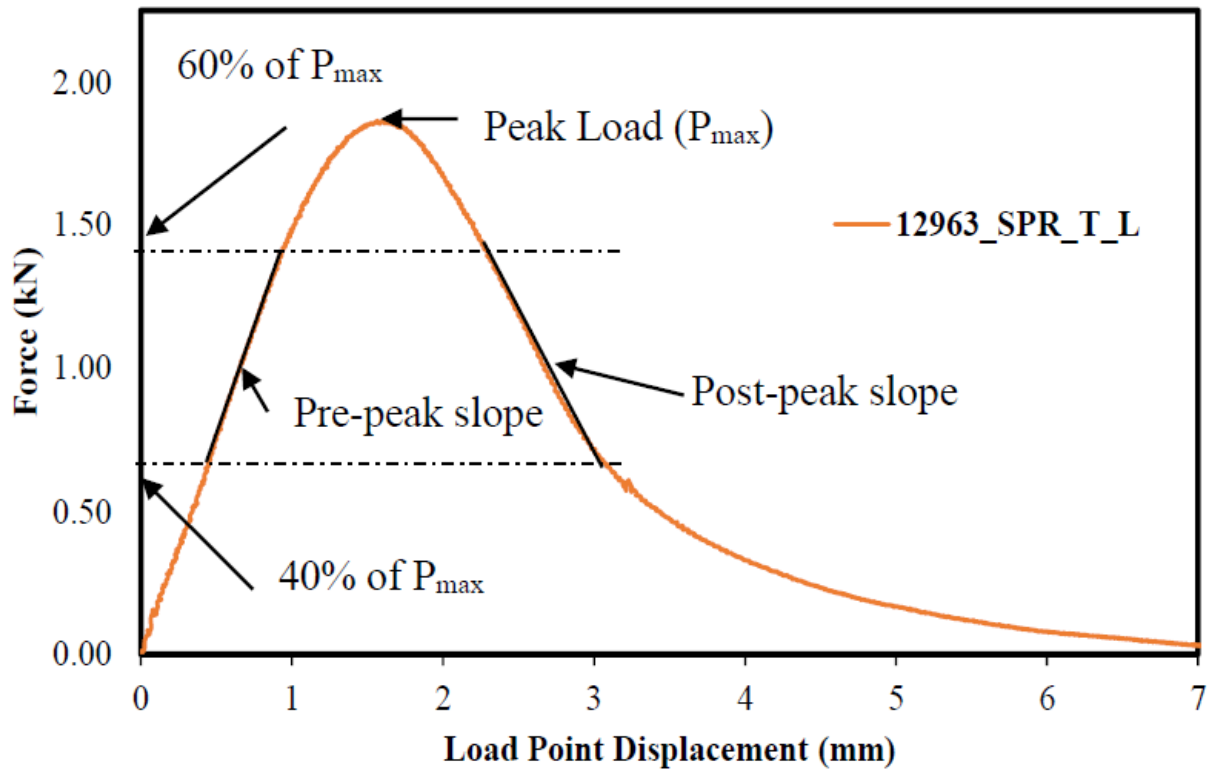


Figure 5-6: A typical force Load Point Displacement (LPD) curve from the SCB test After [96]

5.3. Results and Discussion

5.3.1. Compaction Evaluation

In this section, the compaction evaluation results are presented regarding the volumetric properties, the construction densification index for the 15% RAP and 50% RAP mixtures, and the number of gyrations achieving a particular volume for the 100% RAP mixtures.

5.3.1.1. Volumetric Properties

Figures 5-7, 8, and 9 show %Va, %VMA, and %VFA at the design number of gyrations for 15% RAP mixtures. The control mixtures were produced at conventional HMA temperatures and did not contain fly ash products. The fly ash products substituted 11% of the asphalt binder weight in the mixtures. In designing asphalt mixtures mix design, at least two trials are needed to obtain the Asphalt Content (AC%) corresponding to 4% AV. However, due to the lack of PMA binder material, the unmodified binder AC% was adopted for the PMA binder mixtures. Worth noting that the compaction stopped at N_{max} (160 Gyrations); thus, the variations in densification levels between the different mixture combinations are due to the influence of the fly ash products since the RAP source, RAP content, and production conditions (mixing and compaction temperatures) of the mixtures are the same.

Figure 5-7 shows that the control mixture is within the acceptable range of %AV for the unmodified binder. OFA /rej. #2 products introduction to the unmodified binder mixtures increases the %AV for both RH and SBH fly ashes, indicating less workability and need more energy to compact. On the other hand, Introducing the OFA/SCGO rejuvenator products to the unmodified mixtures reduce the AV % for both RH and WE fly ashes, indicating more workable mixtures and easier to compact. WE fly ash shows the best workability influence when introduced to the unmodified mixtures for both rejuvenators. WE/rej. #2 product remained the %AV as the control, and WE fly ash showed its strongest influence when introduced with the SCGO rejuvenator.

For the PMA binder mixtures, the control mixture is out of the acceptable range of %AV. Fly ash/ SCGO mixtures are more workable and easier to compact than OFA/ rej. #2 mixtures. SBH fly ash shows the best workability influence when introduced to the PMA mixtures for both rejuvenators. SBH/SCGO product almost remained the %AV as the control.

Figure 5-8 shows that the control mixture is within the acceptable range of %VMA, higher than 14%, for the unmodified binder. Lower %VMA is interpreted to higher densification of the mixtures under the applied compaction energy from the gyratory compactor. Following %AV trend, OFA/ SCGO products are more positively influence workability when introduced to the unmodified binder mixtures than OFA/ rej. #2 products. RH/ SCGO and WE/ SCGO mixtures are showing less %VMA than the control, which means more workable mixtures with 11% less asphalt binder.

For the PMA mixtures, All OFA/SCGO products are showing less %VMA than the control mixture. Following the %AV trend, SBH fly ash shows the best workability influence when introduced to the PMA mixtures for both rejuvenators. SBH/SCGO product positively influences workability when introduced to the PMA mixtures.

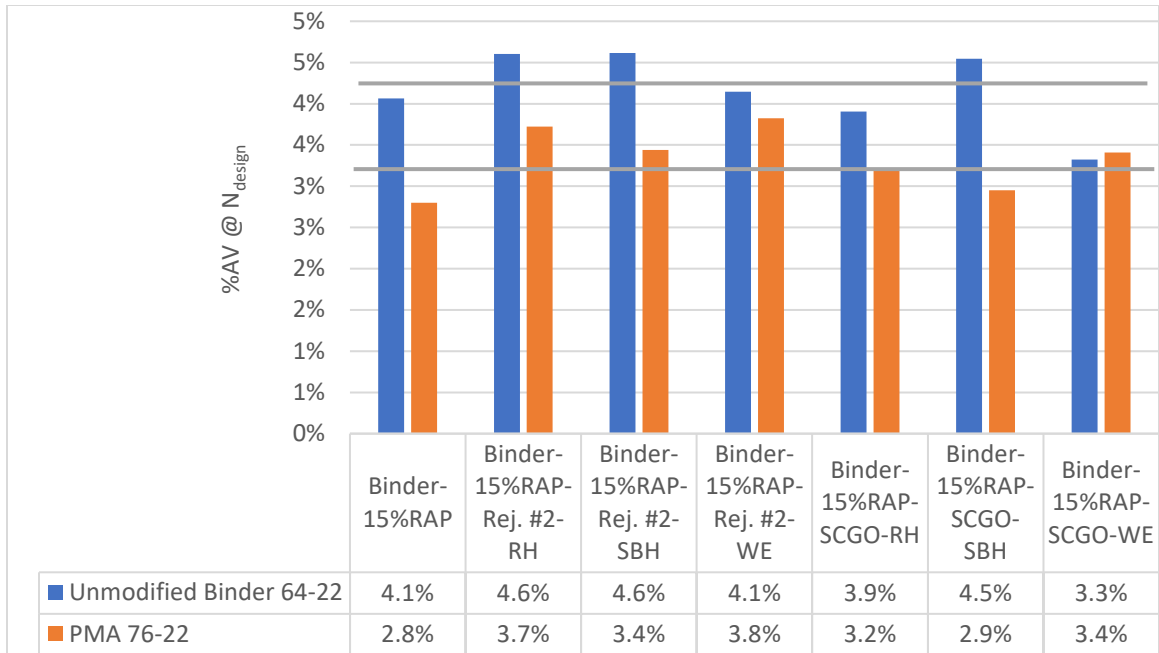


Figure 5-7: The influence of the introduction of the different fly ash products on %AV for the 15% RAP mixtures

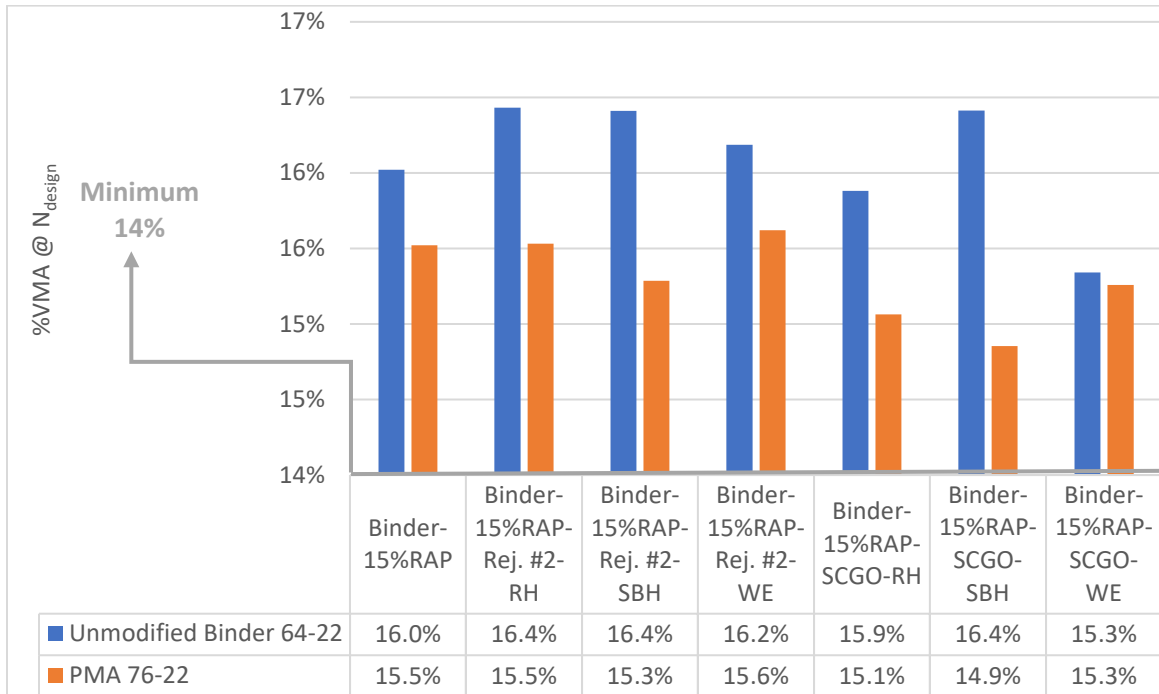


Figure 5-8: The influence of the introduction of the different fly ash products on % VMA for the 15% RAP mixtures

The %VFA values show an opposite trend to that seen for the %Va and %VMA, as shown in Figure 5-9. This is logical, given that lower %Va indicates more voids between the aggregate particles filled by the asphalt binder in the mix and vice versa. For the unmodified binder mixtures, OFA/ SCGO products significantly influence workability than OFA/ rej#2 on asphalt mixtures. Following the previously illustrated trends, RH and WE fly ashes show more positive synergy with SCGO in terms of workability.

For the PMA binder mixtures, following the %AV trend, none of the fly ashes products could improve the workability of the PMA mixtures. However, OFA/SCGO products show more significant improvement in PMA mixtures workability than OFA/rej.#2 products. SBH fly ash shows the highest synergy with both rejuvenators compared to the other two fly ashes. Still, SBH/SCGO rejuvenator shows the most significant improvement in the workability of PMA mixtures. Figure 5-9 shows that, in general, the PMA binder mixtures are more workable than the unmodified binder due to the lower % AV of the PMA binder mixtures compared to the unmodified binder.

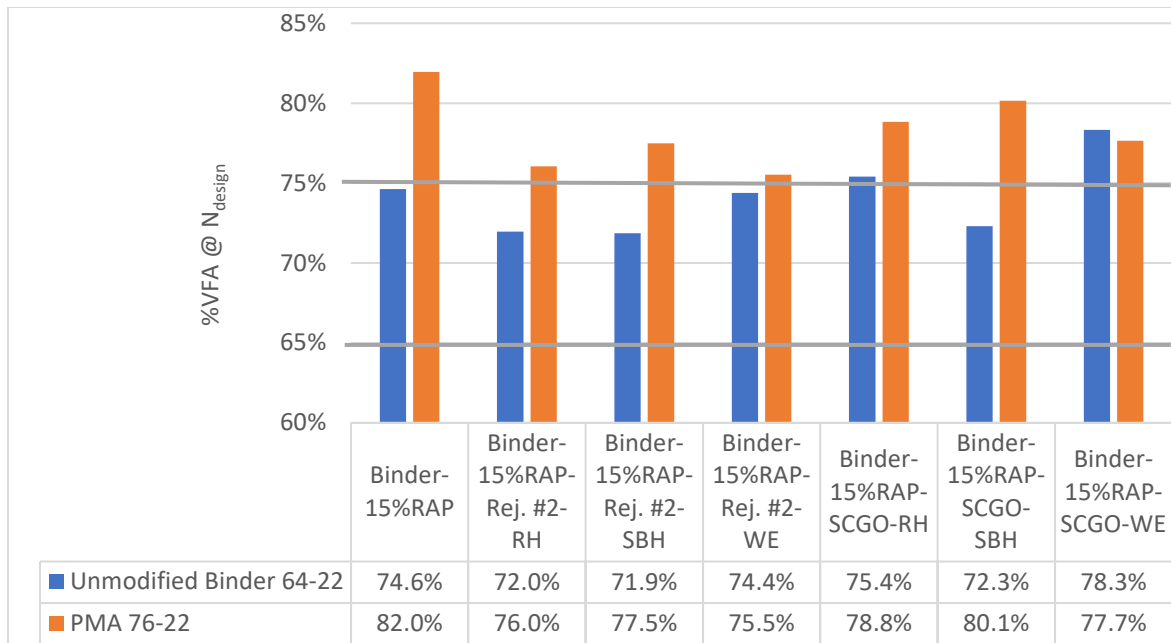


Figure 5-9: The influence of the introduction of the different fly ash products on % VFA for the 15% RAP mixtures

Figures 5-10, 11, and 12 show %Va, %VMA, and %VFA at the design number of gyrations for 50% RAP mixtures. Due to the lack of materials, and since the study focuses on the SCGO rejuvenator, the 50% RAP mixtures are only investigated for OFA/ SCGO rejuvenator products for both the unmodified and PMA binder.

Figure 5-10 shows that the control mixture is within the acceptable range of %AV for the unmodified binder. Introducing the SCGO rejuvenator is found to be associated with lowering the %AV, indicating high workability, compared to the control mixture. Conversely, OFA/ SCGO rejuvenator products introduction to the unmodified binder mixtures, except with RH/SCGO rejuvenator, increases the %AV, indicating less workability and need more energy to compact.

For the PMA binder mixtures, All the mixtures are out of the acceptable range of %AV, except with the WE/SCGO rejuvenator mixture.

Introducing the SCGO rejuvenator shows a minimal increase to the AV% compared to the control mixture. The same is observed with OFA/ SCGO mixtures introduction except with WE/SCGO rejuvenator mixture

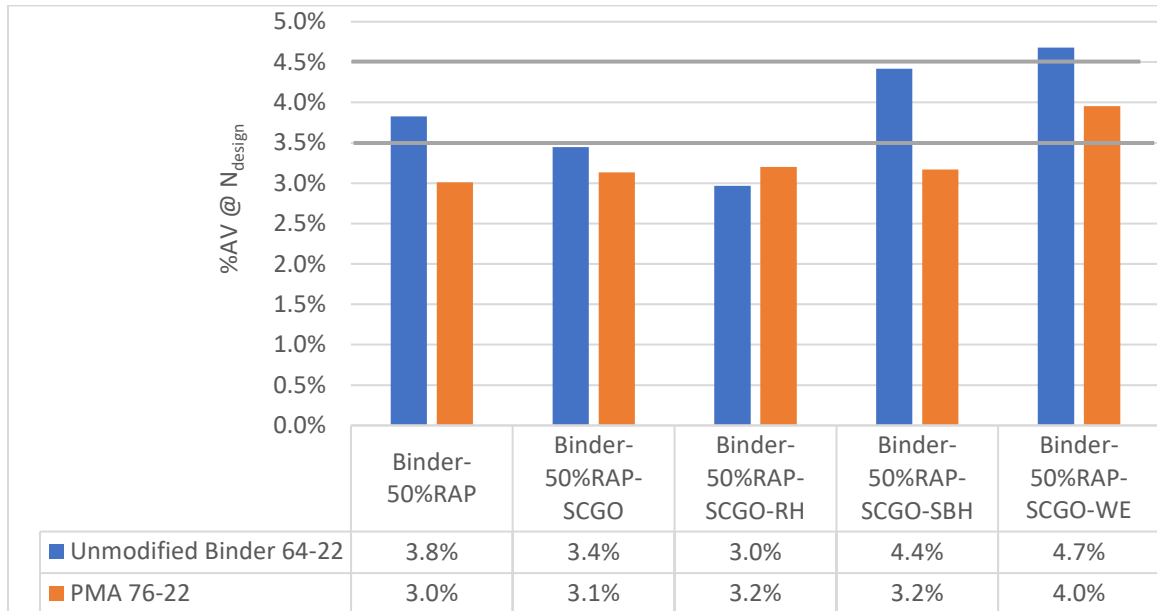


Figure 5-10. The influence of the introduction of the different fly ash products on %AV for the 50% RAP mixtures

Figure 5-11 shows that the control mixture is within the acceptable range of %VMA, higher than 14%, for the unmodified binder. As mentioned, lower %VMA is interpreted to higher densification of the mixtures under the applied compaction energy from the gyratory compactor. Following %AV trend, SCGO rejuvenator introduction is found to be associated with workability enhancement compared to the control 50% RAP mixture. Introducing the OFA/SCGO products minimally influences workability negatively when introduced to the unmodified binder mixtures. RH/ SCGO shows less %VMA than the SBH/SCGO and WE/SCGO products, which means more workable mixtures. For the PMA mixtures, the same previous illustrated findings for the unmodified binder are observed.

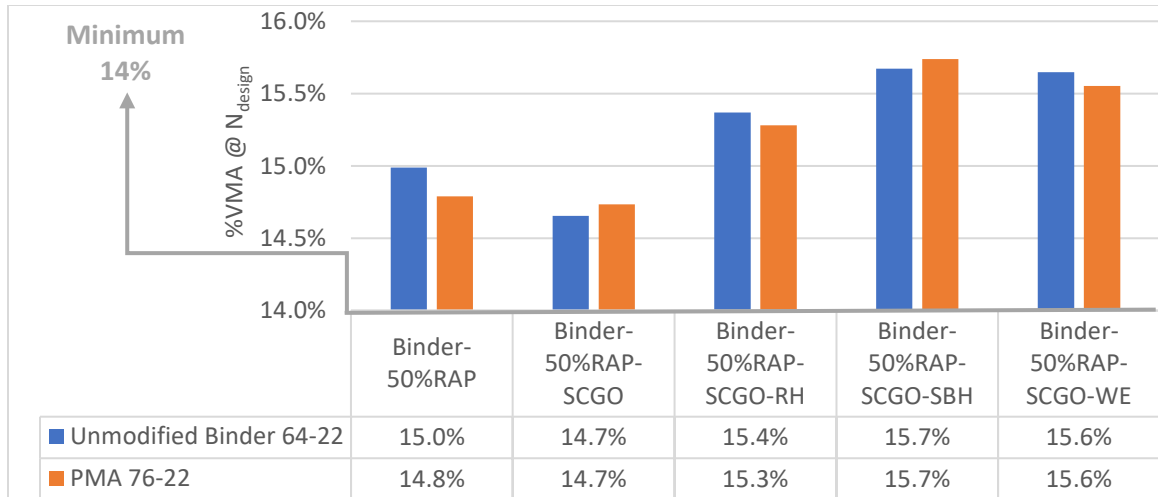


Figure 5-11. The influence of the introduction of the different fly ash products on %VMA for the 50% RAP mixtures

Figure 5-12 shows the %VFA for the 50% RAP mixtures. Following the %AV and %VMA trends, the SCGO rejuvenator significantly enhances the workability when introduced to the 50% RAP mixture. RH/SCGO product shows a dominant positive influence on workability when introduced to the unmodified binder 50% RAP mixture compared to the SBH and WE products.

For the PMA binder mixtures, following the %AV trend, the SCGO rejuvenator could not improve the workability of the PMA 50% RAP mixture. However, the workability reduction is minimal. Still, SBH/SCGO rejuvenator shows the most significant improvement in the workability of PMA mixtures.

Generally, it can be concluded that RH/SCGO product has a very significant influence when introduced to both 15% RAP and 50% RAP unmodified binder mixtures. While SBH/SCGO product has a dominant positive behavior on workability when introduced to 15% RAP and 50% RAP PMA binder mixtures.

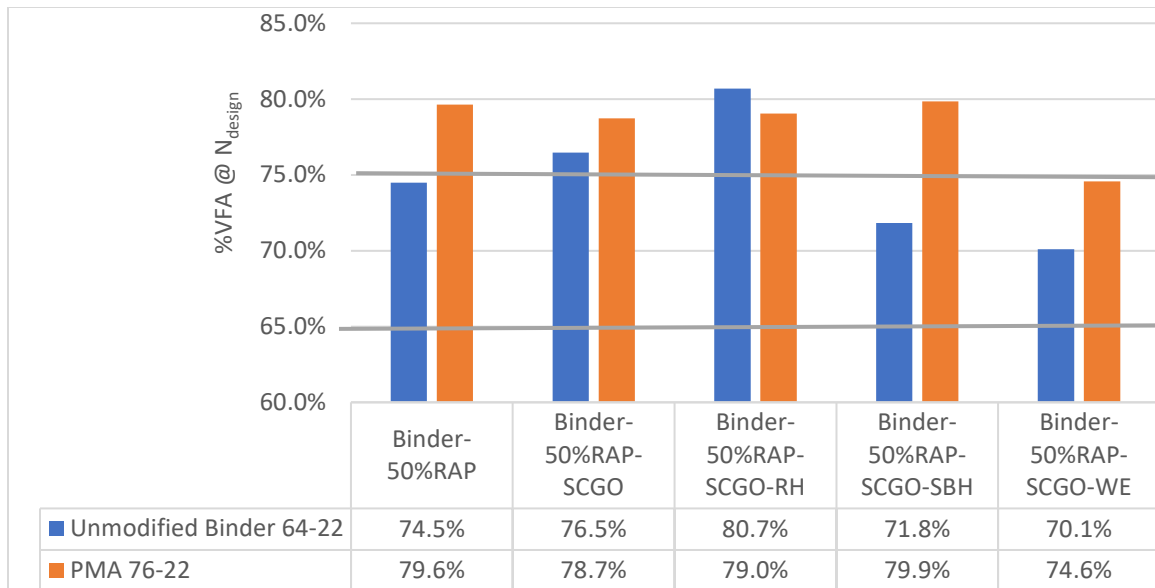


Figure 5-12. The influence of the introduction of the different fly ash products on %VFA for the 50% RAP mixtures

5.3.1.2. Asphalt Mixtures' Workability

It is necessary to remember that all the previously illustrated results are for the 15% RAP and 50% RAP mixtures only since volumetric properties were initially developed for virgin mixtures (not containing RAP). Accordingly, adopting the volumetric properties for 100% RAP mixtures was not possible. Also, RAP aggregate particles are coated by asphalt binder that melts and diffuses when reheated in a new mixture, necessitating caution when volume-based properties such as %VMA and %VFA are utilized to explain the compaction of mixes containing high RAP.

Therefore, volumetric properties were used in this study to describe the compaction of the mixtures because current standard specifications are based on the use of these properties to evaluate mixtures and set quality control criteria. However, in addition to the volumetric properties, the CDI values were also used to evaluate the compaction of the 15% and 50%

RAP mixtures. For the 100%RAP mixture, the numbers of gyrations of the SGC 4900±10 grams specimens to achieve the same specimen height (115 mm) was found a reasonable approach to evaluate the workability of the mixtures [97].

Figure 5-13 demonstrates the CDI values for the 15%RAP mixtures produced for the unmodified asphalt and PMA binders. The higher the CDI, the lower the workability of the mix. As mentioned before, the compaction stopped at N_{max} (160 Gyration). Thus the variations in densification levels between the different mixture combinations are due to the influence of the aging additive (Rej.+Ash), as the RAP source, RAP content, and production conditions (mixing and compaction temperatures) of the mixtures are the same.

For the unmodified binder mixture, the introduction of the fly ash additives in general reduced the workability of the mixtures, by at least 17%, as the percentage of the virgin binder is reduced. However, it can be noticed that the OFA/SCGO additives enhance the unmodified binder mixtures' workability compared to the OFA/rej. #2 additives. That promotes the theory studied in the previous phase that the fly ash depicts higher synergy with the vegetable-based SCGO than the PBO Rej.#2.

Following the trends demonstrated in the volumetrics section, the WE fly ash shows the best workability influence when introduced to the unmodified mixtures for both rejuvenators, compared to the other fly ashes. In addition, the WE/SCGO additive performs the best with the unmodified binder, as it enhances the workability by 10% compared to the control mixture.

For the PMA binder mixtures, following the volumetrics trend, none of the fly ashes products could improve the workability of the PMA mixtures compared to the control

mixture. However, OFA/SCGO products show more significant improvement in PMA mixtures workability than OFA/rej.#2 products. Still, SBH fly ash shows the highest synergy with both rejuvenators compared to the other two fly ashes. SBH/SCGO rejuvenator shows the most significant improvement in the workability of PMA mixtures.

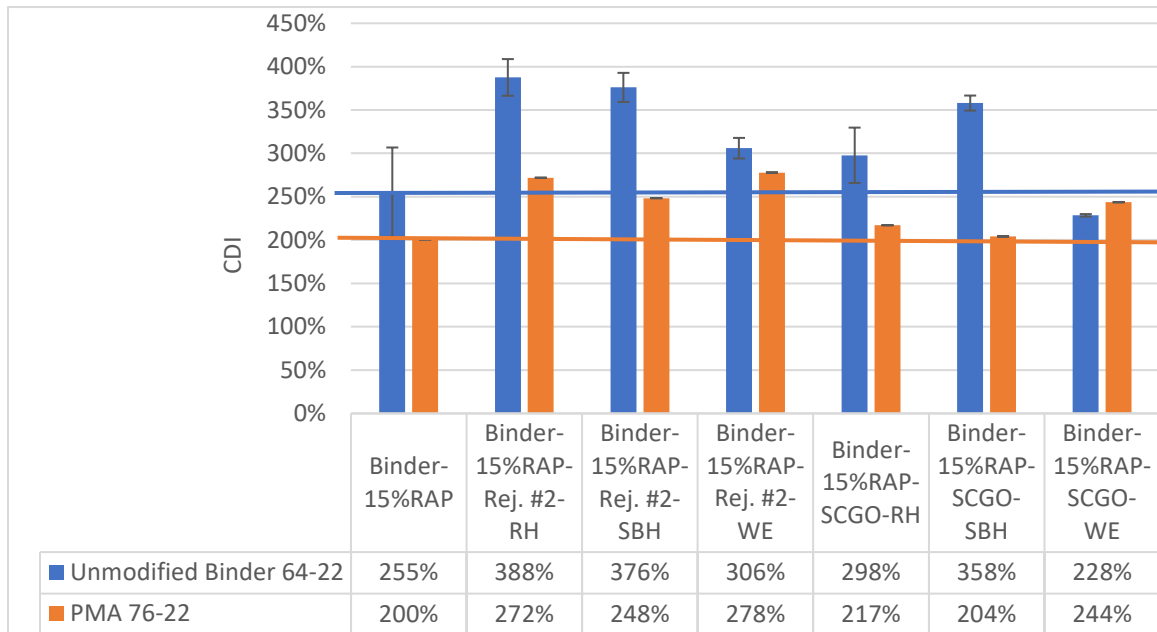


Figure 5-13: Effect of Fly Ash/ Rejuvenator Products on CDI values for Both Unmodified and PMA 15% RAP Mixtures.

Figure 5-14 demonstrates the CDI values for the 50%RAP mixtures produced for the unmodified asphalt and PMA binders. Following the volumetric results trend, the SCGO rejuvenator can enhance the workability of the unmodified mixtures. On the other hand, the significance of the SCGO rejuvenator is very minimal with the PMA mixture. The introduction of all the OFA/SCGO products enhances the workability compared to the control unmodified mixture. Following the previous illustrated results, RH/SCGO product still shows the most workability enhancement compared to the SBH and WE products. Following the 15% RAP mixtures, none of the fly ashes products could improve the

workability of the PMA mixtures compared to the control mixture. Still, SBH/SCGO rejuvenator shows a significant improvement in the workability of PMA mixtures. These findings are valuable considering mixtures with 11% less binder.

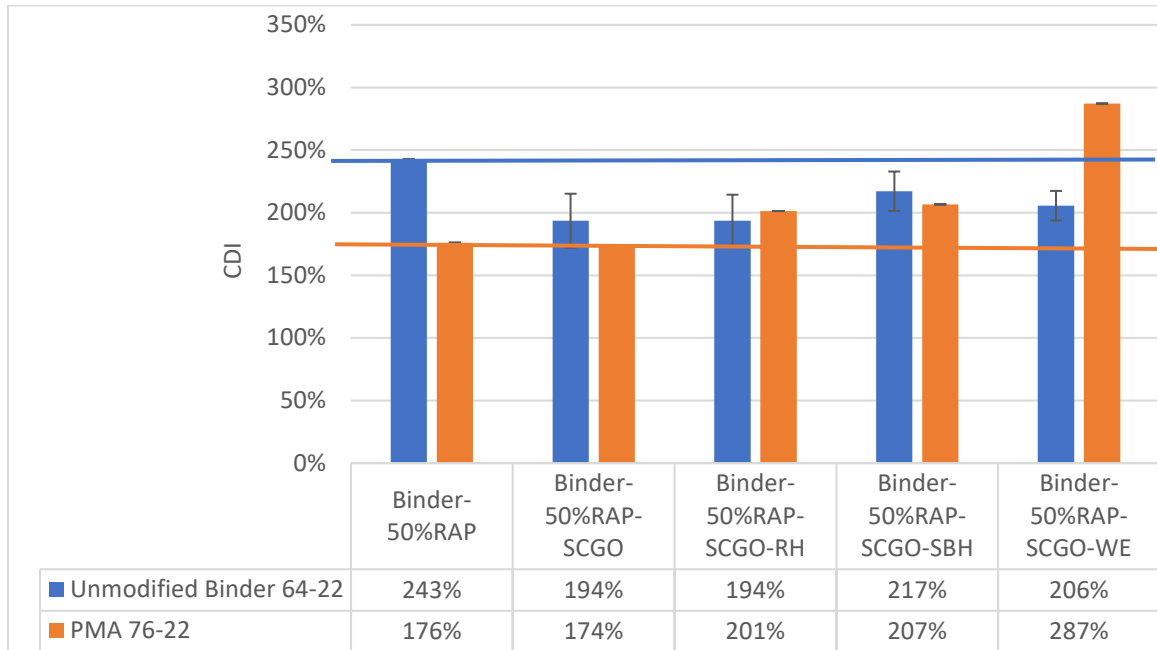


Figure 5-14. Effect of Fly Ash/ Rejuvenator Products on CDI values for Both Unmodified and PMA 50% RAP Mixtures.

Figure 5-15 demonstrates the influence of the OFA/ rejuvenator products on the 100% RAP mixtures. The higher the number of gyrations to achieve a specific specimen height, the less the workability. The introduction of both rejuvenators to the 100% RAP mixture is accompanied by workability enhancement. Following the previous illustrated trends, OFA/SCGO products enhance the workability of the 100% RAP mixtures more than the OFA/rej. #2 products. That also confirms the findings discussed in the previous phase. Unlike the 15% RAP mixtures, neither WE/ SCGO nor SBH/ SCGO products improved the workability of the mixture the most, as with the unmodified and PMA binder, respectively.

The RH/ SCGO product improved the workability the most to a degree close to the rejuvenators.

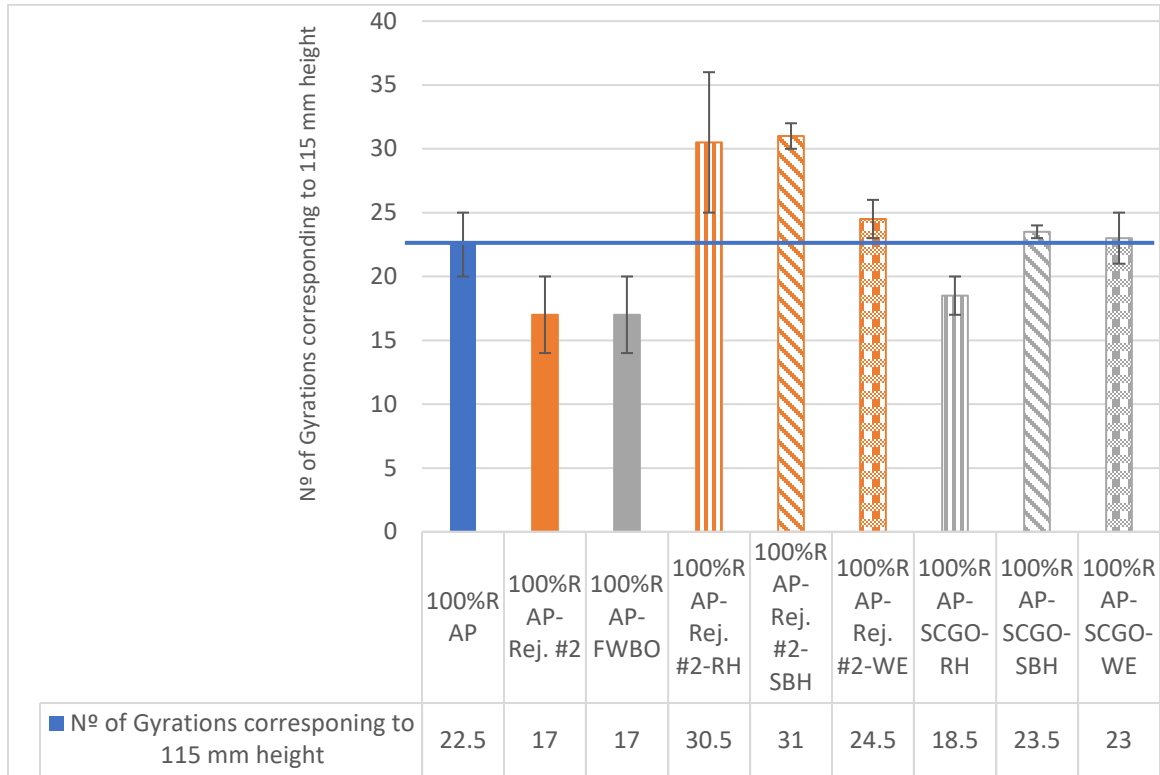


Figure 5-15: Effect of Fly Ash/ Rejuvenator Products on the Number of Gyration Corresponding to 115 mm Height for 100% RAP Mixtures.

5.3.2. Rutting Evaluation (High-Temperature Performance)

Figure 5-16 shows the IDT-HT test results for the unmodified and PMA 15% RAP mixtures. The coefficient of variance ranged from 2.5% to 11.2%. Two replicas were tested for all the unmodified binder mixture combinations, while one replica was tested for the PMA mixture combinations due to limited material availability. However, the relatively low average COV% obtained for the tested mixtures (6.5%) gives confidence in the accuracy of the results. For the 100% RAP mixtures illustrated in Figure 5-17, two replicas were testes achieving CoV varies from 0.2% to 11.3%.

All the 15% RAP mixtures for unmodified and PMA binders have the same total binder content. Accordingly, the IDT-HT test can clearly distinguish the effect of binder grade, as a higher binder grade (PMA binder) shows higher tensile strength than the lower binder grade (unmodified binder) accordingly, higher permanent deformation resistance, as shown in Figure 5-16. While the unmodified binder mixtures are within the 270 kPa and 430 KPa, which is interpreted to a traffic level of 10-30 million ESALs, the PMA mixtures are within the 430 KPa and 660 kPa, which is interpreted to a traffic level of 30-100 million ESALs. Also, the IDT-HT test shows sensitivity towards the RAP ratios within the mixtures system. The 100% RAP mixtures have higher tensile strength than the 15% and 50% RAP mixtures due to the presence of the aged asphalt binder in the system.

For the 15% RAP mixtures, the OFA/rejuvenators' introduction reduced the tensile strength for both the unmodified and PMA binder mixtures compared to the control mixtures.

The introduction of the OFA/SCGO products enhances the viscous behavior of the mixtures, thus less resistance to the permanent deformation than the OFA/ Rej. #2. However, all the mixtures' high-temperature performance is within the same tensile strength limit; 10-30 million ESALs for the unmodified binder and 30-100 million ESALs for the PMA mixtures.

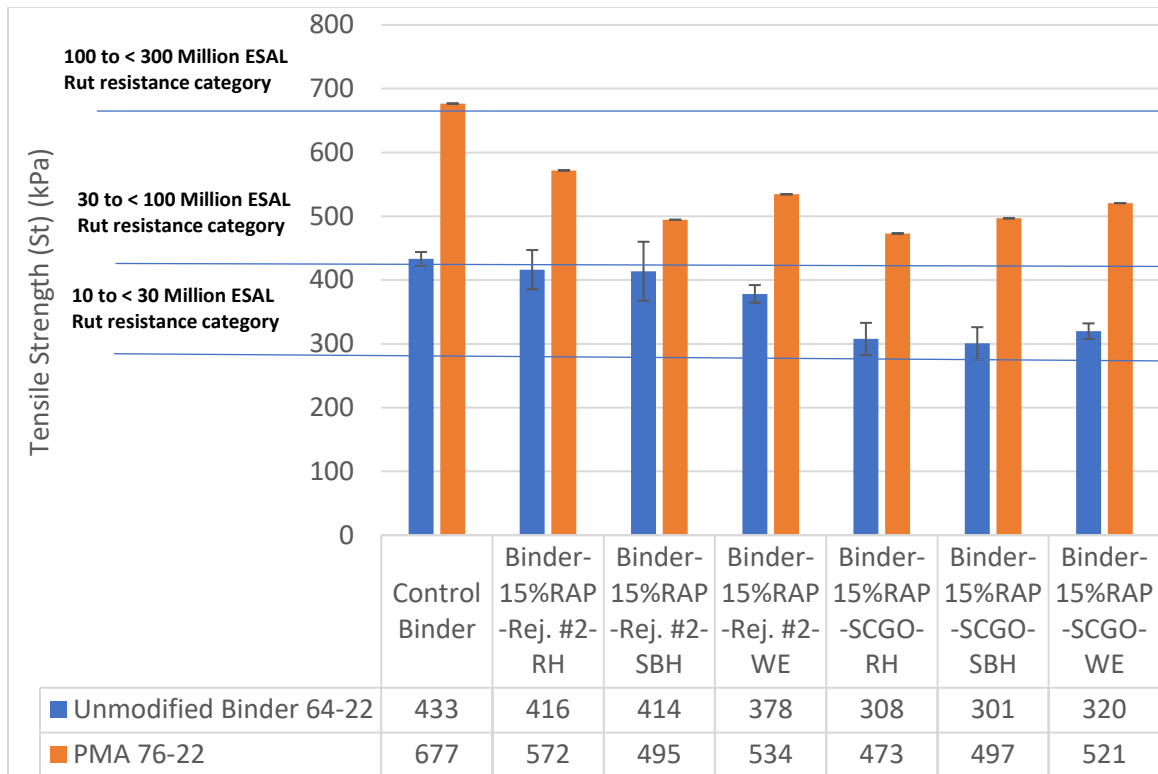


Figure 5-16: Tensile Strength Obtained from IDT-HT Test for both unmodified and PMA 15% RAP Mixtures

Figure 5-17 shows the IDT-HT test results for the unmodified and PMA 50% RAP mixtures. It can be noticed that the SCGO rejuvenator introduction to the 50% RAP mixtures drops the tensile strength significantly for both binders, which can be interpreted to lower rutting resistance. That means that the SCGO rejuvenator increases the viscous behavior of the mixtures.

The introduction of OFA/SCGO rejuvenator is noticed to have a softening effect on both unmodified and PMA mixtures 50% RAP mixtures. However, all OFA/SCGO mixtures' have a similar high-temperature performance to the 15% RAP mixtures. The high-temperature performance is within the same tensile strength limit; 10-30 million ESALs

for the unmodified binder, except with WE/SCGO mixture, and 30-100 million ESALs for the PMA mixtures.

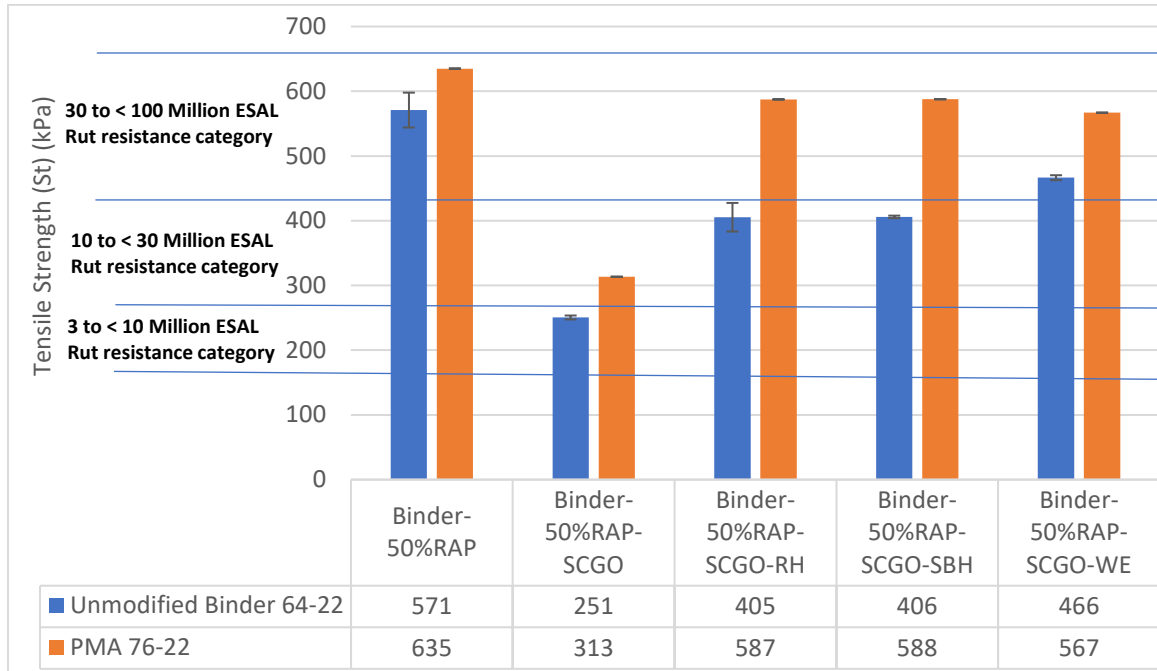


Figure 5-17. Tensile Strength Obtained from IDT-HT Test for both unmodified and PMA 50% RAP Mixtures

Figure 5-18 shows the IDT-HT test results for the 100% RAP mixtures. Introducing the rejuvenators to 100% RAP mixtures reduces the tensile strength from 100-300 million ESALS category with the control mixture to 10-30 million ESALS with rej. #2, and to 3-10 million ESALS with SCGO rejuvenator. The OFA/ SCGO products have a softening effect higher than the OFA/ rej. #2 products.

However, introducing the fly ash/ rejuvenators products to the 100% RAP mixtures categorizes the mixtures' high-temperature performance as 30-100 million ESALs, except with WE/ rej. #2. These results conform with the findings demonstrated for the 15% RAP mixtures.

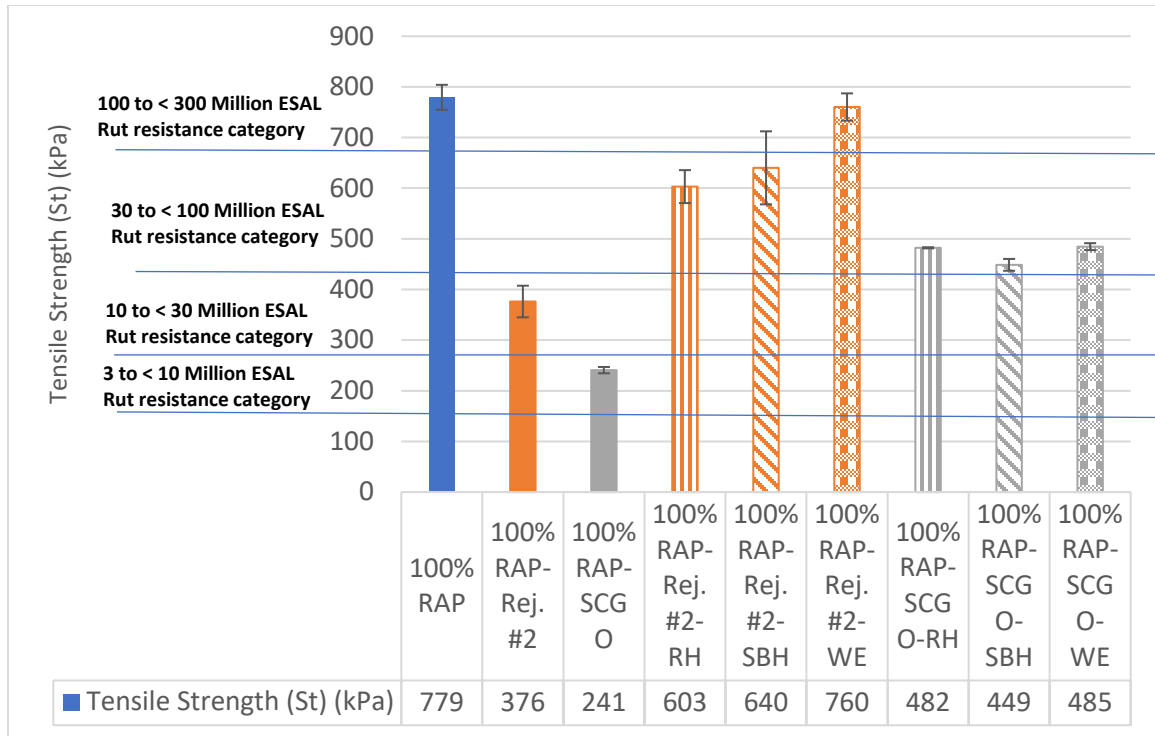


Figure 5-18: Tensile Strength Obtained from IDT-HT Test for 100% RAP Mixtures

5.3.3. Cracking Evaluation (Intermediate-Temperature Performance)

Figures 5-20 and 21 show the fracture energy (FE) and flexibility index (FI) for the unmodified and PMA 15% RAP mixtures. The fracture energy exhibits a grade dependency on the binder grade of the virgin binder. The higher the binder grade, the higher the energy required for crack propagation through the mixture specimen. The average FE value for the unmodified binder 15% RAP is approximately 3,024 J/m², while for the PMA 15% RAP mixtures, the average FE is about 3,428 J/m².

Moreover, the FE shows sensitivity to the RAP ratios, while the 100% RAP mixtures’ average FE is 1,377 J/m². One issue with using FE to evaluate mixture performance is that two mixtures may have similar fracture energies but different failure behaviors.

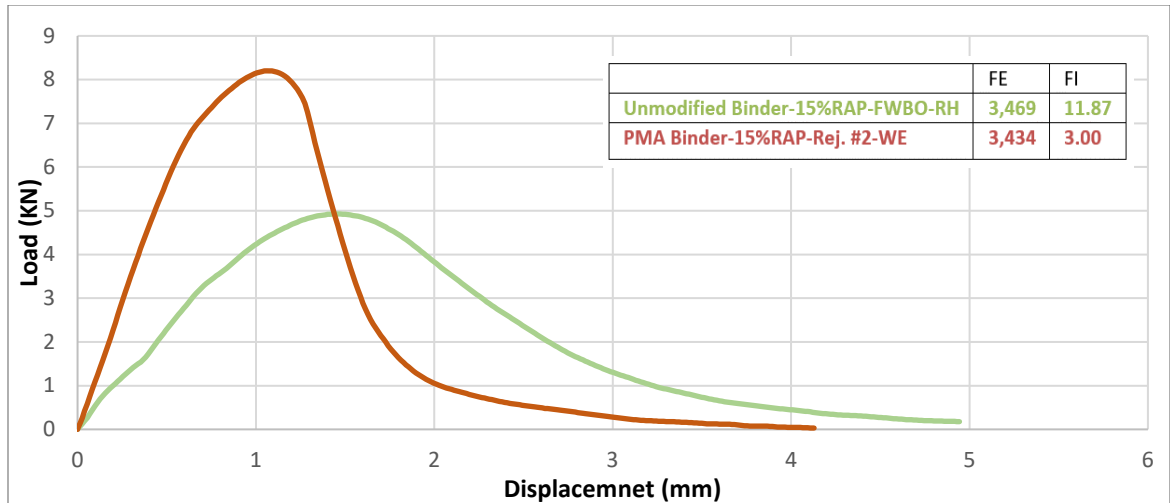


Figure 5-19. Two Specimens with the Same Fracture Energy and Different Flexibility Index

Figure 5-19 shows mixtures with very similar fracture energies. For example, the unmodified binder-15%RAP-SCGO-RH mixture has a FE of 3,496 J/m² and FI 11.87, while the PMA binder-15%RAP-Rej. #2-WE mixture has a FE of 3,434 J/m² and FI 3.00. The area under the two curves is approximately the same, accordingly the similar fracture energy values. However, the PMA binder-15%RAP-Rej. #2-WE mixture curve shows a much higher peak load (8 kN) and post-peak slope (-11.44) than the unmodified binder-15%RAP-SCGO-RH mixture curve's peak load (4 kN) and post-peak slope (-2.92). Al-qadi *et al.* (2015), and Mohammed A. J. Alsalihi (2020) [98], [99] had also reported the same observations about the inability of the fracture energy parameter alone to distinguish between different mixtures. Because of the limitations of the fracture energy parameter, the flexibility index of the mixtures was also determined.

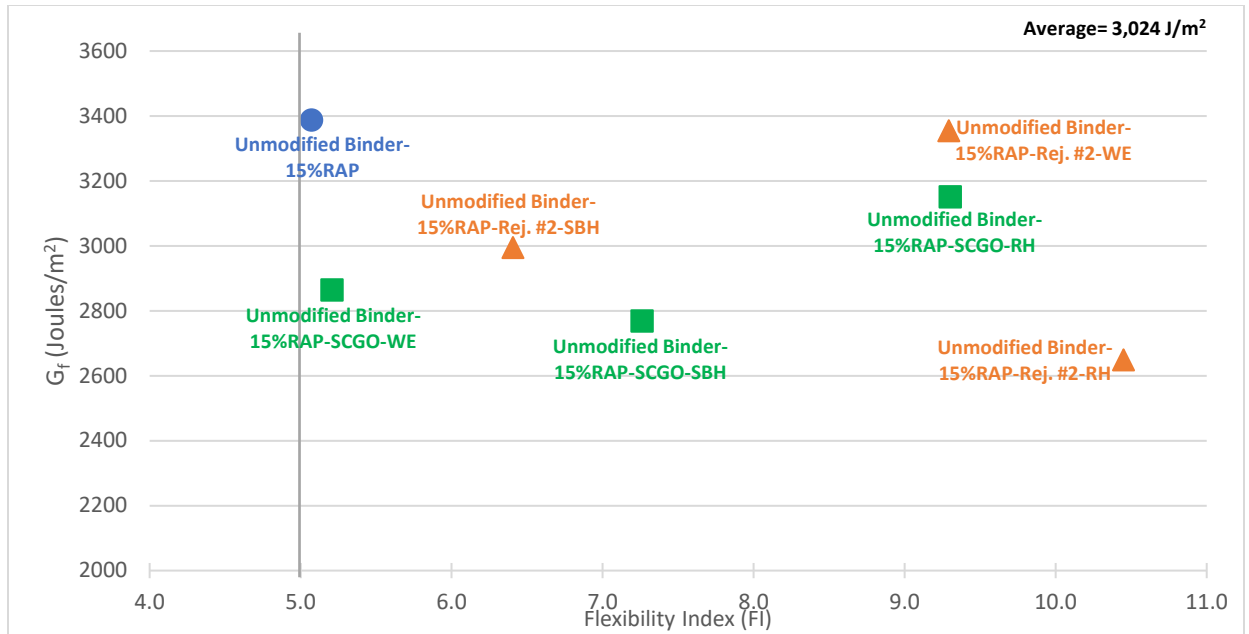


Figure 5-20: The Fracture Energy and the Flexibility Index of the Unmodified Binder 15% RAP Mixtures

The limit of 5 of FI is adopted from the Illinois department of transportation for LTOA I-FIT specimens [100]. It is only used here as an approximate limit to distinguish mixtures that perform adequately from those with low cracking resistance.

For the unmodified binder 15% RAP mixtures, introducing the OFA/ rejuvenator products reduces the FE by a range that varies from 1% to 22% for the WE/ rej. #2 and RH/ rej. #2, respectively. For the FI, all the fly ash/rejuvenator products enhanced the ductile failure behavior for the unmodified binder 15% RAP mixtures, as reflected by the adopted FI threshold of 5. RH fly ash shows a stronger influence on the FI with the unmodified binder. It performs well with both rej. #2 and SCGO rejuvenator.

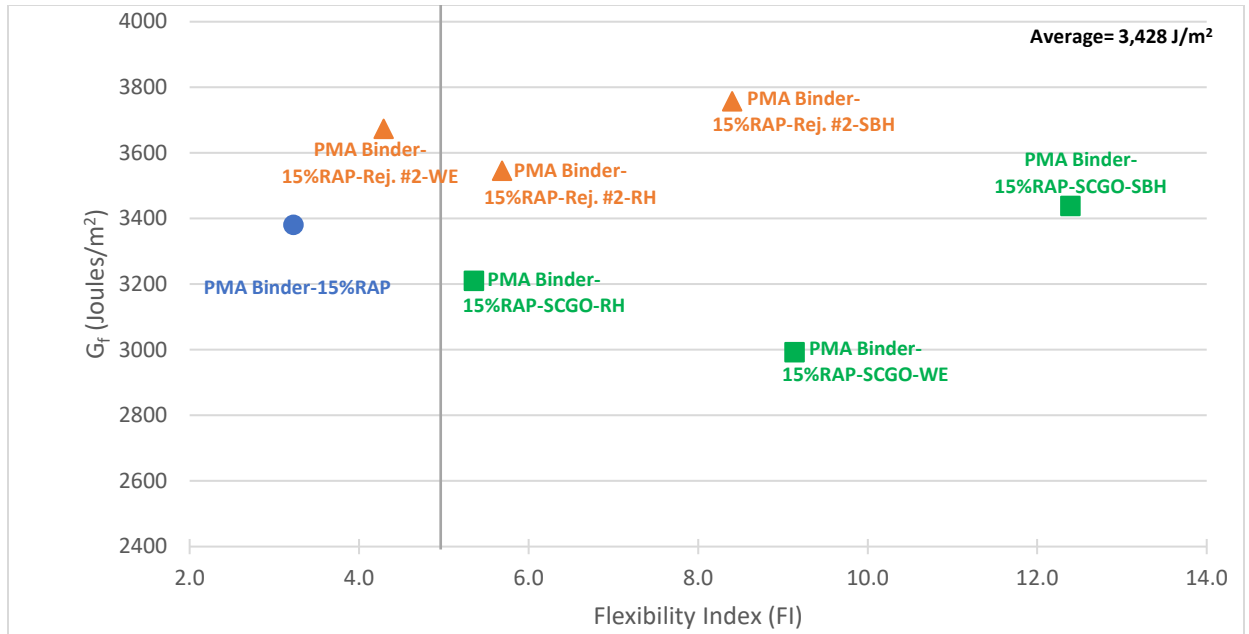


Figure 5-21: The Fracture Energy and the Flexibility Index of the PMA Binder 15% RAP Mixtures

For the PMA 15% RAP mixtures, all the OFA/ rej. #2 products show higher FE than the control mixture. The SCGO rejuvenator shows a higher FE than the control mixture when introduced with SBH fly ash. All OFA/ rejuvenator products improve the FI compared to the control mixture. SBH fly ash depicts a more substantial influence on the FI with the PMA binder when introduced with both rejuvenators.

It is important to note that the FI is critical in characterizing the cracking potential of mixtures. As seen in the results, all mixtures exceeded the minimum threshold for the fracture energy. On the other hand, the FI can distinguish these samples in terms of the of their ductility. The results strongly suggests that the effect of the OFA is maximized by the presence of the rejuvenators. The results also show that the success of the OFA additive appear to be dependent on the binder type.

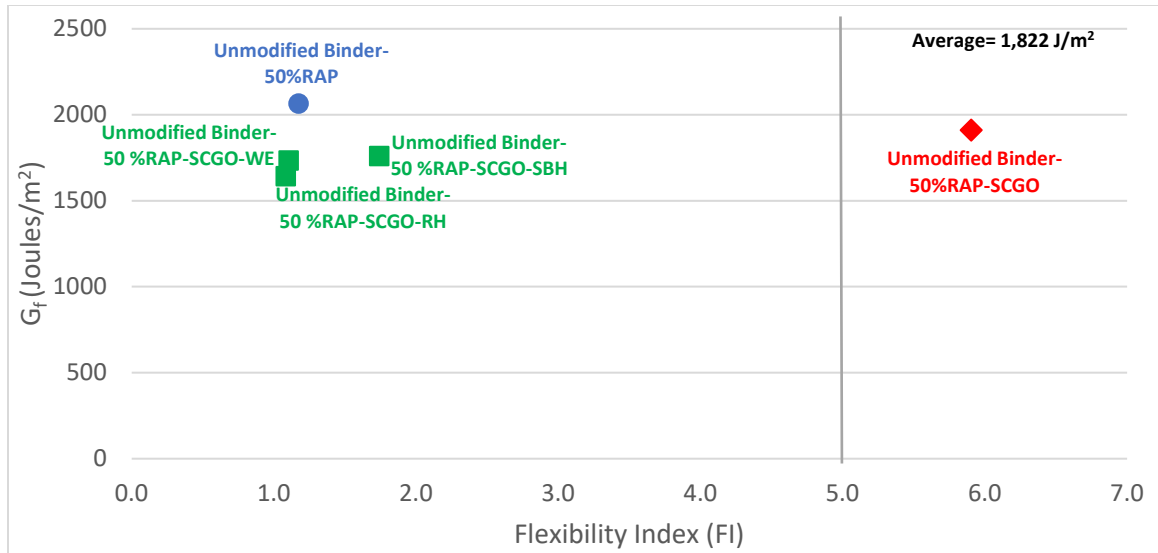


Figure 5-22. The Fracture Energy and the Flexibility Index of the Unmodified Binder 50% RAP Mixtures

Figures 5-22 and 23 show the fracture energy (FE) and flexibility index (FI) for the unmodified and PMA 50% RAP mixtures. The SCGO rejuvenator significantly enhances the 50% RAP mixture's ductile failure as measured by FI. It manages to increase the FI to over the 5.0 adopted threshold.

The presence of the SCGO rejuvenator minimally reduces the FE compared to the control unmodified 50% RAP mixture. However, the OFA/ SCGO products' introduction did not show similar improvement as the SCGO oil. Only SBH/ SCGO product enhanced the FI compared to the control mixture. However, the enhancement is very minimal and did not reach the 5.0 threshold.

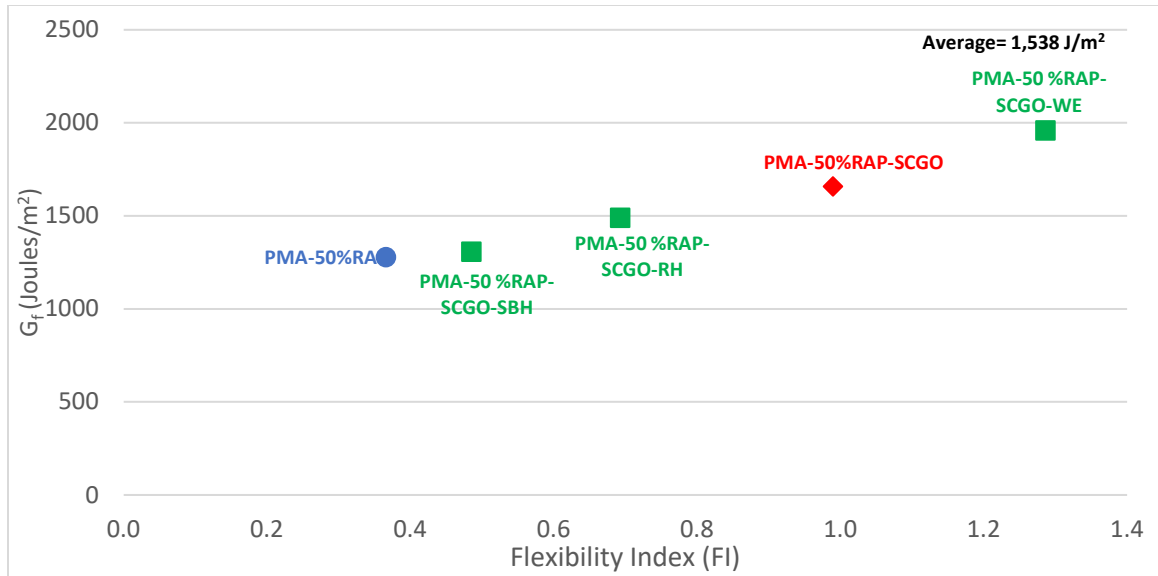


Figure 5-23. The Fracture Energy and the Flexibility Index of the PMA Binder 50% RAP Mixtures

For the PMA 50% RAP mixtures, all the FI are less than the adopted 5.0 threshold. However, all the products' presence increases the FE compared to the control mixture. Only WE/SCGO product and SCGO rejuvenator mixtures show FI higher than 1.00. these results strongly align with the binder testing illustrated in the previous phases indicating a binder dependency. That means that a higher dosage might be needed for the PMA mixtures.

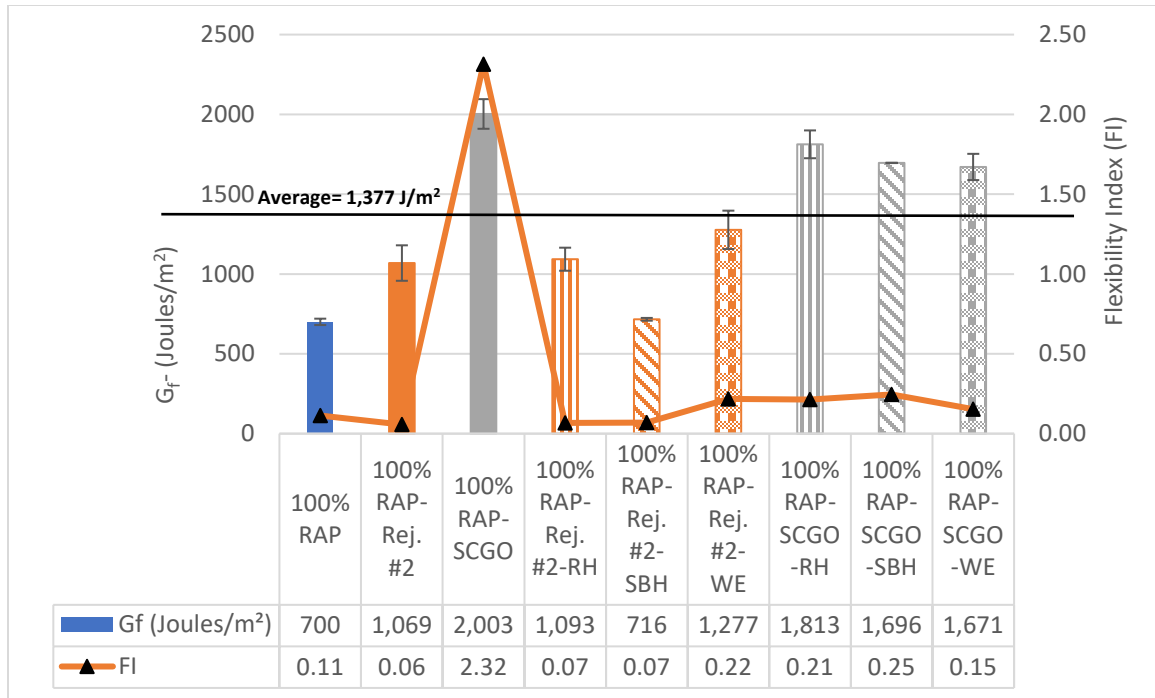


Figure 5-24: The Fracture Energy and the Flexibility Index of the 100% RAP Mixtures

Figure 5-24 shows the FE and the FI of the 100% RAP mixtures. All the FE are less than 15% and 50% RAP mixtures' FE due to the high RAP content and no existence of the virgin binder in the 100% RAP mixtures. Moreover, the FI for all the mixtures is less than the 5 thresholds. The introduction of the SCGO rejuvenator shows the highest FE and FI among all the additives combinations. It can be noticed that the OFA/ SCGO products have higher FE and FI than their rej.#2 comparisons. All OFA/ SCGO products have FE above the average FE. This is because the OFA/ SCGO products improve the mixtures' ductile failure behavior than the fly ash/ rej. #2, and the control 100%RAP mixture, as measured by the FI. Still, the FI is very low compared to the 15% and 50% RAP mixtures. However, that is a validation of the rejuvenation efficiency evaluated in the second phase of that study. The SCGO rejuvenator had a superior rejuvenation efficiency when tested with the field extracted RAP.

5.3.3.1. Optimum RAP Content According to the Intermediate Temperature Performance

In this section, the optimum RAP content will be interpolated from the 15% RAP, 50% RAP, and 100% RAP previously illustrated results.

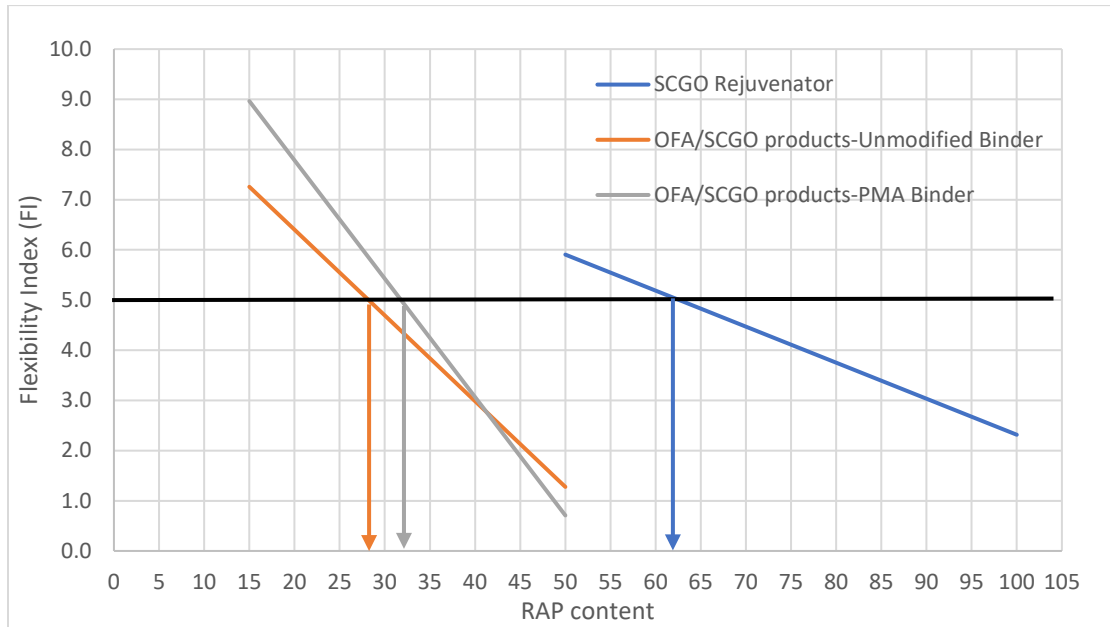


Figure 5-25. Optimum RAP Content According to the Intermediate Temperature Performance

Figure 5-25 shows the optimum RAP content according to the FI. For the SCGO rejuvenator. Two points are used, the 50% RAP-SCGO rejuvenator (5.90) and the 100% RAP SCGO rejuvenator (2.32). The optimum RAP content corresponding to FI of 5.0 is about 62%.

For the OFA/SCGO products, the average of the FI of the three OFA/SCGO products was calculated for 15% RAP (7.26 and 8.96) and 50% RAP (1.28 and 0.71) for both unmodified and PMA binder, respectively. Therefore, the optimum RAP content corresponding to FI of 5.0 is hovering around 30% for unmodified and PMA binders.

5.3.4. Thermal Cracking (Low-Temperature Performance)

Figures 5-27, 28, 29,30, and 31 demonstrate the fracture energy, toughness, and pre-peak slope of the 15% RAP and 50% RAP (unmodified and PMA, respectively) 100% RAP mixtures. A minimum value of 350 J/m² is adopted as a limiting value for the SCB fracture energy to protect the pavement against low-temperature cracking. Moreover, a minimum value of 800 kPa.m^{0.5} is proposed as a limiting value for the SCB fracture toughness by Marasteanu *et al.*(2012) [92].

Fracture toughness is a fundamental material property, indicating a material's strain energy-absorbing ability prior to fracture. The higher the fracture toughness, the higher the material resistance to crack propagation. Likewise, the higher the fracture energy, the higher the crack resistance of the asphalt mixture.

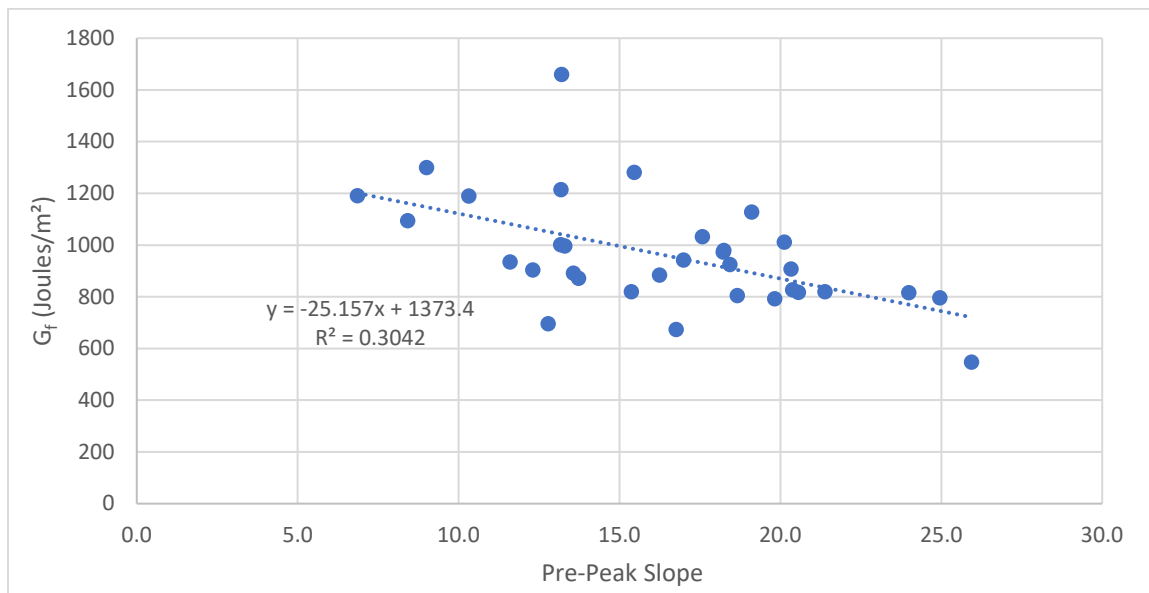


Figure 5-26. The Relation the Pre-peak Slope and the Fracture Energy for the tested Mixtures

A certain ratio of stiffness and brittleness of the mixture can be obtained from the pre-peak slope. It is essential to consider that the test occurs in a pure elastic regime when testing at low temperatures. Accordingly, the lower the slope, the more elastic the asphalt mixture is, as it reaches a higher deformation at the same load. Thus, higher fracture energy is usually required to break the test specimen, as demonstrated in Figure 5-26.

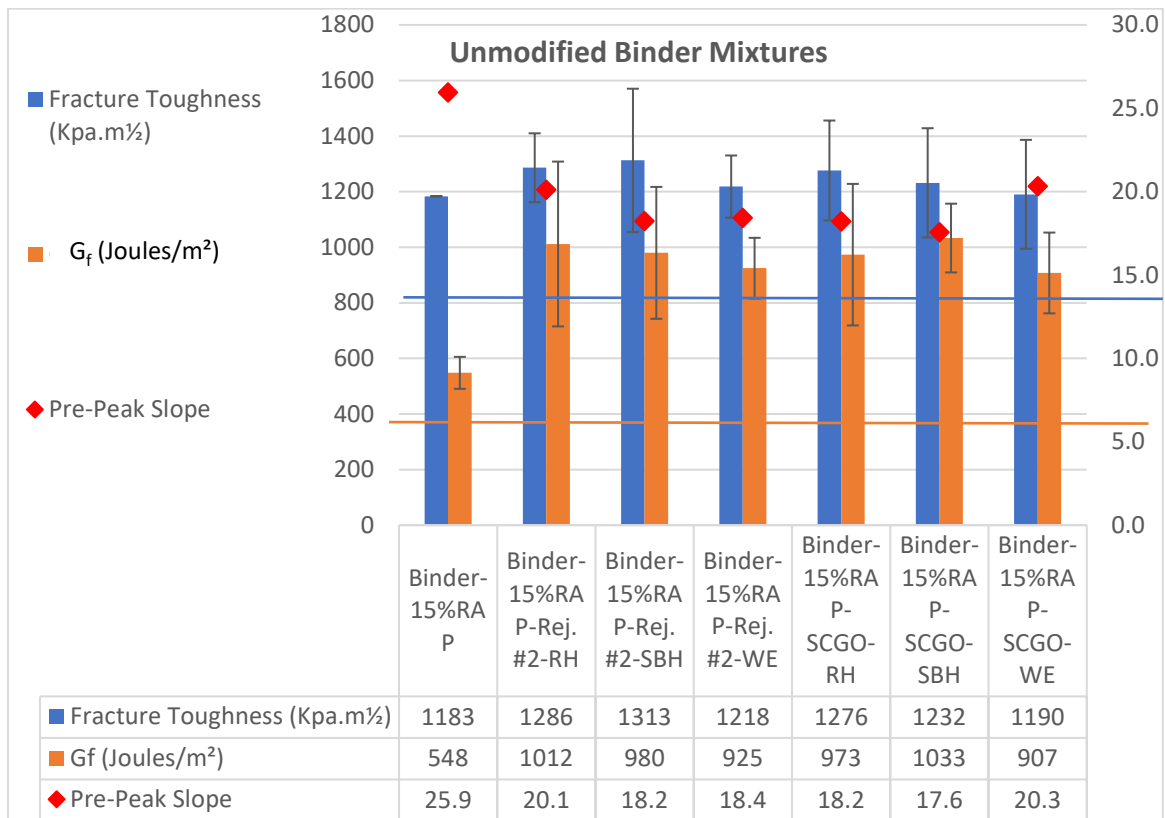


Figure 5-27. The Fracture Toughness, Fracture Energy, and the Pre-Peak Slope of the Unmodified binder 15% RAP Mixtures

Figure 5-27 shows that all fracture toughness values for the 15% RAP unmodified binder mixtures are above the adopted 800 kPa.m^{0.5}. In addition, the introduction of the fly ash/rejuvenator products further increases the fracture toughness of the mixtures compared to the control mixture. The OFA/ rej. #2 products enhance the low temperature cracking resistance of the unmodified binder mixtures compared to the OFA/ SCGO products. For

the fracture energy, the control mixture shows the lowest fracture energy. However, still above the adopted 350 J/m². Introducing the OFA/rejuvenator products increases the required energy to cause a complete failure to the mixtures. The control mixture acquires the highest slope indicating the lowest stiff mixture for the pre-peak slope. Introducing the OFA/ rejuvenator products decreases the pre-peak slope, indicating more energy required for crack propagation and higher low-temperature cracking resistance.

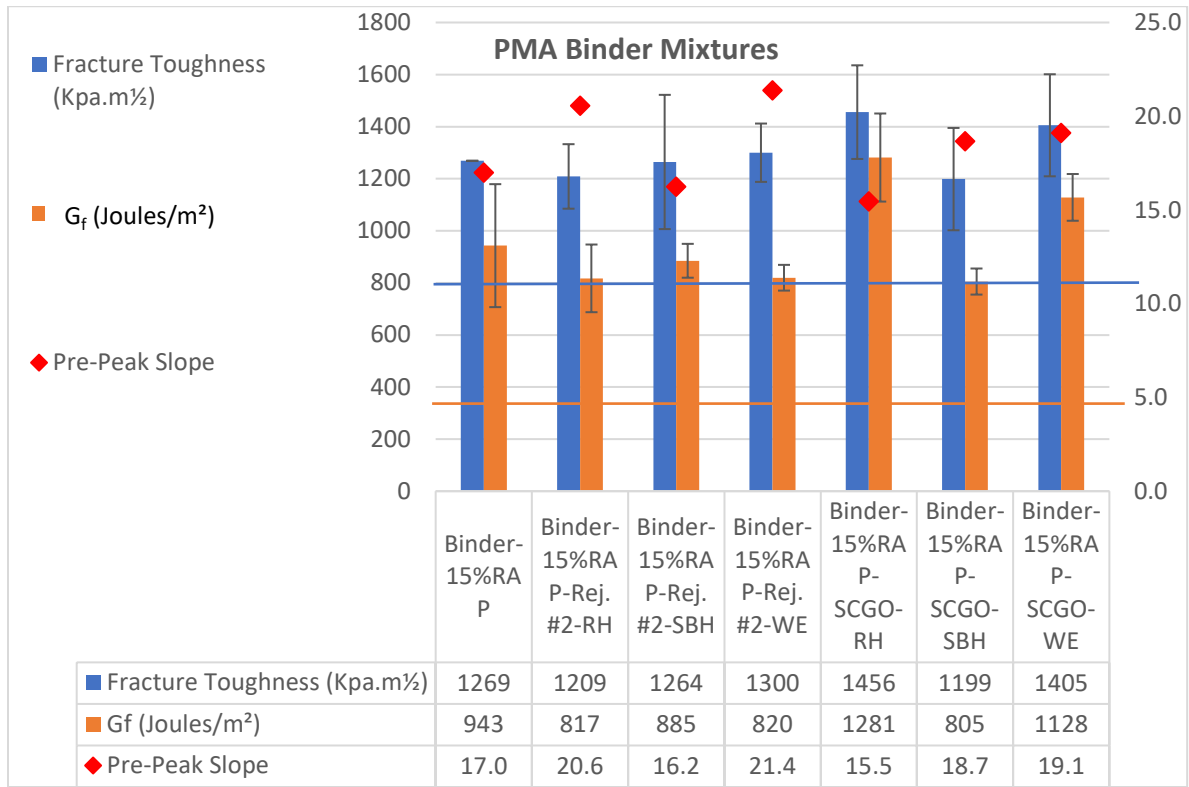


Figure 5-28: The Fracture Toughness, Fracture Energy, and the Pre-Peak Slope of the PMA 15% RAP Mixtures

As demonstrated in Figure 5-28, all fracture toughness values for the 15% RAP PMA binder mixtures are above the adopted 800 kPa.m^{0.5}. Introducing WE/ Rej. #2, RH/ SCGO, and WE/ SCGO products to the PMA mixtures increase the fracture toughness of the mixtures compared to the control mixture. All the investigated mixtures for fracture energy

are above the adopted 350 J/m^2 . Introducing RH/ SCGO and WE/ SCGO products to the PMA mixtures improve the low-temperature fracture energy compared to the control mixture. The introduction of SBH/ Rej. #2 and RH/ SCGO lower the pre-peak slope indicating higher low-temperature cracking resistance than the control PMA mixture.

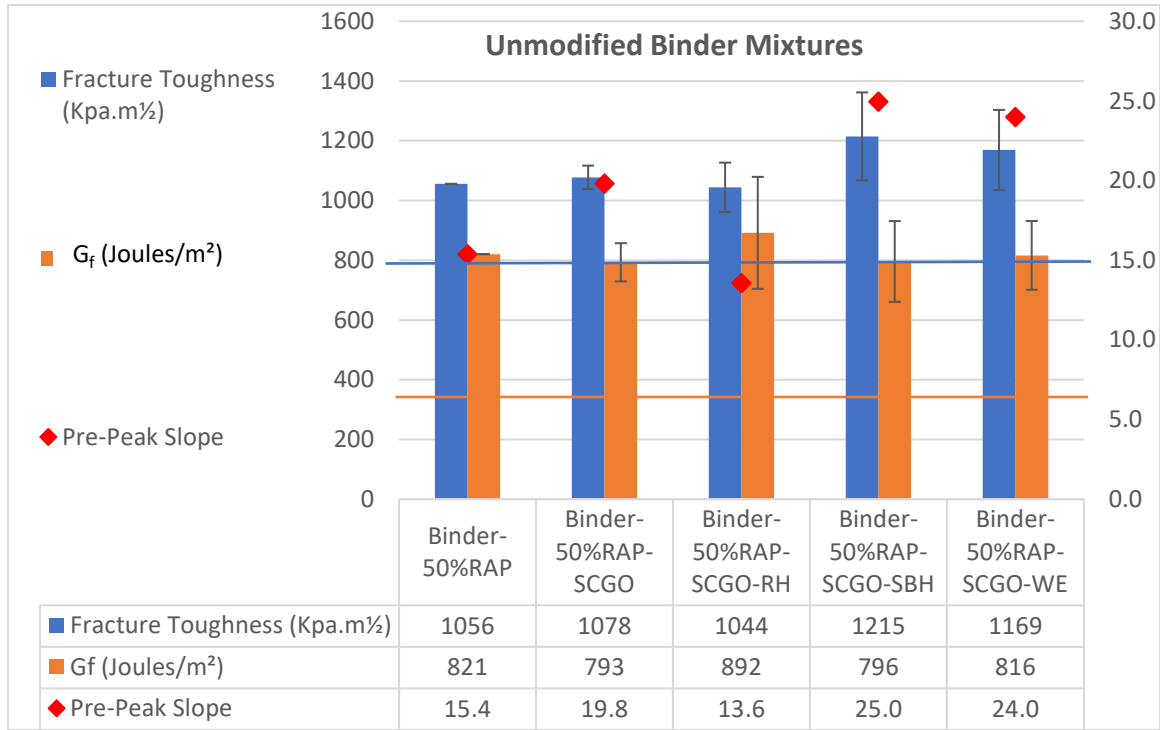


Figure 5-29. The Fracture Toughness, Fracture Energy, and the Pre-Peak Slope of the Unmodified binder 50% RAP Mixtures

As demonstrated in Figure 5-29, all fracture toughness values for the unmodified binder 50% RAP mixtures are above the adopted $800 \text{ kPa}\cdot\text{m}^{0.5}$. Introducing the SCGO rejuvenator minimally enhances the fracture toughness compared to the control mixture. The introduction of SBH/SCGO and WE/ SCGO products to the unmodified binder mixtures increased the fracture toughness of the mixtures the most compared to the control mixture. All the investigated mixtures for fracture energy are above the adopted 350 J/m^2 . The introduction of the SCGO rejuvenator is found to be associated with less fracture energy

and higher pre-peak slope, indicating less energy for crack propagation and less low-temperature crack resistance. Only RH/SCGO product increases the fracture energy and decreases the pre-peak slope among all the additives combinations.

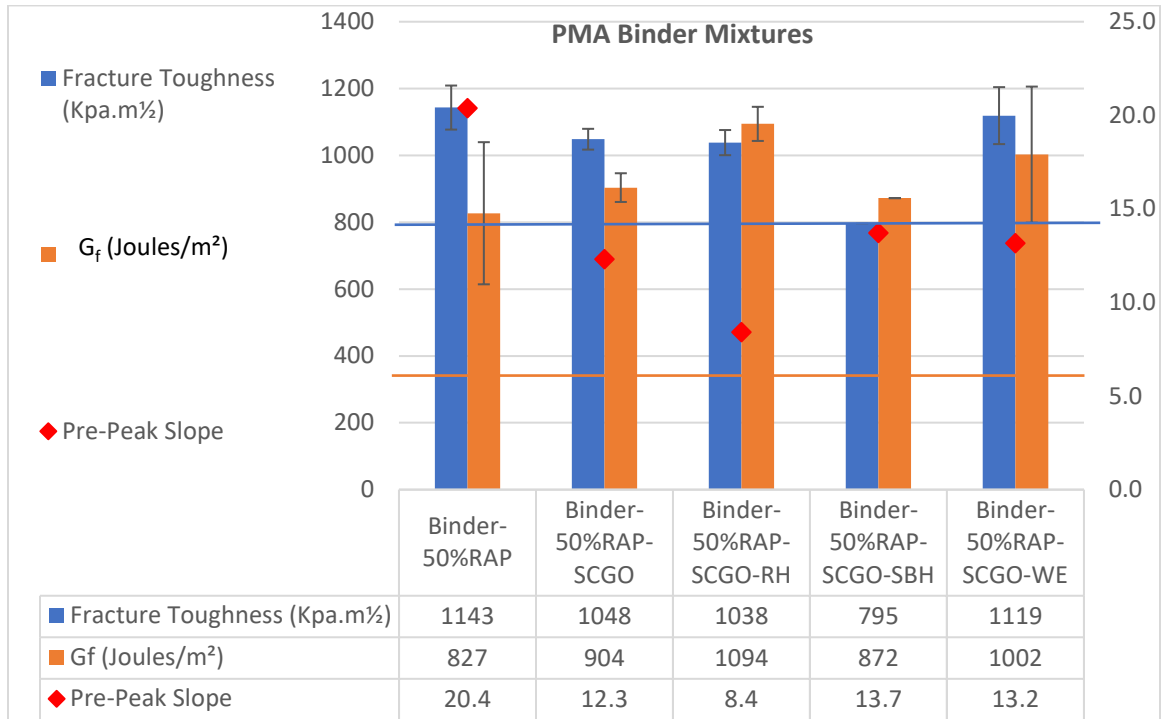


Figure 5-30. The Fracture Toughness, Fracture Energy, and the Pre-Peak Slope of the Unmodified binder 50% RAP Mixtures

As depicted in Figure 5-30, all fracture toughness values for the PMA binder 50% RAP mixtures are above the adopted $800 \text{ kPa}\cdot\text{m}^{0.5}$, except for SBH/SCGO product mixture. Introducing the SCGO rejuvenator minimally reduces the fracture toughness compared to the control mixture. The introduction of RH/SCGO and WE/ SCGO products to the PMA mixtures reduces the mixtures' fracture toughness compared to the control mixture. All the investigated mixtures for fracture energy are above the adopted 350 J/m^2 . The introduction of the SCGO rejuvenator is found to be associated with higher fracture energy and lower pre-peak slope, indicating higher energy for crack propagation and higher low-temperature

crack resistance. In general, the introduction of the OFA/SCGO products increases the fracture energy and decreases the pre-peak slope. Following the unmodified binder trend, RH/SCGO product increases the fracture energy and decreases the pre-peak slope the most among all the additives combinations.

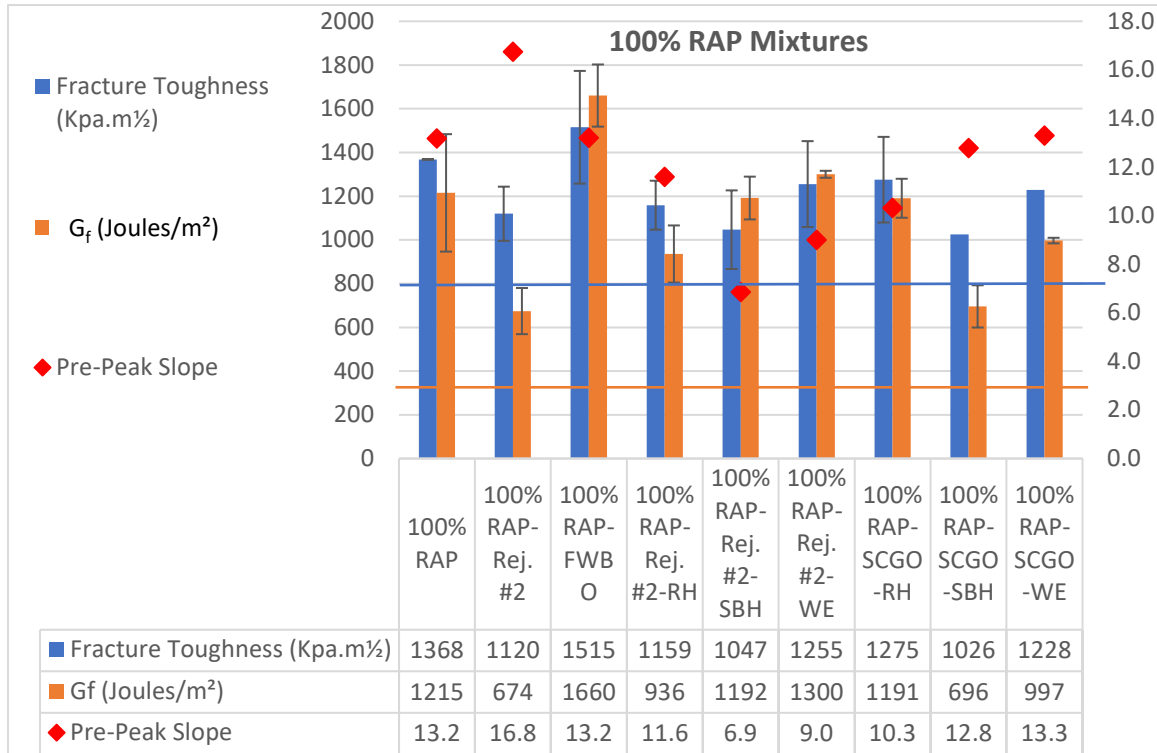


Figure 5-31: The Fracture Toughness, Fracture Energy, and the Pre-Peak Slope of the 100% RAP Mixtures

For the 100% RAP mixtures, all fracture toughness values for the investigated mixtures are above the adopted 800 kPa.m^{0.5}. None of the OFA/ rejuvenator products increase the fracture toughness compared to the control 100% RAP mixture. Only introducing the new proposed SCGO improves the fractures toughness compared to the control mixture. The same trend is observed with fracture energy. While none of the OFA/ rejuvenator products enhance the fracture energy, except with WE/Rej. #2 product, only the SCGO rejuvenator enhances the fracture energy significantly compared to the control 100% RAP mixture.

However, introducing all the OFA/ rejuvenator products, except with WE/ SCGO, reduces the pre-peak slope compared to the 100% RAP mixtures, indicating more deformation required for initiating the low-temperature cracks.

5.3.5. Analysis of Test Method Sensitivity

Statistical analysis was performed to evaluate the sensitivity of the test methods regarding binder type, RAP content, fly ash, and rejuvenator type. One-way ANOVA is used to determine if the changes in the shown parameters had statistical significance towards the outcome of six performance-related test methods: tensile strength (IDT-Rutting), fracture energy, and flexibility index (SCB-intermediate temperature), and fracture energy, fracture toughness, and pre-peak slope (SCB-low temperature). Table 5-4 shows the ANOVA table of the test methods adopted in this study results from 33 mixtures. The null hypothesis was rejected by comparing the p-value with a given α -level (0.05) since the p-value is less than the α -level.

Table 5-4: Significance of Changes in Binder Type, RAP Content, and Fly Ash/ Rejuvenator Products on the Test Method Results Using ANOVA

Test method	Performance Parameter	Mix parameters	ANOVA results					
			DF	Sum of Squares	Mean Square	F Ratio	Prob > F	Significance
IDT-Rutting	Tensile Strength (St) (kPa)	Binder Type	2.00	166706.12	83353.06	5.86	<.00*	YES
		RAP Content	2.00	37404.31	18702.16	1.01	0.38	NO
		Fly Ash Type	3.00	4789.76	1596.59	0.08	0.97	NO
		Rejuvenator Type	2.00	165140.48	82570.24	5.79	<.00*	YES
SCB-Intermediate Temperature	G _f (Joules/m ²)	Binder Type	2.00	10215276.03	5107638.02	8.60	<.00*	YES
		RAP Content	2.00	24081772.65	12040886.33	91.54	<.00*	YES
		Fly Ash Type	3.00	1226916.92	408972.31	0.44	0.72	NO

		Rejuvenator Type	2.00	416468.41	208234.20	0.23	0.80	NO
	Flexibility Index (FI)	Binder Type	2.00	136.06	68.03	6.66	<.00*	YES
		RAP Content	2.00	324.32	162.16	41.23	<.00*	YES
		Fly Ash Type	3.00	30.20	10.07	0.71	0.55	NO
		Rejuvenator Type	2.00	20.92	10.46	0.74	0.48	NO
SCB- Low Temperature	G _f (Joules/m ²)	Binder Type	2.00	109304.17	54652.08	1.21	0.31	NO
		RAP Content	2.00	245528.02	122764.01	3.03	0.06	NO
		Fly Ash Type	3.00	19938.46	6646.15	0.13	0.94	NO
		Rejuvenator Type	2.00	194237.63	97118.82	2.30	0.12	NO
	Fracture Toughness (Kpa.m ^{0.5})	Binder Type	2.00	7445.21	3722.61	0.18	0.84	NO
		RAP Content	2.00	242793.18	121396.59	9.25	<.00*	YES
		Fly Ash Type	3.00	44765.11	14921.70	0.73	0.54	NO
		Rejuvenator Type	2.00	7395.07	3697.54	0.18	0.84	NO
	Pre-Peak Slope	Binder Type	2.00	32.65	16.32	0.73	0.49	NO
		RAP Content	2.00	296.17	148.08	10.91	<.00*	YES
		Fly Ash Type	3.00	34.60	11.53	0.50	0.69	NO
		Rejuvenator Type	2.00	242.61	121.30	7.90	<.00*	YES

The binder type significantly influences the tensile strength and the rejuvenator utilized. Neither the RAP content nor the fly ash type parameters produced significant differences in the test results. However, looking at the tensile strength results, it can be observed that the 100% RAP content mixtures have much higher rutting resistance. The 15% RAP mixture results are categorized as 10 to <30 million ESALS rut resistance category, while some of the 100% RAP mixtures are categorized as 100 to < 300 million ESAL Rut resistance category. This demonstrates that the test is not sensitive enough towards the

design of high RAP mixtures. Therefore, it should not be used for optimizing high RAP mixtures.

The binder type and the RAP content significantly influence the fracture energy and flexibility index calculated at intermediate temperature. Although, the binder phase testing is significantly influenced by the rejuvenators utilized and the fly ash type on the aging and intermediate temperature performance. However, they did not show any influence on the mixture testing. This could be due to the high gap in the RAP ratios adopted in this study.

Any of the parameters do not influence the fracture energy at low temperatures. However, the fracture energy at low temperature is found to have some kind of sensitivity to RAP content and rejuvenator type, as reflected by their low p-value. On the other hand, the fracture toughness shows sensitivity to the RAP content. Worth noting that the fracture toughness is only dependent on the sample geometry (the notch length, specimen radius, specimen thickness) and the peak load.

The reason behind that the fracture toughness is not sensitive to any of the parameters, other than the RAP content, is that the sample geometry is the same for all the tested samples, and the peak load is not enough to capture the significance of any of the parameters. The fracture energy is not sensitive to any of the parameters could be due to the 5 mm/min loading rate adopted in this study. A lower loading rate could be more efficient in making the fracture energy more sensitive to the parameters, especially at lower temperature testing. However, the 5mm/min loading rate is sufficient for the pre-peak slope to be sensitive to the RAP content and the rejuvenator type. Worth noting that it is expected that none of the fracture toughness, energy, nor the pre-peak slope to be sensitive to the

binder type since the two binders used in this study are with similar low PG grade (-22), and their mixtures were tested at the same low temperature (-12 C°). None of the parameters are sensitive to the fly ash suggests that the rejuvenators may have a more dominant effect on the mixtures than the fly ash.

CHAPTER 6

LIFE CYCLE ASSESSMENT OF ECO-FRIENDLY ASPHALT PAVEMENT

6.1. Background

Roads are an essential part of a society's transportation modes in the United States. More than 60% of people and freight transportation is being done through road networks [101]. That explains why road infrastructure is one of the essential industries in construction engineering. The U.S. has about 3,600 asphalt production sites and produced about 420 million tons in 2019. Out of the 2.8 million miles of paved roads in the U.S., about 94% are surfaced with asphalt. In addition, approximately 80% of the nearly 3,330 runways in the Federal Aviation Administration (FAA's) national airport system are surfaced with asphalt pavement. In 2014, total spending on highway improvements such as new construction, reconstruction, resurfacing, and rehabilitation by all levels of government was \$105 billion. In addition, approximately \$4 billion per year from Airport Improvement Program grants and passenger facility charges is spent on airfield runways, taxiways, and aprons [102]. These facts show how big and important the roads infrastructure industry is in the U.S.

One of the first and best-known formal definitions of sustainability term emerged from the 1987 report "Our Common Future" and also known as the "Brundtland Report": "Sustainable development is the development that meets the needs of the present without compromising the ability of future generations to meet their own needs" [103]. However,

asphalt mixtures production processes compromise the concept of sustainable development, as a considerable amount of Greenhouse gases (GHG) and airborne pollutants are released into the atmosphere through the production process. GHG and its effect on climate change are increasingly spotlighted regarding policy, legislation, and the general public's concern. As a result, the pavement industry and scientific community have been challenged to improve conventional asphalt mixtures production processes by developing more sustainable technologies and behaviors [104], [105]. The United States Energy Administration (USEA) reported that in 2020, fossil fuels, petroleum, natural gas, and coal accounted for about 79% of total U.S. primary energy production. The total energy consumption share from natural gas, petroleum, coal, renewable energy, and nuclear electric power is 32%, 33%, 62%, 22%, 45%, and 26%, respectively. It is almost universally accepted that releasing GHG into the atmosphere from these fossil fuels is partly responsible for climate change [106]. Accordingly, transportation agencies are increasingly interested in investigating new technologies that will reduce the cost of asphalt pavement materials while maximizing long-term and reducing the release of GHG emitting into the atmosphere from these fossil fuels.

Applying reclaimed asphalt pavement (RAP) and recycled asphalt shingles (RAS) in new pavement construction can have significant environmental and economic advantages. Studies show that the reuse of RAP saves approximately \$2.5 billion annually, avoiding the need for vast landfill space and preserving natural resources [55]–[58]. Increased usage of reclaimed asphalt pavement (RAP) in hot mix asphalt (HMA) has increased the need for recycling agents such as asphalt binder rejuvenators.

Improving the material's mechanical performance, waste reduction in landfills, natural aggregates' extraction, and the energy requirement to produce, build, and maintain asphalt pavements are indicators of a solution's environmental sustainability. The life cycle assessment (LCA) is a methodology intended to assess the environmental impacts associated with all stages of the life cycle of a solution, or product, during materials extraction, manufacturing, distribution, usage, and after the end of life, similarly to the operations associated with road pavement construction [107]. LCA is a crucial element to prevent negative impacts on the environment from one stage of the life cycle to another and help decision-makers compare multiple solutions and select the one with the lowest impact on the environment. As shown in Figure 6-1, according to the ISO 14044:2006 standards, it consists of four main phases: (i) goal and scope definition, (ii) life cycle inventory analysis (LCI), (iii) life cycle impact assessment (LCIA), and (iv) interpretation.

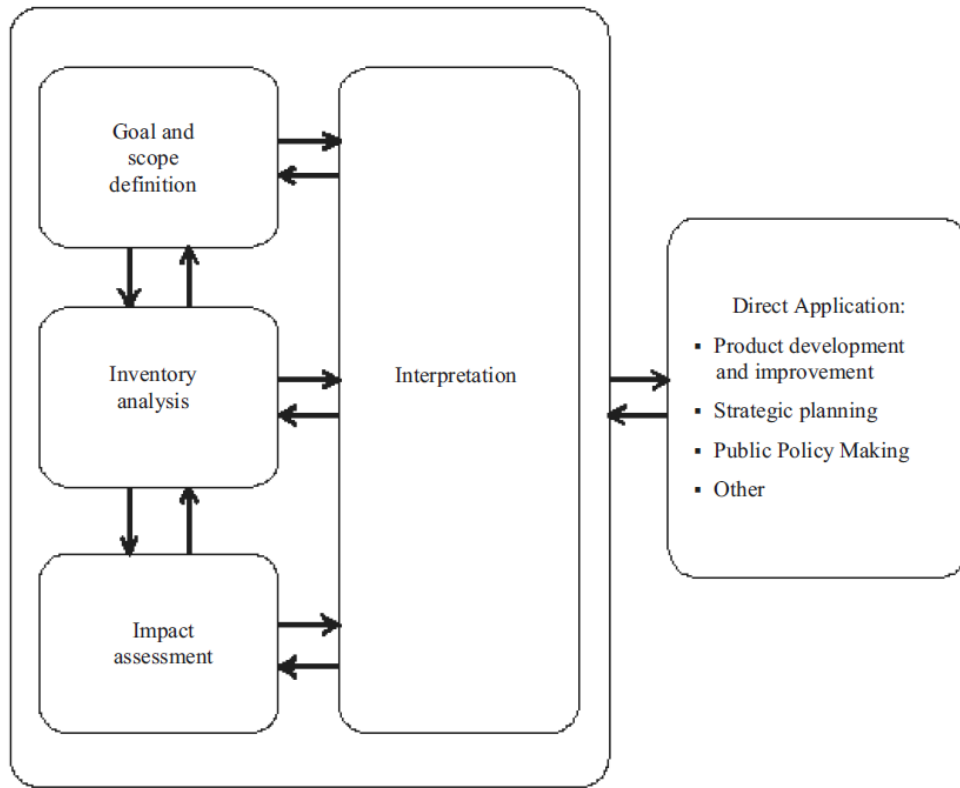


Figure 6-1. Life Cycle Assessment Framework (After the ISO 14044) [107]

Several LCA analyses have been carried out on innovative road materials and maintenance techniques to estimate the environmental compatibility of previously eco-designed asphalt materials and compare them to traditional hot mix asphalt solutions. Studies highlighted that the increased amount of recycled material in material production phases in the asphalt mixture most certainly decreases environmental impacts [108]–[110]. Yang, Kang, *et al.* (2015) [99] assessed the use of RAP and RAS in partial substitution of virgin aggregates to check the different environmental impacts, considering the vehicle's fuel consumption as a function of the International Roughness Index (IRI) index.

In 2016, Md Uzzal Hossain *et al.* [111] compared the environmental consequences of recycled and natural aggregates production. It was found that coarse recycled aggregates produced from Construction and Demolition Wastes (CDW) reduce by 65% the GHGs emissions and by 58% the consumption of non-renewable energy, compared to coarse natural aggregates. Pratic *et al.* (2020) [112] evaluated the environmental impacts of a road-pavement wearing course made up of warm-mix asphalt (WMA), an asphalt mixture produced at a temperature of 140–150 °C, with 45% RAP used in substitution for coarse aggregates, according to the ILCD midpoint impact indicators and the global energy requirement (GER) and compared them to those of a traditional hot asphalt mixture. The results showed that the combination of WMA and RAP allows the consumption of energy, virgin bitumen, and aggregates to be reduced, causing a reduction equal to 19, 14, and 8% of the GER, climate change, and potential acidification indicators, respectively, compared to those of a traditional wearing course.

Numerous studies have proved the mechanical and environmental effects of using different waste to enhance asphalt mixtures' sustainability. However, the focus is mainly on evaluating the environmental impacts of specific eco-designed materials involving one, or at most two, types of waste. LCA results rely on the geographic conditions (e.g., the position of the production facilities, the origin of the waste, and transportation distances) and the boundary considered for the system under analysis (i.e., the processes included in the analysis). That leads to complexity in accurately comparing the studied materials' environmental impacts with newly designed asphalt mixtures.

6.2. Phase Objective and Scope

The LCA analysis was performed considering the four-step methodology defined by the ISO 14040 guidelines and the Federal Highway Administration's (FHWA's) Pavement LCA Framework [113]. Further details on the methods, model development, and calculations conducted in this research study are provided in the following sections.

6.2.1. Goal of the Study

The demands to industries across all sectors and points in the value chain, including pavements to develop the potential environmental impacts of their products, made the availability of accurate life cycle inventory (LCI) and life cycle impact assessment (LCIA) a necessity. As a result, the Department of Transportations (DOTs) across the nation are starting to utilize these data in their projects and design [114].

The current phase aims to analyze the environmental, human health, and the availability of natural resources impacts of several asphalt pavement solutions involving virgin materials extraction and the production of innovative eco-designed materials, previously analyzed and tested for their positive influence on the performance of HMA mixtures (as discussed in details in sections 4.2 and 5.3). The innovative eco-designed materials utilized in this study as asphalt mixture aging additives are Off-spec Fly Ash (OFA) and the newly proposed Spent Coffee Ground Bio-oil (SCGO) rejuvenator. The SCGO is presented in two different ways in this study. The first way is as an asphalt mixture rejuvenator. The second is as a mixing delivery system to the OFA. The SCGO is blended with the OFA in a 1:2 ratio for the latter.

These innovative eco-designed materials are utilized to work as asphalt extenders with highly recycled asphalt mixtures involving high rates of RAP.

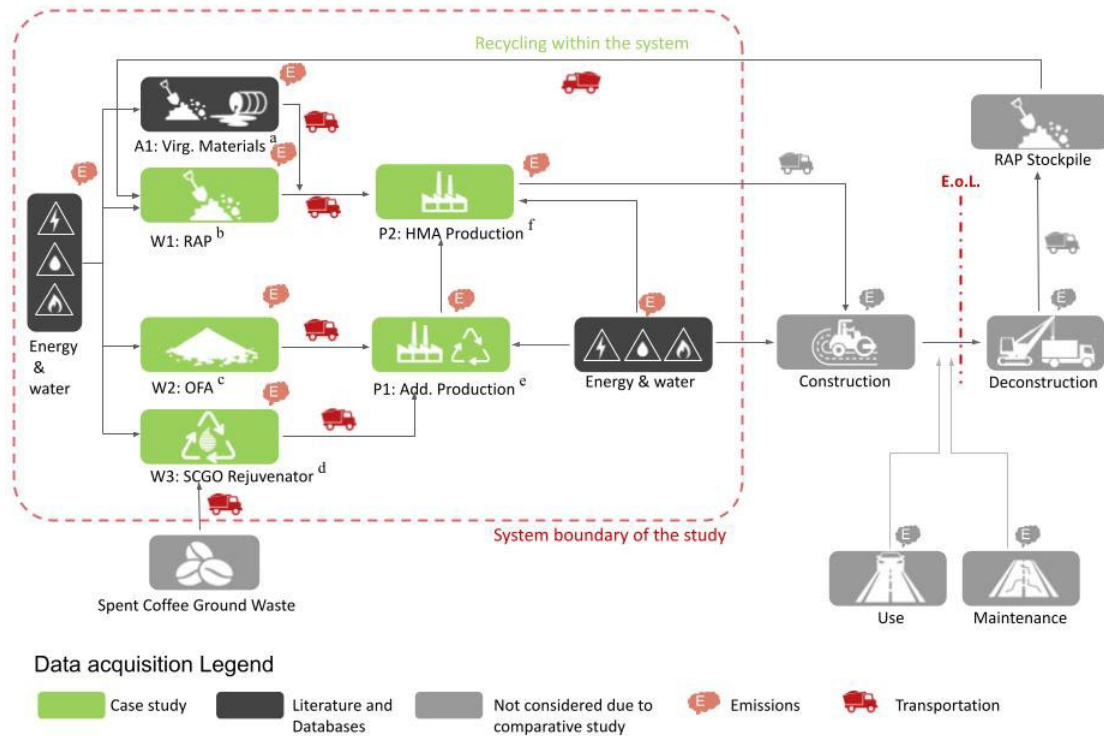
The target audience includes a broad cross-section of researchers, DOTs, green building standards agencies and green initiatives (e.g., LEED, Living Building Challenge, IgCC), internal and external stakeholders with concerns and interests about the potential life cycle environmental impacts of asphalt and its applications, and maybe more.

It is worth mentioning that this research aims to be published and shared with any interested section of the target audience.

6.2.2. System Description and Boundaries

Figure 6-2 demonstrates that the system boundary mainly focused on material extraction, transportation, and mixing due to the research scope, data availability, and quality. The use phase impacts are mainly derived by traffic information, the fuel consumption of vehicles, and pavement-vehicle interactions. The usage phase is excluded in life cycle assessments primarily for its overwhelmingly significant environmental impact than the other phases [115]–[117]. The construction phase is excluded based on the assumption that pavements with or without RAP and the new proposed aging additives would be subjected to the same construction work, M&R, and service life after construction. At the end of pavement life, it turns to RAP and is commonly disposed of without recycling, applying excessive environmental impacts. Therefore, the environmental impact of RAP is studied, as it will be recycled and utilized at high rates in this study.

Most importantly, materials extraction and mixtures production was found to be the phase that plays the most significant environmental impact compared to pavement construction, M&R, and deconstruction phases [105].



- ^a Virgin Materials (aggregates and binder) production.
- ^b RAP waste production
- ^c OFA waste production
- ^d SCGO rejuvenator production
- ^e Aging additive (OFA+SCGO rejuvenator) Production
- ^f HMA production

Figure 6-2. LCA System Boundary of The Study Based on FHWA's Pavement LCA Framework [113].

6.2.3. Functional Unit

The functional unit defines the system that will be studied and acts as the reference for scaling of input and output data in any of the life-cycle stages of the product or service [118]. For pavement systems, the functional unit should represent the physical dimensions and the quantified performance of the pavement [119]. However, a declared unit may be used instead of a functional unit when the scope of the LCA does not include all stages of the life cycle beyond delivery to the plant gate. The excluded stages could be due to the uncertainty of the application of the product and its functional requirements. The defined unit is typically identified in terms of its physical quantity (such as mass, length, area, or volume) and does not include any functionality definitions [113].

As previously illustrated, the construction and usage phases are excluded from the LCA system studied. The exclusion is due to the comparative study, the uncertainty in the data used, and uncertainty in predicting future changes in traffic and technology. Accordingly, this study identified a defined unit of one ton of HMA produced in the United States of America.

6.2.4. Life Cycle Inventory Analysis

The life cycle inventory (LCI) analysis stage consists of the system's real data collection and modeling. In addition, the data sources rely on the several models selected for modeling the processes analyzed by the several considered sub-systems that make up the whole system.

Two types of data are used for this LCA study. The first is primary data, which is specific for the product or service's production processes. This data is obtained from the goods' producers, the operators of processes and services, and their associations. The second is secondary data which presents generic and/or average data for the studied solution, considering the products and operations. Secondary data can be obtained from primary data sources, sometimes with some modifications, and from national databases, consultants, and research groups [108], [120].

The LCA presented in this study was performed using the OpenLCA V1.10.3 software from GREENDELTA combined with the Ecoinvent database, SimaPro database, U.S. Life Cycle Inventory (USLCI) Database, and GaBi LCA Database. This software provides a broad set of database combinations as one of the most widely disseminated LCA tools. Furthermore, it provides the user with an interface, several comprehensive environmental information databases, and various methods to perform the impact assessment [121]. In addition, the software provides a straightforward interface to perform a complete LCA, comprising the four steps described in EN ISO 14040:2006. The USLCI database provides individual gate-to-gate, cradle-to-gate, and cradle-to-grave accounting of the energy and material flows into and out of the environment associated with producing a material, component, or assembly in the U.S. [122]. The Ecoinvent database is the most widely used in the construction sector. The database used was the Ecoinvent 3-allocation, cut-off by classification-unit base [108].

The underlying philosophy of the cut-off approach is that the producer does not obtain any credit for the provision of recyclable materials but is nonetheless fully responsible for their waste disposal [123]. GaBi LCA Database contains data sets based on know-how from GaBi's long-term co-operation with industry as well as patent, technical and scientific literature, which makes the GaBi Databases one of the most comprehensive LCI databases worldwide [124].

For this study, the data selected are related to raw material extraction and production inventory, energy (diesel and electricity), and transportation vehicles and machines. The data is demonstrated in detail in section 3 of this phase.

6.2.4.1. Data Acquisition of Materials Extraction and Production

6.2.4.1.a. Mixtures Composition Different Scenarios

This section illustrates the alternative mixtures investigated to undertake a comprehensive comparative study evaluating the potential environmental impacts of each mixture with and without RAP. The control mixture is determined to be a conventional HMA with no RAP and no added rejuvenators or aging additives. Different incorporation of RAP rates is considered in this LCA to assess the use of RAP material in HMA. Side by side, the environmental impacts of the inclusion of the innovative eco-designed materials are investigated. The key 'LCX-Y' was adopted to identify the studied mixtures. According to this key, 'X' refers to the type of RAP percentage in the mixture. On the other hand, 'Y' refers to the type of additive added to the mix (either 'A' for OFA/SCGO additive or 'R'

for SCGO rejuvenator). Table 6-1 demonstrates the features of the several mixtures evaluated in this case study.

Table 6-1. Scenarios of the Asphalt Mixtures Analyzed in LCA Study.

Material	Mixture scenarios									
		LC0-0	LC15-0	LC15-A	LC30-A	LC50-A	LC80-A	LC80-R	LC100-A	LC100-R
Virgin aggregate (%/m)^a	94.80	81.2	81.2	66.4	48.7	19.8	19.8	0.0	0.0	
RAP (%/m)	0.0	14.4	14.4	30.0	48.7	79.2	79.2	99.4	99.4	
Virgin Asphalt Binder (%/m)	5.2	4.4	3.8	3.0	2.0	0.4	0.4	0.0	0.0	
Aging Additive (%/m)	0.0	0.0	0.6	0.6	0.6	0.6	0.0	0.6	0.0	
SCGO Rejuvenator (%/m)	0.0	0.0	0.0	0.0	0.0	0.0	0.6	0.0	0.6	

^a (%/m) percentage by mass of the mixture

6.2.4.1.b. Virgin Materials (A1)

Table 6-2 shows the data and data resources and processes associated with virgin aggregate and asphalt binder production.

Table 6-2. Life Cycle Inventory Data for Virgin Material Extraction Processes

Material	Data (P/S) ^a	Record Name
Production of virgin bituminous binder	S [124]	Bitumen at refinery, production mix, at refinery, from crude oil, 38.7 MJ/kg net calorific value {RNA} ^b
Production of virgin aggregate	P [123]	Gravel, crushed {RoW} ^c market for gravel, crushed Cut-off

^a P/S stands for whether the data is primary or secondary

^b RNA refers to North America [126]

^c RoW refers to Rest of World [126]

6.2.4.1.c. RAP Production Process (W1)

RAP production process sub-phase is divided into pre-processing and post-processing. RAP pre-processing is associated with the construction and M&R phases. RAP post-processing is attributed to the mixture production phase. Four main activities are involved in RAP post-processing (crushing, stacking, conveying, and screening) [127]. Table 6-3 illustrates the four main RAP production activities mentioned above for producing one ton of RAP.

Table 6-3. Life Cycle Inventory Data for RAP Production Processes (Per 1 Ton of RAP)

Process name	Data (P/S) ^a	Record Name	Data value	Data unit	Notes
Crushing of RAP by a crushing unit	S [128], [129]	Diesel equipment operation; industry average; > 56 kW and < 560 kW	3.00	MJ	Productivity: 358 ton/hr.
Stacking of RAP by a wheel loader	S [123], [127]	Excavation, skid-steer loader {RNA}	0.47	m ³	RAP unit weight: 1940 - 2300 kg/m ³
Conveying of RAP on a conveyor belt	S [129], [130]	Diesel equipment operation; industry average; > 56 kW and < 560 kW	0.21	MJ	Average Productivity: 650 ton/hr.
Screening by a mobile screener	S [129], [131]	Diesel equipment operation; industry average; > 56 kW and < 560 kW	4.04	MJ	Average Productivity: 250 ton/hr.

^a P/S stands for whether the data is primary or secondary

6.2.4.1.d. SCGO Production Process (W3)

In phase II, the study investigated the potential of extracted SCGO to mitigate the effects of aging on unmodified, Polymer Modified Asphalt (PMA) binder and field extracted RAP. Two market rejuvenators were evaluated side by side with a new SCGO rejuvenator. Furthermore, rejuvenators' efficiency was evaluated through leading aging indicators, such as Fourier Transform Infrared Spectroscopy (FTIR), ΔT_c , the Glover-Rowe (G-R) parameter, Crossover frequency, and modulus (ω_c , G_c^*). According to that research, SCGO acquires the merit of being a promising eco-friendly rejuvenator in the asphalt pavement industry, with effectiveness comparable to the two investigated market rejuvenators tested.

The investigated SCGO rejuvenator extraction process discussed in detail in section 3.2.2

Table 6-4. Life Cycle Inventory Data for SCGO Extraction Processes (Per 1 Kg of SCGO)

Process name	Data (P/S) ^a	Record Name	Data value	Data unit	Notes
Input					
SCG Waste	P [123]	Food residue, processed	7	Kg	Measured
n-Hexane (Pure)	P [123]	Hexane {GLO} market for Cut-off, S	24.1	Kg	Hexane Density: 655 kg/m ³
Extraction Thimble	P [123], [132]	Kraft paper, unbleached production mix at plant {RER} ^b	0.6	Kg	Measured
Water	P [129]	Tap water, at user {RNA}	31063.0	Kg	Water flow rate 0.2 Gallon/min
SCG Waste Transportation to the Extraction Location	S [129]	Transport, lorry >28t, fleet average {RNA}	0.21	Ton-meter	The distance: 300 Km
Electricity for SCG Waste Drying	S [129], [133]	Electricity, Eastern US, 2014	50.64	KWh	Time: 24 hours Oven Power: 2.11 KW
Electricity for Extraction Process	S [129], [134]	Electricity, Eastern US, 2014	210	KWh	Time: 700 hours Heater Power: 0.3 KW
Electricity for n-Hexane Recovery	S [129], [134]	Electricity, Eastern US, 2014	1.5	KWh	Distillation time: 5 hours Heater Power: 0.3 kW
Output					
SCG Waste Bio-char	S [135]	biochar; produced from thermochemical conversion; at plant	6.0	Kg	Measured
Wastewater	P [129] [129]	Treatment, sewage, to wastewater treatment-US	31.0	m ³	Calculated
Waste Extraction Thimbles	P [123]	Waste paper	0.6	Kg	Measured
Evaporated n-Hexane (air emissions)	S [123]	hexane	10.5	Kg	Measured
Recovered n-Hexane	P [123]	Hexane {GLO} market for Cut-off, S	13.6	Kg	Measured

^a P/S stands for whether the data is primary or secondary

^b RER refers to Europe [126]

6.2.4.1.e. New Proposed OFA/SCGO Aging Additive Production Process (P1)

In the previous phases, the study evaluated the upcycled OFA/rejuvenator synergetic influence on unmodified and PMA binder aging as demonstrated in sections 4.2 and 5.3. Results showed that all OFA additives either reduce or maintain the oxidation level as that of the neat binder. This indicates a slower aging rate for the OFA blends than the binders alone. Further, rejuvenators' introduction improved the aging resistance of OFA blends, suggesting high potential synergy. Finally, the results encouraged utilizing the SCGO rejuvenator as a delivery system for the OFA, facilitating the mixing process. The new OFA/SCGO aging additive is produced by blending SCGO and OFA in a 1:2 ratio. This percentage achieves a dynamic viscosity close to the binder's viscosity at 155°C (mixing temperature).

The OFA/SCGO additive production process is illustrated in details in section 4.2.2.

Table 6-5. Life Cycle Inventory Data for OFA/SCGO Aging Additive Production (Per 1 Kg of OFA/SCGO Aging Additive)

Process name	Data (P/S) ^a	Record Name	Data value	Data unit	Notes
OFA: W2	S [129]	CUTOFF Disposal, fly ash, to unspecified landfill {RNA}	0.67	Kg	Measured
SCGO Rejuvenator: W3	S	See Table 6-5	0.33	Kg	Measured
OFA Transportation to the Production Location	S [129]	Transport, lorry >28t, fleet average {RNA}	0.11	Ton-meter	The distance: 170 Km
Heating the OFA and SCGO	S [129], [133]	Electricity, Eastern US, 2014	4.22	KWh	Time: 2 hours Oven Power: 2.11 KW
Mixing Process	S [129], [136]	Electricity, Eastern US, 2014	0.095	KWh	Time: 0.5 hours Stirrer Power: 0.19 KW
Heating during the mixing process	S [129], [137]	Electricity, Eastern US, 2014	0.9	KWh	Time: 0.5 hours Oven Power: 1.8 KW

^a P/S stands for whether the data is primary or secondary

6.2.4.1.f. HMA Production Process (P2)

The HMA production process addresses the potential environmental impacts arising from the production of the different mixtures considered in this case study. The Thermal Energy (TE) consumed to produce the different investigated mixtures is determined according to Equation 6-1. The equation assumes that conventional heavy fuel oil (HFO) is combusted for production. The calculated TE accounts for variations in composition, mixing temperature, moisture content of aggregates, and initial temperature of raw materials [105].

The environmental impact resulting from HMA production was modeled based on “*Heat, district or industrial, other than natural gas {RoW}*” heat production, heavy fuel oil, at industrial furnace IMW | Cut-off, S - Copied from Ecoinvent”.

$$TE = \left[\sum_{i=0}^M m_i \times C_i \times (t_{mix} - t_0) + m_{bit} \times C_{bit} \times (t_{mix} - t_0) + \sum_{i=0}^M m_i \times W_i \times C_w \times (100 - t_0) + L_v \times \sum_{i=0}^M m_i \times W_i + \sum_{i=0}^M m_i \times W_i \times C_{vap} \times (t_{mix} - 100) \right] \times (1 + CL)$$

Equation (6-1)

Where,

- TE is the thermal energy (MJ/ton-mixture) necessary to produce one ton of bituminous mixture;
- m_i is the mass of aggregates of fraction i ;
- C_i is the specific heat capacity coefficient of aggregate fraction i ;
- M is the total number of aggregate fractions;
- t_{mix} is the mixing temperature of a bituminous mixture;
- t_0 is the ambient temperature;
- m_{bit} is the mass of bitumen;
- C_{bit} is the specific heat capacity coefficient of bitumen;
- W_i is the water content of aggregates of fraction i ;
- C_w is the specific heat capacity coefficient of water;

- L_v is the latent heat required to evaporate water;
- C_{vap} is the specific heat capacity coefficient of water vapor;
- CL is the casing losses factor.

CL is thermal energy used to heat plant iron (for example, the drum's shell), then radiated to the atmosphere rather than heat the mixture components [138]. This factor was considered the same for all mixtures presented in this study, following the findings presented by Santos et al. (2018) [139]. Table 6-6 demonstrates the values of the parameters used to calculate the TE.

Table 6-6. Parameters Considered Calculating TE According to Equation (1)

Parameter	Value	Unit
T_0 -Ambient temperature	15	°C
t_{mix} Mixing temperature of HMA	155	°C
C_{agg} Specific heat of natural aggregates ^a	0.74	KJ/Kg/°C
W_{agg} Water content of natural aggregates	3	% by mass of aggregates
W_{RAP} Water content of RAP	3	% by mass of RAP
C_{RAP} Specific heat of natural RAP ^a	0.74	KJ/Kg/°C
C_{water} Specific heat of water at 25°C	4.18	KJ/Kg/°C
L_v Latent heat of vaporization of water	2256	kJ/kg
C_{vap} Specific heat of water vapor	1.83	kJ/kg
C_{bit} Specific heat of bitumen	2.09	KJ/Kg/°C
C_{rej} Specific heat of SCGO ^b	1.95	KJ/Kg/°C
C_{add} Specific heat of OFA/SCGO additive ^c	2.09	KJ/Kg/°C
CL Casing loses factor ^d	27	%

^a Value for granitic aggregates [105]

^b Value adopted based on average of various vegetable oils' specific heat [140]

^c assumed to be the same as bitumen

^d Value considered from the literature [138]

Table 6-7 illustrates the calculated TE required to produce 1 ton of the mixtures studied in this research.

Table 6-7. Calculated Thermal Energy (TE) for 1 Tonne of Mixtures' production

Material	Mixture scenarios								
	LC0-0	LC15-0	LC15-A	LC30-A	LC50-A	LC80-A	LC100-A	LC80-R	LC100-R
TE (MJ/ton mixture)	231.6	230.6	230.6	229.6	228.4	226.5	226.0	226.4	225.9

6.2.4.1.g. Materials' Transportation to the Production Locations

This study considered the environmental impacts resulting from materials' transportation. The environmental impacts resulting from transportation are due to the emissions released during the fuel combustion process. All materials and mixtures are assumed to be hauled by Heavy Duty Vehicle (HDV). Transport, lorry >28t, fleet average {RNA}, with a default unit of ton-kilometer (t.km) used to determine the environmental burdens associated with the transportation of materials movements. The total mass of transported material and the distance between the materials' extractions sites and the mixing plant site were calculated to define the t.km units for each scenario. Table 6-8 illustrates the assumed distances between the different locations involved in this study.

Table 6-8. Transportation Distances Considered in the Case Study

Materials' Location ^a	Production Locations	
	OFA/SCGO Production Location	Mixing Plant Location
OFA Landfill	170 Km	NA
SCG Waste Landfill	300 Km	NA
Virgin Aggregate	NA	145 Km
Virgin Binder	NA	55 Km
RAP	NA	145 Km
OFA/SCGO additive	NA	97 Km

^a The Virgin materials, RAP, mixing plant, and Landfills locations are based on existing locations around Philadelphia, Pennsylvania. Only the OFA/SCGO production location is assumed.

6.2.5. Life Cycle Impact Assessment (LCIA)

The LCIA phase aims to transfer the input and output flows of the LCI into impact category indicators, which are comprehensible assessments of specific environmental concerns that can influence the environment, human health, and the availability of natural resources. The LCI results were conducted and analyzed in this study per the characterization factors defined by the Tool for the Reduction and Assessment of Chemical and Other Environmental Impacts (TRACI) version 2.1 impact assessment methodology [125].

TRACI 2.1 focuses on the U.S. average characterization of the following impact categories: (1) ozone depletion (OD), (2) global warming (GW), (3) photochemical smog formation (PSF), (4) acidification (Ac), (5) eutrophication (Eu), (6) human health cancerous (HHC), (7) human health noncancerous (HHN), (8) human health particulate (HHP), and (9)

ecotoxicity (Ec). Table 6-9 demonstrates the emissions-related categories characterization factors available for the media listed for each impact category.

Table 6-9. Characterization Factors are available for the media listed for each impact category After H. Gu and R. Bergman (2016) [125]

Impact Category	Media
Ozone Depletion	Air
Global Warming	Air
Photochemical Smog Formation	Air
Acidification	Air, Water
Eutrophication	Air, Water
Human Health Cancerous	Urban Air, Nonurban Air, Freshwater, Seawater, Natural Soil, Agricultural Soil
Human Health Noncancerous	Urban Air, Nonurban Air, Freshwater, Seawater, Natural Soil, Agricultural Soil
Human Health Particulate	Air
Ecotoxicity	Urban Air, Nonurban Air, Freshwater, Seawater, Natural Soil, Agricultural Soil

6.3. Results and Discussion

The potential environmental impacts are calculated based on the LCA methodology, assumptions, and the collected inventory data illustrated above. Table 6-10 shows the LCIA results for the investigated scenarios.

Table 6-10. Total LCIA Results for the Investigated Scenarios

Impact Category	Unit	LC0-0	LC15-0	LC15-A	LC30-A	LC50-A	LC80-A	LC100-A	LC80-R	LC100-R
Acidification	kg SO ₂ eq	1.50E+00	1.31E+00	1.28E+00	1.07E+00	8.19E-01	4.32E-01	3.18E-01	6.44E-01	5.43E-01
Carcinogenic	CTUh	1.41E-05	1.21E-05	1.15E-05	9.31E-06	6.67E-06	2.59E-06	1.34E-06	4.16E-06	3.00E-06
Ecotoxicity	CTUe	3.67E+02	3.29E+02	4.20E+02	3.77E+02	3.27E+02	2.49E+02	2.16E+02	4.67E+02	4.46E+02
Eutrophication	kg N eq	1.18E-01	1.05E-01	1.66E-01	1.51E-01	1.34E-01	1.08E-01	9.86E-02	2.44E-01	2.42E-01
Global warming	kg CO ₂ eq	3.04E+02	2.65E+02	2.51E+02	2.06E+02	1.54E+02	7.34E+01	5.00E+01	1.01E+02	7.88E+01
Non carcinogenic	CTUh	2.11E-05	1.87E-05	2.18E-05	1.91E-05	1.58E-05	1.09E-05	9.05E-06	1.99E-05	1.87E-05
Ozone depletion	kg CFC ₁₁ eq	2.91E-05	2.61E-05	3.76E-05	3.43E-05	3.04E-05	2.47E-05	2.35E-05	5.26E-05	5.30E-05
Respiratory effects	kg PM _{2.5} eq	1.07E-01	9.51E-02	9.98E-02	8.57E-02	6.91E-02	4.33E-02	3.44E-02	6.82E-02	6.07E-02
Smog	kg O ₃ eq	1.01E+01	8.98E+00	9.34E+00	8.10E+00	6.62E+00	4.34E+00	3.55E+00	6.43E+00	5.75E+00

Figure 6-3 illustrates the relative environmental impacts of the alternative HMA scenarios studied in relation to the conventional asphalt mixture (LC0-0). The negative relative value refers to a decrease in the measured impact category. On the contrary, the relative positive value can be interpreted to increase the environmental impact profile.

All the investigated scenarios with the different RAP incorporation and the new eco-friendly additives show a consistent decrease in six environmental impacts out of nine. Those six impacts are Acidification, Carcinogenic, Non-carcinogenic, Global Warming, Respiratory effects, and Smog. It can be noted that the higher the RAP incorporation, the higher the reduction in those six environmental impacts.

Looking at the LC15 scenarios Acidification, Carcinogenic, and Global Warming, it can be noticed that the inclusion of the new OFA/SCGO additive reduces these environmental

impacts. Investigating the LC80 and LC100 scenarios, the new proposed SCGO rejuvenator shows higher environmental risks than the OFA/SCGO aging additive.

LC15-0, LC50-A, LC80-A, and LC100-A scenarios reduce Ecotoxicity environmental impact category relative to the control scenario LC0-0. All the investigated scenarios, except with LC15-0, LC80-A, and LC100-A, show an increase in Eutrophication and Ozone depletion impact categories relative to the LC0-0 scenario. However, higher incorporation of RAP with OFA/SCGO additive inclusion translates to a reduction in Eutrophication and Ozone depletion environmental impact categories. LC80-R and LC100-R scenarios show that the SCGO rejuvenator increases the Ecotoxicity, Eutrophication, and Ozone Depletion environmental impacts significantly. Investigating the SCGO production process and its related environmental impacts, it is concluded that these significant increases in the mentioned impact categories are due to the hexane production process and the hexane evaporated during the SCGO extraction process, as illustrated in Figure 6-4.

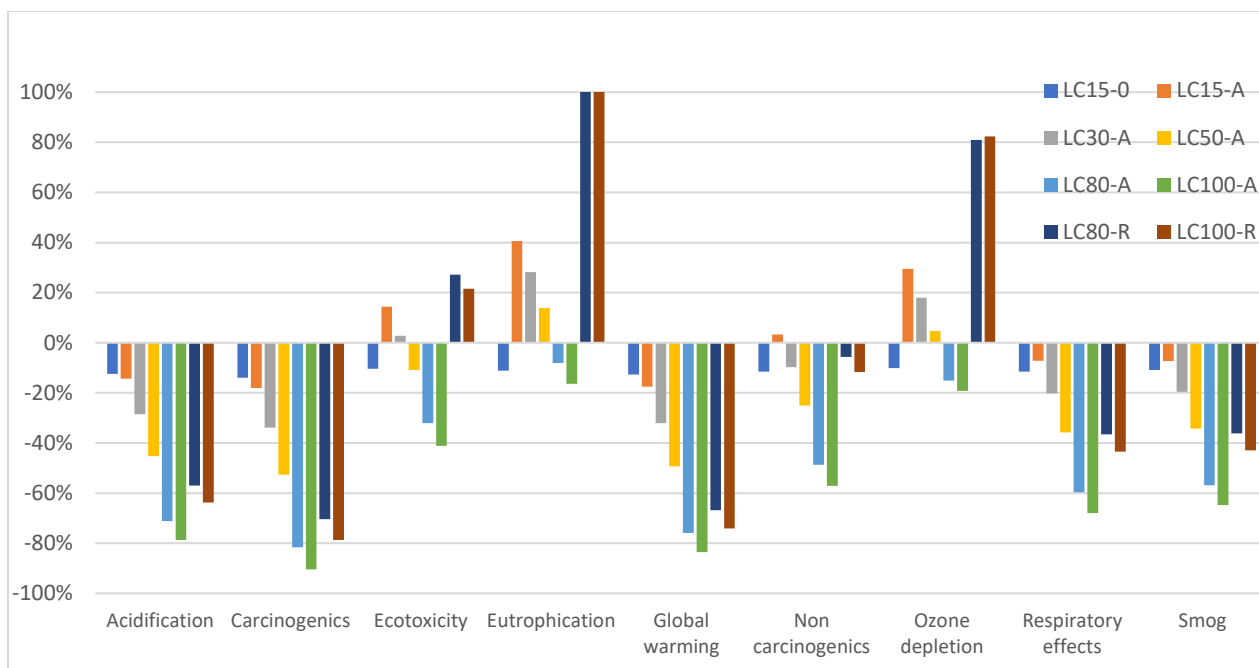


Figure 6-3. LCIA Results Relative to the Control Scenario (LC0-0)

Figure 6-4 shows the contribution of each sub-process involved in the SCGO rejuvenator production process. It can be concluded that utilization of n-Hexane as an extraction solvent has a dominant influence over all the environmental impacts, with a minimum value of 85% with Carcinogenic environmental impact.

Other bio-oil extraction techniques such as pyrolysis, hydrothermal liquefaction, Ultrasonic Assisted Extraction (UAE) are recommended for decreasing the negative influence on those mentioned environmental impacts [132], [141]–[143], especially when aiming for mass production.

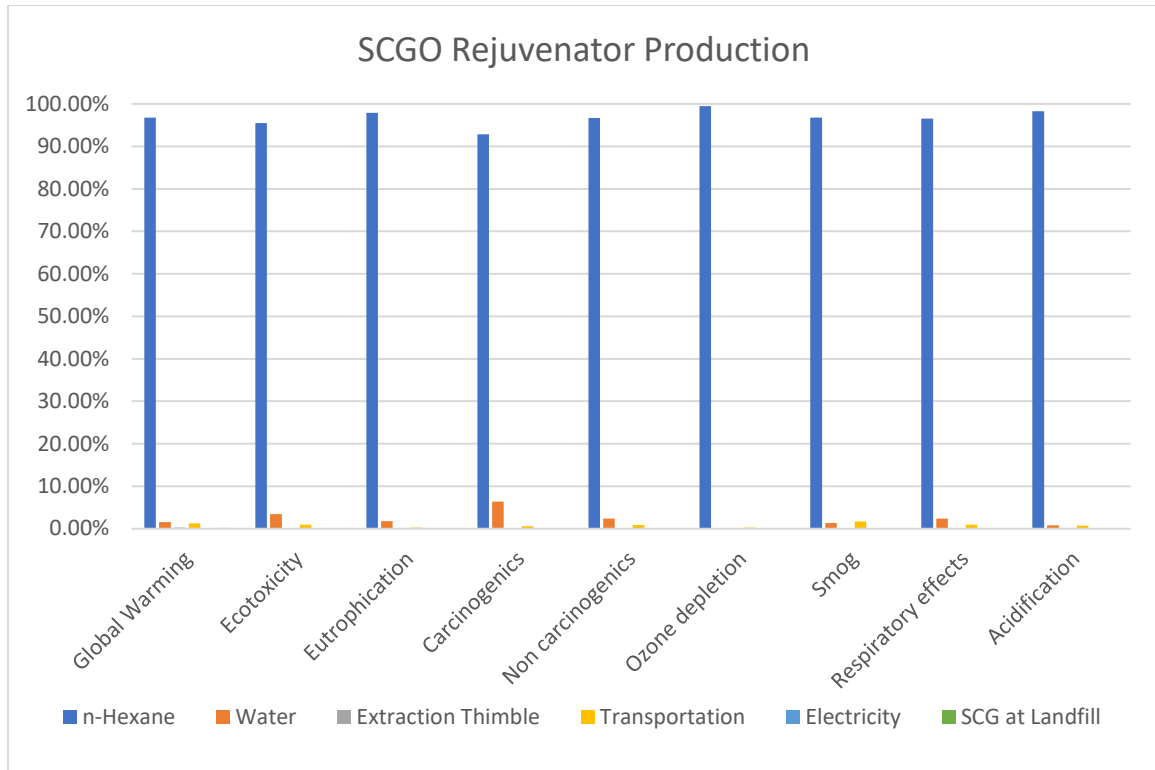


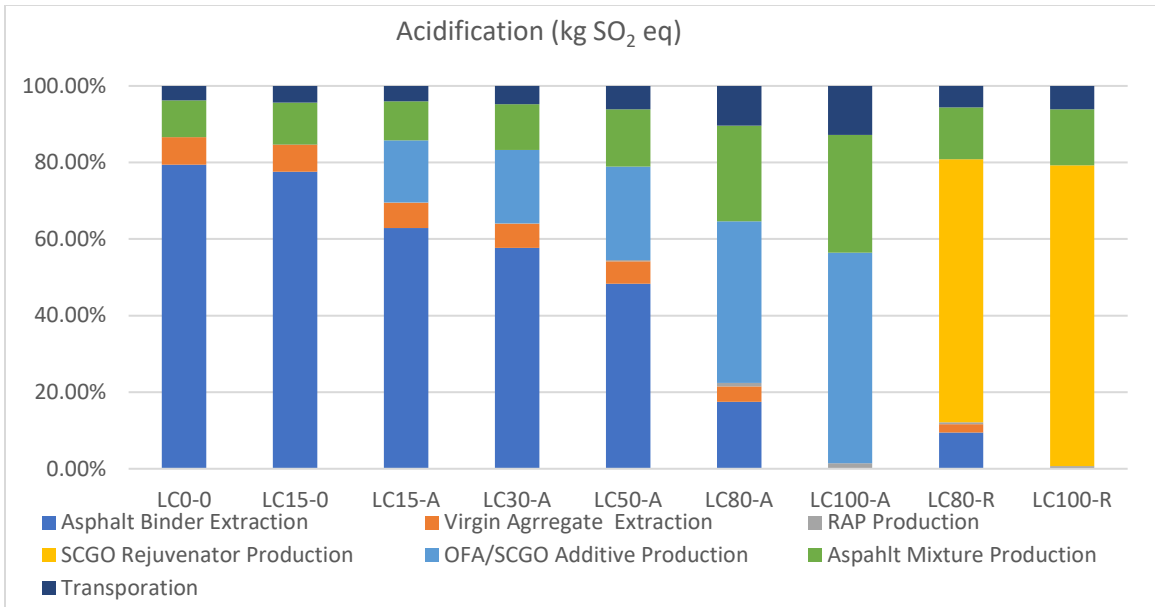
Figure 6-4. Sub-process contribution on the Different Environmental Impacts.

6.3.1. Process Contribution Analysis

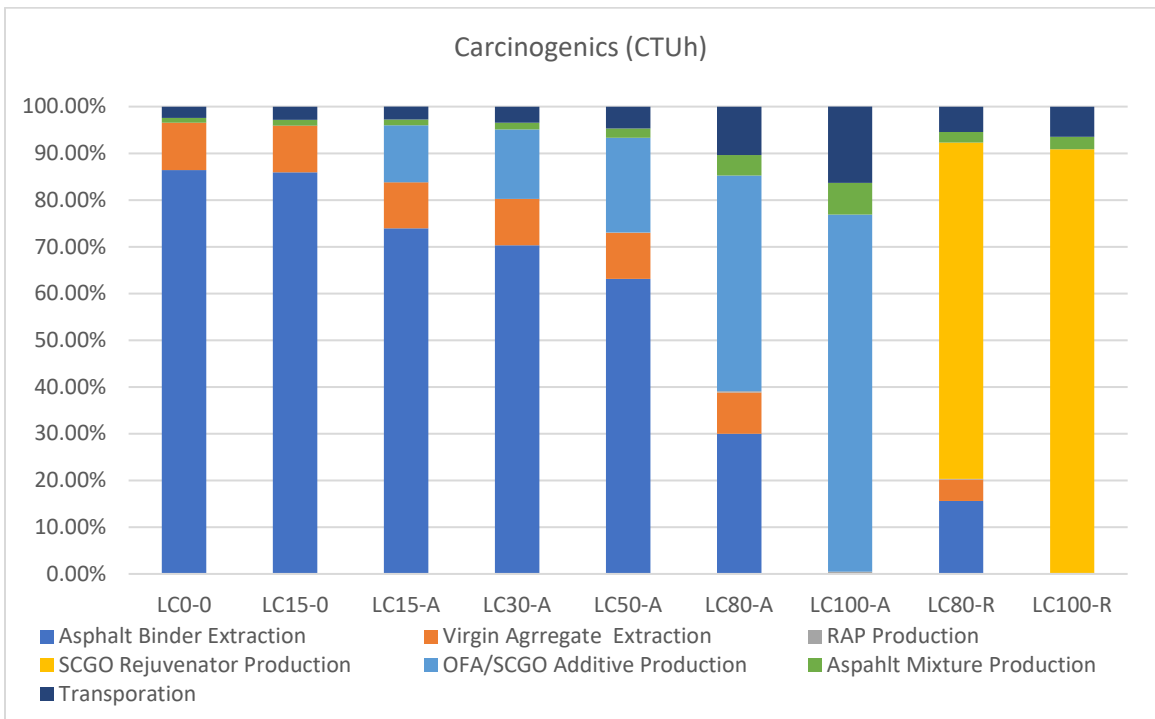
It is essential to study each process contribution to each environmental impact to understand the abovementioned environmental impacts results comprehensively. Analyzing each process's contribution also allows us to improve each process to curb the different environmental impact risks. Figure 6-5 shows each process and its relative contribution to the overall environmental impact. The asphalt binder production process significantly influences Acidification, Carcinogenic, Global Warming, Ozone depletion, and Respiratory effects. For the control scenario LC0-0, Asphalt binder production contributes with a range from 60% to 83% for the mentioned impacts. Virgin Aggregate production has a dominant influence on Ecotoxicity and Eutrophication environmental

impacts with a range of 37% to 40% with the control scenario LC0-0. The HMA production process typically has an average relative contribution impact of about 15% on the different environmental impacts. The highest contribution of the HMA production process is observed on Acidification, Global Warming, and Respiratory effects with LCA80-A and LCA-100A. The explanation behind this could be due to the lower incorporation of the virgin materials in the LCA80-A and LCA-100A. Also, a noticeable contribution is observed on Ozone depletion with LC0-0 and LC15-0. Materials transportation to the mixing plant has a fair impact on Ecotoxicity, Non-carcinogenic, and smog.

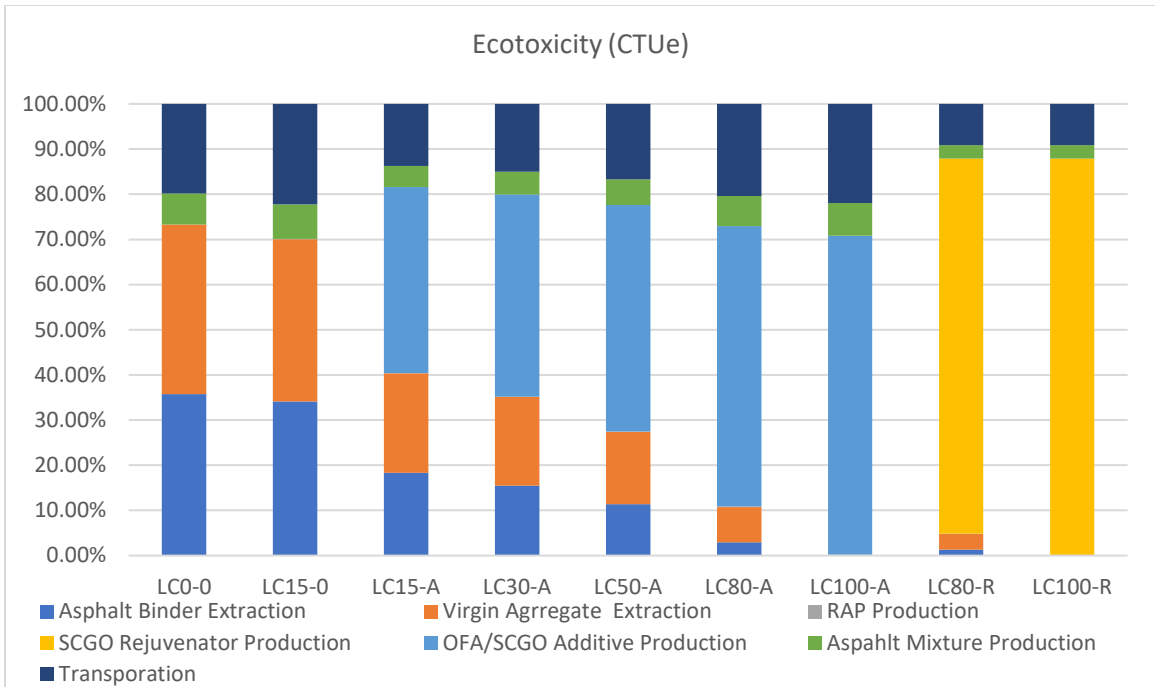
As expected, the contribution of RAP production is insignificant for all environmental categories across all scenarios. The maximum influence was with LC100-A with a maximum value of 5.6% on the Smog category. Otherwise, the RAP effect is insignificant and does not exceed 3% with all environmental impacts. Most of the above-illustrated findings align with other studies [105], [108], [144], [145].



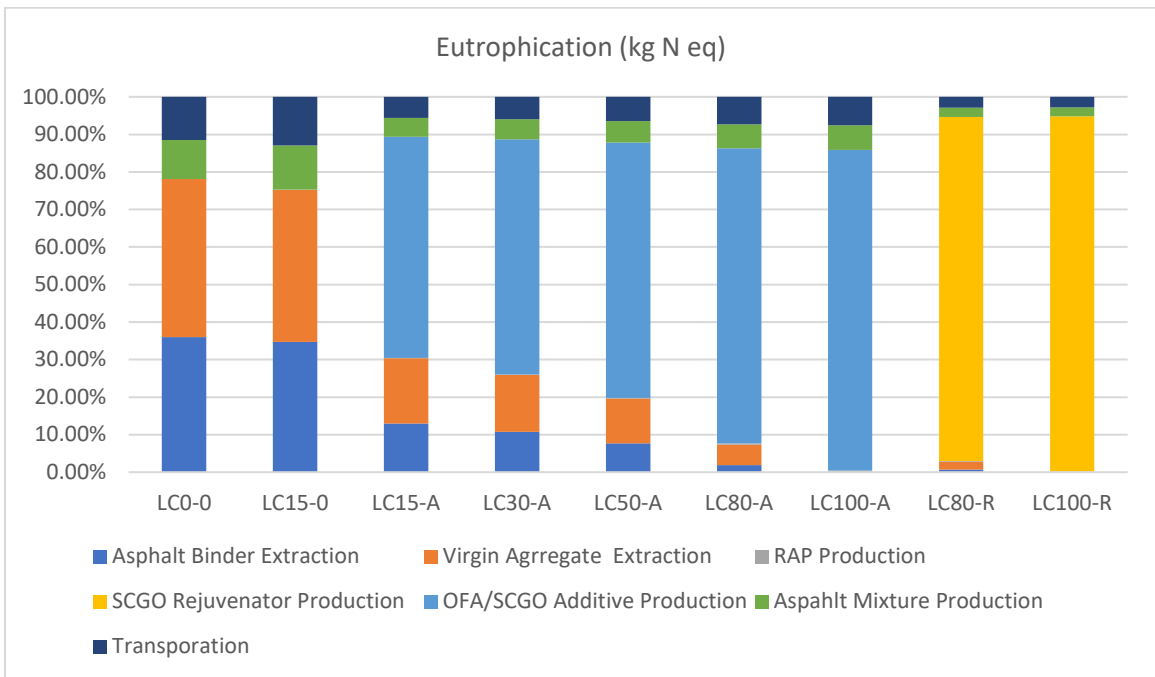
(a)



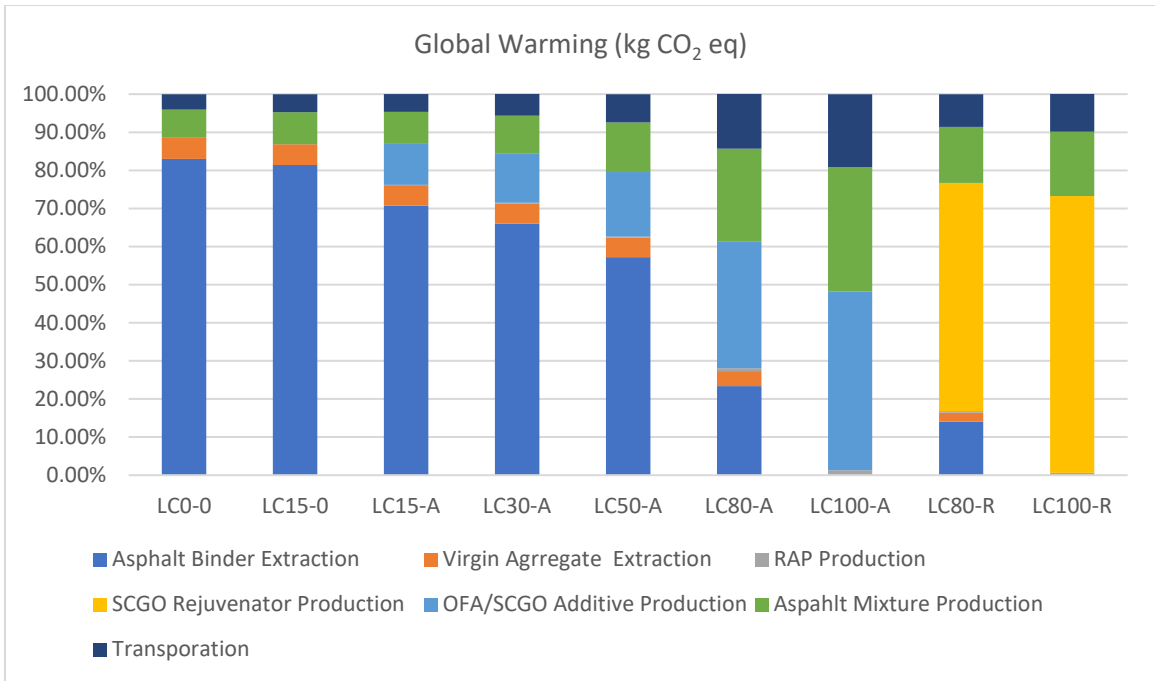
(b)



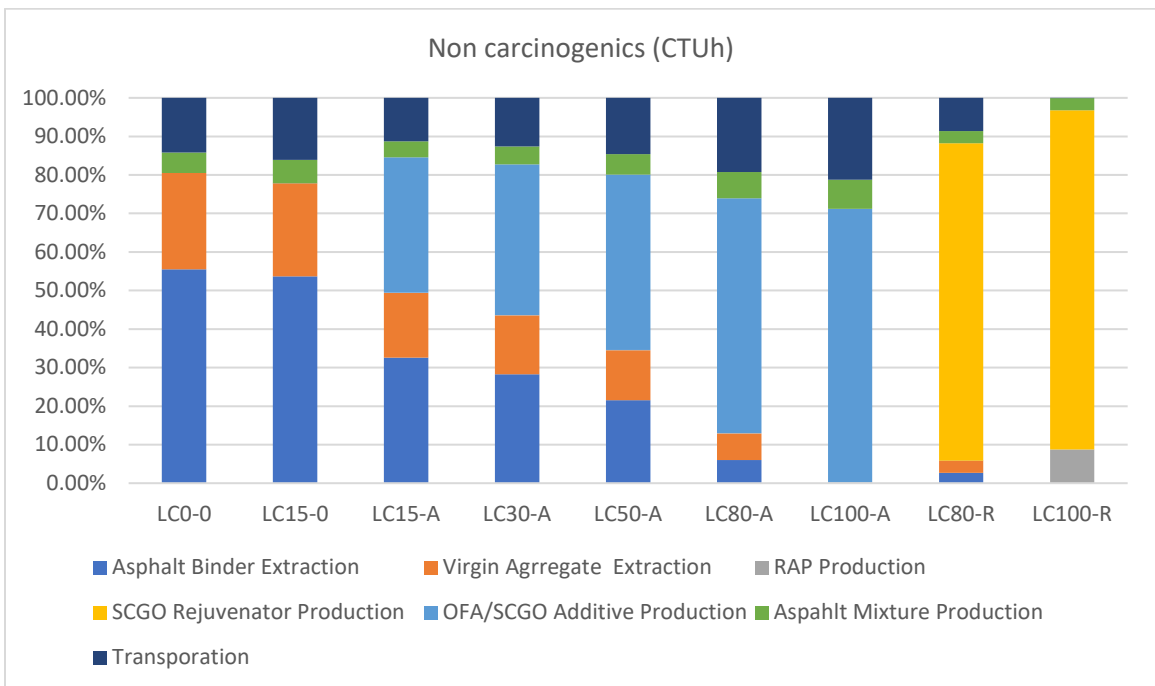
(c)



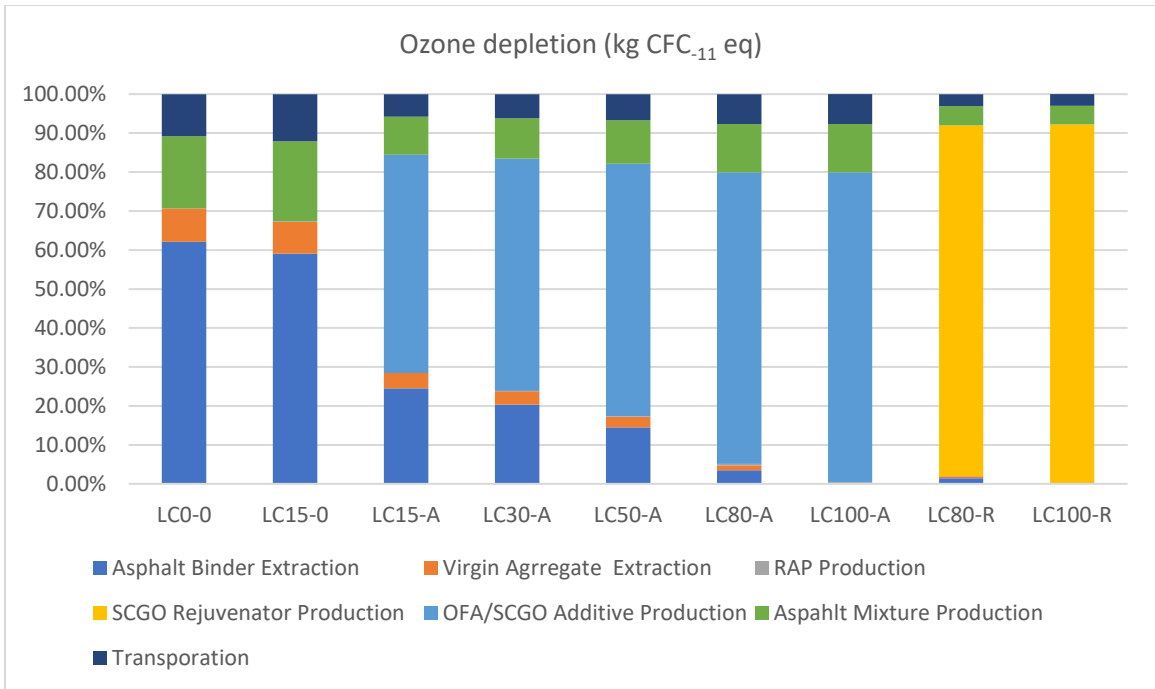
(d)



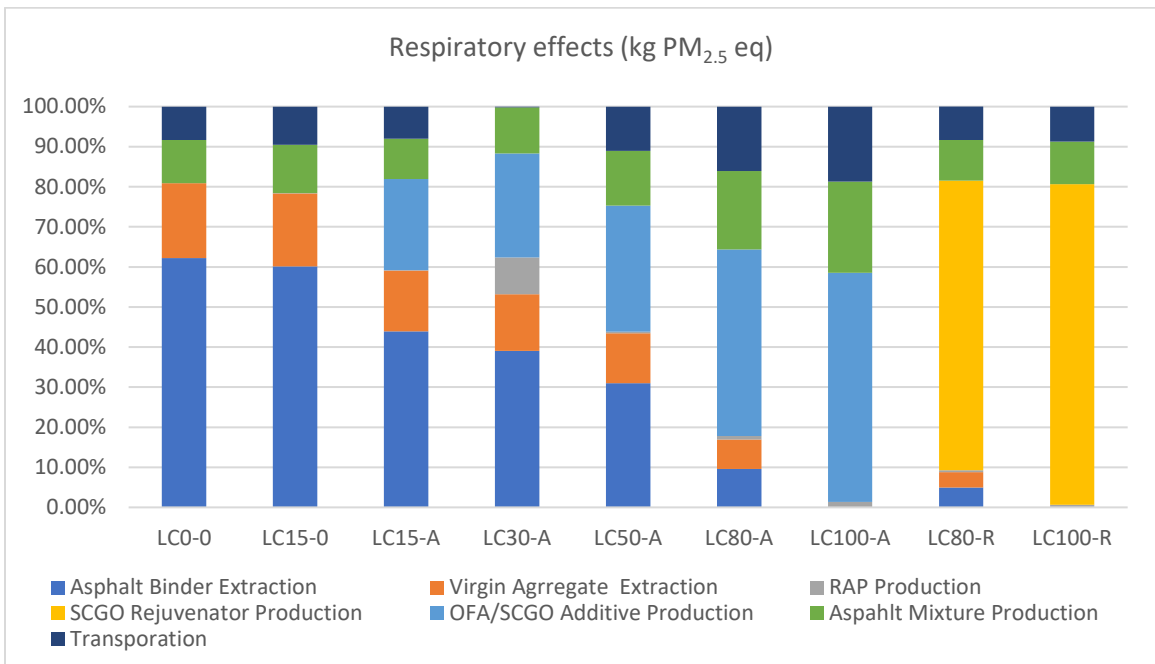
(e)



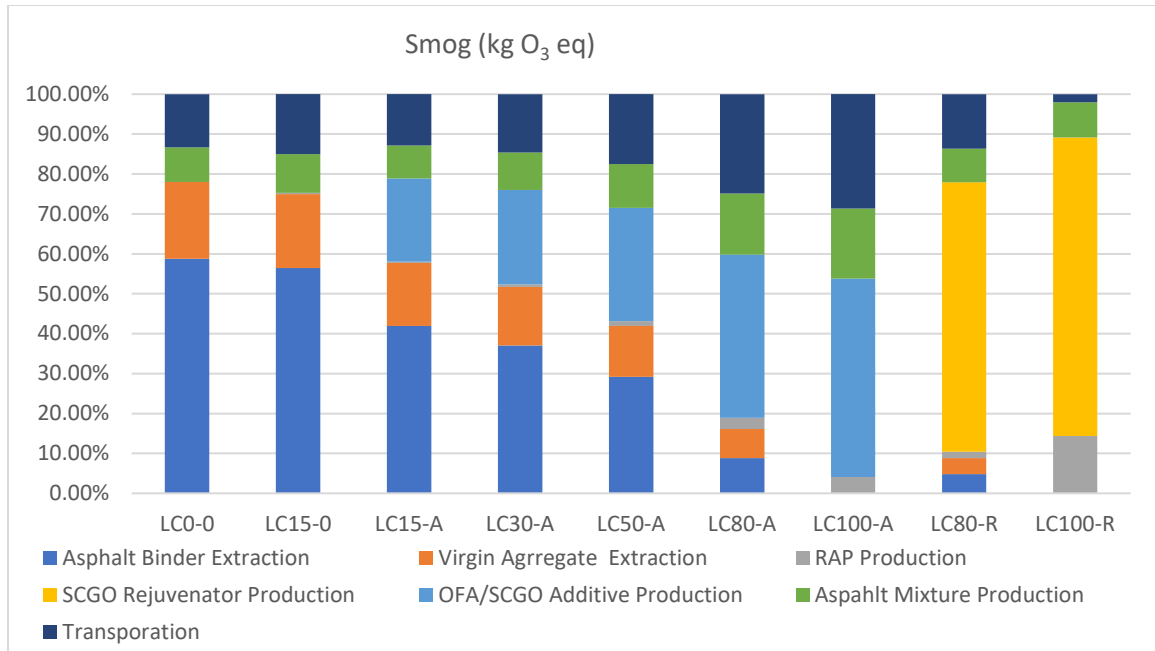
(f)



(g)



(h)



(i)

Figure 6-5. Relative Contribution of the Main Processes to the Total Impact Scores: (a) Acidification, (b) Carcinogenic, (c) Ecotoxicity, (d) Eutrophication, (e) Global Warming, (f) Non-carcinogenic, (g) Ozone depletion, (h) Respiratory effects, and (i) Smog

For the new eco-friendly products presented in this study, OFA/SCGO additive shows a significant contribution over Ecotoxicity, Eutrophication, Non-carcinogenic, and Ozone depletion. The lower the reliance is on virgin materials, the stronger the influence of the OFA/SCGO additive on the mentioned environmental categories. The new SCGO rejuvenator has a significant impact on all environmental categories because of the minimum incorporation of the virgin materials and the use of n-hexane as an extraction solvent, as shown in Figure 6-4.

6.3.2. Scenario Analysis

This section illustrates the scenario analysis undertaken by changing the methodological assumptions to add more validity to the results presented in the previous sub-sections.

The scenario alternative, hereafter named AS1, considers adopting another extraction method with less solvent consumption. Lowering the solvent is found to be more efficient than changing the solvent type through the Soxhlet extraction process since n-Hexane is the most effective extractant for this specific SCG waste [148]–[152]. Therefore, AS1 considers adopting Ultrasonic Assisted-oil Extraction (UAE) method. The UAE provides further extraction improvement, which combines low investment costs (less solvent and energy consumed), a fast extraction rate, and high efficiency. Many researchers found that UAE increased the oil yield and reduced the n-Hexane required for oil extraction from waste coffee grounds by a range from 20% to 39% [151], [153]–[156]. UAE process input and output followed Barjoveanu *et al.* (2020) [132] work. The solvent consumed is reduced by 30% of the Soxhlet extraction process.

Figure 6-6 shows the UAE method's influence relative to the Soxhlet extraction baseline scenario on the different environmental impacts. The negative relative numbers mean that AS1 causes a reduction in the risks of the environmental impact compared to the baseline scenario. In contrast, positive relative numbers mean a worsening of the environmental profile. Using the UAE method is more environmentally friendly than Soxhlet extraction since all the environmental impacts are reduced with all the scenarios investigated. That is again due to the less solvent used in the extraction process. In addition, it is observed that

the higher RAP incorporation is associated with a significant reduction in all the environmental impacts, especially with Carcinogenic, Ecotoxicity, Eutrophication, and Ozone depletion.

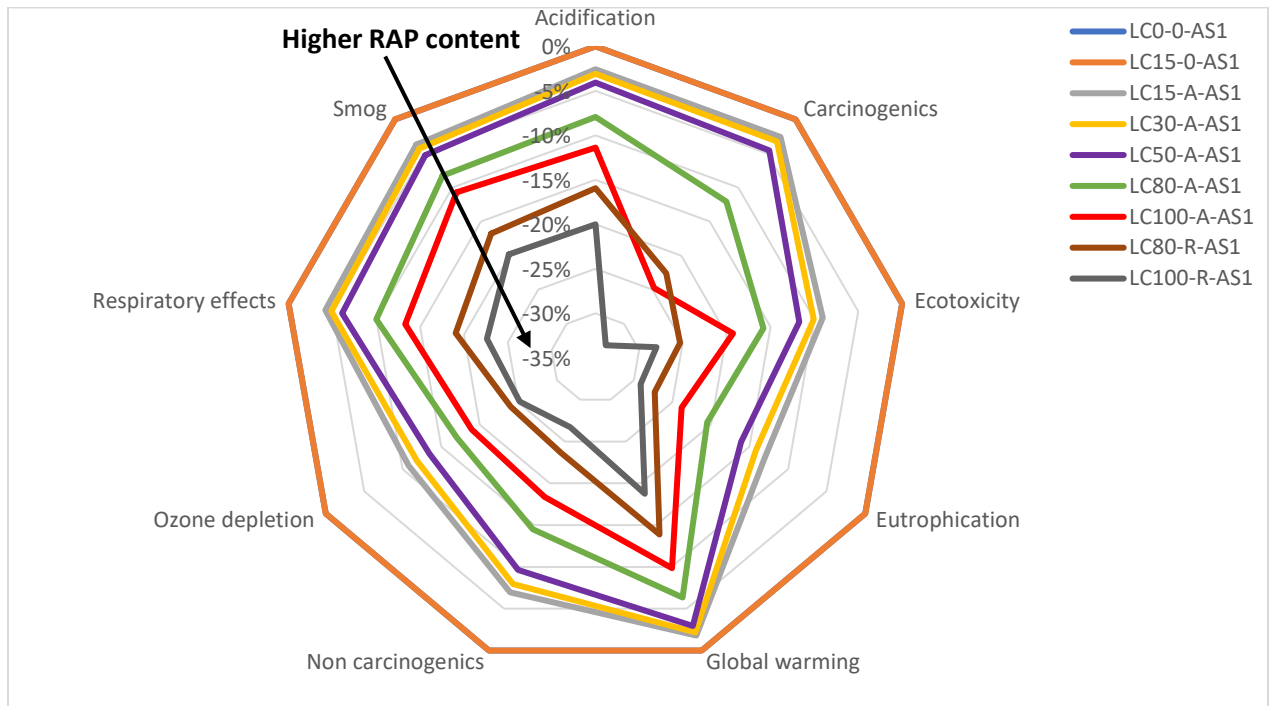


Figure 6-6. The Variation of the LCIA Results of Adopting the Ultrasonic Assisted-oil Extraction (UAE) Method as an Alternative Scenario Relative to the Baseline Scenario (Soxhlet Extraction).

CHAPTER 7

CONCLUSION AND RECOMMENDED FUTURE WORK

7.1. Phase I Conclusion and Recommended Work

The results and analysis presented in this phase show that significant improvements in asphalt performance can be attained in the presence of some types of CCW. The testing program is designed to study the hypothesis that some CCWs can act as an additive to the asphalt binder. The results show that improvement in binder performance can be attained depending on the CCW used.

The following points summarize the concluding statements of this phase:

- 1- The presence of the particulates increases the stiffness of all the blends. This follows findings in the literature and the fundamental behavior of viscoelastic particulate composites.
- 2- The oxidative aging of most of the blends indicates retardation in aging. This is a critical finding. In fact, the results suggest that the mechanistic improvement in the blends is due to the retardation in aging. This means that the delay in aging allows the binder to maintain its flexibility, and durability is one of the influencing mechanisms of the CCW/Binder interaction. For example, all the blends exhibiting a consistent reduction in the aging indices are associated with the most improvement in the low-temperature relaxation measured by the ΔT_c .

- 3- The interaction between the binder and the CCW is also measurable by the phase angle of the blend. It is the most statistically significant parameter in all the regression models presented. This parameter is fundamentally a true reflection of the rheological change in the blends.
- 4- The combination of aging and the measured phase angle can be proposed as criteria for screening the CCW to distinguish between potential additives and fillers. The screening can be found valuable if the CCW is intended for implementation and commercialization. This is especially critical given the large quantity already deposited in landfills worldwide.
- 5- According to the results shown in this phase, three of the CCW used are associated with a significant change in the overall performance. These are HT, WE, and SBH. All three of these CCWs are considered off-spec and would end up in landfills. The other CCWs appear to act as fillers with some indications of conditional interaction depending on the binder used.
- 6- The storage stability of the blended binder is recommended to be studied as part of the CCW's feasibility to be utilized as an asphalt binder additive. Especially when aiming for mass production.

7.2. Phase II Conclusion and Recommended Work

In this phase, three asphalt binder asphalt rejuvenators were introduced to three aged asphalt binders and RAP. Two market rejuvenators were evaluated side by side with a new SCGO rejuvenator. The two market rejuvenators are VBO and PBO. The new SCGO rejuvenator is a VBO rejuvenator. The binders used in this study are unmodified and PMA asphalt binders. Investigated binders underwent the RTFO cycle and the 1st PAV cycle, then testing samples were taken. Then, the rejuvenators are introduced to the different asphalt binders. Further, each sample underwent the 2nd PAV cycle. The main goal of this research was to evaluate rejuvenators' efficiency on asphalt binder aging. The efficiency of rejuvenators was evaluated through leading aging indicators, such as FTIR, ΔT_c , G-R parameter, ω_c , and G_c^* . This section summarizes an extensive testing program that included many samples and testing.

1- Oxidation (FTIR)

- When introduced to the different investigated ARAP/RAP, the proposed SCGO is the only rejuvenator showing a consistent reduction in the ICO aging index.
- Compared to the PBO rejuvenator, the VBO rejuvenators are more efficient in reducing the oxidation levels when introduced to the unmodified binder and RAP. On the contrary, the PBO rejuvenator performs more efficiently when introduced to the PMA binder.
- The new SCGO rejuvenator has superior efficiency in lowering the oxidation levels of the extracted RAP.

2- Low-Temperature Durability (ΔT_c)

- In general, introducing the rejuvenators to the aged asphalt binders and RAP is associated with a higher relaxation at low temperatures.
- The VBO rejuvenators significantly enhance the low-temperature thermal cracking resistance of all samples. On the other hand, the PBO rejuvenator is especially synergetic with the PMA binder, and its enhancement of the thermal cracking resistance is more pronounced.
- There is a strong correlation between the chemical oxidation index, ICO, and the low-temperature durability index, ΔT_c .

3- Intermediate temperature Durability (G-R)

- Introducing the rejuvenators to the aged asphalt binder and RAP associates with a lower G-R parameter, indicating an intermediate temperature rheological performance enhancement.
- Compared to the PBO rejuvenator, the VBO rejuvenators have higher efficiency in enhancing the intermediate temperature cracking resistance when introduced to all investigated aged binders and RAP.

4- Rejuvenator vs. Softener (Crossover frequency and modulus (G_c^*), (ω_c))

- All the investigated rejuvenators are found to perform as softeners when introduced to the unmodified binder NC, as they increase the crossover frequency and do not increase the crossover modulus.
- The PBO rejuvenator has higher rejuvenation efficiency in restoring both the viscous and elastic behavior when introduced to the PMA binder. On the

contrary, the VBO rejuvenators are found to have a higher rejuvenation efficiency when introduced to the unmodified binders.

- When introduced to the extracted RAP, the proposed SCGO increases the crossover modulus and frequency, indicating high rejuvenation efficiency.
- 5- Based on the results, SCGO acquires the merit of being an eco-friendly rejuvenator in the asphalt pavement industry compared to the two market-available rejuvenators.

7.3. Phase III Conclusion and Recommended Work

In this phase, four fly ashes were blended with two asphalt binders, unmodified and PMA. One sample of neat asphalt was also taken for each. Each binder/OFA blend underwent the RTFO cycle and the 1st PAV cycle, then testing samples were taken. Then, each of the ten binder/OFA blends was blended with the two market rejuvenators or the proposed SCGO rejuvenator. Further, each sample underwent the 2nd PAV cycle. The main goal of this phase was to evaluate the upcycled OFA/rejuvenator synergetic influence on asphalt binder aging. This was evaluated through main aging indicators testing, such as FTIR, ΔT_c , G-R parameter, and G_c^* . This section summarizes an extensive testing program that included many samples and testing.

1- Oxidation (FTIR)

- All OFA either reduce oxidation level or maintain the same level as the binder. This indicates a slower aging rate for the ash blends, compared to the binder alone, for both cycles of PAV aging.
- The use of rejuvenators further improved the aging resistance of the blends, suggesting high potential synergy.
- Rejuvenator #2 is a dominating influence reducing the aging for PMA compared to rejuvenator #1 and SCGO, which indicates a binder dependency compared to the unmodified binder.
- SBH, RH, and WE consistently show potential improvement and synergy with the rejuvenators. However, BH demonstrates no improvement against aging-related damage or rheological changes within the binder.

2- Low-Temperature Durability (ΔT_c)

- Unmodified PG 64-22 binder benefits significantly from using the OFA and the addition of the rejuvenator. Especially the VBO rejuvenators. On the other hand, the PBO, rejuvenator #2, shows a dominant influence with PMA binder/OFA blends.
- SCGO had a significant synergetic influence with unmodified ARAP-RH and ARAP-WE blends. Overall, SCGO interaction with RH and WE fly ash improved the thermal cracking aging resistance the most, compared to all OFA/rejuvenators combinations after two cycles of PAV aging.

3- Durability (G-R)

- OFA introduction reduces the cracking resistance for both binders at different aging levels.
- However, the addition of the rejuvenator eliminates this trend and consistently improves durability. This further validates the research goal of using a rejuvenator to deliver the OFA mixture to maximize benefits.
- For unmodified OFA blends, SCGO shows the sharpest decrease in the G-R (which indicates an improvement in cracking resistance) compared to the unrejuvenated blends.
- SCGO rejuvenator introduction to the PMA ARAP OFA blends is associated with an enhancement in intermediate temperature cracking resistance. However, not as significant as with the unmodified binder OFA blends.

4- Flexibility (Crossover Modulus (G_c^* , ω_c))

- The presence of fly ash improves the flexibility with the unmodified binder, while it did not show any flexibility enhancement with the PMA binder one cycle of PAV aging.
- The crossover modulus and frequency for all the investigated unmodified and PMA ARAP binder/OFA blends consistently drop after applying an additional cycle of PAV aging.

- While the VBO rejuvenator#1 could not enhance both binders' ARAP OFA blends, the PBO shows consistent positive rejuvenation efficiency with the PMA ARAP OFA blends.
 - The proposed SCGO rejuvenator shows consistent improvement when introduced to both binders' ARAP OFA blends. However, its most significant rejuvenation influence appears with the unmodified binder ARAP OFA blends.
- 5- Overall, the results from both the unmodified and the PMA binder and blends tests promote the idea that there is a binder dependency, as the polymers may dominate the low-temperature durability performance, not hindered by the OFA or significantly assisted by the rejuvenators. That is observed in the previously illustrated correlations. Furthermore, it is found that correlations are consistently strong with the unmodified binder compared to the PMA binder.
- 6- The results show that OFA/rejuvenator combinations have a tremendous synergetic influence on asphalt binder oxidation, thermal cracking resistance, aging behavior, and flexibility.

7.4. Phase IV Conclusion and Recommended Work

In this phase, three fly ashes were blended with two different rejuvenators, a petroleum-based rejuvenator, and a new proposed SCGO rejuvenator. Three ratios of RAP were studied for this phase. Two binders were used; a neat PG 64-22 binder and a Styrene-Butadiene-Styrene (SBS) Polymer Modified (PMA) binder PG 76-22 for the 15% RAP and 50% RAP mixtures. No neat binder was added to the 100% RAP mixtures. The fly ash

products substituted 11% of the asphalt binder weight in the mixtures. The mixtures were evaluated through the Indirect Tension test for high-temperature performance and Semi-Circular Bend (SCB) for intermediate and low-temperature performance. Moreover, the influence of the OFA/rejuvenator products on mixtures' workability is evaluated. This section summarizes an extensive testing program that included many samples and testing.

1- Workability

- OFA/ SCGO products enhance the workability of the 15%RAP and 100% RAP mixtures more than the OFA/ Rej. #2 products.
- RH/SCGO product has a very significant influence when introduced to 15% and 50% RAP unmodified binder mixtures. While SBH/SCGO product has a dominant positive behavior on workability when introduced to 15% and 50% RAP PMA binder mixtures.
- The RH/ SCGO product improved the workability of the 100% RAP mixture the most to a degree close to the rejuvenators.

2- Rutting Evaluation (High-Temperature Performance)

- The 100% RAP mixtures have higher tensile strength than the 15% and 50% RAP mixtures due to the presence of the aged asphalt binder in the system.
- The introduction of the OFA/SCGO products enhances the viscous behavior of the mixtures, thus less resistance to the permanent deformation than the OFA/ rej. #2 for the 15%, 50% and 100% RAP mixtures.

- All the mixtures' high-temperature performance is within the same tensile strength limit; 10-30 million ESALs for the unmodified binder and 30-100 million ESALs for the PMA mixtures for both 15% and 50% RAP mixtures.
- SCGO rejuvenator introduction to the 50% and 100% RAP mixtures drops the tensile strength significantly for both binders, which can be interpreted to lower rutting resistance.

3- Cracking Evaluation (Intermediate-Temperature Performance)

- The higher the RAP content, the lower the FE and FI.
- FE and FI are found to be sensitive to both binder type and RAP content.
- For the unmodified binder 15% RAP mixtures, introducing the OFA/rejuvenator products reduces the FE.
- All the OFA/ rej. #2 products show higher FE than their OFA/SCGO products when introduced to the PMA 15% RAP mixtures. That conforms with the findings illustrated in the binder phase since the PBO rejuvenator shows higher intermediate temperature performance than VBO rejuvenators as measured by G-R and G_c^* .
- For the FI, all the OFA/rejuvenator products enhanced the ductile failure behavior for the unmodified binder and PMA 15% RAP mixtures.
- While RH fly ash shows a stronger influence with the unmodified binder, SBH fly ash depicts a more substantial influence with the PMA binder when introduced with both rejuvenators, as measured by FI.

- For the 50% and 100% RAP mixtures, the OFA/ rejuvenator products did not increase the FI to the adopted 5.0 threshold due to the high RAP content.
- SCGO rejuvenator shows a superior positive influence on the intermediate temperature performance when introduced to the unmodified binder 50% RAP mixture and the 100% RAP mixture. That aligns with the findings illustrated in phase II.
- The optimum RAP content for utilizing an 11% SCGO rejuvenator was estimated to be 62%. In comparison, an average estimate of 30% RAP content is found suitable for an 11% dosage of OFA/rejuvenator products for both unmodified and PMA binder mixtures.

4- Thermal Cracking (Low-Temperature Performance)

- All fracture toughness values are above the adopted $800 \text{ kPa}\cdot\text{m}^{0.5}$ for the 15%, 50%, and 100% RAP mixtures.
- All the investigated 15%, 50%, and 100% RAP mixtures are above the adopted 350 J/m^2 for fracture energy.
- The SCGO rejuvenator decreases the pre-peak slope and enhances the fracture energy significantly compared to the PBO rejuvenator when introduced to the 100% RAP mixture. That conforms with the results depicted in phase II.
- While fracture energy is found not sensitive to any of the parameters measured, the fracture toughness is found to be efficient in capturing the influence of the RAP content only, as investigated by ANOVA.

- However, the pre-peak slope is very sensitive to RAP content and the rejuvenators used.
- The fracture energy is inversely correlated with the pre-peak slope, which is expected at a pure elastic regime when testing at low temperatures.

7.5. Phase V Conclusion and Recommended Work

This phase presented the utilization of three different recycled materials (RAP, OFA, and SCGO) as a replacement to the virgin materials used with the conventional HMA. The LCA is performed considering the ISO 14040:2006 and ISO 14044:2006 series and the FHWA's Pavement LCA Framework, as far as possible and suitable. One ton of asphalt mixture is considered a functional unit. TRACI v.2.1. impact assessment methodology is adopted to characterize the environmental performance of different HMA scenarios with different RAP incorporation rates (0%, 15%, 30%, 50%, 80%, and 100% RAP). Also, two alternative scenarios are investigated by utilizing natural gas as HFO replacement and adopting UAE instead of Soxhlet extraction. Based on the conditions considered in this case study, the following conclusions can be drawn:

- 1- The higher the RAP incorporation, the less environmental impacts, compared to the conventional mixture;
- 2- The inclusion of the new OFA/SCGO additive with RAP mixtures reduces environmental impacts;
- 3- SCGO rejuvenator increases the Ecotoxicity, Eutrophication, and Ozone Depletion environmental impacts significantly, compared to OFA/SCGO additive;

- 4- The utilization of n-Hexane as an extraction solvent in the SCGO extraction process has a dominant influence over the environmental profile;
- 5- Asphalt binder production is the main factor for the life cycle environmental burdens of the scenarios studied;
- 6- RAP production contribution is insignificant for all environmental categories across all scenarios;
- 7- The UAE method consumes less energy and solvent, making it more environmentally friendly since all the environmental impacts are reduced with all the scenarios investigated.
- 8- An LCA study is recommended to adopt the most efficient approach to extract the SCGO rejuvenator, especially for mass production.

REFERENCES

- [1] W. Tillson, *Street Pavements and Paving Materials*. New York, 1900.
- [2] J. N. Wilford, “World’s Oldest Paved Road Found in Egypt,” *New York Times*, p. 13, 1994.
- [3] F. L. Roberts, P. S. Kandhal, E. R. Brown, D.-Y. Lee, and T. W. Kennedy, *HOT MIX ASPHALT MATERIALS, MIXTURE DESIGN AND CONSTRUCTION*, vol. 2nd Editio. 1991.
- [4] W. D. Powell, J. F. POTTER, H. C. Mayhew, and M. E. NUNN, “THE STRUCTURAL DESIGN OF BITUMINOUS ROADS,” *Transp. Road Res. Lab.*, no. 1115, p. 62 P., 1984.
- [5] D. Croney and P. CRONEY, *THE DESIGN AND PERFORMANCE OF ROAD PAVEMENTS*. 1991.
- [6] A. Self, J. Read, R. Gerlis, R. Taylor, and E. Hobson, *The Shell Bitumen Handbook, (6th Edition)*. 2015.
- [7] AASHTO Designation: M 145-91 (2012), “Classification of Soils and Soil-Aggregate Mixtures for Highway Construction Purposes,” *AASHTO*, vol. 91, no. 2012, 2013.
- [8] USDOT, “Transportation Statistics Annual Report 2019,” *Transp. U.S. Dep. of, Transp. Off. Secr.*, 2019.

- [9] U.S. Federal Highway Administration, “Moving 12-Month Total Vehicle Miles Traveled [M12MTVUSM227NFWA], retrieved from FRED, Federal Reserve Bank of St. Louis; <https://fred.stlouisfed.org/series/M12MTVUSM227NFWA>.” .
- [10] ACAA, “Coal Ash Recycling Rate Declines Amid Shifting Production and Use Patterns.pdf,” Washington, D.C., 2019.
- [11] A. road and transportation builder association (ARTBA), “Production and use of coal combustion products in the U.S. Published by American coal ash association.,” 2015.
- [12] K. Sobolev, I. F. Vivian, and A. Faheem, “Application of Fly Ash in ASHphalt Concrete : from Challenges to Opportunities Application of Fly Ash in ASHphalt Concrete : from Challenges to Opportunities,” *World Coal Ash Conf.*, no. May, 2014.
- [13] E. G. Bautista, J. Flickinger, R. Saha, I. Flores-vivian, A. F. Faheem, and K. Sobolev, “Effect of Coal Combustion Products on high temperature performance of asphalt mastics,” *Constr. Build. Mater.*, vol. 94, pp. 572–578, 2015.
- [14] J. Muhammad *et al.*, “Moisture susceptibility and fatigue performance of asphalt binder modified by bone glue and coal fly ash,” *Constr. Build. Mater.*, vol. 308, no. June, p. 125135, 2021.
- [15] F. Li and Y. Yang, “Experimental investigation on the influence of interfacial effects of limestone and fly ash filler particles in asphalt binder on mastic aging behaviors,”

Constr. Build. Mater., vol. 290, no. 0, 2021.

- [16] T. H. Adams, “Coal Ash Recycling Reaches Record 64 Percent Amid Shifting Production and Use Patterns,” pp. 1–4, 2018.
- [17] J. McKenna, “John McKenna,” *World Economic Forum*, 2018.
- [18] U. S. G. S. (USGS), “STONE (CRUSHED)-Construction Sand and Gravel Statistics and Information,” vol. 1, no. 703, pp. 2021–2022, 2021.
- [19] A. C. A. A. (ACAA), “Fly Ash Use in Concrete Increases Slightly As Overall Coal Ash Recycling Rate Declines,” (*ACAA*), *Am. Coal Ash Assoc.*, vol. d, pp. 1–5, 2020.
- [20] A. F. Faheem and H. U. Bahia, “Modelling of Asphalt Mastic in Terms of Filler-Bitumen Interaction,” *Model. Asph. Mastic Terms Fill. Interact.*, vol. 11, no. sup1, pp. 281–304, 2010.
- [21] A. Faheem, C. Cloutier, E. G. Bautista, and K. Sobolev, “Impact of Coal Combustion Product Incorporation in Asphalt Mixture Performance,” *Transp. Res. Board 96th Annu. Meet.*, 2017.
- [22] C. Cloutier, E. G. Bautista, A. F. Faheem, and K. Sobolev, “Effect of Spray Dryer Absorbers as Mix Enhancer on HMA Performance,” *Int. Congr. Exhib. Sustain. Civ. Infrastructures Innov. Infrastruct. Geotechnol.*, pp. 80–95, 2017.
- [23] Emil G. Bautista, A. F. Faheem, R. Saha, and K. Sobolev, “Characterization of Damage and Aging Resistance of Asphalt Mastics with Coal Combustion By-

Products,” *Airf. Highw. Pavements 2015* © ASCE 2015, pp. 74–85, 2015.

- [24] R. Saha, K. Malloy, E. Bautista, and K. Sobolev, “The investigation of fly ash based asphalt binders using atomic force microscope,” *Front. Struct. Civ. Eng.*, vol. 11, no. 4, pp. 380–387, 2017.
- [25] C. Clopotel, R. Velasquez, and H. Bahia, “Measuring physico-chemical interaction in mastics using glass transition,” *Road Mater. Pavement Des.*, vol. 13:sup1, pp. 304–320, 2012.
- [26] A. F. Faheem, H. U. Bahia, A. F. Faheem, and H. U. Bahia, “Modelling of Asphalt Mastic in Terms of Filler- Bitumen Interaction Modelling of Asphalt Mastic in Terms of Filler-Bitumen Interaction,” vol. 0629, 2011.
- [27] G. Liu, T. Yang, J. Li, Y. Jia, Y. Zhao, and J. Zhang, “Effects of aging on rheological properties of asphalt materials and asphalt-filler interaction ability,” *Constr. Build. Mater.*, vol. 168, pp. 501–511, 2018.
- [28] J. Zhang, X. Li, G. Liu, and J. Pei, “Effects of material characteristics on asphalt and filler interaction ability,” *Int. J. Pavement Eng.*, vol. 8436, pp. 1–10, 2019.
- [29] M. Guo and Y. Tan, “Interaction between asphalt and mineral fillers and its correlation to mastics ’ viscoelasticity,” 2021.
- [30] Lamontagnea, Dumasb, Mouilletb, and Kister, “Comparison by Fourier transform infrared (FTIR) spectroscopy of different ageing techniques: Application to road bitumens.,” *J. Fuel*, vol. 80, no. 4, pp. 483–488, 2001.

- [31] F. FARCAS;, V. Mouillet;, V. BATTAGLIA;, S. BESSON;, C. PETITEAU;, and F. LE CUNFF, “Identification et dosage par spectrométrie infrarouge à transformée de Fourier des copolymères SBS et EVA dans les liants bitumineux,” *Méthode D’Essai 71*, no. ME 71, p. 16P, 2009.
- [32] S. Wu, L. Pang, G. Liu, and J. Zhu, “Laboratory Study on Ultraviolet Radiation Aging of Bitumen,” *J. Mater. Civ. Eng.*, vol. 22, no. 8, pp. 767–772, 2010.
- [33] X. Yang, Z. You, D. Ph, M. Asce, and J. Mills-beale, “Asphalt Binders Blended with a High Percentage of Biobinders: Aging Mechanism Using FTIR and Rheology,” *J. Mater. Civ. Eng.*, vol. 27, no. 4, pp. 1–11, 2015.
- [34] B. Singh, N. Saboo, and P. Kumar, “Use of Fourier transform infrared spectroscopy to study ageing characteristics of asphalt binders,” *Pet. Sci. Technol.*, vol. 35, no. 16, pp. 1648–1654, 2017.
- [35] P. Nayak and U. C. Sahoo, “Rheological, chemical and thermal investigations on an aged binder rejuvenated with two non-edible oils,” *Road Mater. Pavement Des.*, vol. 18, no. 3, pp. 612–629, 2017.
- [36] J. Grenfell *et al.*, “Development of a laboratory bituminous mixtures ageing protocol,” *Adv. Test. Charact. Bitum. Mater.*, pp. 331–346, 2009.
- [37] W. Xie, C. Castorena, C. Wang, and Y. R. Kim, “A framework to characterize the healing potential of asphalt binder using the linear amplitude sweep test,” *Constr. Build. Mater.*, vol. 154, no. 15 November, pp. 771–779, 2017.

- [38] C. Wang *et al.*, “Unified failure criterion for asphalt binder under cyclic fatigue loading,” *Road Mater. Pavement Des.*, vol. 0629, no. 16:sup2, pp. 125–148, 2015.
- [39] R. M. Anderson, G. N. King, D. I. Hanson, and P. B. Blankenship, “Evaluation of the Relationship between Asphalt Binder Properties and Non-Load Related Cracking,” *Asph. Paving Technol.*, vol. 80, p. Asphalt Paving Technology 2011, 2011.
- [40] R. Rahbar-rastegar, “CRACKING IN ASPHALT PAVEMENTS : IMPACT OF COMPONENT PROPERTIES AND AGING ON FATIGUE AND THERMAL,” *Durham Univ. New Hampsh.*, 2017.
- [41] T. Sinsiri, P. Chindaprasirt, and C. Jaturapitakkul, “Influence of fly ash fineness and shape on the porosity and permeability of blended cement pastes,” *Int. J. Miner. Metall. Mater.*, vol. 17, no. 6, p. 683, 2010.
- [42] D. A. Anderson and W. H. Goetz, “MECHANICAL BEHAVIOR AND REINFORCEMENT OF MINERAL FILLER-ASPHALT MIXTURES,” *Jt. Highw. Res. Proj.*, pp. 37–66, 1973.
- [43] D. A. Anderson, J. P. Tarris, and J. D. Brock, “DUST COLLECTOR FINES AND THEIR INFLUENCE ON MIXTURE DESIGN,” *Assoc. Asph. Paving Technol. Proc.*, vol. 51, pp. 363–397, 1982.
- [44] B. J. Smith, “Low-Temperature And Dynamic Fatigue Toughening Mechanisms In Asphalt Mastics And Mixtures,” 2000.

- [45] X. Xu, J. Yu, L. Xue, C. Zhang, Y. Zha, and Y. Gu, "Investigation of Molecular Structure and Thermal Properties of Thermo-Oxidative Aged SBS in Blends and Their Relations," *Materials (Basel)*., vol. 10, no. 768, 2017.
- [46] H. Yu, X. Bai, G. Qian, H. Wei, X. Gong, and J. Jin, "Impact of Ultraviolet Radiation on the Aging Properties of SBS-Modified Asphalt Binders," *Polymers (Basel)*., vol. 11, no. 7, 2019.
- [47] A. E. Cha, M. Herrera-alonso, and R. Herrera-na, "Comparative Study of the Effect of Sulfur on the Morphology and Rheological Properties of SB- and SBS-Modified Asphalt," *J. Appl. Polym. Sci.*, vol. 10, no. 1002, pp. 3409–3422, 2009.
- [48] M. A. Parvez, M. Al-mehthel, H. I. A. Wahhab, and I. A. Hussein, "Utilization of Sulfur and Crumb Rubber in Asphalt Modification," *J. Appl. Polym. Sci.*, vol. 40046, pp. 1–11, 2014.
- [49] G. M. S. Abdullah and H. I. A. Wahhab, "Evaluation of foamed sulfur asphalt stabilized soils for road applications," *Constr. Build. Mater.*, vol. 88, pp. 149–158, 2015.
- [50] G. Polacco, S. Filippi, F. Merusi, and G. Stastna, "Historical perspective A review of the fundamentals of polymer-modified asphalts : Asphalt / polymer interactions and principles of compatibility," *Adv. Colloid Interface Sci.*, vol. 224, pp. 72–112, 2015.
- [51] H. T. Le, S. Inozemtcev, E. Korolev, and A. Grishina, "The efficiency of sulfur

- modifier to neutralize toxic gases in sulfur-asphalt concrete technology,” *IOP Conf. Ser. Mater. Sci. Eng.*, vol. 869, no. 032016, 2020.
- [52] M. Singh, K. Jain, and S. S. Kahlon, “Use of Sulphur as an Additive in Bitumen : A Review,” *Int. Res. J. Eng. Technol.*, vol. 07, no. 10, pp. 36–43, 2020.
- [53] M. Farrar, T. Turner, J.-P. Planche, J. Schabron, and R. Harnsberger, “Evolution of the Crossover Modulus with Oxidative Aging Method to Estimate Change in Viscoelastic Properties of Asphalt Binder with Time and Depth on the Road,” *Transp. Res. Rec. J. Transp. Res. Board*, vol. 2370, no. 1, pp. 76–83, 2013.
- [54] D. Lesueur, M. D. Elwardany, J. Planche, D. Christensen, and G. N. King, “Impact of the asphalt binder rheological behavior on the value of the ΔT_c parameter,” *Constr. Build. Mater.*, vol. 293, p. 123464, 2021.
- [55] E. Y. Hajj, P. E. Sebaaly, R. Shrestha, E. Y. Hajj, P. E. Sebaaly, and R. Shrestha, “Laboratory Evaluation of Mixes Containing Recycled Asphalt Pavement (RAP) Laboratory Evaluation of Mixes Containing Recycled Asphalt Pavement (RAP),” *Road Mater. Pavement Des.*, vol. 0629, no. 10:3, pp. 495–517, 2011.
- [56] B. A. Williams, A. Copeland, and T. C. Ross, “Asphalt Pavement Industry Survey on Recycled Materials and Warm-Mix Asphalt Usage: 2017,” *Natl. Asph. Pavement Assoc.*, 2017.
- [57] M. Mohammadafzali *et al.*, “Effects of Rejuvenation and Aging on Binder Homogeneity of Recycled Asphalt Mixtures,” *J. Transp. Eng. Part B Pavements*,

vol. 5, no. 1, pp. 1–9, 2019.

- [58] E. Fini *et al.*, “Role of Chemical Composition of Recycling Agents in Their Interactions with Oxidized Asphaltene Molecules,” *J. Mater. Civ. Eng.*, vol. 32, no. 9, pp. 1–13, 2020.
- [59] Audrey Copeland, *Reclaimed Asphalt Pavement in Asphalt Mixtures : State of the Practice*. 2011.
- [60] T. B. Moghaddam and H. Baaj, “The use of rejuvenating agents in production of recycled hot mix asphalt : A systematic review,” *Constr. Build. Mater.*, vol. 114, pp. 805–816, 2016.
- [61] M. Zaumanis, R. B. Mallick, and R. Frank, “100 % recycled hot mix asphalt : A review and analysis,” *Resour. Conserv. Recycl.*, vol. 92, pp. 230–245, 2014.
- [62] I. L. Al-Qadi, H. Ozer, and R. Yang, “Hybrid life cycle assessment for asphalt mixtures with high RAP content,” *Resour. Conserv. Recycl.*, vol. 83, pp. 77–86, 2014.
- [63] R. C. West, “RECLAIMED ASPHALT PAVEMENT MANAGEMENT: BEST PRACTICES,” *Natl. Cent. Asph. Technol. Auburn Univ. Auburn, Alabama*, 2010.
- [64] W. Mogawer *et al.*, “Performance characteristics of plant produced high RAP mixtures,” *Road Mater. Pavement Des.*, vol. 0629, no. 13:sup1, pp. 183–208, 2012.
- [65] Z. Yang *et al.*, “Effect of Aging on Chemical and Rheological Properties of

- Bitumen,” *Polymers (Basel)*., vol. 10, no. 12, pp. 1345–1361, 2018.
- [66] M. A. Raouf and R. C. Williams, “Rheology of Fractionated Cornstover Bio-oil as a Pavement Material,” *Int. J. Pavements*, vol. 9, no. 1-2-3, pp. 58–69, 2010.
- [67] H. B. Goyal, D. Seal, and R. C. Saxena, “Bio-fuels from thermochemical conversion of renewable resources: A review,” *Renew. Sustain. Energy Rev.*, vol. 12, no. 2, pp. 504–517, 2008.
- [68] D. Sun *et al.*, “Evaluation of optimized bio-asphalt containing high content waste cooking oil residues,” *Fuel*, vol. 202, pp. 529–540, 2017.
- [69] F. Pahlavan, A. Rajib, S. Deng, P. Lammers, and E. H. Fini, “Investigation of Balanced Feedstocks of Lipids and Proteins to Synthesize Highly Effective Rejuvenators for Oxidized Asphalt,” *ACS Sustain. Chem. Eng.*, vol. 8, no. 20, pp. 7656–7667, 2020.
- [70] E. A. O’Rear, C. R. Dugan, C. R. Sumter, S. Rani, S. A. Ali, and M. Zaman, “Rheology of virgin asphalt binder combined with high percentages of RAP binder rejuvenated with waste vegetable oil,” *ACS Omega*, vol. 5, no. 26, pp. 15791–15798, 2020.
- [71] K. A. Ahmad, M. E. Abdullah, and N. A. Hassan, “Investigating the Feasibility of Using *Jatropha Curcas* Oil (JCO) as Bio Based Rejuvenator in Reclaimed Asphalt Pavement (RAP),” vol. 09013, 2017.
- [72] M. Zahoor, S. Nizamuddin, S. Madapusi, and F. Giustozzi, “Sustainable asphalt

- rejuvenation using waste cooking oil: A comprehensive review,” *J. Clean. Prod.*, vol. 278, p. 123304, 2021.
- [73] X. Yang, Z. You, and Q. Dai, “Performance evaluation of asphalt binder modified by bio-oil generated from waste wood resources,” *Int. J. Pavement Res. Technol.*, vol. 6, no. 4, pp. 431–439, 2013.
- [74] R. Zhang, Z. You, H. Wang, X. Chen, C. Si, and C. Peng, “Using bio-based rejuvenator derived from waste wood to recycle old asphalt,” *Constr. Build. Mater.*, vol. 189, pp. 568–575, 2018.
- [75] C. Xinxin, C. Xuejuan, T. Boming, W. Yuanyuan, and L. Xiaolong, “Investigation on Possibility of Waste Vegetable Oil Rejuvenating Aged Asphalt,” *Appl. Sci.*, vol. 8, no. 765, 2018.
- [76] M. Elkashef, J. Podolsky, R. C. Williams, and E. Cochran, “Preliminary examination of soybean oil derived material as a potential rejuvenator through Superpave criteria and asphalt bitumen rheology,” *Constr. Build. Mater.*, vol. 149, pp. 826–836, 2017.
- [77] I. Menapace *et al.*, “Effect of recycling agents in recycled asphalt binders observed with microstructural and rheological tests,” *Constr. Build. Mater.*, vol. 158, pp. 61–74, 2018.
- [78] C. J. Glover *et al.*, “Development of a New Method for Assessing Asphalt Binder Durability with Field Validation,” vol. 7, no. 2, 2005.

- [79] G. M. P. D. for the A. paper by A. et al. . Rowe, “Evaluation of the Relationship between Asphalt Binder Properties and Non-Load Related Cracking,” *J. Assoc. Asph. Paving Technol.*, vol. 80, pp. 649–662, 2011.
- [80] G. Rowe, G. King, and M. Anderson, “Journal of The Influence of Binder Rheology in the Cracking of Asphalt Mixes in Airport and,” *J. Test. Eval.*, vol. 42, no. 5, pp. 1063–1072, 2014.
- [81] A. I. Rajib *et al.*, “Do all rejuvenators improve asphalt performance ? ABSTRACT,” *Road Mater. Pavement Des.*, vol. 0, no. 0, pp. 1–19, 2020.
- [82] M. Elkashef, J. Podolsky, R. C. Williams, and E. W. Cochran, “Introducing a soybean oil-derived material as a potential rejuvenator of asphalt through rheology, mix characterisation and Fourier Transform Infrared analysis,” *Road Mater. Pavement Des.*, vol. 19, no. 8, pp. 1750–1770, 2018.
- [83] V. Loise, P. Caputo, M. Porto, P. Calandra, R. Angelico, and C. O. Rossi, “A Review on Bitumen Rejuvenation: Mechanisms, Materials, Methods and Perspectives,” *Appl. Sci.*, vol. 9, no. 4316, 2019.
- [84] J. C. Petersen and P. M. Harnsberger, “Asphalt aging: Dual oxidation mechanism and its interrelationships with asphalt composition and oxidative age hardening,” *Transp. Res. Rec.*, no. 1638, pp. 47–55, 1998.
- [85] Y. Liang, R. Wu, J. T. Harvey, D. Jones, and M. Z. Alavi, “Investigation into the Oxidative Aging of Asphalt Binders,” *Transp. Res. Rec.*, vol. 2673, no. 6, pp. 368–

378, 2019.

- [86] M. Elkashef *et al.*, “Effect of Using Rejuvenators on the Chemical, Thermal, and Rheological Properties of Asphalt Binders,” *Energy and Fuels*, vol. 34, no. 2, pp. 2152–2159, 2020.
- [87] E. R. Brown *et al.*, *Hot Mix Asphalt Materials, Mixture Design, and Construction*. NAPA Research and Education Foundation, 2009.
- [88] A. F. Faheem, H. U. Bahia, and H. Ajideh, “Estimating Results of a Proposed Simple Performance Test for Hot-Mix Asphalt from Superpave Gyratory Compactor Results,” *ournal Transp. Res. Board*, vol. 1929, pp. 104–113, 2005.
- [89] Geetha Srinivasan, “Evaluation of indirect tensile strength to identify asphalt concrete rutting potential,” West Virginia University, 2004.
- [90] D. W. Christensen Jr and R. F. Bonaquist, “Using the Indirect Tension Test to Evaluate Rut Resistance in Developing Hot-Mix Asphalt Mix Designs,” *TRB Circ. E-C124 Pract. Approaches to Hot-Mix Asph. Mix Des. Prod. Qual. Control Testing, Transp. Res. Board Natl. Acad.*, pp. 62–77, 2007.
- [91] S. Wu, R. He, H. Chen, and Y. Luo, “Low temperature characteristics of asphalt mixture based on the semi-circular bend and thermal stress restrained specimen test in alpine cold regions,” *Constr. Build. Mater.*, vol. 311, no. 15, p. 125300, 2021.
- [92] M. Marasteanu, W. Buttlar, H. Bahia, and C. Williams, “Investigation of Low Temperature Cracking in Asphalt Pavements National Pooled Fund Study - Phase

II,” 2012.

- [93] M. Alsalihi and A. Faheem, “INTERACTION OF WARM MIX ASPHALT (WMA) TECHNOLOGIES AND HIGH-RECLAIMED ASPHALT PAVEMENT (RAP) IN ASPHALTIC MIXES,” *Conf. Transp. Res. Board 97th Annu. Meet. Washingt. DC, United States*, 2018.
- [94] I. L. Al-qadi *et al.*, “Testing Protocols to Ensure Performance of High Asphalt Binder Replacement Mixes Using RAP and RAS,” 2015.
- [95] I.L.Lim;, I.W.Johnston;, and S.K.Choi, “Stress intensity factors for semi-circular specimens under three-point bending,” *Eng. Fract. Mech.*, vol. 44, no. 3, pp. 363–382, 1993.
- [96] G. Nsengiyumva, Y.-R. Kim, and T. You, “Development of a Semicircular Bend (SCB) Test Method for Performance Testing of Nebraska Asphalt Mixtures,” 2015.
- [97] H. Yu, Z. Leng, Z. Dong, Z. Tan, F. Guo, and J. Yan, “Workability and mechanical property characterization of asphalt rubber mixtures modified with various warm mix asphalt additives,” *Constr. Build. Mater.*, vol. 175, pp. 392–401, 2018.
- [98] Mohammed A. J. Alsalihi, “QUANTIFICATION OF THE ROLE OF THE EFFECTIVE BINDER IN THE PERFORMANCE OF RAP-WMA MIXTURES,” Temple University, 2020.
- [99] R. Yang, S. Kang, H. Ozer, and I. L. Al-Qadi, “Environmental and economic analyses of recycled asphalt concrete mixtures based on material production and

- potential performance,” *Resour. Conserv. Recycl.*, vol. 104, pp. 141–151, 2015.
- [100] I. L. Al-qadi *et al.*, “Development of Long-Term Aging Protocol for Implementation of the Illinois Flexibility Index Test (I-FIT),” *Civ. Eng. Stud. Illinois Cent. Transp. Ser. No. 19-012 UILU-ENG-2019-2012 ISSN 0197-9191*.
- [101] B. of T. S. U.S. Department of Transportation, “Transportation Statistics Annual Report 2020,” Washington, DC, 2020.
- [102] J. A. Epps *et al.*, *NCHRP Report 455: Recommended Performance-Related Specification for Hot-Mix Asphalt Construction: Results of the Westrack Project*, vol. 455, no. 455. National Academies Press, 2002.
- [103] U. N. G. Assembly, “Our Common Future: Report of the World Commission on Environment and Development,” 1987.
- [104] L. P. Thives and E. Ghisi, “Asphalt mixtures emission and energy consumption : A review,” *Renew. Sustain. Energy Rev.*, vol. 72, no. January, pp. 473–484, 2017.
- [105] J. Santos, V. Cerezo, K. Soudani, and S. Bressi, “A comparative life cycle assessment of hot mixes asphalt containing bituminous binder modified with waste and virgin polymers,” *Procedia CIRP*, vol. 69, no. May, pp. 194–199, 2018.
- [106] M. Zaumanis, R. B. Mallick, and R. Frank, “Evaluation of Rejuvenator ’ s Effectiveness with Conventional Mix Testing for 100 % Reclaimed Asphalt Pavement Mixtures,” *Transp. Res. Rec. J. Transp. Res. Board*, no. 2370, pp. 17–25, 2013.

- [107] ISO, “ISO 14044: Environmental management – Life cycle assessment – Requirements and guidelines. Geneva: International Organization for Standardization.,” 2006.
- [108] D. Vandewalle, V. Antunes, J. Neves, and A. C. Freire, “Assessment of Eco-Friendly Pavement Construction and Maintenance Using Multi-Recycled RAP Mixtures,” *recycling*, vol. 5, no. 17, 2020.
- [109] X. Zhou *et al.*, “Life Cycle Assessment of Biochar Modified Bioasphalt Derived from Biomass,” *ACS Sustain. Chem. Eng.*, vol. 8, pp. 14568–14575, 2020.
- [110] C. Oreto, F. Russo, R. Veropalumbo, N. Viscione, G. D. Acqua, and S. A. Biancardo, “Life Cycle Assessment of Sustainable Asphalt Pavement: Solutions Involving Recycled Aggregates and Polymers,” *Materials (Basel)*., vol. 14, no. 3867, 2021.
- [111] Md Uzzal Hossain, C. S. Poon, I. M. Lo, and J. C. Cheng, “Comparative environmental evaluation of aggregate production from recycled waste materials and virgin sources by LCA,” *Resour. Conserv. Recycl.*, vol. 109, pp. 67–77, 2016.
- [112] F. G. Pratic, M. Giunta, and M. Mistretta, “Energy and Environmental Life Cycle Assessment of Sustainable Pavement Materials and Technologies for Urban Roads,” *sustainability*, vol. 12, no. 704, 2020.
- [113] J. T. Harvey, J. Meijer, H. Ozer, I. L. Al-Qadi, A. Saboori, and A. Kendall, “Pavement life cycle assessment framework (No. FHWA-HIF-16-014). United

States. Federal Highway Administration.,” 2016.

- [114] M. Wildnauer, E. Mulholland, J. Liddie, C. Koffler, and S. Murphy, “Life Cycle Assessment of Asphalt Binder,” 2019.
- [115] J. Li, F. Xiao, L. Zhang, and S. N. Amirkhanian, “Life cycle assessment and life cycle cost analysis of recycled solid waste materials in highway pavement: A review,” *J. Clean. Prod.*, vol. 233, pp. 1182–1206, 2019.
- [116] R. Cao, Z. Leng, H. Yu, and S.-C. Hsu, “Comparative life cycle assessment of warm mix technologies in asphalt rubber pavements with uncertainty analysis,” *Resour. Conserv. Recycl.*, vol. 147, pp. 137–144, 2019.
- [117] J. Xie, Z. Wang, F. Wang, S. Wu, Z. Chen, and C. Yang, “The Life Cycle Energy Consumption and Emissions of Asphalt Pavement Incorporating Basic Oxygen Furnace Slag by Comparative Study,” *sustainability*, vol. 13, no. 4540, 2021.
- [118] CEN, “Sustainability of Construction Works - Environmental Product Declarations - Core Rules for the Product Category of Construction Products,” *Eur. Stand. EN 15804:2012+A1. CEN-CENELEC Manag. Centre, Brussels, Belgium.*, 2013.
- [119] J. Harvey, A. Kendall, I.-S. Lee, N. Santero, T. Van Dam, and T. Wang, “Pavement Life Cycle Assessment Workshop: Discussion Summary and Guidelines,” *UCPRC-TM-2010-03. Univ. California, Davis, CA.*, no. May, 2010.
- [120] B. Moins, D. Hernando, M. Buyle, C. France, W. Van den Bergh, and A. Audenaert, “Quantifying the environmental and economic impact of adding RAP and

rejuvenators in asphalt pavements using LCA and LCCA,” 2021.

- [121] A. Cirotto, C. Di Noi, T. Lohse, and M. Srocka, “OpenLCA 1.10: Comprehensive User Manual,” 2020.
- [122] N. R. E. L. (NREL), “U . S . LIFE CYCLE INVENTORY DATABASE ROADMAP,” 2009.
- [123] Ecoinvent 3, “Ecoinvent System Models in Ecoinvent 3.0,” 2019. [Online]. Available: <https://www.ecoinvent.org/database/%0Asystem-models-in-ecoinvent-3/system-models-in-ecoinvent-3.html>.
- [124] GaBi Database, “GaBi LCA Database Documentation :Extension database II: Energy,” 2018. [Online]. Available: <https://gabi.sphera.com/support/gabi/gabi-database-2018-lci-documentation/extension-database-ii-energy/>.
- [125] J. Bare, “Tool for the Reduction and Assessment of Chemical and Other Environmental Impacts (TRACI) User ’ s Guide,” *U.S. Environ. Prot. Agency /600/R-12/554*, no. July, 2012.
- [126] R. Frischknecht *et al.*, “Project ecoinvent data v2.0: Overview and Methodology,” 2007.
- [127] FHWA, “User Guidelines for Waste and Byproduct Materials in Pavement Construction :RECLAIMED ASPHALT PAVEMENT,” 1997. [Online]. Available: <https://www.fhwa.dot.gov/publications/research/infrastructure/structures/97148/rap131.cfm>.

- [128] RubbleMaster, “RM 120X Mobile Impact Crusher,” 2021. [Online]. Available: <https://www.rubblemaster.com/us/products/impact-crushers/rm-120x>.
- [129] USLCIDatabase, “U.S. Life Cycle Inventory Database,” *National Renewable Energy Laboratory, 2012. Accessed November 19, 2012, 2012*. [Online]. Available: <https://www.lcacommons.gov/nrel/search>.
- [130] McCloskeyInternational, “ST80T Tracked Stackers,” 2021. [Online]. Available: <https://mccloskeyinternational.com/product/st80-tracked-stackers/>.
- [131] SCREEN MACHINE, “SCREEN MACHINE 4043TR,” 2021. [Online]. Available: <https://www.machinerytrader.com/listing/for-sale/207719077/2021-screen-machine-4043tr-crusher-aggregate-equipment>.
- [132] G. Barjoveanu, O. Alexandra, C. Teodosiu, and I. Volf, “Life cycle assessment of polyphenols extraction processes from waste biomass,” *Sci. Rep.*, vol. 10, no. 13632, pp. 1–12, 2020.
- [133] Hogentogle, “Quincy lab, Inc. 31-350ER Mechanical Convection Oven,” 2021. [Online]. Available: https://www.hogentogler.com/quincy-lab/31-350er-mechanical-convection-oven.asp?gclid=CjwKCAiAm7OMBhAQEiwArvGi3Muc9060o5NKaEQrezhhtmlwID-2vEul0GTzfnWtSdoCQt_TFHUi7RoCpUUQAvD_BwE.
- [134] Southernlabware, “EM Controlled Electromantle, Heating Mantle, Volume, 1000ml, 115v,” 2021. [Online]. Available: <https://www.southernlabware.com/em->

controlled-electromantle-heating-mantle-volume-1000ml-115v.html?gclid=CjwKCAiAm7OMBhAQEiwArvGi3IKIRVFyx_Gk_UYn0CiE1W-sG8VOK0xa8DIu7Mt0L6QWh6pm3awpghoClX4QAvD_BwE.

- [135] H. Gu and R. Bergman, "LIFE-CYCLE ASSESSMENT OF A DISTRIBUTED-SCALE THERMOCHEMICAL BIOENERGY CONVERSION SYSTEM," *WOOD FIBER Sci.*, vol. 84, no. 2, pp. 129–141, 2016.
- [136] ohaus, "ACHIEVER™ 5000: Reliable Overhead Stirrers with Excellent Performance for Everyday Use: e-A51ST020," 2020. [Online]. Available: <https://us.ohaus.com/en-US/Products/Equipment/Overhead-Stirrers/Achiever-5000/Overhead-Stirrer-e-A51ST020>.
- [137] Coleparmer, "Thermo Scientific Cimarec Stirring Hot Plate, 10x10" Ceramic, 120 VAC," 2020. [Online]. Available: https://www.coleparmer.com/i/thermo-scientific-cimarec-stirring-hot-plate-10x10-ceramic-120-vac/0460044?PubID=UX&persist=true&ip=no&gclid=CjwKCAiAm7OMBhAQEiwArvGi3NLawNgI2rz7QNCz15yiNKSrKX9YNk-CKAoS7A8vXLGxN0mPvxv2oxoCTeIQAvD_BwE. [Accessed: 11-Nov-2021].
- [138] R. West *et al.*, "Field Performance of Warm Mix Asphalt Technologies," (*National Coop. Highw. Res. Progr. Rep. No. 779*). *Transp. Res. Board, Washington, D.C.*, 2014.
- [139] J. Santos, S. Bressi;, V. Cerezo;, M. Dauvergne;, and D. Lo Presti, "Life Cycle

Assessment of low temperature asphalt mixtures for road pavement surfaces : a comparative analysis.,” *Conserv. Recycl.*, vol. 10, no. 1016, pp. 283–297, 2018.

[140] O. O. Fasina and Z. Colley, “Viscosity and Specific Heat of Vegetable Oils as a Function of Temperature : 35 ° C to 180 ° C,” *Int. J. Food Prop.*, vol. 11, no. 4, pp. 738–746, 2008.

[141] P. Steele, M. E. Puettmann, and J. E. Cooper, “Life-Cycle Assessment of Pyrolysis Bio-Oil Production,” *For. Prod. J.*, vol. 62, no. 4, pp. 326–334, 2012.

[142] Y. Heng, C. Raymond, R. T. Suzana, Y. Hon, L. Lam, and A. T. Quitain, “Comparative life cycle assessment (LCA) of bio-oil production from fast pyrolysis and hydrothermal liquefaction of oil palm empty fruit bunch (EFB),” *Clean Technol. Environ. Policy*, vol. 18, no. 6, pp. 1759–1768, 2016.

[143] S. G. Papadaki, K. E. Kyriakopoulou, and M. K. Krokida, “Life Cycle Analysis of Microalgae Extraction Techniques,” *Chem. Eng. Trans.*, vol. 52, pp. 1039–1044, 2016.

[144] J. Santos, A. Ferreira, and G. Flintsch, “A life cycle assessment model for pavement management : methodology and computational framework,” *Int. J. Pavement Eng.*, vol. 16:3, pp. 268–286, 2015.

[145] Angela Farina, M. C. Zanetti, E. Santagata, and G. A. Blengini, “Life cycle assessment applied to bituminous mixtures containing recycled materials: Crumb rubber and reclaimed asphalt pavement,” *Resour. Conserv. Recycl.*, vol. 117, no.

PB, pp. 204–212, 2017.

- [146] M. B. dos Santos, J. Candido, S. de S. Baulé, Y. M. M. de Oliveira, and L. P. Thives, “Greenhouse gas emissions and energy consumption in asphalt plants,” *Rev. Eletrônica em Gestão, Educ. e Tecnol. Ambient.*, vol. 24, 2020.
- [147] D. L. Vega, J. Santos, and G. Martinez-arguelles, “Life cycle assessment of hot mix asphalt with recycled concrete aggregates for road pavements construction,” *Int. J. Pavement Eng.*, vol. 0, no. 0, pp. 1–14, 2020.
- [148] Z. Al-hamamre, S. Foerster, F. Hartmann, M. Kröger, and M. Kaltschmitt, “Oil extracted from spent coffee grounds as a renewable source for fatty acid methyl ester manufacturing,” *Fuel*, vol. 96, no. x, pp. 70–76, 2012.
- [149] K. Somnuk, P. Eawlex, and G. Prateepchaikul, “Optimization of coffee oil extraction from spent coffee grounds using four solvents and prototype-scale extraction using circulation process,” *Agric. Nat. Resour.*, vol. 51, no. 3, pp. 181–189, 2017.
- [150] I. Efthymiopoulos *et al.*, “Industrial Crops & Products Influence of solvent selection and extraction temperature on yield and composition of lipids extracted from spent coffee grounds,” *Ind. Crop. Prod.*, vol. 119, no. September 2017, pp. 49–56, 2018.
- [151] B. Han *et al.*, “Ultrasonic assisted oil extraction and biodiesel synthesis of Spent Coffee Ground,” *Fuel*, vol. 261, no. August 2019, p. 116121, 2020.

- [152] J. Yang, H. Chen, H. Niu, J. Mcnutt, and Q. He, "A Comparative Study on Thermochemical Valorization Routes for Spent Coffee Grounds," *Energies*, vol. 14, no. 3840, pp. 1–10, 2021.
- [153] M. Abdullah and A. B. Koc, "Oil removal from waste coffee grounds using two-phase solvent extraction enhanced with ultrasonication," *Renew. Energy*, vol. 50, pp. 965–970, 2013.
- [154] B. Ahangari and J. Sargolzaei, "Extraction of lipids from spent coffee grounds using organic solvents and supercritical carbon dioxide," *J. Food Process. Preserv.*, 2013.
- [155] M. Valdez et al., "Bioresource Technology Ultrasound-assisted production of biodiesel and ethanol from spent coffee grounds," *Bioresour. Technol.*, vol. 167, pp. 343–348, 2014.
- [156] C. Severini, A. Derossi, and A. G. Fiore, "Ultrasound - assisted extraction to improve the recovery of phenols and antioxidants from spent espresso coffee ground : a study by response surface methodology and desirability approach," *Eur. Food Res. Technol.*, vol. 243, no. 5, pp. 835–847, 2017.